PHASE BEHAVIOUR AND MASS TRANSFER OF SOLVENT(S)-CO_2-HEAVY OIL SYSTEMS UNDER RESERVOIR CONDITIONS

A Thesis

Submitted to the Faculty of Graduate Studies and Research

In Partial Fulfillment of the Requirements

For the Degree of

Doctor of Philosophy

in

Petroleum Systems Engineering

University of Regina

By

Huazhou Li

Regina, Saskatchewan

May, 2013

Copyright 2013: H. Li

UNIVERSITY OF REGINA

FACULTY OF GRADUATE STUDIES AND RESEARCH

SUPERVISORY AND EXAMINING COMMITTEE

Huazhou Li, candidate for the degree of Doctor of Philosophy in Petroleum Systems Engineering**,** has presented a thesis titled, **Phase Behaviour and Mass Transfer of Solvent(s)-CO_2-Heavy Oil Systems Under Reservoir Conditions*,*** in an oral examination held on May 14, 2013. The following committee members have found the thesis acceptable in form and content, and that the candidate demonstrated satisfactory knowledge of the subject material.

External Examiner:	Dr. Gordon R. Moore, University of Calgary
Supervisor:	Dr. Daoyong Yang, Petroleum Systems Engineering
Committee Member:	*Dr. Yongan Gu, Petroleum Systems Engineering
Committee Member:	Dr. Farshid Torabi, Petroleum Systems Engineering
Committee Member:	Dr. Guoxiang Chi, Department of Geology
Chair of Defense:	Dr. Cory Butz, Faculty of Science

*Not present at defense, submitted questions

ABSTRACT

CO_2 has been found to be an efficient agent for recovering heavy oil resources worldwide through an immiscible displacement process. One major disadvantage of CO_2 immiscible process is the limited solubility of CO_2 in heavy oil, resulting in limited enhanced oil recovery. Addition of light alkane solvents to CO_2 stream may provide a better recovery efficiency of heavy oil, though it is not well understood how addition of solvents will affect the phase behaviour and mass transfer of CO_2-heavy oil systems. Therefore, it is of fundamental and practical importance to study phase behaviour and mass transfer of the solvent(s)-CO_2-heavy oil systems under reservoir conditions.

In order to improve the phase behaviour modeling of highly asymmetric systems, e.g., solvent(s)-CO_2-heavy oil systems, a new alpha function for the Peng-Robinson equation of state (PR EOS) is first developed. In comparison with the existing alpha functions evaluated in this study, the modified alpha function with the redefined acentric factor at a reduced temperature of 0.6 provides more accurate prediction of vapour pressures of non-hydrocarbon and hydrocarbon compounds, especially heavy hydrocarbons. Subsequently, the enhanced swelling effect and viscosity reduction of CO_2-heavy oil systems with the addition of solvent C_3H_8 or *n*-C_4H_{10} are experimentally measured and theoretically determined. An increased swelling effect of heavy oil is obtained by adding gas solvent C_3H_8 or *n*-C_4H_{10} into the CO_2 stream, while an enhanced viscosity reduction of the CO_2-heavy oil system is also achieved in the presence of either solvent C_3H_8 or *n*-C_4H_{10}. By treating the heavy oil sample as a single pseudocomponent, three binary interaction parameter (BIP) correlations have been proposed for respectively characterizing CO_2-heavy oil binaries, C_3H_8-heavy oil binaries and *n*-C_4H_{10}-heavy oil binaries. The PR EOS

with the modified alpha function and BIP correlations can be used to predict the saturation pressures and swelling factors of the aforementioned systems with a generally good accuracy.

Equilibrium interfacial tensions (IFT) between solvent(s)-CO_2 mixture and heavy oil have also been experimentally measured with an axisymmetric drop shape analysis (ADSA) setup. Addition of C_3H_8 and/or *n*-C_4H_{10} into CO_2 stream leads to an obvious reduction of IFT between heavy oil and CO_2, though the degree of reduction depends on the added amount of the light alkane solvent(s). Theoretically, an optimized mechanistic parachor model provides a qualitative agreement with the measured equilibrium IFTs between solvent(s)-CO_2 mixture and heavy oil.

The liquid-liquid-vapour (L_1L_2V) phase boundaries of solvent(s)-CO_2 heavy oil mixtures in the pressure-temperature (*P*-*T*) diagram are also experimentally and visually determined with the PVT setup. The addition of an alkane solvent to the CO_2-heavy oil system tends to expand the pressure span of the L_1L_2V phase boundary, while the L_1L_2V phase boundary of solvent(s)-CO_2-heavy oil system shows its tendency to move towards the high-temperature and low-pressure side of the *P*-*T* diagram.

Experimental and theoretical methods have been performed to determine the diffusion coefficient of each component in the solvent(s)-CO_2 mixture or the apparent diffusion coefficient of the mixture in heavy oil. It is found that the gas-phase solvent fraction decreases as diffusion proceeds, while the gas-phase CO_2 fraction decreases during the diffusion test. As for the solvent(s)-CO_2 mixtures tested, the molecular diffusion coefficient of an individual solvent in heavy oil is found to be significantly larger than that of CO_2 in heavy oil. Also, at the same pressure, the C_3H_8-CO_2 mixture leads to an accelerated growth in swelling-factor compared to pure CO_2.

ACKNOWLEDGEMENTS

I would like to express my sincere gratitude to my academic supervisor, Dr. Daoyong (Tony) Yang, for providing me the precious opportunity together with his continuous encouragement and support throughout the course of my Ph.D. graduate studies. This dissertation could have not been possible without his excellent guidance.

I also wish to thank the following individuals or organizations for their help and friendship during my Ph.D. study at the University of Regina:

- My past and present research group members: Dr. Heng Li, Dr. Shengnan Chen, Dr. Mohamed Arhuoma, Mr. Yin Zhang, Mr. Sixu Zheng, Ms. Xiaoli Li, Mr. Chengyao Song, Mr. Feng Zhang, Ms. Min Yang, Mr. Deyue Zhou, and Ms. Ping Yang;
- Natural Sciences and Engineering Research Council (NSERC) of Canada to Dr. Daoyong Yang;
- Petroleum Technology Research Center (PTRC) for the innovation fund to Dr. Daoyong Yang;
- Faculty of Graduate Studies and Research (FGSR) at the University of Regina for awarding the FGSR Dean's Scholarship (2011 Fall to 2012 Fall) and the Graduate Studies Scholarship (2010 Fall);
- Dr. Yongan Gu for using the interfacial interaction apparatus and Mr. Bart Schnell from Saskatchewan Research Council (SRC) for his technical assistance on operating the DBR PVT system; and
- Many wonderful friends and families who showed their love, friendship and care to my wife and me during our stay in the beautiful city Regina of Canada.

DEDICATION

This dissertation is dedicated to my dearest parents, Mrs. Kaixiu Yuan and Mr. Weixiu Li, my beloved wife, Dr. Huijuan Sun, and my dear brother, Mr. Huadeng Li

TABLE OF CONTENTS

ABSTRACT ..... **i**

ACKNOWLEDGEMENTS ..... **iii**

DEDICATION ..... **iv**

TABLE OF CONTENTS ..... **v**

LIST OF TABLES ..... **x**

LIST OF FIGURES ..... **xii**

NOMENCLATURE ..... **xx**

CHAPTER 1 INTRODUCTION **1**

1.1 CO_2-based Processes for Heavy Oil Recovery 1

1.2 Objective of This Study 2

1.3 Outline of the Dissertation 3

CHAPTER 2 LITERATURE REVIEW **5**

2.1 Immiscible CO_2 Processes 5

2.2 Phase Behaviour and Physical Properties 6

2.2.1. CO_2-alkane systems 7

2.2.2. CO_2-heavy oil systems 11

2.3 Correlations for Physical Properties 20

2.3.1. CO_2 solubility 20

2.3.2. Swelling factor 23

2.3.3. Viscosity 25

2.4 Phase Behaviour of Solvent(s)-Heavy Oil Systems 27

2.4.1. Short-chain alkane and long-chain alkane system 28

2.4.2. C_3H_8/*n*-C_4H_{10} with heavy oil 32

2.5 Phase Behaviour of Solvent(s)-CO_2-Heavy Oil Systems 32

2.6 Mass Transfer of Solvent(s)-CO_2-Heavy Oil Systems 37

2.7 Summary 40

CHAPTER 3 A MODIFIED ALPHA FUNCTION FOR PENG-ROBINSON EQUATION OF STATE TO IMPROVE VAPOUR PRESSURE PREDICTION OF NON-HYDROCARBON AND HYDROCARBON COMPOUNDS 42

3.1 Introduction 42

3.2 Mathematical Formulation 44

3.2.1. Alpha function 44

3.2.2. Determination of the correlation coefficients 56

3.2.3. Enthalpy of vaporization 65

3.3 Results and Discussion 67

3.3.1. Vapour pressure 67

3.3.2. Enthalpy of vaporization 76

3.4 Summary 76

CHAPTER 4 ENHANCED SWELLING EFFECT AND VISCOSITY REDUCTION OF SOLVENT(S)-CO_2-HEAVY OIL SYSTEMS 80

4.1 Introduction 80

4.2 Experimental 81

4.2.1. Materials 81

4.2.2. Viscosity measurements 84

4.2.3. Density measurements 91
4.2.4. PVT measurements 95
4.3 Mathematical Formulation 103
4.3.1. PR EOS model 103
4.3.2. BIP correlations 105
4.3.3. Mixing rules for mixture viscosity 115
4.4 Results and Discussion 117
4.4.1. Validation of the BIP correlations 117
4.4.2. Solvent(s)-Lloydminster heavy oil systems 121
4.4.3. Solvent(s)-CO_2-Lloydminster heavy oil systems 132
4.4.4. Formation of foamy heavy oil 137
4.5 Summary 139
CHAPTER 5 DETERMINATION OF EQUILIBRIUM INTERFACIAL TENSION FOR SOLVENT(S) -CO_2-HEAVY OIL SYSTEMS 141
5.1 Introduction 141
5.2 Experimental 142
5.2.1. Materials 142
5.2.2. IFT measurements 143
5.3 Mathematical Formulation 147
5.3.1. PR EOS model 147
5.3.2. Mechanistic parachor model for equilibrium IFT 148
5.4 Results and Discussion 151
5.4.1. Dynamic IFT of the solvent(s)-CO_2-heavy oil systems 151

5.4.2. Equilibrium IFT of the solvent(s)-CO_2-heavy oil systems 154

5.5 Summary 168

CHAPTER 6 DETERMINATION OF THREE-PHASE BOUNDARIES OF SOLVENT(S)-CO_2-HEAVY OIL SYSTEMS UNDER RESERVIOR CONDITIONS 169

6.1 Introduction 169

6.2 Experimental 170

6.2.1. Materials 170

6.2.2. Experimental setup 170

6.2.3. Experimental procedures 170

6.3 Mathematical Formulation 173

6.3.1. PR EOS model 173

6.3.2. Determination of the L_1L_2V phase boundaries 174

6.4 Results and Discussion 175

6.4.1. CO_2-heavy oil system 178

6.4.2. C_3H_8-CO_2-heavy oil system 180

6.4.3. *n*-C_4H_{10}-CO_2-heavy oil system 182

6.5 Summary 186

CHAPTER 7 DETERMINATION OF MOLECULAR DIFFUSION COEFFICIENTS OF SOLVENT(S)-CO_2 MIXTURES IN HEAVY OIL 188

7.1 Introduction 188

7.2 Experimental 189

7.2.1. Materials 189
7.2.2. Experimental setup 189
7.2.3. Experimental procedures 189
7.3 Mathematical Formulation 193
7.3.1. Mass transfer model 193
7.3.2. Determination of molecular diffusion coefficients 197
7.4 Results and Discussion 201
7.4.1. Diffusion profiles 203
7.4.2. Molecular diffusion coefficients 208
7.4.3. Swelling factor 214
7.5 Summary 216
CHAPTER 8 CONCLUSIONS AND RECOMMENDATIONS 218
8.1 Conclusions 218
8.2 Recommendations 222
REFERENCES 225

LIST OF TABLES

TABLE 2-1: Phase behaviour of CO_2-heavy oil systems documented in the literature .. 17

TABLE 2-2: Phase behaviour of solvent(s)-heavy oil systems documented in the literature 33

TABLE 3-1: Vapour pressure database used in this study..... 51

TABLE 3-2: Alpha functions examined in this study..... 54

TABLE 3-3: Critical properties and acentric factors of the substances used in this study 57

TABLE 3-4: Standard errors of the fitted coefficients in Equations [3-17] and [3-18]... 62

TABLE 3-5: Standard errors of the fitted coefficients in alpha functions #4-1 and 4-2.. 64

TABLE 3-6: Vaporization enthalpy data 68

TABLE 3-7: The predicted vapour pressures by using PR EOS with different alpha functions 70

TABLE 3-8: The predicted vaporization enthalpy using PR EOS with different alpha functions 77

TABLE 4-1: Compositional analysis result of the Lloydminster heavy oil..... 82

TABLE 4-2: SARA fraction analysis of the Lloydminster heavy oil 83

TABLE 4-3: Measured viscosity of the Lloydminster heavy oil at different temperatures 85

TABLE 4-4: The coefficient values in Equations [4-3] and [4-6] 92

TABLE 4-5: Compositions of the C_3H_8-*n*-C_4H_{10}-CO_2-heavy oil mixtures tested 96

TABLE 4-6: BIP matrix for the *n*-C_4H_{10}-C_3H_8-CO_2-heavy oil system 107

TABLE 4-7: Database for developing the BIP correlation for CO_2-heavy oil systems. 108

TABLE 4-8: Database for developing the BIP correlation for C_3H_8-heavy oil systems 109

TABLE 4-9: Physical properties of CO_2, C_3H_8, *n*-C_4H_{10} and Lloydminster heavy oil.. 122

TABLE 5-1: Compositions of seven solvent mixtures 144

TABLE 5-2: Physical properties of the three solvents and Lloydminster heavy oil used in the mechanistic parachor model 155

TABLE 6-1: Compositions of solvent(s)-CO_2-heavy oil systems examined in this study 172

TABLE 6-2: Raw experimental data obtained in this study 176

TABLE 7-1: Overall compositions for the three feeds and initial conditions of the three diffusion tests 192

TABLE 7-2: Compositional analysis results of C_3H_8-CO_2 mixture and *n*-C_4H_{10}-CO_2 mixture measured at the beginning and the end of the diffusion tests 209

TABLE 7-3: Comparison of the measured molecular diffusion coefficients in different oils 210

TABLE 7-4: Measured and calculated mole fractions of solvent(s)-CO_2 in heavy oil at the end of diffusion tests 213

LIST OF FIGURES

FIGURE 2-1: Phase behaviour classification for binary mixtures. 8

FIGURE 2-2: Phase behaviour of CO_2/*n*-hexadecane mixtures at 70ºF and 90ºF showing liquid-vapour and liquid-liquid equilibria (Orr, 1984)..... 10

FIGURE 2-3: Phase diagrams of binary CO_2-alkane mixtures. Three phase lines are omitted (Liphard and Schneider, 1975)..... 12

FIGURE 2-4: Three-phase loci for binary CO_2-alkane mixtures (Larson *et al.*, 1989) .. 14

FIGURE 2-5: Conceptual phase diagrams of a pseudo CO_2-heavy oil system based on phase behaviour of CO_2-heavy alkane systems. Dotted line denotes vapour pressure of CO_2 15

FIGURE 2-6: Vapour pressure lines of six gases N_2, CH_4, CO_2, C_2H_6, C_3H_8 and *n*-C_4H_{10}. Bold dots denote the critical points (Lide, 2009) 29

FIGURE 2-7: Binaries of short and long *n*-alkanes first showing partial miscibility in the liquid phase characterized by their carbon numbers (Peters *et al.*, 1989) 31

FIGURE 2-8: Critical loci for the L_1L_2V regions of the systems of CO_2-N_2-*n*-nonadecane and CO_2-C_3H_8-*n*-nonadecane. 35

FIGURE 3-1: Temperature dependence of the alpha function in the PR EOS for heavy normal alkanes expressed in Soave-type form (based on the experimental data (Mazee, 1948))..... 47

FIGURE 3-2: Temperature dependence of the alpha function in PR EOS for heavy normal alkanes expressed in logarithm-type form (based on the experimental data (Mazee, 1948))..... 48

FIGURE 3-3: Dependence of acentric factor on carbon number of normal alkanes..... 60

FIGURE 3-4: Variation of alpha function #4-2 with reduced temperature for CO_2 66

FIGURE 3-5: Overall %AAD of the predicted vapour pressures of normal alkanes using different alpha function models..... 75

FIGURE 4-1: Effect of BPR pressure on the measured differential pressures across the capillary viscometer at different flow rates for (a) viscosity standard S60; and (b) viscosity standard S20..... 87

FIGURE 4-2: Effect of pressure on the water viscosity and C_3H_8 viscosity at different temperatures, respectively (Nagashima, 1977; Vogel *et al.*, 1998; Younglove and Ely, 1987)..... 89

FIGURE 4-3: Effect of temperature on the calculated *k* constant of the capillary viscometer 90

FIGURE 4-4: Comparison of the measured and calculated density of Lloydminster heavy oil 94

FIGURE 4-5: Comparison of the calculated saturated-densities and viscosities via Equations [4-3] and [4-6] and the measured data (Younglove and Ely, 1987; Vesovic *et al.*, 1990; Span and Wagner, 1996) for (a) CO_2, (b) C_3H_8 and (c) *n*-C_4H_{10}, respectively..... 97

FIGURE 4-6: Schematic diagram of experimental setup for conducting the PVT measurements for solvent(s)-CO_2-heavy oil systems..... 98

FIGURE 4-7: Parity chart of the measured and calculated phase behaviour data for CO_2-heavy oil systems by using the PR EOS with Equations [4-7] and [4-18]: (a) CO_2 solubility; and (b) swelling factor of CO_2-saturated heavy oil . 111

FIGURE 4-8: Comparison of the measured and calculated phase behaviour data for C_3H_8-heavy oil systems by using PR EOS with Equations [4-7] and [4-19]: (a) C_3H_8 solubility; and (b) swelling factor of C_3H_8-saturated heavy oil 113

FIGURE 4-9: The experimentally optimized BIPs and the linearly regressed values for the *n*-C_4H_{10}-heavy oil binaries (Feeds #8 and #9) as a function of temperature 114

FIGURE 4-10: Comparison of the measured saturation pressures (Badamchi-Zadeh *et al.*, 2009b) and calculated values with different models for the ternary mixtures: (a) Mixture #1 (24.0 wt% C_3H_8, 6.2 wt% CO_2, 69.8 wt% bitumen); and (b) Mixture #2 (13.5 wt% C_3H_8, 11.0 wt% CO_2, 75.5 wt% bitumen) 118

FIGURE 4-11: Comparison of the measured L_1L_2V boundaries (Badamchi-Zadeh *et al.*, 2009b) and calculated ones with the PR-EOS used in this study and the APR EOS (Díaz *et al.*, 2011) for Mixture #3 (13.1 wt% C_3H_8, 19.2 wt% CO_2, 67.7 wt% bitumen) 120

FIGURE 4-12: *P-V* relations measured by the continuous depressurization method and discrete depressurization method for (a) Feed #3 (20.9 wt% C_3H_8, 79.1 wt% heavy oil) at 298.85 K; and (b) Feed #4 (11.6 wt% C_3H_8, 88.4 wt% heavy oil) at 323.85 K 123

FIGURE 4-13: Measured and predicted saturation pressures and swelling factors for the C_3H_8-Lloydminster heavy oil system (a) Feeds #1-3 at 298.85 K; and (b) Feeds #4-6 at 323.85 K, respectively 124

FIGURE 4-14: Comparison of the measured saturation pressures and swelling factors and their predicted values for the C_3H_8-Lloydminster heavy oil binary: Feed #7 126

FIGURE 4-15: Comparison of the measured saturation pressures and swelling factors and their predicted values for the *n*-C_4H_{10}-Lloydminster heavy oil binaries: Feeds #8 and #9 127

FIGURE 4-16: Comparison of the measured saturation pressures and swelling factors and their predicted values for the ternary C_3H_8-*n*-C_4H_{10}-Lloydminster heavy oil system: Feed #10 129

FIGURE 4-17: Measured viscosity and predicted viscosity by using different mixing rules for (a) C_3H_8-heavy oil mixtures at 298.85 K and (b) *n*-C_4H_{10}-heavy oil mixtures at 298.85 K 131

FIGURE 4-18: Asphaltene precipitation observed on the PVT cell wall for Feed #3 (29.3 wt% C_3H_8, 70.7 wt% heavy oil) at 1500.0 kPa and 323.85 K..... 133

FIGURE 4-19: Measured and predicted saturation pressures and swelling factors for the C_3H_8-CO_2-heavy oil system with Feed #11 (10.3 wt% C_3H_8, 11.0 wt% CO_2, 78.7 wt% Lloydminster heavy oil) and the *n*-C_4H_{10}-CO_2-heavy oil system with Feed #12 (10.1 wt% *n*-C_4H_{10}, 7.1 wt% CO_2, 82.8 wt% Lloydminster heavy oil) 134

FIGURE 4-20: Predicted swelling factor and mixture viscosity for the CO_2-Lloydminster heavy oil system at 298.85 K, respectively. 136

FIGURE 4-21: Sequential images of the foamy C_3H_8-*n*-C_4H_{10}-heavy oil system Feed #10 which is released to atmosphere from the PVT cell at saturation

pressure and 298.85 K after the viscosity measurements at: (a) 0 s; (b) 30 s; (c) 60 s; (d) 90 s; and (e) 120 s. The total volume of the ternary mixture discharged is around 10 cm^3 at saturation conditions 138

FIGURE 5-1: Schematic diagram of experimental setup for measuring the dynamic and equilibrium IFT of solvent(s)-CO_2-heavy oil systems by using the ADSA technique for the pendant drop case 145

FIGURE 5-2: Measured dynamic IFT as a function of time between various solvents and heavy oil at 21.0°C 153

FIGURE 5-3: Variation of the objective function $RMSRE_{IFT}$ with the parachor of Lloydminster heavy oil P_{ao} and the mass transfer exponent n in the mechanistic model 156

FIGURE 5-4: Comparison of the measured and calculated equilibrium IFT using the mechanistic model Equation [5-11] for the pure solvent-heavy oil systems: (a) CO_2-heavy oil system at 21.0°C and 44.0°C, respectively; (b) C_3H_8-heavy oil system at 21.0°C and 46.1°C, respectively; and (c) *n*-C_4H_{10}-heavy oil system at 21.0°C and 48.6°C, respectively 158

FIGURE 5-5: Calculated *P-X* diagrams for CO_2-heavy oil system by using PR EOS with the modified alpha function: (a) at 21.0°C and (b) at 44.0°C, respectively 161

FIGURE 5-6: Comparison of the measured and calculated equilibrium IFT using Equation [5-11] for the CO_2-heavy oil system, CO_2-C_3H_8-heavy oil system (i.e., Mixtures #1, #2 and #3), and C_3H_8-heavy oil system at 21.0°C, respectively. 162

FIGURE 5-7: Comparison of the measured and calculated equilibrium IFT using Equation [5-11] for the CO_2-heavy oil system, CO_2-*n*-C_4H_{10}-heavy oil system (i.e., Mixture #4), and *n*-C_4H_{10}-heavy oil system at 21.0°C, respectively. The composition of Mixture #4 is (81.5 mol% CO_2, 18.5 mol% *n*-C_4H_{10}) 164

FIGURE 5-8: Comparison of the measured and calculated equilibrium IFT using Equation [5-11] for the C_3H_8-heavy oil system, C_3H_8-*n*-C_4H_{10}-heavy oil system (i.e., Mixtures #5 and #6), and *n*-C_4H_{10}-heavy oil system at 21.0°C, respectively. The compositions of Mixtures #5 and #6 are (76.8 mol% C_3H_8, 23.2 mol% *n*-C_4H_{10}) and (61.4 mol% C_3H_8, 38.6 mol% *n*-C_4H_{10}), respectively..... 165

FIGURE 5-9: Comparison of the measured and calculated equilibrium IFT using Equation [5-11] for the CO_2-heavy oil system and CO_2-C_3H_8-*n*-C_4H_{10}-heavy oil system (i.e., Mixture #7) at 21.0°C, respectively. The composition of Mixture #7 is (93.0 mol% CO_2, 5.9 mol% C_3H_8, 1.1 mol% *n*-C_4H_{10})..... 167

FIGURE 6-1: Digital images of typical phase equilibria captured for the C_3H_8-CO_2-heavy oil system (Feed #14): (a) L_1L_2 phase equilibrium at 298.55 K and 6501.0 kPa; (b) L_1L_2V phase equilibrium at 298.55 K and 5538.0 kPa; and (c) L_1V phase equilibrium at 298.55 K and 5306.0 kPa..... 177

FIGURE 6-2: Comparison of the measured L_1L_2V phase boundary and the predicted L_1L_2V phase boundary by using the PR EOS with Equations [4-7] and [4-18] for the general CO_2-heavy oil system: Feed #13 179

FIGURE 6-3: Comparison of the measured L_1L_2V phase boundary and the predicted L_1L_2V phase boundary with Equations [4-7], [4-18] and [4-19] for the ternary C_3H_8-CO_2-heavy oil system: Feed #14 181

FIGURE 6-4: Comparison of the measured L_1L_2V phase boundary and the predicted L_1L_2V phase boundary by using the PR EOS with Equations [4-7], [4-18] and [4-20] for the ternary *n*-C_4H_{10}-CO_2-heavy oil system: Feed #15 183

FIGURE 6-5: (a) Calculated phase volumes for 1 mole of Feed #15 as a function of pressure at 298.65 K; Correspondingly calculated phase compositions as a function of pressure at 298.65 K; (b) V phase; (c) L_2 phase; and (d) L_1 phase. The phase behaviour calculations are performed by using the volume-translated PR EOS (Peneloux *et al.*, 1982) with Equations [4-7], [4-18] and [4-20] for the ternary *n*-C_4H_{10}-CO_2-heavy oil system 185

FIGURE 7-1: Schematic of PVT system for conducting molecular diffusion experiments 190

FIGURE 7-2: Schematic of dynamic process of molecular diffusion of the solvent(s)-CO_2 mixture into heavy oil in a closed PVT cell at a constant temperature 194

FIGURE 7-3: Schematic of domain discretization 198

FIGURE 7-4: Flowchart of determining the individual molecular diffusion coefficients 199

FIGURE 7-5: Measured and correlated pressure decay profile as a function of time for the CO_2-heavy oil system 204

FIGURE 7-6: Measured and correlated pressure decay profile as a function of time for the C_3H_8-CO_2-heavy oil system 205

FIGURE 7-7: Measured and correlated pressure decay profile as a function of time for the *n*-C_4H_{10}-CO_2-heavy oil system..... 206

FIGURE 7-8: Gas-phase volume-decay profiles as a function of time for the three diffusion tests 207

FIGURE 7-9: Measured and calculated swelling factor based on the individual molecular diffusion coefficients for the CO_2-heavy oil system, C_3H_8-CO_2-heavy oil system and *n*-C_4H_{10}-CO_2-heavy oil system..... 215

NOMENCLATURE

a	attraction parameter in Equations [3-1]
a_c	constant in Equation [3-2]
$a_1, a_2, \ldots, a_{12}$	empirical constants
A	cross-sectional area of the diffusion cell, cm^2
% AAD	percentage average absolute deviation
ADSA	axisymmetric drop shape analysis
b	van der Waals volume, $m^3/kmol$
$b_1, b_2, \ldots, b_7$	empirical constants
B	constant in Equation [3-28]
% BIAS	percentage bias
BIP	binary interaction parameter
c_i	concentration of *i*th component in heavy oil in mole fraction
$c_{i,\mathrm{sat}}$	saturation concentration of *i*th component in heavy oil in mole fraction
$c_1, c_2, \ldots, c_7$	empirical constants in Equations [2-4] and [2-5]
C	volume correction factor, $m^3/kmol$
C_n	carbon number
d, e, f, g, h, l, n	coefficients in Equations [4-3] and [4-6]
d_1, d_2, d_3	empirical constants in Equation [2-6]
D_{AB}	diffusivity of solute A in solvent B, m^2/s

D_i	individual molecular diffusion coefficient of the *i*th component in heavy oil, m^2/s
F, G, H, K	coefficients in Equation [4-16]
H	enthalpy, kJ/mol
H_{CO_2}	Henry's constant
H^{IG}	ideal gas enthalpy, kJ/mol
$\Delta_l^g H(T)$	enthalpy of vaporization at temperature *T*, kJ/mol
i	integer
IFT	interfacial tension
k	characteristic constant in Equations [3-9] and [3-10], temperature-dependant characteristic factor in Equation [4-2]
k_1	characteristic constant in Equations [3-11] and [3-13], coefficient in Equation [7-10]
k_1'	characteristic constant in Equation [3-12]
k_2	characteristic constant in Equations [3-11]-[3-13], coefficient in Equation [7-10]
l	constant in Equation [3-13]
L_0	initial height of heavy oil in diffusion cell, m
$L(t)$	height of gas-diluted heavy oil in diffusion cell at a given time, m
L_1, L_2, L_m	liquidity of solvent, solute and mixture, respectively
m	total number of compound species

m_1 , m_2	coefficients in Equation [7-10]
M	molar mass, g/mol
% MAD	percentage maximum absolute deviation
MW	molecular weight
n	number of coexisting phases in Equation [2-1]
n_j	molar mass of jth component in liquid bulk phase, mol
nc	number of components in the system
ng	number of gas-phase components in the system
N	total number of data point
$NPTS$	number of data points
$O(c)$	objective function
P	pressure, kPa
P_{a}	Parachor
P_{ao}	Parachor of Lloydminster heavy oil
P_c	critical pressure, kPa
P_{eq}	equlibrium pressure, kPa
P_r	reduced pressure
P_v^{cal}	calculated vapour pressure, kPa
P_v^{exp}	experimental vapour pressure, kPa
ΔP	differential pressure, kPa
PR EOS	Peng-Robinson equation of state

Q	flow rate, $\mathrm{cm}^3/\mathrm{min}$
R	universal gas constant, $\mathrm{J}/(\mathrm{mol}\cdot\mathrm{K})$
R_s	gas solubility in oil
$RMSRE$	root-mean-squared relative error
SF	swelling factor
SG	specific gravity
t	time, s
T	temperature, K
T_{br}	reduced temperature at normal boiling point, K
T_c	critical temperature, K
T_r	reduced temperature
V	molar volume, m^3/kmol
V_{A}	molar volume at normal boiling point, m^3/kmol
V_{c}	critical molar volume, m^3/kmol
$V_{\mathrm{corrected}}$	corrected molar volume, m^3/kmol
V_{s1}	molar volume of oil at saturation temperature and atmospheric pressure, m^3/kmol
V_{s2}	molar volume of saturated oil at saturation temperature and pressure, m^3/kmol
$V(t)$	molar volume of solvent-diluted oil at time t, m^3/kmol

V_0 molar volume of heavy oil at the beginning of pressure decay experiment, m^3/kmol

V^* molar volume of heavy oil at 60°F

w weight fraction

x_i mole fraction of the *i*th component in the bulk liquid phase, distance from the bottom of the diffusion cell in *x*-direction, m

x_i^{cal} calculated mole fraction of *i*th component in heavy oil

x_i^{exp} measured mole fraction of *i*th component in heavy oil

X solvent solubility in mole fraction

X_i^{cal} calculated solvent solubility of *i*th data point in heavy oil

X_i^{exp} measured solvent solubility of *i*th data point in heavy oil

y parameter in Equation [2-4]

y_i mole fraction of the *i*th component in the vapour phase

Z compressibility factor

Z_l compressibility factor of liquid phase

Z_{RA} Rackett parameter

Z_v compressibility factor of vapour phase

Greek letters

α empirical constant having a value in the range of 0 to 1 in Equation [2-12b]; and alpha function in Equation [3-2]

β parameter in Equation [4-5b]

γ	IFT, mN/m
δ_{ij}	BIP between *i*th component and *j*th component
μ	viscosity, $\text{mPa}\cdot\text{s}$
ρ	density, kg/cm^3
ρ^{L}, ρ^{V}	molar densities of liquid and vapour phases, mol/cm^3
σ	surface tension, mN/m
ϕ	volume fraction
ω	acentric factor defined at $T_r = 0.7$
ω'	acentric factor defined at $T_r = 0.6$

CHAPTER 1 INTRODUCTION

1.1 CO_2-based Processes for Heavy Oil Recovery

Heavy oil and tar sands are an important part of the energy supply of the world, while they have been exploited increasingly as the demand for petroleum increases (Farouq Ali, 2003). Canada's energy future depends on heavy oil resources that are mainly discovered in Saskatchewan and Alberta, of which only 8-9% of the original oil in place (OOIP) can be recovered with currently available technologies due to the fact that the oil is highly viscous and contained in thin payzones.

About 62% of Canada's total heavy oil resources is discovered in Saskatchewan (Bowers and Drummond, 1997), including 3.4 billion m^3 of proved reserves in the west-central region of the province (Ministry of Energy and Resources of Saskatchewan, 2008). As for the proved heavy oil reserves in Saskatchewan, about 97% is contained in payzones of less than 10 m, while 55% is located in payzones of less than 5 m (Strivastava *et al.*, 1999). The depth of these thin payzones ranges from 300 m to 1400 m, while a large portion of these reservoirs are underlain by a bottomwater. These heavy oils possess high carbon intensity, require more effort and energy to recover than the conventional oils, resulting in adverse environmental consequences during exploitation. The major challenge lies in developing techniques for recovering these heavy oil resources while minimizing greenhouse gas emissions (mainly CO_2) and thus reducing the carbon footprint.

It has been found that cyclic steam stimulation (CSS), steam-assisted gravity drainage (SAGD) and vapour extraction (VAPEX) often do not work for recovering heavy oil in such thin reservoirs (Dyer and Farouq Ali, 1994). Alternatively, CO_2 has been found to be an efficient agent for recovering heavy oil resources worldwide through an immiscible displacement process (Saner and Patton, 1986; Mohammed-Singh and Singhal, 2005; Sahin *et al.*, 2008). Such immiscible displacement processes mainly include CO_2 cyclic injection (i.e., CO_2 huff-*n*-puff), continuous CO_2 injection and water-alternating-CO_2 injection, among which CO_2 huff-*n*-puff appears to be more efficient to increase heavy oil recovery, though the recovery factor is still low (Sayegh and Maini, 1984; Sahin *et al.*, 2008).

Addition of solvents to the CO_2 stream will generally accelerate the processes of swelling heavy oil and reducing its viscosity, achieving a higher oil recovery in the VAPEX process (Talbi and Maini, 2008). Although some laboratory efforts have been conducted to study the mechanisms for heavy oil recovery by CO_2 injection, it is still not well understood how addition of solvents will affect the CO_2 injection for enhancing heavy oil recovery. Therefore, it is of fundamental and practical importance to study phase behaviour and mass transfer of the solvent(s)-CO_2-heavy oil systems and determine potential of CO_2 cyclic injection in combination with solvents for enhancing oil recovery in such thin heavy oil reservoirs where other processes are not applicable.

1.2 Objective of This Study

The major objective of this proposed research is to provide a pragmatic method and correlations/theoretical models for determining and simulating phase behaviour and

physical properties of solvent(s)-CO_2-heavy oil systems for enhanced heavy oil recovery. The detailed objectives are listed as follows,

1) To conduct PVT tests to study phase behaviour of CO_2-heavy oil systems and solvent(s)-CO_2-heavy oil systems under subcritical and supercritical conditions, respectively;
2) To measure the equilibrium properties including swelling factor, equilibrium interfacial tension (IFT) and molecular diffusion coefficients for the above-mentioned systems; and
3) To develop correlations and/or theoretical models for simulating phase behaviour and mass transfer determined in Objectives #1 and 2.

1.3 Outline of the Dissertation

There are eight chapters in this dissertation. Chapter 1 introduces the research topic together with its major research objectives. Chapter 2 provides an updated literature review on phase behaviour and mass transfer of CO_2-heavy oil systems, C_3H_8-heavy oil systems, and *n*-C_4H_{10} heavy oil systems, respectively. Chapter 3 presents a new alpha function in the Peng-Robinson equation of state (PR EOS) to more accurately predict the vapour pressure of non-hydrocarbons and hydrocarbon compounds, respectively. Chapter 4 includes the experimental measurements and theoretical determination of saturation pressures, swelling factors and viscosities of the solvent(s)-CO_2-heavy oil systems with the PR EOS. Chapter 5 presents the measured equilibrium interfacial tensions (IFTs) of the solvent(s)-CO_2-heavy oil systems together with the mechanical parachor model. Chapter 6 focuses on the measurements made on the liquid-liquid-vapour (L_1L_2V) three-

phase behaviour of solvent(s)-CO_2-heavy oil systems. The measured molecular diffusion coefficients of solvent(s)-CO_2-heavy oil systems are discussed in Chapter 7. Finally, conclusions of the current research and recommendation for future work are presented in Chapter 8.

CHAPTER 2 LITERATURE REVIEW

2.1 Immiscible CO_2 Processes

In principle, there exist three categories of CO_2 flooding processes: miscible, near miscible and immiscible (Blunt *et al.*, 1993). Miscible displacement of crude oil by CO_2 is the most desirable scenario that can yield maximum recovery efficiency. This is ascribed to the favourable mechanisms initiated by forming a single-phase containing CO_2 and crude oil through multiple contacts. Oil swelling, oil viscosity reduction, elimination of interfacial tension, and vaporization and extraction of intermediate components from the crude oil all contribute to a low residual oil saturation (Orr and Taber, 1984). In general, minimum miscibility pressure (MMP) is decreased with the API gravity of crude oil (Alston, 1985; Shokir, 2007; Li *et al.*, 2012). As for oil reservoir containing crude oil with 30°API or lower, the MMP would be too high to achieve such that only immiscible state could prevail during CO_2 injection processes in a hydrocarbon reservoir (Mangalsingh and Jagai, 1996).

Although the immiscible CO_2 flooding is a non-thermal recovery method, it shows considerable potential for a range of heavy oil reservoirs. During the immiscible flooding process, CO_2 is injected into the formation, highly mobilizing the oil contacted and displacing it towards the production wells. Oil mobility is improved due to solubility of CO_2 in the oil that causes a reduction in the viscosity, and an increase in oil volume (Al-Abri and Amin, 2010). Recovery mechanisms related to immiscible CO_2 flooding consist of viscosity reduction, oil swelling effect, and interfacial tension reduction.

***Viscosity reduction*:** It is mainly attributed to the dissolution of CO_2 into the crude oil. The viscosity of CO_2 saturated oil is a function of temperature, pressure, and concentration of dissolved CO_2. A decrease in viscosity due to carbonation is generally unimportant for light oils, but plays a significant role in the recovery of heavy oil. For example, when temperature is set at 75°F, the viscosity of a Wilmington oil sample with 15°API is reduced from 2000 cP to 20 cP with pressure increasing from 0 psia to 1500 psia (Spivak and Chima, 1984).

***Oil swelling*:** When CO_2 comes into contact with crude oil, it is expanded due to the dissolution of CO_2. Degree of swelling depends on pressure, temperature, and oil composition. Swelling is important in that the residual oil saturation is inversely proportional to the swelling factor (Hatzignatiou and Lu, 1994; Mangalsingh and Jagai, 1996).

***Interfacial tension reduction*:** Reduction of interfacial tension takes place due to the dissolution of CO_2 into heavy oil. For a heavy oil at moderate pressures (4-6 MPa) and temperature (293.15-298.15 K) with dissolved CO_2 of 50-100 m^3/m^3, a 30% reduction of interfacial tension can be observed (Kamal, 1986; Mangalsingh and Jagai, 1996). Reduction of interfacial tension increases the capillary number and thus enhances oil recovery.

2.2 Phase Behaviour and Physical Properties

Most of the aforementioned mechanisms associated with immiscible CO_2 flooding depend on the phase behaviour and mass transfer of CO_2-heavy oil systems. Phase behaviour is a critical factor in determining both the displacement efficiency and oil

recovery by CO_2 injection (Orr and Silva, 1983; Orr *et al.*, 2003). The mechanism of CO_2 flooding of heavy oil is complicated by the low temperature usually encountered in heavy oil reservoirs. At a low temperature which is close to 304.19 K (i.e., the critical temperature of CO_2), phase behaviour of liquid (L_1) equilibrium, liquid/vapour (L_1V) equilibrium, liquid/liquid (L_1L_2) equilibrium, and liquid/liquid/vapour (L_1L_2V) equilibrium can take place in CO_2-light oil systems (Orr, 1981; Suehiro *et al.*, 1996). Analogous to a CO_2-light oil system, L_1, L_1V, L_1L_2 and L_1L_2V equilibria have been also observed in CO_2-heavy oil systems (Badamchi-Zadeh *et al.*, 2009).

2.2.1. CO_2-alkane systems

It is necessary to examine the phase behaviour of CO_2 with pure hydrocarbons to better understand the phase behaviour of CO_2-crude oil systems. For an arbitrary binary mixture, nine types of phase diagrams have been identified through either laboratory experiments or theoretical calculations (van Konynenburg and Scott, 1980; Wang and Sadus, 2003). FIGURE 2-1 shows the conceptual layouts of the nine types of phase diagrams.

Phase behaviour of CO_2-alkane systems demonstrates more asymmetrical characteristics with the increase of carbon number of alkanes since the length of alkane chain is extended by adding more carbon atoms. In general, three types of phase behaviour have been observed for CO_2-alkane systems: Types I, II, and III (Liphard and Schneider, 1975; Orr *et al*., 1981). Mixtures of CO_2 with alkanes from methane up to hexane demonstrate only L_1V equilibria, as indicated by phase diagram of Type I in FIGURE 2-1. For such systems the critical line commences at the critical point of one pure component and moves smoothly to the critical point of the other component as the

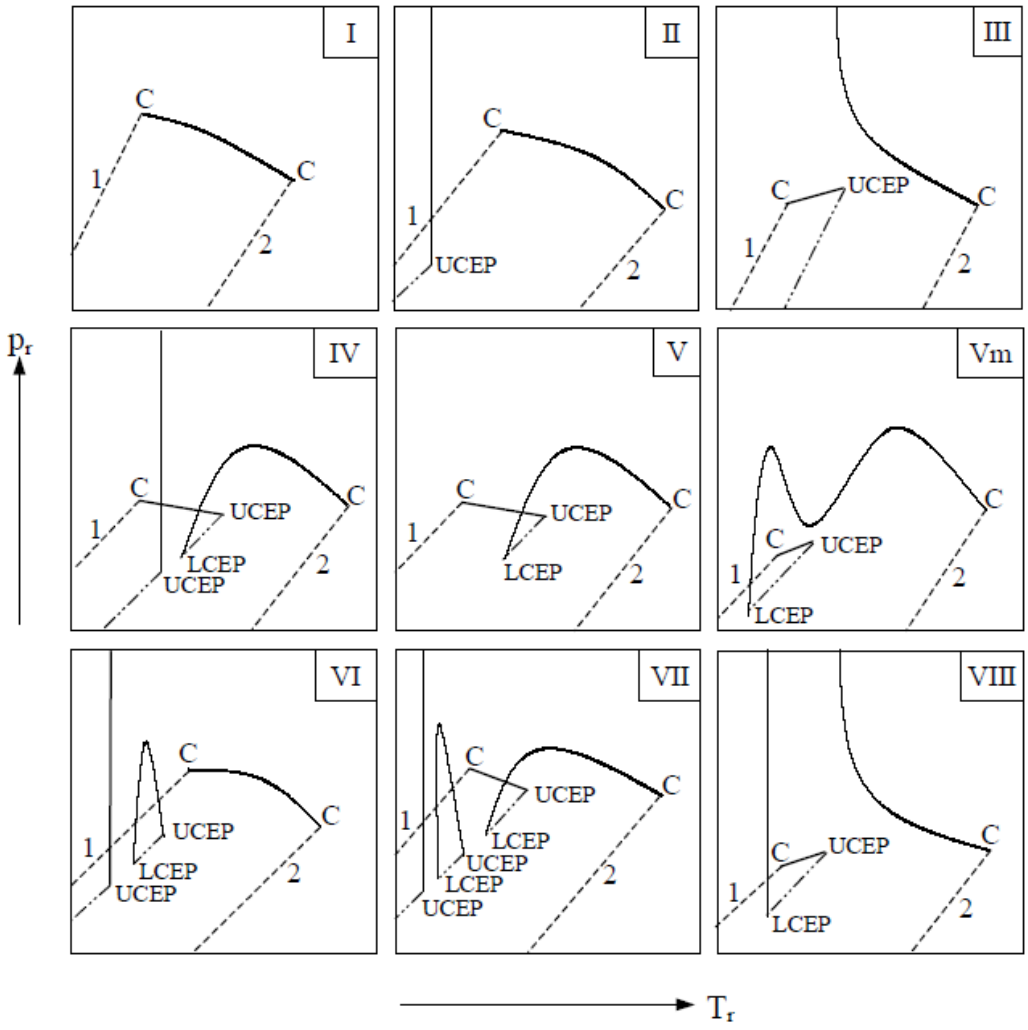

FIGURE 2-1: Phase behaviour classification for binary mixtures. Types I, II, III, IV, V and VI behaviour are observed experimentally, whereas behaviour of Types Vm, VII and VIII have only been reported in the literature from calculations. Critical equilibria of the binary mixtures (—), the critical points of the pure components (C), the vapour pressure curves (- - -, 1 and 2) and three-phase liquid-liquid-vapour (– · · – · · –) equilibria are illustrated. UCEP and LCEP denote upper critical end point (where L_2 and V become identical) and lower critical end point (where L_1 and L_2 become identical), respectively (Wang and Sadus, 2003)

mixture becomes richer in the second component. Mixtures of CO_2 with alkanes from *n*-heptane and *n*-tridecane (C_{13}) show L_2V, L_1L_2 and L_1L_2V equilibria, as illustrated by phase diagram of Type II in FIGURE 2-1. Type II phase behaviour is slightly more complicated in that there is a L_1L_2 region at low temperatures and high pressures, while a three phase region L_1L_2V occurs at low temperatures and low pressures (Sandler, 1999). Binary mixture of CO_2 and alkane *n*-tetradecane (C_{14}) and heavier illustrates Type III phase behaviour as shown in FIGURE 2-1. Compared to Type II phase behaviour, the L_1L_2 critical locus moves to a higher temperature and merges with the L_2V critical locus into a continuous critical curve (Orr *et al.*, 1981). As can be observed from FIGURE 2-1, one vapour-liquid critical line originates at critical point of CO_2 and terminates at the upper-critical-end-point (UCEP), whereas the other starts at critical point of the alkane and then smoothly merges into the L_1L_2 critical line.

Orr (1984) reported the phase behaviour of CO_2/*n*-hexadecane mixtures at 70ºF and 90ºF showing liquid/vapour and liquid/liquid equilibria. As can be seen from FIGURE 2-2, at 70ºF and pressure below about 800 psia, a C_{16}-rich phase containing dissolved CO_2 is in equilibrium with a vapour that is composed of almost pure CO_2. For the binary mixture of CO_2 and *n*-hexadecane, the degree of freedom of three-phase coexistence is 1 according to the Gibbs phase rule,

$$F = nc - n + 2 \qquad [2\text{-}1]$$

where *nc* is the number of components in the system and *n* is the number of coexisting phases. This indicates that the three-phase locus in the *P*-*T* diagram exists as a line. Thus, three phases can coexist at only one pressure for the binary CO_2-*n*-hexadecane at a fixed temperature. At pressure above the three-phase pressure but below the vapour pressure of

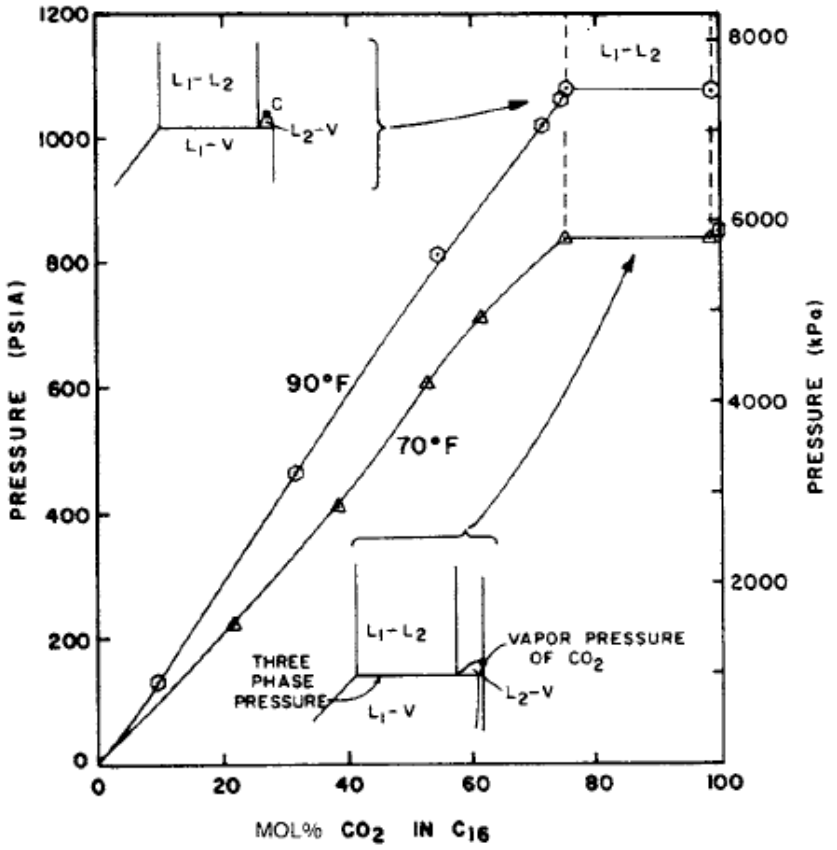

FIGURE 2-2: Phase behaviour of CO_2/*n*-hexadecane mixtures at 70ºF and 90ºF showing liquid-vapour and liquid-liquid equilibria (Orr, 1984)

CO_2 (i.e., 855 psia), the L_1L_2 region is separated from the tiny L_2V region by a mall single L_2 region. The L_2V region will disappear at the vapour pressure of CO_2, whereas the L_1L_2 region persists to higher pressures. Similar phase behaviour is observed for the binary system at 90ºF. It is worthwhile noting that, at a higher temperature, the pressure at which three phases coexist shows a higher value. In addition, it can be observed that in the L_1V region, the solubility of CO_2 in *n*-hexadecane increases as pressure increases while decreases as temperature increases. The phase behaviour of the binary CO_2-hexadecane system is very useful to understand the phase behaviour of CO_2-heavy oil system since heavy oil is mainly composed of heavy hydrocarbons.

As shown in FIGURE 2-3, Liphard and Schneider (1975) found that the critical locus of L_1L_2 moves to a higher temperature as the molecular weight of the alkane increases. This observation suggests that the maximum temperature where the L_1L_2 immiscibility can occur in a CO_2-alkane system also increases with the carbon numbers of the alkane. After comparing the phase behaviour of several CO_2-crude oil systems and CO_2-alkane systems, Orr *et al.* (1981) concluded that oils with a C_{14+} fraction of higher molecular weight would show L_1L_2 behaviour at a higher temperature than oils with a lower molecular weight C_{14+} fraction. In the case of heavy oil, the L_1L_2 immiscibility can be expected to exist at a high pressure and elevated temperature. However, the phase behaviour at such a high pressure is of no practical importance to heavy oil recovery since the original pressure of most of the heavy oil reservoirs is fairly low.

2.2.2. CO_2-heavy oil systems

Due to low temperatures and low pressures encountered in most heavy oil reservoirs, it is of more practical significance to study the phase behaviour of CO_2-heavy oil systems

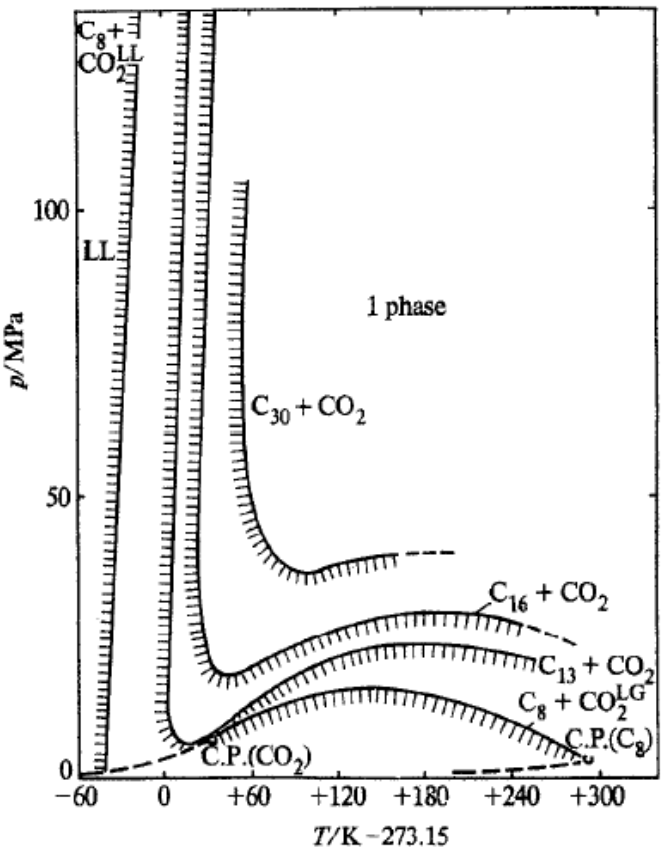

FIGURE 2-3: Phase diagrams of binary CO_2-alkane mixtures. Three phase lines are omitted (Liphard and Schneider, 1975)

at low pressures and temperatures. The binary CO_2-heavy oil system is expected to exhibit Type III phase behaviour, analogous to that of CO_2-heavy alkane systems with carbon number greater than 13. FIGURE 2-4 illustrates the three-phase co-existing loci for CO_2 and alkanes heavier than C_{13} (Larson *et al.*, 1989). As illustrated in FIGURE 2-4, the three-phase loci lie just below the real and extrapolated vapour pressure line of CO_2. With the increase of carbon number of alkane, the three-phase line tends to move closer to the vapour pressure of CO_2. The *K* point at which the L_2 and V phase interface disappears also lies closer to the critical point of CO_2.

FIGURE 2-5 is a conceptual phase diagram of a pseudo CO_2-heavy oil system based on phase behaviour of CO_2-heavy alkane systems. According to the Gibbs phase rule, the coexisting three-phase region is an enclosed area instead of a line. The three-phase region should lie close to the vapour pressure line of CO_2, while the *K* point of the CO_2-heavy oil system should be also close to the critical point of CO_2. Mehrotra and Svrcek (1984) and Badamchi-Zadeh *et al*. (2009) experimentally demonstrated the conceptual phase diagram of CO_2-heavy oil system. Mehrotra and Svrcek (1984) observed a three phase region for the CO_2-bitumen system at 285.15 K and around 4.5 MPa. The three phases included a liquid phase rich in hydrocarbon, a liquid phase rich in carbon dioxide, and a vapour phase that was essentially filled with CO_2. Badamchi-Zadeh *et al*. (2009) discovered that, for a given binary mixture of CO_2 and bitumen, there was a transition zone from liquid-liquid to vapour-liquid-liquid to vapour-liquid phase regimes as the pressure was reduced at a constant temperature below the critical point of pure CO_2. The L_1L_2V region was narrow, spanning at most 800 kPa (116 psia) at any given temperature. Above the critical point of CO_2, only two phases were observed at all measured

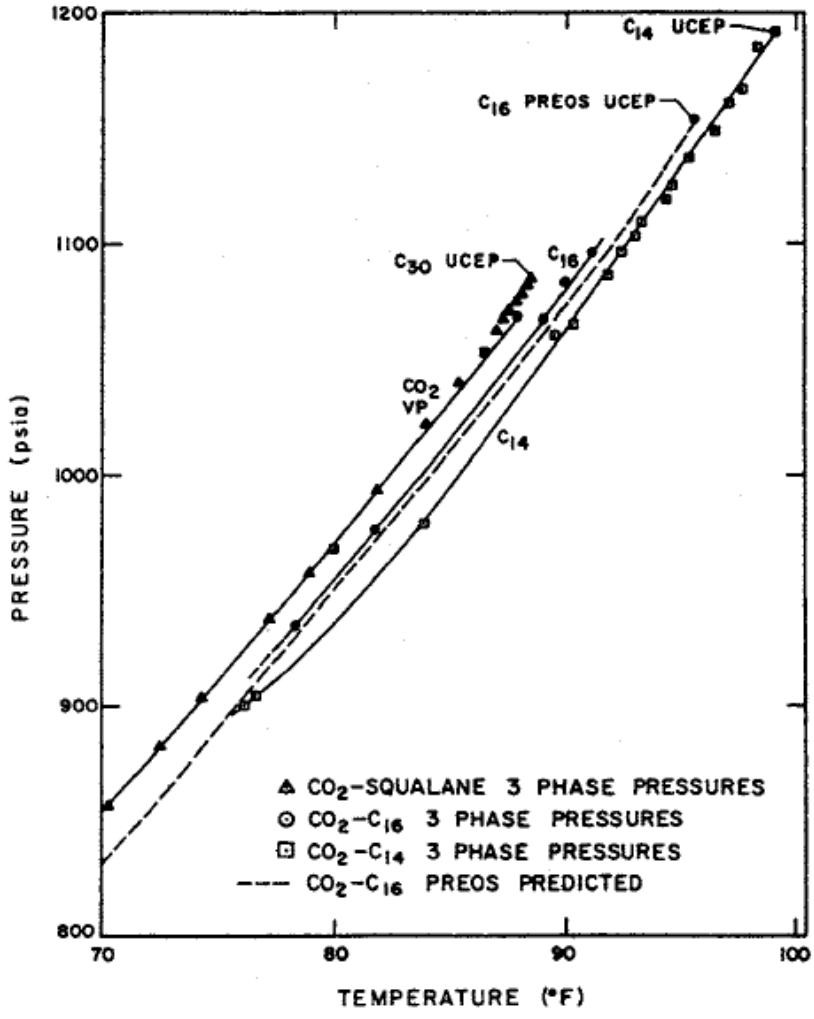

FIGURE 2-4: Three-phase loci for binary CO_2-alkane mixtures (Larson *et al.*, 1989)

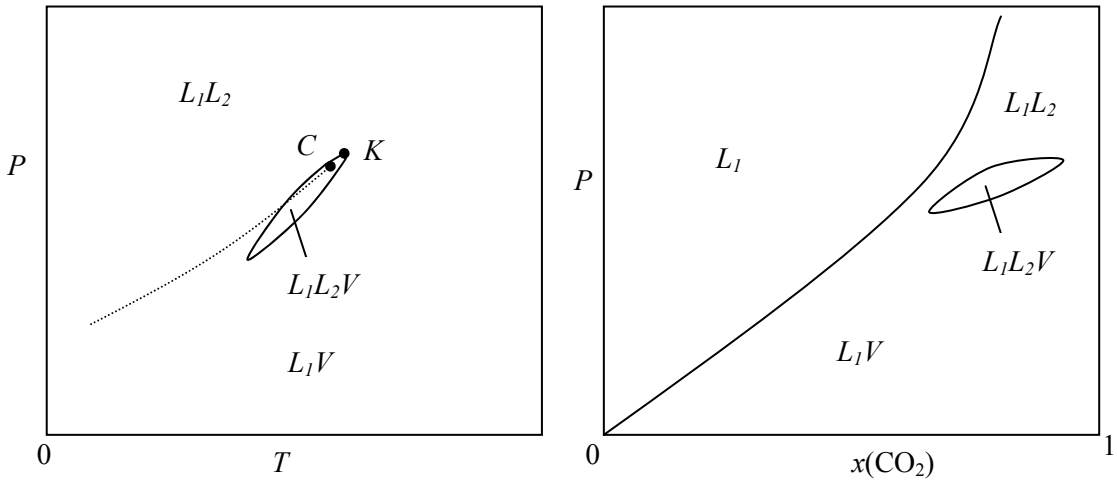

FIGURE 2-5: Conceptual phase diagrams of a pseudo CO_2-heavy oil system based on phase behaviour of CO_2-heavy alkane systems. Dotted line denotes vapour pressure of CO_2

temperatures and pressures.

Most of the previous efforts have been devoted to investigating both the L_1V region (involving subcritical CO_2) and liquid-fluid (involving supercritical CO_2) region that take place in CO_2-heavy oil systems. Solubility of CO_2 in heavy oil or bitumen is usually used as an important index to quantify the maximum amount of CO_2 that can be dissolved in a given amount of heavy oil. Solubility is normally a function of pressure, temperature and oil properties. Data on solubility of subcritical and supercritical CO_2 in light oils or heavy oils under different conditions have been extensively documented in the literature.

TABLE 2-1 lists an exhaustive review of the published data on solubility, density and viscosity of CO_2 in heavy oil or bitumen with API gravity less than 20º. Several major points can be obtained from the studies on phase behaviour of CO_2 with various heavy oils in the literature:

(1) CO_2 cannot achieve miscibility with heavy oil under all the conditions studied;

(2) In general, solubility of CO_2 in heavy oil decreases as temperature increases. At temperatures below the *K* point of the CO_2-heavy oil system, CO_2 solubility increases with pressure but levels off when system pressure reaches a certain point. This observation corresponds to the three-phase L_1L_2V region or two liquid phase L_1L_2 region as depicted in Figure 2-4. The corresponding pressure can be either approximated with the CO_2 vapour pressure with temperature lower than its critical temperature or extrapolated its vapour pressure with temperature between its critical temperature and the *K* point of the CO_2-heavy oil system. At temperatures above the *K* point of the CO_2-heavy oil system, solubility of CO_2 in

TABLE 2-1: Phase behaviour of CO_2-heavy oil systems documented in the literature

Oil Sample	API @ 60ºF	Viscosity, cP	MW g/mol	Temperature ºF	Reference
Wyoming heavy oil	17.0	600 @ 80ºF	N/A	80	Welker and Dunlop, 1963
A[a]	17.3	87 @ 110ºF	350	110, 200	Simon and Graue, 1965
D[a]	18.3	74 @120ºF	358	120, 250	Simon and Graue, 1965
E[a]	13.5	1300 @ 120ºF	463	120, 200	Simon and Graue, 1965
F[a]	12.1	105 @ 120ºF	330	120	Simon and Graue, 1965
H[a]	11.9	499 @130ºF	458	130	Simon and Graue, 1965
I[a]	18.2	58.6 @ 145ºF	370	145	Simon and Graue, 1965
Wyoming heavy oil	17.0	800 @ 75ºF	N/A	75, 140, 200	Miller and Jones, 1981
Cat Canyon heavy oil	10.0	4500 @ 140ºF	N/A	140, 200	Miller and Jones, 1981
Wyoming heavy oil	15.0	2000 @ 75ºF	N/A	75, 140, 200	Miller and Jones, 1981
Athabasca bitumen	9	>10000 @ 110.3ºF	554.6	73.4-207.32	Mehrotra and Svrcek, 1982
Marguerite Lake bitumen	N/A	271000 @ 56ºF	N/A	53.6-217.4	Mehrotra and Svrcek, 1984
Peace River bitumen	10.0	14700 @ 104.4ºF	542	74.3-224.6	Mehrotra and Svrcek, 1985a
Athabasca bitumen	9.0	N/A	554.6	212	Fu *et al.*, 1985
Wabasca bitumen	8.9	8100 @ 55.4ºF	446.5	70.52-302.00	Mehrotra and Svrcek, 1985b
Saskatchewan heavy oil	15.3	2600 @ 68ºF	423	82.4	Jha, 1986
Bartlett heavy oil	16.8	1484.35 @ 75ºF	N/A	75, 140, 200	Chung *et al.*, 1988
Senlac heavy oil	15.0	2600 @ 68ºF	N/A	82.31	Quail *et al.*, 1988
Aberfeldy oil sample 1	17.0	1032 @ 73.4ºF	425	73.4	Rojas and Farouq Ali, 1988
Aberfeldy oil sample 2	14.0	4681 @ 73.4ºF	460	73.4	Rojas and Farouq Ali, 1988
Cold Lake bitumen	N/A	15700 @ 86.9ºF	533	59.0-217.4	Mehrotra and Svrcek, 1988
Cold Lake bitumen	N/A	N/A	533	122-482	Yu *et al.*, 1989

TABLE 2-1: Phase behaviour of CO_2-heavy oil systems documented in the literature (continued)

Oil Sample	API @ 60ºF	Viscosity, cP	MW, g/mol	Temperature, ºF	Reference
Peace River bitumen	10.0	14700 @ 104.4ºF	542	58.46-234.86	Mehrotra and Svrcek, 1989
Peace River bitumen	10.0	14700 @ 104.4ºF	542	175.3-391.8	Svrcek *et al.*, 1989
Lindbergh heavy oil	14.7	12086 @ 69.8ºF	490	69.8-284	Sayegh *et al.*, 1990
Athabasca bitumen	8.9	10000 @ 121ºF	640	185.1, 248.1	Deo *et al.*, 1991
Tar Sand Triangle bitumen	8.9	10000 @ 140.3ºF	701	185.1, 248.2	Deo *et al.*, 1991
PR Spring bitumen	8.0	100000@ 161.3ºF	541	185.1, 248.3	Deo *et al.*, 1991
Suffield heavy oil	17.0	685 @ 69.8ºF	358	68-284	Kodal and Sayegh, 1992
West Sak heavy oil 1	18.5	241.5 @ 75ºF	330	65	DeRuiter *et al.*, 1994
West Sak heavy oil 2	14.0	5243.7 @ 75ºF	446	60	DeRuiter *et al.*, 1994
Aberfeldy oil	17.0	1050 @ 73.4ºF	N/A	73.4	Nguyen and Farouq Ali, 1998
Jiangsu heavy oil	N/A	N/A	384	131, 167	Liu *et al.*, 1999
Senlac heavy oil	14.1	3580 @ 68ºF	440	82.4	Srivastava *et al.*, 1999
Athabasca bitumen	9.0	>10000 @110.3ºF	552	77	Badamchi-Zadeh *et al.*, 2009

Note:
a: These designations were used in the original literature
MW: Molecular weight

heavy oil increases with pressure and no level-off phenomenon has been reported in the literature;

(3) The effect of CO_2 solubility on the density of CO_2-saturated heavy oil or bitumen is ambiguous. This may be explained by the fact that an increase of pressure leads to a volume increase of heavy oil but compresses the volume at the same time;

(4) The swelling factor increases with CO_2 solubility in heavy oil and shows its highly linear relationship (Welker and Dunlop, 1963; Chung *et al.*, 1988); and

(5) The viscosity of heavy oil saturated with CO_2 decreases dramatically with CO_2 solubility. It is worth noting that the decline trend normally terminates when the three-phase or two-liquid phase region is encountered and begins to level off afterwards. In addition, effect of viscosity reduction caused by CO_2 dissolution is more pronounced for heavy oils than that of light oils. In some scenarios as observed by Chung *et al.* (1988), dissolution of CO_2 is even capable of reducing viscosity of heavy oil more than heating the heavy oil.

Interfacial tension is another important physical property that affects CO_2 flooding efficiency (Yang and Gu, 2005). A reduced interfacial tension of heavy oil due to CO_2 dissolution is favourable for increasing heavy oil recovery since the capillary number is increased with the reduced interfacial tension. Yang and Gu (2006) measured the change of equilibrium interfacial tension with pressure at 298.15 K for a CO_2-Ontario heavy oil system. It was found that the interfacial tension decreases linearly with the pressure in the tested pressure range. As mentioned previously, at pressure lower than L_1L_2 or L_1L_2V pressure of the CO_2-heavy oil system, the solubility of CO_2 in heavy oil increases with

saturation pressure. The dissolved CO_2 functions as a surface-active agent, which is responsible for the interfacial reduction (Yang and Gu, 2006).

2.3 Correlations for Physical Properties

Physical properties of CO_2-heavy oil system, including CO_2 solubility, swelling factor, density, and viscosity are of great importance for designing a successful CO_2 immiscible flooding project in a heavy oil reservoir. In the literature, many correlations have been documented to predict the physical properties of CO_2-light oil systems, only some of which are specially designed for CO_2-heavy oil systems.

2.3.1. CO_2 solubility

Welker and Dunlop (1963) studied the physical properties of several light oils and heavy oils saturated with CO_2 at 80ºF. They graphically expressed the CO_2 solubility as a function of saturation pressure and API gravity. It was the first attempt to provide correlations regarding CO_2 solubility in light and heavy oils. Similarly, Simon and Graue (1964) conducted a comprehensive study of phase behaviour of CO_2 with nine crude oil samples including six heavy oil samples, resulting in graphical correlations in which CO_2 solubility is expressed as a function of saturation pressure, temperature and the UOP (Universal Oil Product) characterization factor. These graphical correlations have been widely used in the petroleum industry since their development. However, such correlations are expressed in a graphical form, which is not convenient for computer calculations or reservoir simulation studies.

Mehrotra and Svrcek (1982) presented an empirical correlation for CO_2 solubility in bitumen based on the experimental results as below,

$$R_s\left(m^3/m^3\right) = a_1 + a_2 p + a_3\left(\frac{P}{T}\right) + a_4\left(\frac{P}{T}\right)^2 \qquad [2\text{-}2]$$

where R_s is volumetric solubility of CO_2 in bitumen, P is saturation pressure, T is temperature, and $a_1 - a_4$ are empirical constants. Note that the saturation pressure should be less than or equal to the vapour pressure of CO_2 at temperature lower than the critical point of CO_2.

Chung *et al.* (1988) provided a correlation for solubility of CO_2 in heavy oil in the following form,

$$R_s\left(\text{scf}/\text{bbl}\right) = \frac{1}{b_1\gamma^{b_2}T^{b_3} + b_4 T^{b_5}\exp\left(-b_6 p + b_7/P\right)} \qquad [2\text{-}3]$$

where b_1-b_7 are empirical constants.

Emera and Sarma (2006) developed correlations to predict CO_2 solubility, oil swelling factor, CO_2-oil density and CO_2-oil viscosity for both light or heavy oils using a genetic algorithm (GA)-based technique. Their correlations recognized not only all major parameters that affect each physical property, but also took into account the effects of CO_2 liquefaction pressure and oil molecular weight (MW). For temperatures greater than the critical temperature of CO_2 (for all pressures) and temperatures less than critical temperature of CO_2 (for pressures less than CO_2 L_1L_2 and L_1L_2V phase pressure),

$$R_s\left(\text{mole }\%\right) = c_1 + c_2 y + c_3 y^{c_4} + c_5 y^{c_6} \qquad [2\text{-}4]$$

where

$$y = SG\left[\frac{c_7 T}{P}\right]^{\exp\left(1/MW\right)} \qquad [2\text{-}5]$$

where $c_1 - c_7$ are empirical constants and SG is the oil specific gravity. They also presented solubility correlation for pressures greater than three-phase or liquid-liquid phase pressure of a CO_2-oil system. According to this correlation, solubility of CO_2 will increase further with system pressure. According to TABLE 2-1, it has been found that the solubility of CO_2 in heavy oil may keep unchanged or even decrease with pressure that is greater than the L_1L_2 and L_1L_2V phase pressure of the CO_2-oil system. Therefore, it is not recommended to use the correlation developed by Emera and Sarma (2006) for this pressure range, whereas a constant CO_2 solubility in heavy oil is recommended.

Based on the simplified Henry's Law, Badamchi-Zadeh *et al.* (2009) obtained a correlation for CO_2 solubility in crude oil based on the data of Simon and Graue (1964),

$$R_s\left(\text{mole \%}\right) = \frac{P}{H_{CO_2}} = \frac{P}{\ln d_1 + \frac{d_2}{T} + \frac{d_3 P}{RT}} \qquad [2\text{-}6]$$

where H_{CO_2} is Henry's constant at T, R is universal gas constant, d_1-d_3 are empirical constants. Their correlation is claimed to fit well with the experimental data with absolute average error of 1.7%.

Another approach adopted in the literature is to use the cubic equation of state (CEOS) to correlate the experimental data on CO_2 solubility in heavy oil. Fu *et al.* (1985) treated bitumen as a single pseudocomponent and used the PR EOS to reproduce the solubility data with good accuracy. The similar methodology had also been adopted by Jamaluddin *et al.* (1991) to successfully reproduce the solubility of CO_2 in eleven heavy oil or bitumen samples and the density data of these systems with a different EOS.

Kariznovi *et al.* (2010) used six universal pseudocomponents that are optimized to characterize Alberta bitumen, which are independent of bitumen type and can be used in the PR EOS to predict the solubility of CO_2 in Alberta bitumen (Athabasca, Wabasca, Peace River, and Cold Lake) with satisfactory accuracy. Their results also showed that the Lee-Kesler correlation was the most appropriate correlation for CO_2-bitumen systems to determine the critical properties of the pseudocomponents.

2.3.2. Swelling factor

According to Welker and Dunlop (1963), swelling factor is defined as the volume of crude oil saturated with CO_2 at reservoir pressure and temperature divided by the volume of crude oil at atmospheric pressure (0.1 MPa) and reservoir temperature. This definition has become a norm in the petroleum industry since its introduction. The swelling of heavy oil is mainly attributed to the dissolution of CO_2 into oil. Thereby, a strong dependence of swelling factor on solubility is expected. Welker and Dunlop (1963) provided a correlation for swelling factor as a function of CO_2 solubility,

$$SF = 1.0 + \frac{0.35 R_s}{1000} \qquad [2\text{-}7]$$

where SF is swelling factor, and R_s is CO_2 solubility in scf/bbl. Chung *et al.* (1988) measured the swelling factors of four different heavy oils saturated with CO_2. Equation [2-7] provides a fairly good fit to their experimental data, suggesting a strong linear relationship between swelling factor and solubility for heavy oil. Simon and Graue (1964) devised a graphical correlation for predicting swelling factor of different crude oil saturated with CO_2. In order to eliminate the inconvenience brought along by the graphical representation of swelling factor correlation, Emera and Sarma (2006)

developed a expression for swelling factor as a function of oil molecular weight and CO_2 solubility based on the experimental data including those of Simon and Graue (1964).

Since the Simon-Graue correlations are completely empirical and lack of theoretical basis, the extrapolation outside their range or extension to other systems is expected to introduce a large error. The EOS modelling is a possible approach to calculate swelling factor of CO_2 saturate oil. It has been shown by Teja and Sandler (1980) that the swelling factor can be calculated by *molar volume* and *molar solubility* in the following form,

$$SF = \frac{V_{s2}}{V_{s1}} \times \frac{1}{1-X} \qquad [2\text{-}8]$$

where V_{s1} is the molar volume of CO_2 saturated oil at saturation temperature and atmospheric pressure, V_{s2} is the molar volume of CO_2 saturated oil at saturation temperature and saturation pressure, and X is the CO_2 solubility in mole fraction.

Mullken and Sandler (1980) treated the crude oil as a single pseudocomponent and characterized it with specific gravity and normal boiling point or Watson K factor. They firstly calculated the solubility of CO_2 in crude oil and density of the mixture using PR EOS and then obtained the swelling factor of CO_2 saturated oil based on Equation [2-8]. Such a method showed comparable accuracy compared to the graphical correlations of Simon and Graue (1964), while a binary interaction parameter (BIP) formula was obtained by regressing the CO_2 solubility data,

$$\delta = 0.5010 - 0.3576T_r - 0.18285SG - 0.0961\omega \qquad [2\text{-}9]$$

where δ is BIP between CO_2 and oil, T_r, SG, and ω are reduced temperature, specific gravity and acentric factor of crude oil, respectively, which are calculated from the Lee-Kesler correlation.

2.3.3. Viscosity

Viscosity is an important parameter to characterize the flowing property of heavy oil. Significant reduction of heavy oil viscosity after being saturated with CO_2 has been extensively documented in the literature. Since it is extremely difficult to quantify the individual contribution of each component in heavy oil to the viscosity of the mixture, CO_2-heavy oil mixture is usually treated as a pseudo-binary system with two components: CO_2 and heavy oil. Viscosity of CO_2-heavy oil mixtures is generally a function of the mixture composition. The viscosity reduction degree of heavy oil is dependent on how much CO_2 is dissolved in the heavy oil. Therefore, if the concentration of CO_2 in the crude oil and viscosities of CO_2 and heavy oil are known, a correlation can be developed to predict the viscosity of CO_2-heavy oil mixtures. According to Chung *et al.* (1988), the viscosity ratio of heavy oil to CO_2 falls in the range of 10^3 to 10^6. Several correlations have been developed for estimating the viscosity of solvent-solute mixture with such large viscosity ratios.

Based on the fact that the mixture viscosity is not a simply linear function of the solvent fraction, Cragoe (1933) developed a widely used method for liquid mixture viscosity predictions. Mixing rules are used in their model to combine the "Liquidity" L of the solvent and solute. Liquidity is expressed as,

$$L = \frac{1000 \ln 20}{\ln \mu - \ln\left(5 \times 10^{-4}\right)} \qquad [2\text{-}10]$$

where μ is the viscosity of the solvent or solute. The mixture liquidity is calculated from the following mixing rule,

$$L_m = w_1 L_1 + \left(1 - w_1\right) L_2 \qquad [2\text{-}11]$$

where L_m is mixture liquidity, w_1 is the weight fraction of solvent in the mixture, L_1 and L_2 are the liquidity of solvent and solute, respectively. Then the mixture viscosity can be calculated by Equation [2-10]. The Cragoe correlation can be used for calculating the viscosity of heavy oil saturated with CO_2. However, the weight fraction of CO_2 should be known prior to calculation.

Lederer (1933) presented an equation for mixture viscosity which was modified from the classic Arrhenius expression,

$$\ln \mu = x_s \ln \mu_s + (1 - x_s) \ln \mu_o \qquad [2\text{-}12a]$$

and

$$x_s = \frac{\alpha V_s}{\alpha V_s + V_o} \qquad [2\text{-}12b]$$

where μ is mixture viscosity, μ_s is solvent viscosity, μ_o is oil viscosity, V_s and V_o are volume fraction of solvent and oil in the mixture, and α is an empirical constant having a value in the range of 0 to 1. It had been shown by Rahmes and Nelson (1948) that the Lederer correlation exhibited an excellent fit to their experimental data for systems of 26 blends of 17 petroleum fractions.

Shu (1984) extended the Lederer equation to higher viscosity ratios by using a generalized expression for the empirical constant α which is expressed as a function of the component viscosities and densities on the basis of the experimental data for mixtures of heavy oils with light petroleum fractions,

$$\alpha = \frac{17.04(\rho_o - \rho_s)^{0.5237} \rho_o^{3.2745} \rho_s^{1.6316}}{\ln\left(\mu_o / \mu_s\right)} \qquad [2\text{-}13a]$$

where ρ_s and ρ_o are specific gravity of the solvent and heavy oil, respectively. This correlation was tested with heavy oil/bitumen-solvent blending data and provided an excellent prediction of the mixture viscosities. However, the correlation developed by Shu is based on organic solvents (e.g., kerosene) and cannot be applied for CO_2-heavy oil systems where CO_2 density may be higher than heavy oil density at high pressures. Chung *et al.* (1988) obtained a modified α correlation that was a function of temperature (T in ºR), pressure (P in psia) and specific gravity (SG) of heavy oil,

$$\alpha = 0.225SG^{-4.16}\left(\frac{T}{547.57}\right)^{1.85}\left[\frac{e^{7.36}-e^{7.36\left(1-P/1071\right)}}{e^{7.36}-1}\right] \qquad \text{[2-13b]}$$

Equations [2-12] and [2-13b] generated excellent reproduction of the viscosity data of CO_2-heavy oil mixture for four heavy oils. It is worth noting that EOS is able to provide information on volume fraction of CO_2 in heavy oil, which is needed prior to calculating mixture viscosity by using Equations [2-12] and [2-13b].

Obviously, EOS modeling of CO_2-heavy oil systems provides an integrated method for predicting CO_2 solubility, mixture density, swelling factor, and even mixture viscosity. Therefore, it is important to study phase behaviour of CO_2-heavy oil systems and numerical simulating CO_2 flooding of heavy oil by conducting EOS modeling.

2.4 Phase Behaviour of Solvent(s)-Heavy Oil Systems

It has been found that a gas solvent with a higher critical temperature and boiling point is more soluble than the one with a lower critical temperature, for the vapour pressure is lower for the former, which leads to an increased nonvolatility (Hildebrand,

1936). FIGURE 2-6 shows the vapour pressure lines and critical point of six gas solvents N_2, CH_4, CO_2, C_2H_6, C_3H_8 and *n*-C_4H_{10}. The nonvolatility of the pure gas solvent is increased with the vapour pressure line moving to the right side of FIGURE 2-6. Then the ranking of solubility of the gas solvents in a given solute shown in FIGURE 2-6 is supposed to follow the order: N_2<CH_4<CO_2<C_2H_6<C_3H_8<*n*-C_4H_{10}.

As for a CO_2-based solvent flooding process for heavy oil recovery, the promising solvent additives appear to be C_3H_8 and *n*-C_4H_{10}. This may be accounted for by two major considerations. These two solvents show a much lower nonvolatility, implying a high solubility in heavy oil. On the other hand, they demonstrate a relatively large vapour pressure, enabling the CO_2-solvent(s) mixture to exist in the gas state under reservoir conditions. Therefore, it is meaningful to review the phase behaviour of C_3H_8-heavy oil or *n*-C_4H_{10}-heavy oil system. Rather than directly running into the phase behaviour of solvent(s)-heavy oil systems, the phase behaviour of short-chain alkane and long-chain alkane system will be firstly covered in the following discussion.

2.4.1. Short-chain alkane and long-chain alkane system

The phase behaviour of short-chain alkane (normally CH_4, C_2H_6, C_3H_8, or *n*-C_4H_{10}) and long-chain alkane systems has been an intensive research topic which is of great interests to various industry applications. Similar to the CO_2-alkane systems, the homologous alkane-alkane series show a classical transition between different types of phase behaviour (See FIGURE 2-1). The binary mixture of methane and alkane up to *n*-entane demonstrates Type I phase behaviour (Rowlinson and Swinton, 1982). Partial miscibility in the liquid state appears first in the mixture of methane and *n*- hexane and a change from Type I phase behaviour to Type V occurs. When the *n*-alkane

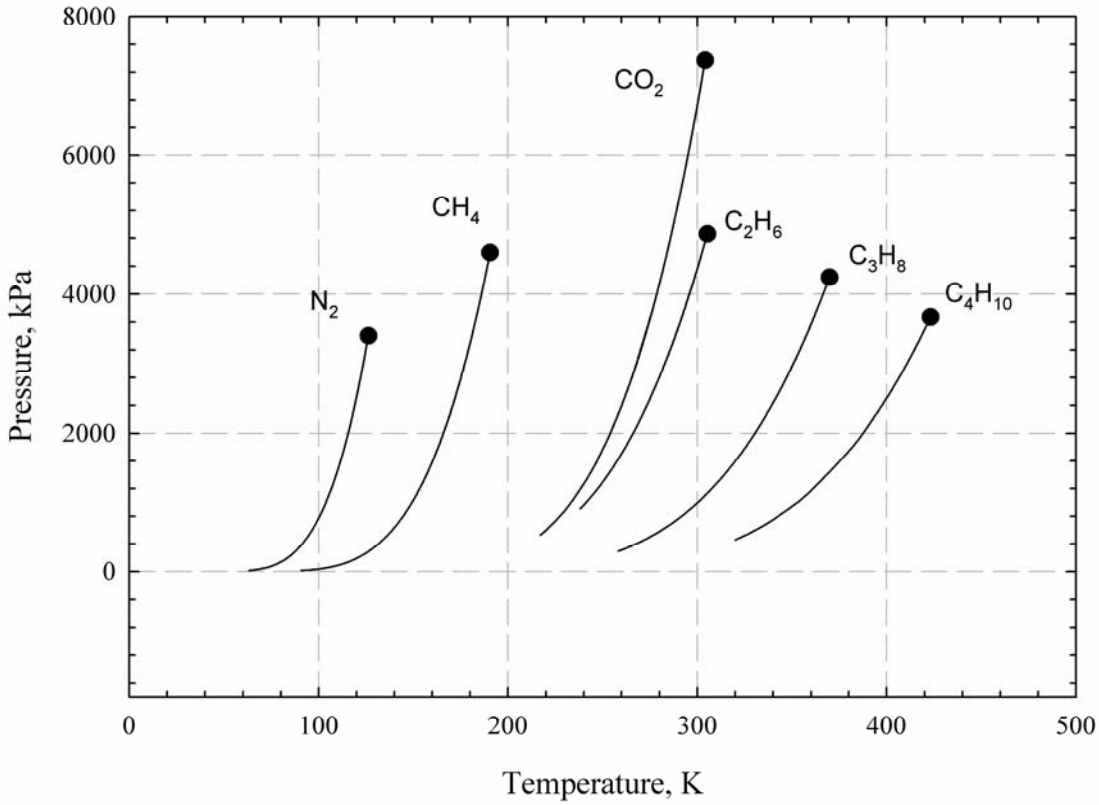

FIGURE 2-6: Vapour pressure lines of six gases N_2, CH_4, CO_2, C_2H_6, C_3H_8 and *n*-C_4H_{10}. Bold dots denote the critical points (Lide, 2009)

chain length increases, the phase behaviour becomes more complicated. The global phase behaviour of methane and *n*-heptane system shows a Type III phase behaviour (Aparicio-Martínez and Hall, 2007).

Analogous to the methane-alkane mixture, the global phase behaviour of a binary C_2H_6-alkane mixture changes from a Type I pattern to a Type V and then to a Type III as the carbon number of alkane increases. According to the experimental observation of Specovius *et al.* (1981), the phase behaviour changing from Type I to Type V happens first for *n*-octadecane. The phase behaviour for binary systems of alkanes heavier than CH_4 or C_2H_6 is analogous to that of CH_4-alkane system and C_2H_6-alkane system, respectively. These mixtures show Type I behaviour for the lower members of the series, and a Type V transition range appears when carbon number reaches a certain value. Then a Type III phase behaviour occurs with the further increase of carbon number.

Based on experimental observation, Peters *et al.* (1989) estimated that partial miscibility in the liquid state appeared first in the mixture of C_3H_8 and alkanes with carbon number between 29 and 30. In addition, binaries of short and long alkanes first showing partial miscibility in the liquid phase has been characterized by their carbon numbers (see FIGURE 2-7) by Peters *et al.* (1989). It can be seen from this figure that a linear relationship between the carbon numbers of solvent and solute exists. According to FIGURE 2-7, a carbon number of 42 can be expected for the binary alkane mixture involving *n*-C_4H_{10}. The appearance of partial miscibility implies that the solubility of one lighter alkane solvent in one heavier alkane solute is decreased.

Phase behaviour of a binary system of heavy alkane with C_3H_8/*n*-C_4H_{10} is helpful to interpret the phase behaviour of C_3H_8/*n*-C_4H_{10} and heavy oil system. Since heavy oil is

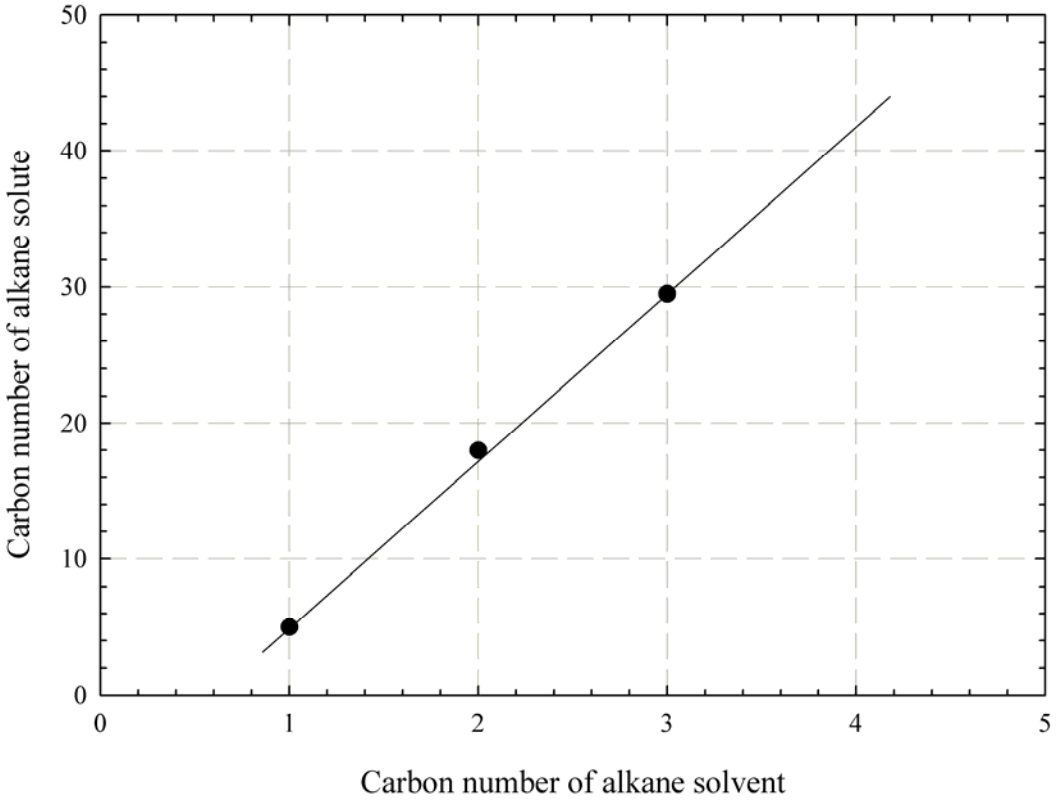

FIGURE 2-7: Binaries of short and long *n*-alkanes first showing partial miscibility in the liquid phase characterized by their carbon numbers (Peters *et al.*, 1989)

mainly composed of heavy hydrocarbons, the pseudo binary system of C_3H_8/*n*-C_4H_{10} and heavy oil may exhibit Type III or V pattern.

2.4.2. C_3H_8/*n*-C_4H_{10} with heavy oil

Phase behaviour study of binary system of heavy oil and solvent (including C_3H_8 and *n*-C_4H_{10}) is of great importance to the solvent-based heavy oil recovery methods, for example, the solvent flooding process and vapour extraction (VAPEX) process (Upreti *et al*., 2007). Analogous to CO_2-heavy oil systems, complex phase behaviours, for example, L_1L_2V equilibrium, can also take place under certain circumstances as depicted in FIGURE 2-4. However, no L_1L_2V equilibrium has been reported in the literature for the aforementioned systems. TABLE 2-2 lists a review of the published data on phase behaviour of C_3H_8/*n*-C_4H_{10} and heavy oil systems.

Badamchi-Zadeh *et al*. (2009a) provided a correlation for C_3H_8 solubility in Athabasca bitumen by using a modified Raoult's Law,

$$x_{C3} = \frac{P}{1.158 p_{C3}^{s}} \qquad [2\text{-}14]$$

where x_{C3} is C_3H_8 solubility in the bitumen in mole fraction, P is saturation pressure of the C_3H_8-bitumen system in kPa, and p_{C3}^{s} is C_3H_8 vapour pressure in kPa. Equation [2-14] fits the saturation pressures with an average relative deviation of 5.1%.

2.5 Phase Behaviour of Solvent(s)-CO_2-Heavy Oil Systems

Although some laboratory efforts have been conducted to study the mechanisms for enhancing heavy oil recovery by CO_2 injection (Simon *et al.*, 1978; Klins and Farouq Ali,

TABLE 2-2: Phase behaviour of solvent(s)-heavy oil systems documented in the literature

Sample	Solvent	MW g/mol	Specific gravity	Temperature °F	Reference
Peace River bitumen	C_3H_8	537	1.013	69.8-95	Das and Butler, 1996
Peace River bitumen	*n*-C_4H_{10}	537	1.013	95	Das and Butler, 1996
Fengcheng bitumen	C_3H_8	503	N/A	381	Han *et al.*, 1998
Winter heavy oil	C_3H_8	412	0.973	59-82.4	Freitag *et al*., 2005
Lloydminster heavy oil	C_3H_8	432	0.988	68-75.2	Luo *et al.*, 2007; Luo and Gu, 2009
Athabasca bitumen	C_3H_8	552	1.007	50-122	Badamchi-Zadeh *et al*., 2009
Frog Lake heavy oil	*n*- C_4H_{10}	400	0.989	233.6-257	Yazdani and Maini, 2010

1982; Sayegh and Maini, 1984; Chung *et al.*, 1988; Dyer and Farouq Ali, 1994; Strivastava *et al.*, 1999), few attempts have been made to evaluate the phase behaviour and physical properties of the solvent(s)-CO_2-heavy oil systems under subcritical and supercritical conditions (Badamchi-Zadeh *et al.*, 2009a; b). Nevertheless, some investigations have been made to study phase behaviour of ternary solvent-CO_2-alkane systems. Phase behaviour of CO_2-C_3H_8-*n*-hexadecane system were reported by Stewart and Nielsen (1954) and Meldrum and Nielsen (1955). Complex phase behaviour took place for the ternary CO_2-C_3H_8-*n*-hexadecane system. The three-phase coexisting region was found to expand to a larger region in the *P-T* diagram due to the addition of C_3H_8. Similar observation was also reported by Fall and Luks (1986). They reported the phase equilibria data for two ternary systems, i.e., CO_2-C_3H_8-*n*-hexadecane system and CO_2-N_2-*n*-hexadecane system. As shown in FIGURE 2-8, addition of nitrogen to CO_2-*n*-nonadecane resulted in a three-phase region developing to the low-temperature and high-pressure side of the binary L_1L_2V locus of CO_2-*n*-nonadecane system, while addition of C_3H_8 causes the three-phase region to extend to the high-temperature side of the L_1L_2V locus.

Nguyen and Farouq Ali (1998) studied the effect of nitrogen on CO_2 solubility in Aberfeldy heavy oil and discovered that, even if the partial pressure of CO_2 in a CO_2-N_2 mixture was equal to the pressure of pure CO_2 system, CO_2 solubility in the gas mixture was lower than the pure CO_2 solubility. For pure CO_2, its critical temperature and normal boiling point are 304.19 K and 194.67 K, respectively (Yaws, 2003). For the mixture ($x(CO_2)$=0.9, $x(N_2)$=0.1), the critical temperature and normal boiling point are about 286.35 K and -183.09K, respectively. Comparing pure CO_2 and CO_2-N_2 mixture, it

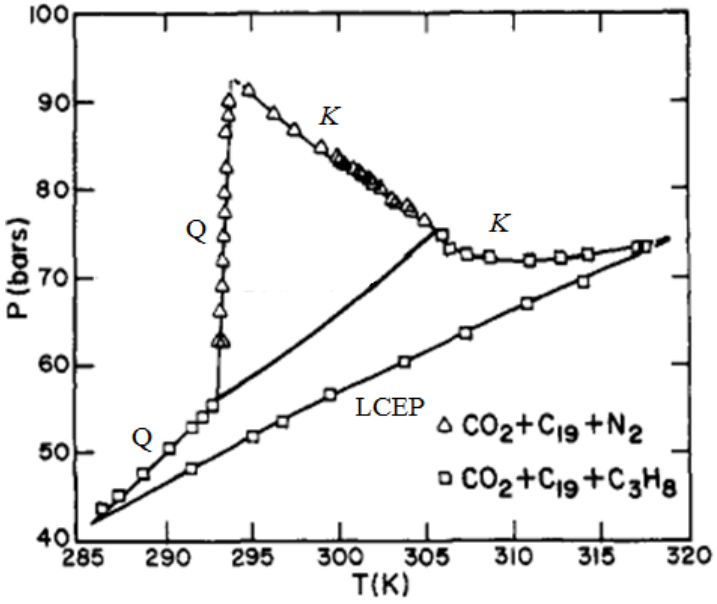

FIGURE 2-8: Critical loci for the L_1L_2V regions of the systems of CO_2-N_2-*n*-nonadecane and CO_2-C_3H_8-*n*-nonadecane. Q refers to the point where four-phase solid-liquid-liquid-vapour equilibrium coexists. The solid line denotes the three-phase coexisting line for CO_2-*n*-nonadecane system (Fall and Luks, 1986)

is obvious that pure CO_2 has a higher critical temperature and boiling point than the CO_2-N_2 mixture. As discussed previously, a gas with a higher critical temperature and boiling point temperature is more soluble than the one with a lower critical temperature. This discussion also implies that addition of more soluble solvents including C_3H_8 or *n*-C_4H_{10} to CO_2 stream is expected to result in an increased solubility of the mixture in heavy oil than that of pure CO_2 because C_3H_8 and *n*-C_4H_{10} have higher critical temperatures and boiling point temperatures than CO_2.

Talbi and Maini (2008) have shown that addition of solvents including C_3H_8 and *n*-C_4H_{10} can generally accelerate the processes of swelling heavy oil and reducing its viscosity in the VAPEX process to a larger extent than pure CO_2. Badamchi-Zadeh *et al.* (2009b) measured the saturation pressures of CO_2 and C_3H_8 in Athabasca bitumen as well as the liquid-phase densities and viscosities for three ternary CO_2-C_3H_8-bitumen mixtures at temperatures from 283.15 K to 298.15 K. In addition to the observed L_1V phase equilibria and L_1L_2 phase equilibria, L_1L_2V phase equilibria have also been observed in the C_3H_8-CO_2-heavy oil systems. The liquid-phase viscosity of two C_3H_8-CO_2-bitumen mixtures was also presented and suggested that the ternary mixture with a larger concentration of C_3H_8 exhibits a greater viscosity reduction effect.

The existence of three-phase equilibria impose a significant impact on the displacing efficiency of heavy oil since the relative permeability curves can be largely altered due to the presence of multiple phases. Recent studies show, as for CO_2-light oil systems, L_1L_2V phase behaviour is a critical mechanism for achieving high displacement efficiency (Okuno *et al.*, 2011). With regard to the solvent(s)-CO_2-heavy oil systems, how the L_1L_2V phase behaviour affects the recovery performance is still not well understood.

Several important mechanisms can come into play when L_1L_2V phase behaviour appears in the porous media. The heavy oil is diluted and swollen by solvent(s) and CO_2 in the L_1 phase with a low viscosity, which is beneficial for improving heavy oil recovery. The existence of L_2 phase can impose double-sided effect on the *in situ* fluid flow in porous media. On one hand, the L_2 phase is more movable in the porous media with a lower viscosity in comparison to the L_1 phase and can be easily recovered from the production end (Talbi and Maini, 2008). On the other hand, one possible benefit arising from emergence of the L_2 phase is that the L_2 phase reduces the gas-phase saturation in the pores. A reduction in gas saturation suppresses the gas-phase relative permeability, hence delays the gas breakthrough and results in a better sweeping efficiency (Feizabadi *et al.*, 2012).

Addition of alkane solvents to the CO_2 stream generally accelerates the processes of swelling heavy oil, reducing its viscosity, and decreasing the IFT between heavy oil and CO_2, and thus leading to a higher oil recovery in the vapor extraction (VAPEX) process (Talbi and Maini, 2008). Most recently, the synergetic mechanisms of solvent(s)-enriched CO_2 flooding are proved by both linear and radial coreflooding experiments with using CO_2 only and C_3H_8-enriched CO_2 stream, respectively. Compared to the pure CO_2 flooding process, a significantly higher heavy oil recovery factor, as well as less solvent consumption, can be achieved with the C_3H_8-enriched CO_2 flooding process (Luo *et al*., 2012).

2.6 Mass Transfer of Solvent(s)-CO_2-Heavy Oil Systems

The foregoing sections of this chapter have been focused on discussing the phase

behaviour of solvent(s)-CO_2-heavy oil systems and equilibrium physical properties. Intrusive forces, e.g., the shearing force caused by the rotation of a magnetic stirrer in a typical PVT setup, can be applied to significantly accelerate the mass transfer between solvent(s)-CO_2 mixture and heavy oil. However, it takes a long time for the solvent(s)-CO_2 mixture to reach equilibrium *in situ* with heavy oil during a huff-*n*-puff process. It is found that the solvent(s)-CO_2 mixture naturally dissolves into heavy oil in a reservoir, making the swollen heavy oil less viscous and hence more mobile (Qazvini Firouz and Torabi, 2012). During dissolution of the solvent(s)-CO_2 mixture into heavy oil, the molecular diffusion coefficients can be used to quantify the mass transfer rate of solvent(s)-CO_2 mixture into heavy oil.

In the literature, several methods have been developed and applied to determine the molecular diffusion coefficient of a pure gas in heavy oil. These methods include the pressure decay method (Zhang *et al.*, 1999; Upreti and Mehrotra, 2000; Upreti and Mehrotra, 2002; Tharanivasan *et al.*, 2006), volume decay method (Jamialahmadi *et al.*, 2006), constant-pressure technique (Etminan *et al.*, 2010), dynamic pendant drop shape analysis (DPDSA) (Yang and Gu, 2006a), dynamic interfacial tension method (Yang *et al*., 2006; Yang and Gu, 2008), and microfluidic method (Fadaei *et al.*, 2011). Some methods are developed by recording the gas phase parameters, e.g., pressure (Zhang *et al.*, 1999; Upreti and Mehrotra, 2000; Upreti and Mehrotra, 2002; Tharanivasan *et al.*, 2006) or volume (Jamialahmadi *et al.*, 2006), while the other are focused on monitoring the swelling of heavy oil due to gas dissolution (Yang and Gu, 2006a; Fadaei *et al.*, 2011). The pressure decay method is the most commonly used and non-intrusive method to determine the molecular diffusion coefficient of a pure gas in heavy oil because it reflects

the actual molecular diffusion process with the absence of any exterior forces, though oil swelling is normally neglected. Accordingly, such determined diffusion coefficient may become less accurate because oil swelling can be significant during the diffusion of a gas mixture into heavy oil, in particular, at a high pressure. During the diffusion process, not only does the system pressure decrease, but also the gas-phase volume decreases due to the swelling of the liquid phase. It is desirable to simultaneously monitor both pressure- and volume-history of either gas or liquid phase for more accurate determination of the molecular diffusion coefficient.

Although all the aforementioned methods are suitable for estimating the apparent molecular diffusion coefficient in the case of a gas mixture diffusing into heavy oil, they cannot be used to determine the individual molecular diffusion coefficient of each component in the gas mixture. For example, as for the constant-pressure method, it has been found that the addition of nitrogen into CO_2 reduces the apparent gas diffusivity in heavy oil (Nguyen and Farouq Ali, 1998). As for the DPDSA method, the addition of C_3H_8 into CO_2 is found to increase the apparent gas diffusivity in heavy oil (Yang and Gu, 2006). However, the individual contribution of each component in the gas mixture to the bulk diffusion cannot be quantified with the aforementioned methods. Compositional measurements of the gas phase must be carried out before the diffusion test and after the diffusion test to determine individual molecular diffusion coefficients of different gases in heavy oil, thus enabling the evaluation of preferential diffusion of different gases into heavy oil.

It is of fundamental and practical importance to perform further research on phase behaviour and mass transfer of solvent(s)-CO_2-heavy oil systems due to the scarcity of

experimental data for these systems as well as accurate theoretical foundations. The scientific findings will provide fundamental data and important insights for designing solvent-assisted CO_2 flooding processes for enhancing heavy oil recovery.

2.7 Summary

The following summary can be made from the previous discussions:

1) CO_2-heavy oil system can exhibit complex phase behaviour including L_1, L_1V, L_1L_2, L_1L_2V equilibria;
2) Solubility of CO_2 in heavy oil decreases as temperature increases. At temperatures below the *K* point of the CO_2-heavy oil system, CO_2 solubility increases with pressure but levels off when system pressure reaches a L_1L_2 or L_1L_2V pressure;
3) Dissolution of CO_2, C_3H_8 or *n*-C_4H_{10} in heavy oil at the L_1 or L_1V equilibrium state contributes to an enhanced swelling factor, a reduced mixture viscosity and a reduced interfacial tension, which is fundamentally beneficial for enhancing heavy oil recovery;
4) The solubility of a gas in heavy oil depends proportionally on its nonvolatility. Therefore, C_3H_8 and *n*-C_4H_{10} are potentially good solvent additives for the CO_2-heavy oil system due to their high solubility in heavy oil and consequently desirable physical properties of the solvent-heavy oil mixture; and
5) Although the existing methods are suitable for estimating the apparent molecular diffusion coefficient of a gas mixture diffusing into heavy oil, they cannot be used to determine the individual molecular diffusion coefficient of each component in the solvent(s)-CO_2 mixture. Gas-phase compositional measurements may need to

be carried out before the diffusion test and after the diffusion test in order to determine the individual molecular diffusion coefficients of different gases in heavy oil.

CHAPTER 3 A MODIFIED ALPHA FUNCTION FOR PENG-ROBINSON EQUATION OF STATE TO IMPROVE VAPOUR PRESSURE PREDICTION OF NON-HYDROCARBON AND HYDROCARBON COMPOUNDS

3.1 Introduction

The cubic equation of state (CEOS)-based phase behaviour simulation of highly asymmetric systems plays a critical role in many enhanced oil recovery (EOR) processes, such as CO_2 injection (Kokal and Sayegh, 1989) and VAPEX processes (Upreti *et al.*, 2007). These processes are closely associated with both the injected light compounds (e.g., CO_2 and C_3H_8) and light-to-heavy hydrocarbons. Although accurate prediction of phase behaviour of mixtures using EOS depends on the appropriately chosen binary interaction parameters and mixing rules, accurate representation of saturation conditions of pure substances by the alpha function in CEOS lays a sound foundation for successfully applying the EOS to mixtures.

The two-parameter CEOS has been widely used in the petroleum and chemical industries due to its simplicity and capability in predicting properties of pure substances and mixtures in both vapour and liquid phases. It has been well-accepted that the most popular two-parameter CEOS includes the PR EOS (Peng and Robinson, 1976) and the Soave-Redlich-Kwong equation of state (SRK EOS) (Soave, 1972). The attractive term associated with the alpha function in the CEOS plays an important role in accurately predicting the characteristics of a real pure substance deviated from its ideal behaviour. In general, an improved representation of the vapour pressures of pure substances leads to

an improved saturation pressure prediction for mixtures (Hernández-Garduza *et al.*, 2002; Joshipura *et al.*, 2009; Neau *et al.*, 2009a). In the literature, numerous efforts have been made to modify the original alpha function for better phase behaviour simulation; however, most of the existing modified alpha functions are associated with non-hydrocarbon compounds and light hydrocarbons (Mathias, 1983; Mathias and Copeman, 1983; Stryjek and Vera, 1986; Melhem *et al.*, 1989).

To modify the alpha function, the following three basic requirements should be satisfied: 1) the alpha function must be finite and positive at all temperatures; 2) alpha function equals unity at the critical point; and 3) the alpha function approaches a finite value as the temperature approaches infinity (Hernández-Garduza *et al.*, 2002). In fact, the first two requirements can be easily satisfied for any alpha function. It is worthwhile noting that the traditional Soave-type alpha function fails to meet the third requirement since it does not demonstrate a limiting behaviour when the reduced temperature approaches infinity (Soave, 1972). However, as suggested by Neau *et al.* (2009a; b), the temperature point where the Soave alpha function begins to show upward trend is usually very high and beyond the interest of industrial applications. Thereafter, the third requirement is somewhat less restrictive.

The logarithm-type alpha function, which was proposed by Heyen (1981), and later modified by Trebble and Bishnoi (1987), and Twu *et al*. (1991; 1995a; b), shows an asymptotic behaviour when the reduced temperature is approaching infinity. Twu's alpha function employs a switching function which is defined by two sets of coefficients for the subcritical and supercritical conditions, respectively.

In this chapter, the functionality of two basic forms of the alpha function (i.e., the Soave-type alpha function and logarithm-type alpha function including the one recently modified by Gasem *et al.* (2001) for heavy hydrocarbons) in predicting the saturation properties of diverse pure substances was first examined. A new alpha function that combines the characteristics of both Soave-type and logarithm-type alpha functions is then developed, validated, and compared with the commonly used alpha functions. In addition, the acentric factor has been redefined at a reduced temperature of 0.6, rather than 0.7 as initially defined by Pitzer (1955) and Pitzer *et al.* (1955), and subsequently redefined as 0.5 by Twu *et al.* (1994), in an attempt to improve the saturation representation of both non-hydrocarbon and hydrocarbon compounds. The vapour pressure database in this study includes 59 chemical species from both light compounds, such as CO_2, CH_4 and C_3H_8, to heavy hydrocarbons up to *n*-tritetracontane (*n*-$C_{43}H_{88}$).

3.2 Mathematical Formulation

3.2.1. Alpha function

Due to its wide application in the petroleum and chemical industries, the PR EOS is chosen as the primary CEOS for this study. The same methodology discussed here will be also applicable to the SRK EOS. The PR EOS (Peng and Robinson, 1976) was originated from Redlich-Kwong EOS (1949) and SRK EOS (Soave, 1972) and can be expressed as follows,

$$P = \frac{RT}{V-b} - \frac{a}{V\left(V+b\right)+b\left(V-b\right)} \qquad [3\text{-}1]$$

$$a = a_c \alpha\left(T_r, \omega\right) \qquad [3\text{-}2]$$

$$a_c = \frac{0.457235 R^2 T_c^2}{P_c} \qquad [3\text{-}3]$$

and

$$b = \frac{0.0777969 R T_c}{P_c} \qquad [3\text{-}4]$$

where $\alpha\left(T_r, \omega\right)$ is the so-called alpha function which is dependent on both the reduced temperature T_r and the acentric factor ω, P is the pressure, T is the temperature, V is the molar volume, R is the universal gas constant, P_c is the critical pressure, and T_c is the critical temperature. Many modified versions of the alpha function have been made available in an attempt to enhance the vapour pressure prediction. A comprehensive review of the available alpha functions can be found elsewhere (Gasem *et al.*, 2001).

In principle, the existing alpha functions can be divided into two categories, i.e., Soave-type alpha function and logarithm-type alpha function. The Soave-type alpha function is based on the observation that α varies with the reduced temperature in the following manner,

$$\alpha^{0.5} \propto \left(1 - T_r^{0.5}\right) \qquad [3\text{-}5]$$

The Soave-type alpha function used in the PR EOS is given by,

$$\alpha = \left[1 + \left(0.37464 + 1.54226\omega - 0.26992\omega^2\right)\left(1 - T_r^{0.5}\right)\right]^2 \qquad [3\text{-}6]$$

A new form of the alpha function for $\omega > 0.49$ is later proposed by Robinson and Peng (1978),

$$\alpha = \left[1 + \left(0.3796 + 1.485\omega - 0.1644\omega^2 + 0.01667\omega^3\right)\left(1 - T_r^{0.5}\right)\right]^2 \qquad [3\text{-}7]$$

As for the logarithm-type alpha function, variation of α with the reduced temperature can be expressed by,

$$\ln \alpha \propto \left(1 - T_r\right) \qquad [3\text{-}8]$$

The original logarithm-type alpha function was proposed by Heyen (1981) in the following form,

$$\alpha = \exp\left[k\left(1 - T_r^n\right)\right] \qquad [3\text{-}9]$$

and then was modified by Trebble and Bishnoi (1987) by removing the index, n,

$$\alpha = \exp\left[k\left(1 - T_r\right)\right] \qquad [3\text{-}10]$$

For both types of alpha functions, there exists an approximately linear relationship between α and the acentric factor, ω. The α value for a substance at a subcritical temperature can be obtained by using a procedure that forces the fugacity of the gas phase to equate with that of liquid phase at the saturation pressure and temperature by using the CEOS (McCain, 1990). In order to explore the applicability of the Soave-type and logarithm-type alpha functions in representing vapour pressures of heavy hydrocarbons, the alpha values in the PR EOS for several heavy alkanes at different reduced temperatures are calculated and depicted in FIGUREs 3-1 and 3-2, respectively. It can be seen that both Soave-type and logarithm-type alpha functions are sufficiently accurate for representing the relation between α and the reduced temperature for heavy hydrocarbons up to *n*-tritetracontane (*n*-$C_{43}H_{88}$). This justifies the fact that either the Soave-type or logarithm-type relationship can be employed to accurately define the alpha function in the PR EOS.

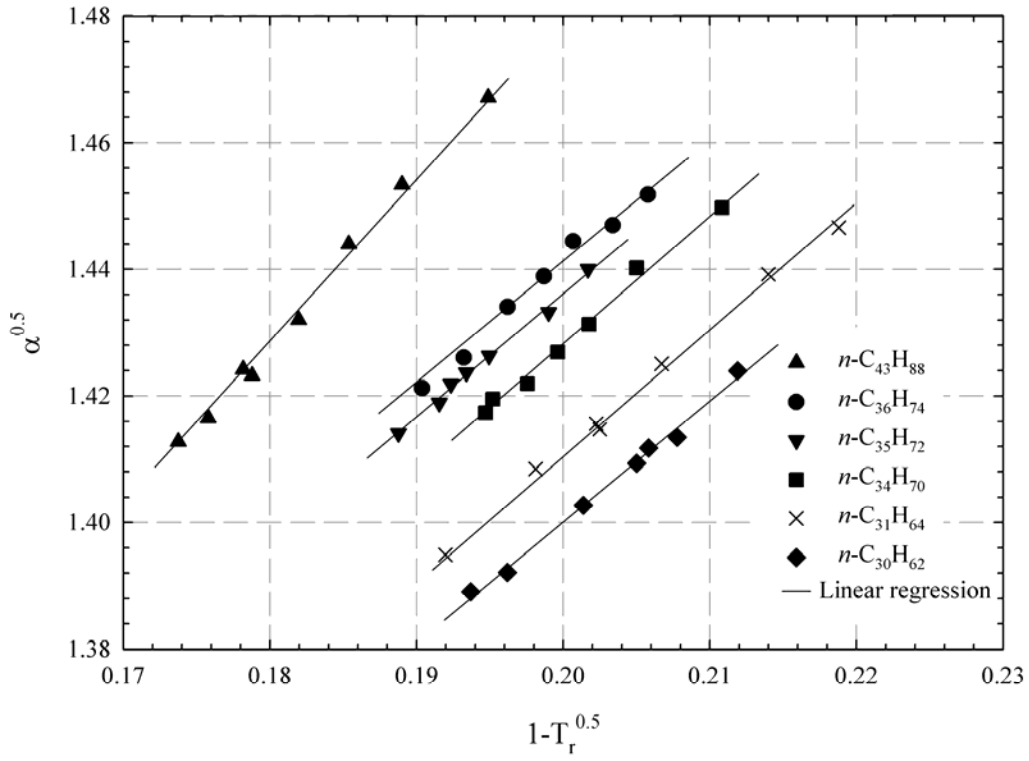

FIGURE 3-1: Temperature dependence of the alpha function in the PR EOS for heavy normal alkanes expressed in Soave-type form (based on the experimental data (Mazee, 1948))

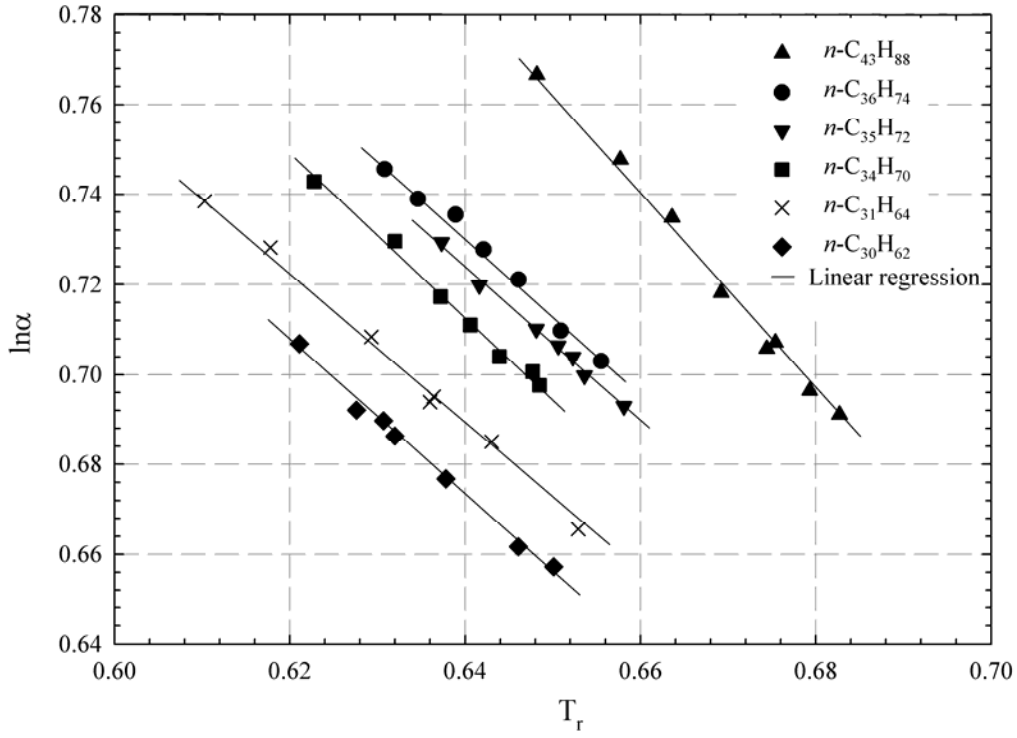

FIGURE 3-2: Temperature dependence of the alpha function in PR EOS for heavy normal alkanes expressed in logarithm-type form (based on the experimental data (Mazee, 1948))

In this chapter, a new alpha function has been developed by combining the advantages of both the Soave-type and logarithm-type alpha function with the following two possible methodologies. One is to sum the Soave-type alpha function and logarithm-type alpha function by using a weighting factor as shown below,

$$\alpha = w\exp\left[k_1\left(1-T_r\right)\right]+\left(1-w\right)\left[1+k_2\left(1-\sqrt{T_r}\right)\right]^2 \qquad [3\text{-}11]$$

where w is the weighting factor with values between 0 and 1. It can be found that the alpha defined by Equation [3-11] satisfies the first two aforementioned requirements; however, it can be easily derived that such type of alpha function does not show asymptotic behaviour when temperature approaches infinity. The alternative option would be to multiply the Soave-type with logarithm-type alpha function by using a weighting factor as a power index, i.e.,

$$\alpha = \left\{\exp\left[k_1'\left(1-T_r\right)\right]\right\}^w\left[1+k_2\left(1-\sqrt{T_r}\right)\right]^{2(1-w)} \qquad [3\text{-}12]$$

Obviously, Equation [3-12] can be reduced to Equation [3-6] with w equal to 0 and Equation [3-10] with w equal to 1, respectively. After carrying out some mathematical manipulations, Equation [3-12] can be simplified as,

$$\alpha = \exp\left\{k_1\left(1-T_r\right)+l\ln\left[1+k_2\left(1-\sqrt{T_r}\right)\right]^2\right\} \qquad [3\text{-}13]$$

with

$$k_1 = k_1'w = a_1 + a_2\omega + a_3\omega^2 + a_4\omega^3 \qquad [3\text{-}14a]$$

$$k_2 = a_5 + a_6\omega + a_7\omega^2 + a_8\omega^3 \qquad [3\text{-}14b]$$

and l is a constant that needs to be optimized. It can be shown that the new alpha function satisfies all the three basic requirements for a generalized alpha function, provided that the coefficient $k_1 > 0$.

For the existing alpha functions, the numerical coefficients appearing in the α expressions are determined by minimizing the deviation of the theoretically calculated and experimentally measured vapour pressures of a pure substance. Since Equations [3-6] and [3-7] are intrinsically developed on the basis of a limited number of substances including some light compounds and light-to-medium heavy hydrocarbons (Peng and Robinson, 1976; Robinson and Peng, 1978), extrapolation of these two equations to heavy hydrocarbons is expected to result in large deviations between the predicted vapour pressures and measured values. Gasem *et al.* (2001) modified the logarithm-type alpha function and obtained best reproduction of the vapour pressures of heavy hydrocarbons up to *n*-octacosane (*n*-$C_{28}H_{58}$) in comparison to the existing alpha functions.

Recently, based on the vapour pressure data of 237 hydrocarbons including heavy alkanes up to *n*-hexacosane (*n*-$C_{26}H_{54}$), Nji *et al.* (2009) modified the Soave-type alpha function for the PR EOS so that vapour pressures of heavy hydrocarbons can be more accurately predicted. Since the alpha functions developed by Gasem *et al.* (2001) and Nji *et al.* (2009) include heavy hydrocarbons in the database, these two alpha functions as well as the original Soave-type alpha function will be discussed in this chapter for the purpose of comparison. The experimentally measured vapour pressure data of heavy alkanes up to *n*-tritetracontane (*n*-$C_{43}H_{88}$) from Mazee *et al.* (1948) are included in this study (see TABLE 3-1). The formats of the evaluated alpha functions are summarized in TABLE 3-2.

TABLE 3-1: Vapour pressure database used in this study

Name	Formula	T_r	P_v^{exp} (kPa)	NPTS*	Reference
Carbon dioxide	CO_2	0.714-0.905	530.325-7368.95	55	Michels *et al.*,1950
Nitrogen	N_2	0.500-1.000	12.52-3400.2	67	Wagner, 1973
Argon	Ar	0.556-0.999	68.95-4857.8	57	Wagner, 1973
Neon	Ne	0.611-0.954	101.325-2026.5	5	Stull,1947
Water	H_2O	0.422-1.000	0.6107-22106	78	Ambrose and Lawenson, 1972
Oxygen	O_2	0.420-0.993	0.152-4844.8	22	Chung, 1997
Ammonia	NH_3	0.691-0.996	558-10973.69	30	Baehr, 1976; Holcomb and Outcalt, 1999
Hydrogen fluoride	HF	0.592-0.657	48.03-144.56	14	Sheft *et al.*, 1973
Hydrogen sulfide	H_2S	0.496-0.589	17.399-141.655	8	Stull,1947
Carbon monoxide	CO	0.609-0.976	101.325-3039.75	6	Stull,1947
Nitric oxide	NO	0.674-0.990	101.325-6079.5	9	Stull,1947
Chlorine	Cl_2	0.574-0.959	101.325-6079.5	9	Stull,1947
Sulfur dioxide	SO_2	0.611-0.963	101.325-6079.5	9	Stull,1947
Bromine	Br_2	0.567-0.884	101.325-6079.5	9	Stull,1947
Krypton	Kr	0.578-0.987	101.325-5066.25	10	Stull,1947
Silicon tetrachloride	$SiCl_4$	0.729-0.973	202.65-3039.75	5	Stull,1947
Acetone	C_3H_6O	0.510-0.690	4.267-201.571	29	Ambrose *et al.*, 1974
Ethyl fluoride	C_2H_5F	0.628-0.992	101.5-4713.9	110	Chen *et al.*, 2005
Acetic acid	$C_2H_4O_2$	0.513-0.700	2.891-201.718	27	Ambrose *et al.*, 1977
Methanol	CH_4O	0.562-0.696	9.815-205.653	20	Ambrose and Sprake, 1970
Ethanol	C_2H_6O	0.570-0.713	5.726-179.321	25	Ambrose and Sprake, 1970
1-Pentanol	$C_5H_{12}O$	0.744-0.874	226.8-1220	13	Ambrose *et al.*, 1975

TABLE 3-1: Vapour pressure database used in this study (continued)

Name	Formula	T_r	P_v^{exp} (kPa)	NPTS*	Reference
1-Octanol	$C_8H_{18}O$	0.770-0.849	234.6-649.9	10	Ambrose *et al.*, 1975
Methane	CH_4	0.476-1.000	11.698-4596.087	36	Kleinrahm and Wagner, 1986
Ethane	C_2H_6	0.780-1.000	912.990-4863.500	18	Douslin and Harrison, 1973
Propane	C_3H_8	0.698-1.000	291.79-4239.31	24	Thomast and Harrison, 1982
n-Butane	*n*-C_4H_{10}	0.753-0.995	456.65-3661.2	12	Kratzke, 1982
2-Methylpropane	*i*-C_4H_{10}	0.681-0.844	183.194-1113.365	5	Martinez-Ortlz and Manley, 1978
n-Pentane	*n*-C_5H_{12}	0.745-0.980	338.78-2912.7	14	Kratzke *et al.*,1985
n-Hexane	*n*-C_6H_{14}	0.581-0.692	17.309-133.974	45	Bich *et al.*,1992
n-Heptane	*n*-C_7H_{16}	0.687-0.889	99.663-1597.746	29	Weber, 2000
n-Octane	*n*-C_8H_{18}	0.632-0.691	29.037-86.150	15	Gregorowicz, 1987
n-Nonane	*n*-C_9H_{20}	0.607-0.859	13.238-656.657	10	Carmichael, 1953
n-Decane	*n*-$C_{10}H_{22}$	0.528-0.961	0.8741-1395.0	16	Morgan and Kobayashi, 1994
n-Dodecane	*n*-$C_{12}H_{26}$	0.537-0.894	0.7338-671.13	13	Morgan and Kobayashi, 1994
n-Tetradecane	*n*-$C_{14}H_{30}$	0.538-0.849	0.443-343.45	16	Morgan and Kobayashi, 1994
n-Hexadecane	*n*-$C_{16}H_{34}$	0.544-0.807	0.318-163.53	20	Morgan and Kobayashi, 1994
n-Octadecane	*n*-$C_{18}H_{38}$	0.553-0.707	0.2656-22.730	12	Morgan and Kobayashi, 1994
n-Nonadecane	*n*-$C_{19}H_{40}$	0.560-0.779	0.2550-73.66	16	Morgan and Kobayashi, 1994
n-Eicosane	*n*-$C_{20}H_{42}$	0.564-0.759	0.2440-48.08	32	Morgan and Kobayashi, 1994
n-Docosane	*n*-$C_{22}H_{46}$	0.576-0.729	0.2432-20.720	12	Morgan and Kobayashi, 1994
n-Tetracosane	*n*-$C_{24}H_{50}$	0.566-0.735	0.0901-17.460	13	Morgan and Kobayashi, 1994
n-Octacosane	*n*-$C_{28}H_{58}$	0.586-0.713	0.0821-6.001	14	Morgan and Kobayashi, 1994
n-Triacontane	*n*-$C_{30}H_{62}$	0.621-0.650	0.4000-0.7761	7	Mazee, 1948

TABLE 3-1: Vapour pressure database used in this study (continued)

Name	Formula	T_r	P_v^{exp} (kPa)	NPTS*	Reference
n-Hentriacontane	*n*-$C_{31}H_{64}$	0.610-0.653	0.4000-0.7160	7	Mazee, 1948
n-Tetratriacontane	*n*-$C_{34}H_{70}$	0.623-0.649	0.4000-0.4187	7	Mazee, 1948
n-Pentatriacontane	*n*-$C_{35}H_{72}$	0.637-0.658	0.4000-0.4931	7	Mazee, 1948
n-Hexatriacontane	*n*-$C_{36}H_{74}$	0.631-0.656	0.4000-0.3451	7	Mazee, 1948
n-Tritetracontane	*n*-$C_{43}H_{88}$	0.648-0.683	0.4000-0.5247	8	Mazee, 1948
Benzene	C_6H_6	0.530-0.996	12.471-4772.600	33	Ambrose *et al.*,1970; Ambrose, 1990
Tetralin	$C_{10}H_{12}$	0.492-0.616	1.443-39.128	11	Mokbel *et al.*, 1998
n-Butylbenzene	$C_{10}H_{14}$	0.505-0.633	1.249-37.027	10	Mokbel *et al.*, 1998
Cyclohexylbenzene	$C_{10}H_{16}$	0.545-0.626	4.104-29.700	7	Mokbel *et al.*, 1998
n-Octylbenzene	$C_{14}H_{22}$	0.555-0.637	1.513-14.226	7	Mokbel *et al.*, 1998
n-Undecylbenzene	$C_{17}H_{28}$	0.578-0.610	1.369-3.726	4	Mokbel *et al.*, 1998
Cyclopentane	C_5H_{10}	0.476-0.671	2.781-191.64	13	Mokbel *et al.*, 1995
Trans-decahydronaphtalene	$C_{10}H_{18}$	0.474-0.601	1.329-38.41	10	Mokbel *et al.*, 1995
Methylcyclohexane	C_7H_{14}	0.480-0.686	1.785-163.7	13	Mokbel *et al.*, 1995
Cyclooctane	C_8H_{16}	0.571-0.722	19.920-270.111	15	Mokbel *et al.*, 1995

Note:
* NPTS represents the number of experimental data points

TABLE 3-2: Alpha functions examined in this study

Model No.	Functions	Reference
1	$\alpha = \left[1 + \left(0.37464 + 1.54226\omega - 0.26992\omega^2\right)\left(1 - T_r^{0.5}\right)\right]^2$	Soave, 1972
2	$\alpha = \left[1 + \left(0.388187 + 1.56132\omega - 0.29014\omega^2 + 0.0617513\omega^3\right)\left(1 - T_r^{0.5}\right)\right]^2$	Nji *et al.*, 2009
3	$\alpha = \exp\left[\left(2 + 0.836T_r\right)\left(1 - T_r^{0.134+0.508\omega-0.0467\omega^2}\right)\right]$	Gasem *et al.*, 2001
4	$\alpha = \exp\left\{k_1\left(1 - T_r\right) + l\ln\left[1 + k_2\left(1 - \sqrt{T_r}\right)\right]^2\right\}$	This work

The alpha function in the PR EOS is also dependent on the acentric factor, which reflects the deviation of acentricity or non-sphericity of a compound molecule from that of a simple fluid, such as argon and xenon (Pitzer *et al.*, 1955a). The acentric factor was originally introduced by Pitzer and co-workers (1955a; b) and defined as the following form in terms of the reduced vapour pressure at a reduced temperature of 0.7,

$$\omega = -\log\left(P_r\right)_{T_r=0.7} - 1 \qquad [3\text{-}15]$$

It has been found that, based on the above definition, the generalized correlation developed by Pitzer *et al.* (1955a) can be used to accurately predict the vapour pressures at reduced temperatures between 0.7 and 1.0 but less accurately represent those at reduced temperatures lower than 0.7 (Twu *et al.*, 1994). In other words, the acentric factor defined at reduced temperature of 0.7 can accurately reflect the characteristics of a substance (e.g., carbon dioxide and light hydrocarbons) at a temperature close to 70-100% of its critical temperature. However, it is less accurate of representing the characteristics of a substance (e.g., heavy hydrocarbons) at a temperature usually much lower than 70% of its critical temperature encountered in the industrial applications. Thus, Twu *et al.* (1994) modified the definition of acentric factor at a reduced temperature of 0.5 other than 0.7 and achieved a better representation of vapour pressures of heavy hydrocarbons at low reduced temperatures.

Nji *et al.* (2009) developed an alpha function based on the acentric factor at a reduced temperature of 0.5 and improved vapour pressure predictions for heavy hydrocarbons. Nevertheless, it should be noted that using the acentric factor defined at a reduced temperature of 0.5 may result in a biased representation for non-hydrocarbon compounds since the vapour pressure database used by Nji *et al.* (2009) only contains

hydrocarbons. In this study, the Pitzer acentric factor is redefined at a reduced temperature of 0.6 so as to balance the characteristics of both light compounds and heavy hydrocarbons,

$$\omega' = -\log\left(P_r\right)_{T_r=0.6} - 1 \qquad [3\text{-}16]$$

Herein, it is assumed that the reduced vapour pressure for imaginary simple fluids at a reduced temperature of 0.6 is exactly equal to 0.1 so that the acentric factor for imaginary simple fluids becomes zero according to Equation [3-16].

3.2.2. Determination of the correlation coefficients

In this study, a total of 59 chemical species (including polar and non-polar non-hydrocarbons, light and heavy hydrocarbons) are included in the vapour pressure database. TABLE 3-1 presents the temperature range for each substance within which vapour pressure data are measured, while the critical properties used in this study are listed in TABLE 3-3. Note that the critical properties of some heavy hydrocarbons are estimated using the asymptotic behaviour model (Gao *et al.*, 2001) whenever the experimental critical properties are not available from the literature.

The commonly used Wagner equation is used to smooth the vapour pressure data (Wagner, 1973). Then, the acentric factors defined at a reduced temperature of either 0.7 or 0.6 can be calculated using the regressed Wagner equations, as shown in TABLE 3-3. In particular, for normal alkanes, it is found that the acentric factor increases with carbon number of normal alkanes, as indicated by FIGURE 3-3. Quadratic polynomials are employed to describe the variation trend of acentric factor defined at $T_r = 0.7$ and 0.6 with carbon number. The regressed expressions for acentric factor defined at $T_r = 0.7$ and

TABLE 3-3: Critical properties and acentric factors of the substances used in this study

Name	P_c (kPa)	T_c (K)	Reference	ω [a]	ω' [a]
Carbon dioxide	7377.5	304.14	Shaver *et al.*, 1991	0.2238	0.9276
Nitrogen	3400.2	126.2	Shaver *et al.*, 1991	0.0371	0.6119
Argon	4897.9	150.86	Shaver *et al.*, 1991	-0.0031	0.5422
Neon	2653	44.4	Green and Perry, 2008	0.3451	1.1142
Water	22055	647.13	Shaver *et al.*, 1991	0.3451	1.1142
Oxygen	5042.9	154.581	Shaver *et al.*, 1991	0.0222	0.5852
Ammonia	11304	405.4	Shaver *et al.*, 1991	0.2519	0.9630
Hydrogen fluoride	6480	461.15	Shaver *et al.*, 1991	0.3798	1.0701
Hydrogen sulfide	8970	373.3	Green and Perry, 2008	0.2137	0.7341
Carbon monoxide	3498.75	134.45	Green and Perry, 2008	0.0916	0.5880
Nitric oxide	6480	180.15	Green and Perry, 2008	0.5885	1.4627
Chlorine	7710	417.15	Green and Perry, 2008	0.0735	0.6823
Sulfur dioxide	7884	430.75	Green and Perry, 2008	0.2441	0.9852
Bromine	10300	584.15	Green and Perry, 2008	0.0465	0.7217
Krypton	5520.19	209.46	Green and Perry, 2008	-0.0589	0.5739
Silicon tetrachloride	3720	259	Green and Perry, 2008	0.4768	1.4415
Acetone	4700	508.1	Shaver *et al.*, 1991	0.3074	1.0613
Ethyl fluoride	5027.75	375.31	Chen *et al.,* 2005	0.2170	0.9159
Acetic acid	5786	592.71	Shaver *et al.*, 1991	0.4598	1.2803
Methanol	8097.1	512.64	Shaver *et al.*, 1991	0.5652	1.4737
Ethanol	6148.4	513.92	Shaver *et al.*, 1991	0.6451	1.6455
1-Pentanol	3897	588.1	Shaver *et al.*, 1991	0.5785	1.6294

TABLE 3-3: Critical properties and acentric factors of the substances used in this study (continued)

Name	P_c (kPa)	T_c (K)	Reference	ω [a]	ω' [a]
1-Octanol	2783	652.3	Shaver *et al.*, 1991	0.5801	1.6031
Methane	4599.2	190.564	Lemmon and Goodwin, 2000	0.0103	0.5640
Ethane	4871.8	305.322	Lemmon and Goodwin, 2000	0.0989	0.7090
Propane	4246.2	369.825	Lemmon and Goodwin, 2000	0.1520	0.8007
n-Butane	3786.1	425.12	Lemmon and Goodwin, 2000	0.1978	0.8749
2-Methylpropane	3640	407.8	Martinez-Ortlz and Manley, 1978	0.1852	0.8592
n-Pentane	3366.5	469.7	Lemmon and Goodwin, 2000	0.2501	0.9644
n-Hexane	3018.1	507.49	Lemmon and Goodwin, 2000	0.2988	1.0585
n-Heptane	2727	540.13	Lemmon and Goodwin, 2000	0.3486	1.1384
n-Octane	2486	568.88	Lemmon and Goodwin, 2000	0.3971	1.2251
n-Nonane	2290	594.6	Nikitin *et al.*, 1997	0.4442	1.3093
n-Decane	2110	617.7	Nikitin *et al.*, 1997	0.5381	1.4549
n-Dodecane	1820	658.32	Nikitin *et al.*, 1997	0.5757	1.5381
n-Tetradecane	1570	693	Nikitin *et al.*, 1997	0.6442	1.6671
n-Hexadecane	1400	723	Nikitin *et al.*, 1997	0.7167	1.7962
n-Octadecane	1290	747	Nikitin *et al.*, 1997	0.8160	1.9565
n-Nonadecane	1160	755	Nikitin *et al.*, 1997	0.8624	2.0343
n-Eicosane	1080	768	Nikitin *et al.*, 1997	0.88665[b]	2.0686
n-Docosane	991	786	Nikitin *et al.*, 1997	0.9579	2.2213
n-Tetracosane	871	800	Nikitin *et al.*, 1997	1.0509	2.3841
n-Octacosane	744	824	Nikitin *et al.*, 1997	1.1702	2.60767[c]
n-Triacontane	636	843	Nikitin *et al.*, 1997	1.2188	2.6921

TABLE 3-3: Critical properties and acentric factors of the substances used in this study (continued)

Name	P_c (kPa)	T_c (K)	Reference	ω [a]	ω' [a]
n-Hentriacontane	607.37	847.58	Gao *et al.*, 2001	1.2654	2.7815
n-Tetratriacontane	526.64	862.41	Gao *et al.*, 2001	1.3447	2.9135
n-Pentatriacontane	502.8	866.88	Gao *et al.*, 2001	1.4149	2.9391
n-Hexatriacontane	472	872	Nikitin *et al.*, 1997	1.4243	2.9937
n-Tritetracontane	353.66	896.03	Gao *et al.*, 2001	1.5439	3.3847
Benzene	4889.8	562.161	Shaver *et al.*, 1991	0.2084	0.9088
Tetralin	4889.8	562.161	Mokbel *et al.*,1998	0.3220	1.1156
n-Butylbenzene	2890	660.5	Mokbel *et al.*,1998	0.3517	1.2085
Cyclohexylbenzene	2890	739.6	Mokbel *et al.*,1998	0.4203	1.2280
n-Octylbenzene	1980	726.7	Mokbel *et al.*,1998	0.5943	1.5357
n-Undecylbenzene	1610	765.5	Mokbel *et al.*,1998	0.7156	1.7677
Cyclopentane	4510	511.7	Lide, 2009	0.1972	0.8792
Trans-decahydronaphtalene	3200	703.6	Lide, 2009	0.2089	0.9291
Methylcyclohexane	3480	572.1	Lide, 2009	0.2407	0.9533
Cyclooctane	3560	647.2	Lide, 2009	0.2522	0.9863

Note:
[a] Calculated based on the experimental data and Wagner equation
[b] Smoothed value using Equation [3-17]
[c] Smoothed value using Equation [3-18]

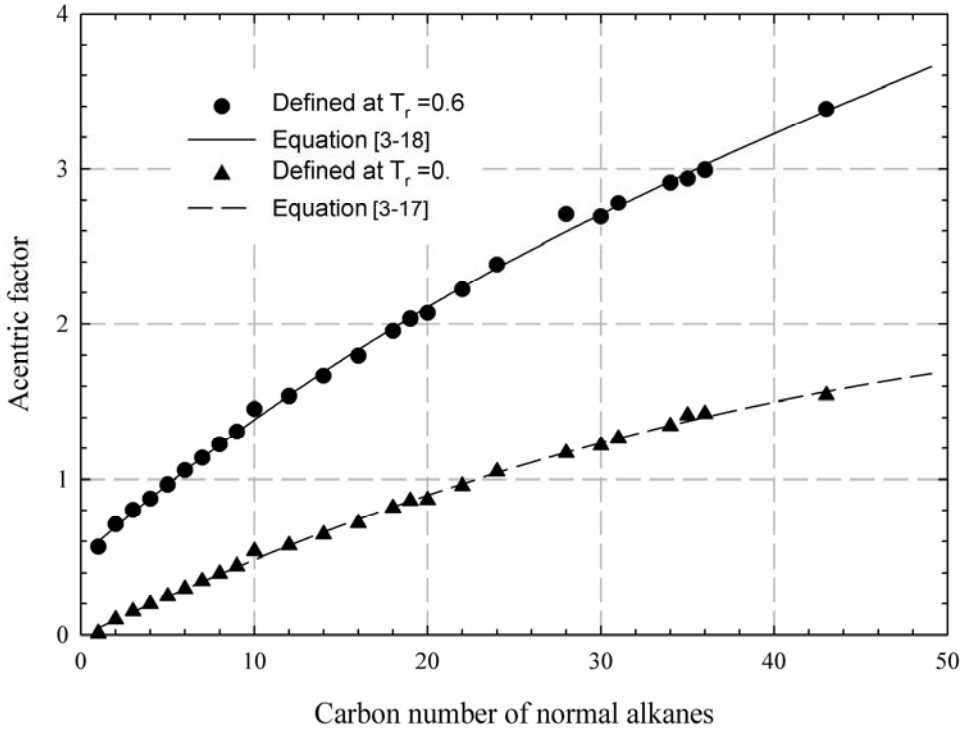

FIGURE 3-3: Dependence of acentric factor on carbon number of normal alkanes

0.6 are respectively provided as follows,

$$\omega = 0.0520C_n\text{-}0.0004C_n^2 \qquad [3\text{-}17]$$

and

$$\omega' = 0.5268 + 0.0907C_n\text{-}0.0006C_n^2 \qquad [3\text{-}18]$$

The above two equations are regressed with a confidence interval of 95%. The standard errors for the fitted coefficients are shown in TABLE 3-4. The purpose of the regression is to obtain the coefficients that appear in the new alpha function expressed by Equation [3-13] based on the vapour pressure database considered. Such regression can be achieved by minimizing the objective function defined as follows,

$$\text{RMSRE} = \sqrt{\frac{1}{NPTS}\sum_{i=1}^{NPTS}\left[\frac{\left(P_v^{\text{cal}}\right)_i - \left(P_v^{\text{exp}}\right)_i}{\left(P_v^{\text{exp}}\right)_i}\right]^2} \qquad [3\text{-}19]$$

All the regressions have been conducted with a confidence interval of 95%. To ensure that the new alpha function demonstrates the asymptotic behaviour when the reduced temperature is approaching infinity, the following constraint is applied.

$$\min\left\{k_1^i = a_1 + a_2\omega_i + a_3\omega_i^2 + a_4\omega_i^3, i = 1,2,3,\cdots,m\right\} > 0 \qquad [3\text{-}20]$$

where m is the total number of compound species considered in this study. This constraint ensures the coefficient $k_1 > 0$.

The alpha function with an acentric factor defined at reduced temperature of 0.7 is obtained as follows,

$$\alpha = \exp\left\{\begin{array}{l}\left(0.13280 - 0.05052\omega + 0.25948\omega^2\right)\left(1 - T_r\right) + \\ 0.81769\ln\left[1 + \left(0.31355 + 1.86745\omega - 0.52604\omega^2\right)\left(1 - \sqrt{T_r}\right)\right]^2\end{array}\right\} \qquad [3\text{-}21]$$

TABLE 3-4: Standard errors of the fitted coefficients in Equations [3-17] and [3-18]

Equation [3-17]		**Equation [3-18]**	
Coefficient	**Standard error**	**Coefficient**	**Standard error**
0.05200	0.00070	0.52680	0.01880
-0.00040	0.00002	0.09070	0.00230
-	-	-0.00060	0.00005

Under supercritical states, the Soave-type function, even with its abnormal minimum at a very high temperature, must be preferred to the logarithm types which usually present inconsistent variations of the alpha function with respect to temperature (Neau *et al*., 2009a; b). Therefore, the proposed Equation [3-21] is recommended for subcritical region ($T_r \le 1$) and the following Soave-type alpha function instead of Equation [3-21] should be used under supercritical states ($T_r > 1$),

$$\alpha = \left[1 + \left(0.38856 + 1.40137\omega - 0.05387\omega^2 - 0.01824\omega^3\right)\left(1 - T_r^{0.5}\right)\right]^2 \qquad [3\text{-}22]$$

The alpha function with an acentric factor defined at reduced temperature of 0.6 is determined as,

$$\alpha = \exp\left\{\begin{array}{l}\left(0.34580 - 0.59700\omega' + 0.27040\omega'^2\right)\left(1 - T_r\right) + \\ 0.92030\ln\left[1 + \left(-0.53261 + 1.75415\omega' - 0.40127\omega'^2\right)\left(1 - \sqrt{T_r}\right)\right]^2\end{array}\right\} \qquad [3\text{-}23]$$

Similarly, Equation [3-23] is recommended for subcritical region ($T_r \le 1$) and the following Soave-type alpha function instead of Equation [3-23] should be used for supercritical conditions ($T_r > 1$),

$$\alpha = \left[1 + \left(-0.12401 + 0.96953\omega' - 0.08591\omega'^2 + 0.00642\omega'^3\right)\left(1 - T_r^{0.5}\right)\right]^2 \qquad [3\text{-}24]$$

The regressed coefficients in Equation [3-13] for acentric factors defined at $T_r = 0.7$ and 0.6 are specified in alpha functions [3-21] and [3-23], respectively. For convenience, the alpha functions expressed by Equations [3-21] and [3-23] are referred to as alpha functions #4-1 and 4-2. It can be found that the k_1 terms in the alpha functions #4-1 and 4-2 do not show a negative value even at a large and positive acentric factor. TABLE 3-5 lists the standard errors of the fitted coefficients appearing in alpha functions #4-1 and 4-

TABLE 3-5: Standard errors of the fitted coefficients in alpha functions #4-1 and 4-2

Coefficients	Alpha function #4-1		Alpha function #4-2	
	Value	**Standard error**	**Value**	**Standard error**
a_1	0.13280	0.02954	0.34580	0.07031
a_2	-0.05052	0.00963	-0.59700	0.09532
a_3	0.25948	0.03896	0.27040	0.02690
a_5	0.31355	0.07627	-0.53261	0.09134
a_6	1.86745	0.10264	1.75415	0.09943
a_7	-0.52604	0.03418	-0.40127	0.02902
l	0.81769	0.09159	0.92030	0.13931

2 with a regression confidence interval of 95%. For a given chemical species, alpha function #4-2 is decreased with an increase in reduced temperature. As shown in FIGURE 3-4, it can be observed that the alpha function developed by this study shows a monotonously decreasing dependence on the reduced temperature that is below 4 for carbon dioxide.

It is worthwhile noting that the recommended Soave-type alpha functions Equation [3-22] and Equation [3-24] for supercritical region are applicable for low-to-medium supercritical temperatures. In this case, the alpha functions will show an upward trend at a high supercritical temperature (about 3 to 4 times critical temperature), though such a high temperature is seldom encountered in petroleum and chemical applications.

3.2.3. Enthalpy of vaporization

The newly proposed alpha function, i.e., Equation [3-23], is used to calculate other thermodynamics properties in order to further validate its applicability. Due to the availability of vaporization enthalpy data for heavy hydrocarbons, vaporization enthalpy is chosen as the thermodynamic property for the purpose of validation. The fundamental enthalpy departure equation on a molar scale is provided as follows (Sandler, 1999),

$$H(T,P)-H^{IG}(T,P)=RT(Z-1)+\int_{V=\infty}^{V=V(T,P)}\left[T\left(\frac{\partial P}{\partial T}\right)_{V}-P\right]dV \qquad [3\text{-}25]$$

More specific expression can be obtained using PR EOS as follows,

$$H(T,P)-H^{IG}(T,P)=RT(Z-1)+\frac{T\left(da/dT\right)-a}{2\sqrt{2}b}\ln\left[\frac{Z+\left(1+\sqrt{2}\right)B}{Z+\left(1-\sqrt{2}\right)B}\right] \qquad [3\text{-}26]$$

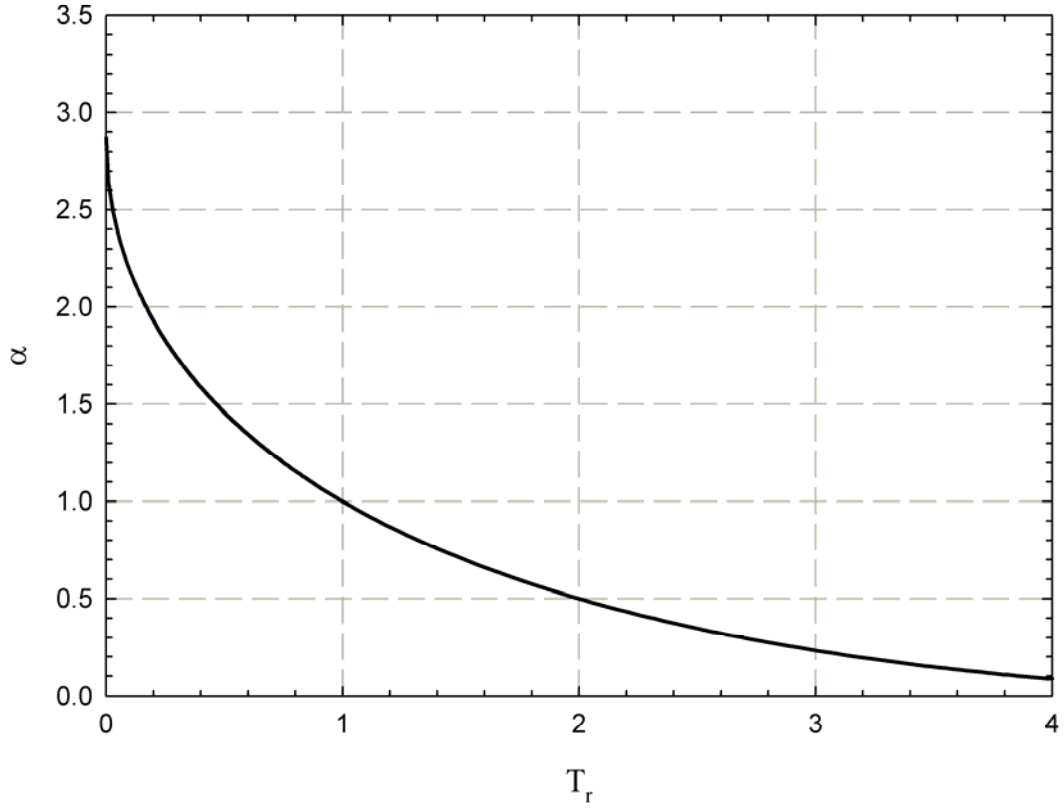

FIGURE 3-4: Variation of alpha function #4-2 with reduced temperature for CO_2

Thus, the enthalpy of vaporization at saturation temperature can be readily expressed by,

$$\Delta_l^g H(T) = RT(Z_v - Z_l) + \frac{T\left(da/dT\right) - a}{2\sqrt{2}b}\left\{\ln\left[\frac{Z_v + \left(1+\sqrt{2}\right)B}{Z_v + \left(1-\sqrt{2}\right)B}\right] - \ln\left[\frac{Z_l + \left(1+\sqrt{2}\right)B}{Z_l + \left(1-\sqrt{2}\right)B}\right]\right\} \quad [3\text{-}27]$$

where

$$B = \frac{bP}{RT} \quad [3\text{-}28]$$

and for the newly proposed alpha function,

$$\frac{\mathrm{d}\alpha}{\mathrm{d}t} = \left\{-\frac{k_1}{T_c} - \frac{lk_2}{T_c\sqrt{T_r}\left[1 + k_2\left(1-\sqrt{T_r}\right)\right]}\right\}\exp\left\{k_1\left(1-T_r\right) + l\ln\left[1 + k_2\left(1-\sqrt{T_r}\right)\right]^2\right\} \quad [3\text{-}29]$$

TABLE 3-6 lists the vaporization enthalpy data of non-hydrocarbon compounds, light hydrocarbons and heavy hydrocarbons, which are found from the literature.

3.3 Results and Discussion

3.3.1. Vapour pressure

The predicted vapour pressures based on the aforementioned alpha functions are presented in TABLE 3-7 in terms of the percentage absolute average deviation (%AAD), the percentage bias (%BIAS), and the percentage maximum absolute deviation (%MAD). Alpha functions #1, 2, 3 and 4-1 shown in TABLE 3-7 are based on an acentric factor which is defined at $T_r = 0.7$, while alpha function #4-2 is based on an acenric factor that is defined at $T_r = 0.6$. It should be noted that the overall %AAD data for various alpha

TABLE 3-6: Vaporization enthalpy data

Name	*T* (K)	$\Delta_l^g H(T)$ (kJ/mol)	NPTS	Reference
Carbon dioxide	244.26-303.71	2.20-12.89	56	Lide, 2009
Nitrogen	63.15-110.00	3.76-6.03	7	Lide, 2009
Argon	83.81-150.00	1.17-6.54	8	Lide, 2009
Water	273.15-643.15	16.07-45.01	28	Lide, 2009
Benzene	295.00-460.00	23.19-33.40	34	Lide, 2009
Oxygen	54.36-150.00	2.54-7.77	11	Lide, 2009
Acetone	260.00-350.00	27.78-33.18	31	Lide, 2009
Methanol	300.00-470.00	29.7-39.29	18	Lide, 2009
Ethanol	300.00-460.00	33.82-44.48	17	Lide, 2009
Methane	90.69-190.00	1.29-8.70	11	Lide, 2009
Ethane	90.37-300.00	4.49-17.84	12	Lide, 2009
Propane	85.53-360.00	6.78-24.76	15	Lide, 2009
n-Pentane	298.15	26.4	1	Chickos and Wilson, 1997
n-Hexane	298.15	31.5	1	Chickos and Wilson, 1997
n-Heptane	298.15	36.6	1	Chickos and Wilson, 1997
n-Octane	298.15	41.6	1	Chickos and Wilson, 1997
n-Nonane	298.15	46.6	1	Chickos and Wilson, 1997
n-Decane	298.15	51.4	1	Chickos and Wilson, 1997
n-Undecane	298.15	56.6	1	Chickos and Wilson, 1997
n-Dodecane	298.15	61.5	1	Chickos and Wilson, 1997
n-Tridecane	298.15	66.7	1	Chickos and Wilson, 1997
n-Tetradecane	298.15	71.7	1	Chickos and Wilson, 1997

TABLE 3-6: Vaporization enthalpy data (continued)

Name	*T* (K)	$\Delta_l^g H(T)$ (kJ/mol)	NPTS	Reference
n-Pentadecane	298.15	76.8	1	Chickos and Wilson, 1997
n-Hexadecane	298.15	81.4	1	Chickos and Wilson, 1997
n-Heptadecane	298.15	86.5	1	Chickos and Wilson, 1997
n-Eicosane	440.00	80.78	1	Chirico *et al.*, 1989
n-Tetracosane	481.75	90.16	1	Mazee, 1948
n-Octacosane	515.15	93.72	1	Mazee, 1948
n-Triacontane	531.65	99.99	1	Mazee, 1948
n-Hentriacontane	539.35	105.00	1	Mazee, 1948
n-Tetratriacontane	558.55	107.90	1	Mazee, 1948
n-Pentatriacontane	565.45	111.50	1	Mazee, 1948
n-Hexatriacontane	571.55	114.80	1	Mazee, 1948
n-Tritetracontane	605.15	131.40	1	Mazee, 1948

TABLE 3-7: The predicted vapour pressures by using PR EOS with different alpha functions

Name	%AAD of each model				
	#1	#2	#3	#4-1	#4-2
Carbon dioxide	0.27	0.87	0.18	0.35	0.48
Nitrogen	0.75	1.11	0.20	0.56	0.50
Argon	0.87	0.88	0.43	0.30	0.43
Neon	5.86	5.13	4.91	5.32	5.21
Water	4.65	8.11	5.84	3.85	2.55
Oxygen	2.05	1.52	1.20	1.72	1.13
Ammonia	0.34	0.92	0.79	0.30	0.51
Hydrogen fluoride	18.10	22.50	17.87	17.83	5.33
Hydrogen sulfide	42.89	46.46	43.24	26.88	3.61
Carbon monoxide	7.66	8.05	7.80	7.64	7.93
Nitric oxide	4.79	5.99	4.49	4.76	5.80
Chlorine	2.16	2.21	1.91	2.20	2.28
Sulfur dioxide	2.12	2.44	2.01	2.27	2.96
Bromine	17.39	16.59	16.94	17.33	13.09
Krypton	14.87	13.91	13.77	14.29	10.07
Silicon tetrachloride	3.42	5.02	3.14	3.68	7.58
Acetone	1.52	7.25	1.64	0.68	0.11
Ethyl fluoride	0.54	1.74	0.89	0.56	0.82
Acetic acid	10.53	16.69	11.83	10.49	4.36
Methanol	3.90	10.64	6.16	5.08	3.44
Ethanol	3.24	5.13	1.44	0.70	1.94
1-Pentanol	3.76	6.31	3.97	4.55	9.01

TABLE 3-7: The predicted vapour pressures by using PR EOS with different alpha functions (continued)

Name	%AAD of each model				
	#1	**#2**	**#3**	**#4-1**	**#4-2**
1-Octanol	1.67	4.33	1.88	2.51	6.40
Methane	0.67	1.04	0.67	0.30	0.43
Ethane	0.34	0.40	0.45	0.23	0.27
Propane	0.26	0.98	0.43	0.38	0.34
n-Butane	0.36	0.77	0.68	0.35	0.34
2-Methylpropane	0.42	0.89	0.83	0.39	0.39
n-Pentane	0.25	2.11	0.52	0.45	0.63
n-Hexane	0.70	3.82	1.46	1.03	0.76
n-Heptane	0.25	2.41	0.77	0.24	0.39
n-Octane	0.52	4.04	1.03	0.56	0.32
n-Nonane	0.80	3.22	0.69	0.85	0.92
n-Decane	3.84	6.32	5.03	3.83	4.05
n-Dodecane	3.19	2.52	1.19	1.83	1.20
n-Tetradecane	0.32	2.46	0.68	1.20	1.59
n-Hexadecane	7.63	2.06	1.33	2.81	1.39
n-Octadecane	11.28	3.60	1.55	0.64	0.92
n-Nonadecane	10.82	3.18	1.73	0.84	1.58
n-Eicosane	14.36	1.51	1.36	2.63	0.85
n-Docosane	19.02	0.78	0.19	1.01	1.08

TABLE 3-7: The predicted vapour pressures by using PR EOS with different alpha functions (continued)

Name	%AAD for each model				
	#1	**#2**	**#3**	**#4-1**	**#4-2**
n-Tetracosane	26.00	0.60	0.79	0.81	2.71
n-Octacosane	38.01	3.51	4.88	6.10	5.52
n-Triacontane	53.47	8.44	6.43	3.50	1.67
n-Hentriacontane	61.44	9.04	6.78	3.02	2.54
n-Tetratriacontane	69.69	8.52	6.28	1.69	1.90
n-Pentatriacontane	60.86	1.56	2.97	5.63	9.37
n-Hexatriacontane	69.93	2.28	1.75	8.47	5.62
n-Tritetracontane	98.70	13.36	12.70	2.82	2.91
Benzene	2.02	1.96	2.28	2.26	1.35
Tetralin	9.85	2.08	8.73	7.78	2.81
n-Butylbenzene	21.62	13.28	20.81	21.01	3.30
Cyclohexylbenzene	7.06	13.58	7.97	6.64	1.07
n-Octylbenzene	2.69	11.81	7.24	5.07	1.97
n-Undecylbenzene	5.57	7.30	3.84	1.20	1.76
Cyclopentane	2.15	3.88	1.22	2.83	2.08
Trans-decahydronaphtalene	22.08	13.61	20.34	21.58	6.85
Methylcyclohexane	1.65	4.53	0.95	2.38	1.72
Cyclooctane	1.62	2.70	2.19	1.87	1.63
Overall %AAD	7.10	4.48	3.26	2.87	1.90
%BIAS	4.10	-2.98	-0.48	-0.25	0.01
%MAD	125.95	52.19	49.22	40.56	21.22

functions listed in TABLE 3-7 are calculated by averaging all the 1165 other than 59 %AAD data points for the 59 compounds. As can be seen from TABLE 3-7, the original form of the Soave-type function used in PR EOS results in the largest error for predicting vapour pressures for heavy hydrocarbons with %AAD increasing as a function of carbon number. This is mainly attributed to the fact that the original alpha function in PR-EOS is developed on the basis of vapour pressure of light hydrocarbons.

Both alpha function #2 and alpha function #3 demonstrate better prediction of vapour pressure for heavy hydrocarbons compared to the original Soave-type alpha function #1. It is worthwhile noting that alpha function #2 produces a second largest %AAD among all the examined alpha functions except for the original Soave-type alpha function #1. This can be ascribed to the fact that the vapour pressure data used to develop alpha function #2 is solely from hydrocarbons. In addition, the newly developed alpha functions #4-1 and 4-2 that combines the Soave-type form and logarithm-type form outperforms the Soave-type alpha functions #1 and 2 as well as the logarithm-type alpha function #3 since a better prediction in terms of %AAD between the experimentally measured and theoretically calculated vapour pressures has been obtained with the newly developed alpha function.

It is also interesting to find that, compared to the acentric factor defined at a reduced temperature of 0.7, this parameter defined at a reduced temperature of 0.6 enables alpha function #4-2 to provide a much better prediction of vapour pressures. For example, the overall %AAD and %MAD by using alpha function #4-2 with an acentric factor defined at $T_r = 0.6$ is reduced to 1.90% and 21.22%, compared to 2.87% and 40.56% resulting from alpha function #4-1 with an acentric factor defined at $T_r = 0.7$. In particular, a much

better prediction of vapour pressures of the polar compounds (e.g., hydrogen fluoride, hydrogen sulphide and acetic acid) and aromatic compounds (e.g., *n*-butylbenzene and trans-decahydronaphtalene) has been also observed by using the alpha function defined at $T_r = 0.6$ other than $T_r = 0.7$. This means that the acentric factor defined at $T_r = 0.6$ outperforms the acentric factor defined at $T_r = 0.7$ in reproducing vapour pressures of non-hydrocarbon compounds, light hydrocarbons and heavy hydrocarbons. Overall, TABLE 3-7 demonstrates that the alpha function #4-2 developed in this study provides the best vapour pressure prediction for all the examined chemical compounds.

FIGURE 3-5 illustrates %AAD variation of PR EOS prediction of normal-alkane vapour pressure against carbon number by incorporating different alpha functions. In general, the original PR EOS is found to be accurate in predicting the vapour pressure of normal alkanes with carbon number less than ten. Unfortunately, the average absolute deviation of vapour pressures between the experimental measurement and theoretical prediction using the original PR EOS increases drastically for normal alkanes with carbon number of ten and higher. This is attributed to the fact that the original alpha function in PR EOS is obtained mainly on the basis of vapour pressure data of light hydrocarbons. The other three alpha functions (#2, 3 and 4-2) show improved predictions of vapour pressure of heavier alkanes since vapour pressure data of heavy alkanes are included in the database with which the three alpha functions are developed. More accurate prediction of the vapour pressures of heavier alkanes can be obtained by using the newly developed alpha function #4-2 in comparison to the other alpha functions evaluated.

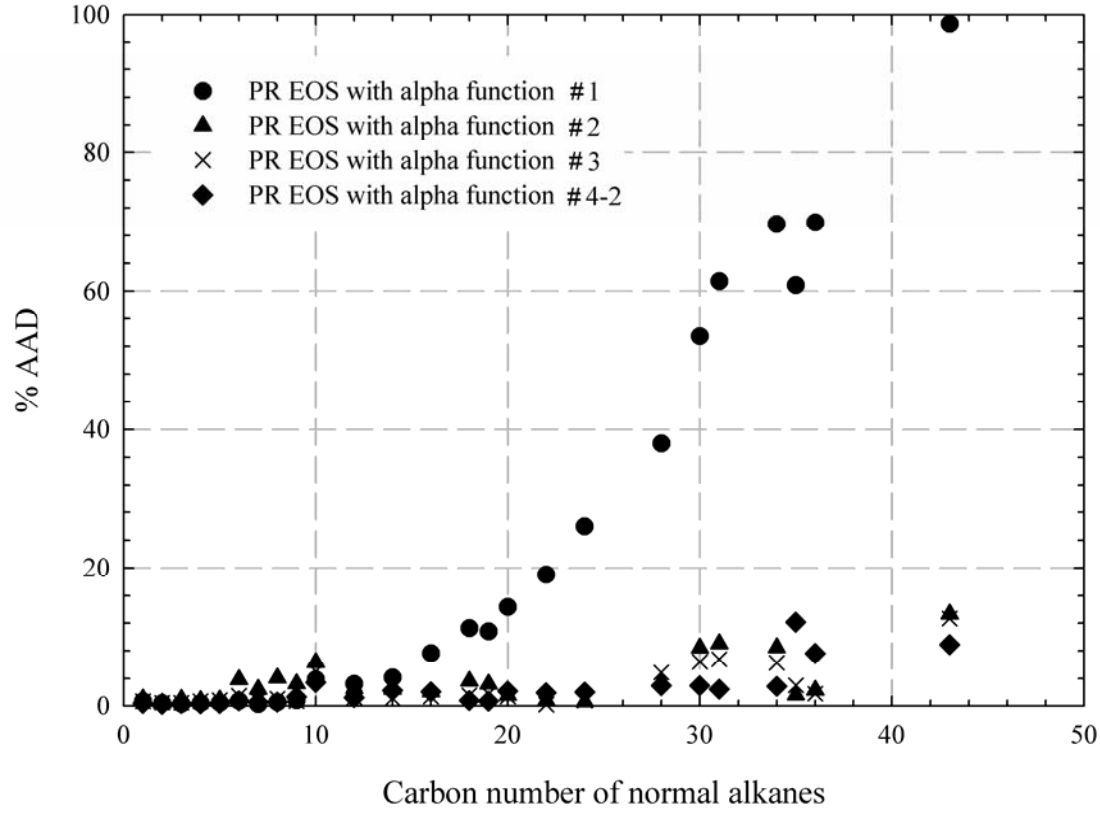

FIGURE 3-5: Overall %AAD of the predicted vapour pressures of normal alkanes using different alpha function models

3.3.2. Enthalpy of vaporization

In order to examine the capability of the newly proposed alpha function in representing other thermodynamic properties, alpha functions #1, 2, 3, and 4-2 are incorporated into the PR EOS to predict the vaporization enthalpy of the compounds as provided in TABLE 3-8. As can be seen from TABLE 3-8, the overall accuracy of the predicted vaporization enthalpy is slightly lower than that of the predicted vapour pressure for each compound. Alpha function #1 is found to yield the largest error in predicting the vaporization enthalpy, especially for the heavy alkanes, while the other three alpha functions demonstrate similar predictive accuracy. Among the four alpha functions examined by this study, the alpha function proposed in this study provides the most accurate prediction of vaporization enthalpy of all the compounds considered in terms of %AAD. This means that the proposed alpha function outperforms either the logarithm-type or Soave-type alpha functions with respect to the predicted vapour pressure and vaporization enthalpy.

3.4 Summary

A new alpha function for the PR EOS is developed to more accurately predict vapour pressure for non-hydrocarbons and hydrocarbon compounds, while the acentric factor is redefined at a reduced temperature of 0.6 and incorporated into the newly developed alpha function. Compared to the other existing alpha functions evaluated, the newly developed alpha function can be used to more accurately predict the vapour pressure for polar or non-polar non-hydrocarbon substances, light hydrocarbons and heavy

TABLE 3-8: The predicted vaporization enthalpy using PR EOS with different alpha functions

Name	%AAD for each model			
	#1	**#2**	**#3**	**#4-2**
Carbon dioxide	5.21	5.17	5.32	5.05
Nitrogen	0.85	0.58	0.32	0.74
Argon	3.24	3.09	3.21	3.10
Water	5.37	4.77	5.91	4.00
Benzene	1.63	1.78	1.18	1.73
Oxygen	1.97	1.57	1.82	1.96
Acetone	2.01	1.28	2.70	1.50
Methanol	8.25	8.19	8.31	7.82
Ethanol	10.96	10.48	9.87	10.52
Methane	3.83	4.18	4.44	3.76
Ethane	2.36	2.35	2.33	2.41
Propane	2.46	2.63	1.53	2.64
n-Pentane	0.14	0.83	0.15	0.47
n-Hexane	0.94	1.72	0.22	0.75
n-Heptane	1.81	2.60	0.67	2.08
n-Octane	2.47	3.19	0.91	1.58
n-Nonane	3.11	3.70	1.16	3.14
n-Decane	0.94	0.75	3.51	0.16
n-Undecane	4.25	4.45	1.62	4.13
n-Dodecane	4.95	4.91	2.04	4.65
n-Tridecane	5.34	4.99	2.16	5.10
n-Tetradecane	7.33	6.83	4.02	6.15

TABLE 3-8: The predicted vaporization enthalpy using PR EOS with different alpha functions (continued)

Name	%AAD for each model			
	#1	**#2**	**#3**	**#4-2**
n-Pentadecane	6.40	5.41	2.81	6.07
n-Hexadecane	8.40	7.33	4.77	6.43
n-Heptadecane	8.38	6.84	4.58	6.34
n-Eicosane	5.54	3.15	2.16	1.51
n-Tetracosane	4.82	0.41	0.08	1.74
n-Octacosane	1.33	8.72	8.36	6.15
n-Triacontane	4.81	1.68	1.48	5.02
n-Hentriacontane	7.56	0.65	0.98	3.03
n-Tetratriacontane	6.65	1.41	0.87	5.00
n-Pentatriacontane	7.19	1.82	1.08	2.29
n-Hexatriacontane	9.37	0.44	1.17	1.23
n-Tritetracontane	17.26	7.56	8.42	1.78
Overall	4.40	4.07	4.17	3.92

hydrocarbons (up to *n*-tritetracontane). It is found that the acentric factor defined at a reduced temperature of 0.6 significantly improves vapour pressure predictions for all the alpha functions evaluated in this study. In addition, the newly developed alpha function has been applied to predict the enthalpy of vaporization of various compounds considered in this study with good accuracy. The modified alpha function obtained in this study leads to the best performance in comparison to either the logarithm-type or Soave-type alpha functions in the literature.

CHAPTER 4 ENHANCED SWELLING EFFECT AND VISCOSITY REDUCTION OF SOLVENT(S)-CO_2-HEAVY OIL SYSTEMS

4.1 Introduction

CO_2 has been found to be an efficient agent for recovering heavy oil resources worldwide through an immiscible displacement process (Tuzunoglu and Bagci, 2000). In a CO_2 immiscible flooding process, oil recovery is enhanced with CO_2 mainly by the following two mechanisms (Al-Abri and Amin, 2010). The most important mechanism is that the lowered crude viscosity due to dissolution of CO_2 in heavy oil results in a reduced average oil saturation by the displacing water. Secondly, dissolution of CO_2 into the oil results in an increased oil volume and a reduced interfacial tension (IFT), and then enhanced production occurs as the reservoir fluid saturations react to accommodate the swollen oil. One major disadvantage associated with CO_2 immiscible process is the limited solubility of CO_2 in heavy oil, resulting in limited swelling effect and viscosity reduction of the CO_2-saturated heavy oil. Addition of alkane solvents (e.g., C_3H_8 and *n*-C_4H_{10}) to the CO_2 stream may enhance performance of CO_2 dissolution in heavy oil. It is essential that swelling effect and viscosity reduction be significantly enhanced for recovering heavy oil in hydrocarbon reservoirs where other EOR methods are not applicable.

In this study, techniques have been developed to examine the advanced swelling effect and viscosity reduction of CO_2-saturated heavy oil with addition of either C_3H_8 or *n*-C_4H_{10}. Experimentally, the enhanced swelling factor of CO_2-heavy oil systems due to addition of either C_3H_8 or *n*-C_4H_{10} is determined. Theoretically, based on the

experimental phase behaviour data in the literature, three binary interaction parameter (BIP) correlations in the PR EOS (Peng and Robinson, 1976) are used for characterizing CO_2-heavy oil systems, C_3H_8-heavy oil systems, and *n*-C_4H_{10}-heavy oil systems, respectively. The PR EOS together with the BIP correlations are used to predict the saturation pressures and swelling factors of the C_3H_8-CO_2-heavy oil system and *n*-C_4H_{10}-CO_2-heavy oil system measured in this study.

4.2 Experimental

4.2.1. Materials

A heavy oil sample is collected from the Lloydminster area in Saskatchewan, Canada. The molecular weight of the Lloydminster heavy oil is measured to be 482 g/mol with a freezing point depression method. The compositional analysis result of the Lloydminster heavy oil is obtained by using the simulated distillation method and provided in TABLE 4-1. It can be seen from TABLE 4-1 that there is no hydrocarbon components lighter than C_9. TABLE 4-2 shows the results of SARA (saturates, aromatics, resins, and asphaltenes) fraction analysis by using an extraction method with alumina. The gas solvents, CO_2, C_3H_8 and *n*-C_4H_{10} (Praxair, Canada), used in the measurements have purities of 99.998 mol%, 99.99 wt%, and 99.5 wt%, respectively. It should be noted that the liquid-phase *n*-C_4H_{10} is originally compressed in a high pressure cylinder. The high pressure cylinder allows for direct withdrawal of liquid *n*-C_4H_{10} from the cylinder. In comparison, only gaseous CO_2 and C_3H_8 can be released from the cylinders and need to be compressed into a liquid phase prior to being injected into the PVT cell.

TABLE 4-1: Compositional analysis result of the Lloydminster heavy oil

Carbon No.	wt%	mol%	Assumed MW*, g/mol	Carbon No.	wt%	mol%	Assumed MW*, g/mol
C_1	0	0	16	C_{31}	1.390	1.42	436
C_2	0	0	30	C_{32}	1.329	1.31	450
C_3	0	0	44	C_{33}	0.981	0.94	464
C_4	0	0	58	C_{34}	1.083	1.01	478
C_5	0	0	72	C_{35}	1.307	1.18	492
C_6	0	0	86	C_{36}	1.343	1.18	506
C_7	0	0	100	C_{37}	0.917	0.78	520
C_8	0	0	114	C_{38}	0.900	0.75	534
C_9	0.786	2.73	128	C_{39}	1.583	1.29	548
C_{10}	0.844	2.64	142	C_{40}	1.600	1.27	562
C_{11}	1.037	2.96	156	C_{41}	0.750	0.58	576
C_{12}	1.267	3.32	170	C_{42}	0.830	0.63	590
C_{13}	1.817	4.39	184	C_{43}	1.380	1.02	604
C_{14}	1.950	4.38	198	C_{44}	0.929	0.67	618
C_{15}	2.300	4.83	212	C_{45}	0.929	0.65	632
C_{16}	2.143	4.22	226	C_{46}	0.700	0.48	646
C_{17}	2.286	4.24	240	C_{47}	0.833	0.56	660
C_{18}	2.238	3.92	254	C_{48}	0.792	0.53	674
C_{19}	2.048	3.40	268	C_{49}	0.792	0.51	688
C_{20}	1.857	2.93	282	C_{50}	0.733	0.46	702
C_{21}	2.071	3.11	296	C_{51}	0.750	0.47	716
C_{22}	1.329	1.91	310	C_{52}	0.717	0.44	730
C_{23}	1.743	2.39	324	C_{53}	0.717	0.43	744
C_{24}	1.571	2.07	338	C_{54}	0.683	0.40	758
C_{25}	1.714	2.17	352	C_{55}	0.650	0.37	772
C_{26}	1.600	1.95	366	C_{56}	0.650	0.37	786
C_{27}	1.583	1.85	380	C_{57}	0.667	0.37	800
C_{28}	1.650	1.86	394	C_{58}	0.667	0.36	814
C_{29}	1.452	1.58	408	C_{59}	0.667	0.36	828
C_{30}	1.281	1.35	422	C_{60+}	36.164	15.01	1072

*Note: The assumed MWs are from Saskatchewan Research Council (SRC).

TABLE 4-2: SARA fraction analysis of the Lloydminster heavy oil

Fraction	Content (wt%)
Saturates	26.2
Aromatics	28.2
Resins	24.2
Asphaltenes	21.4

4.2.2. Viscosity measurements

Ambient conditions: Viscosities of the heavy oil samples at the atmospheric pressure and a temperature range of 298.85 K to 373.15 K were measured by using a cone-plate viscometer (DV-II+, Brookfield Engineering Laboratories, USA). The viscometer has a measurement accuracy of 1.0% of the full scale range. The constant temperature during the viscosity measurement is maintained by using a heated circulating water bath (Haake DC10, Thermo Electron Corporation, USA) with an accuracy of ±0.1 K. The spindle CP-51, which covers the viscosity range of 2.4-48000.0 cP, is used in the measurement. The measured viscosity data for the heavy oil sample are tabulated in TABLE 4-3. A two-parameter double logarithm relation has been applied to fit the measured viscosity data,

$$\log_{10}\left[\log_{10}\left(\mu\right)\right] = -3.7042\log_{10}\left(T\right) + 9.7600 \qquad [4\text{-}1]$$

where μ is the heavy oil viscosity in cP and T is the temperature in K. The fit produces a correlation coefficient of R^2=0.9998.

Reservoir conditions: It is a challenge to determine viscosity of the solvent-saturated heavy oil at a high pressure, which can be measured with either the expensive commercial in-line viscometers or the capillary viscometer (Memon *et al*., 2010). After comparing these two options, Memon *et al.* (2010) concluded that the capillary viscometer is a better choice as the capillary viscometer honours more the bulk flow characteristics of a solvent-saturated heavy oil sample. In this study, a customized-capillary viscometer is constructed and connected to the PVT cell for more accurately determining viscosity of the solvent(s)-saturated heavy oil.

TABLE 4-3: Measured viscosity of the Lloydminster heavy oil at different temperatures

Temperature, K	Viscosity, cP
298.15	8251.0
303.15	5120.0
308.15	2977.0
313.15	1941.0
318.15	1238.0
323.15	825.1
328.15	556.5
333.15	395.0
338.15	287.0
343.15	206.3
348.15	159.7
353.15	127.7
358.15	97.7
363.15	80.5

The capillary tube is a 3 m long stainless steel tubing (Swagelok, Canada) with an inner diameter (ID) of 0.069 in (0.175 cm) and a wall thickness of 0.028 in (0.071 cm). The automatic positive displacement pump (PMP-0500-1-10-MB-316-M4-C0, DBR, Canada) is used to displace the solvent(s)-saturated heavy oil from the PVT cell into the capillary tubing. A back-pressure regulator (BPR) (EB1HP1, Equilibar, USA) is used to maintain its outlet pressure at a desirable point, while a differential pressure transducer (P61, Validyne, USA) is used to measure the pressure drop along the tubing.

Two standard viscosity fluids, i.e., S60 and S20 (Cannon Instrument Company, USA), are used as standard viscosity liquids and injected through the capillary tubing at different injection rates to calibrate the capillary viscometer. The injection rates during calibration are controlled below the flow rates that can induce turbulent flow behaviour. The capillary viscometer is calibrated in the temperature range of 294.15 to 321.55 K and pressure range of 101.3 kPa to 5000.0 kPa by using S60 as well as in the temperature range of 294.15 to 321.85 K and pressure range of 101.3 kPa to 5000.0 kPa by using S20. S60 has viscosities of 132.1 cP at 294.15 K and 32.7 cP at 321.55 K, respectively.

FIGURE 4-1 shows effect of BPR pressure on the measured differential pressures across the capillary viscometer at different flow rates for viscosity standards S60 and S20, respectively. Because the viscosity data for the viscosity standard S60 or S20 at pressures higher than 101.3 kPa are not available, constant viscosity is assumed to be valid at a given temperature and in the pressure range of 101.3 kPa to 5000.0 kPa. This assumption is well supported by FIGURE 4-1. As can be seen in FIGURE 4-1, the measured differential pressures follow a good linear relationship with the flow rates. This implies that a constant k value is accurate to represent the viscosity in the pressure range of 101.3

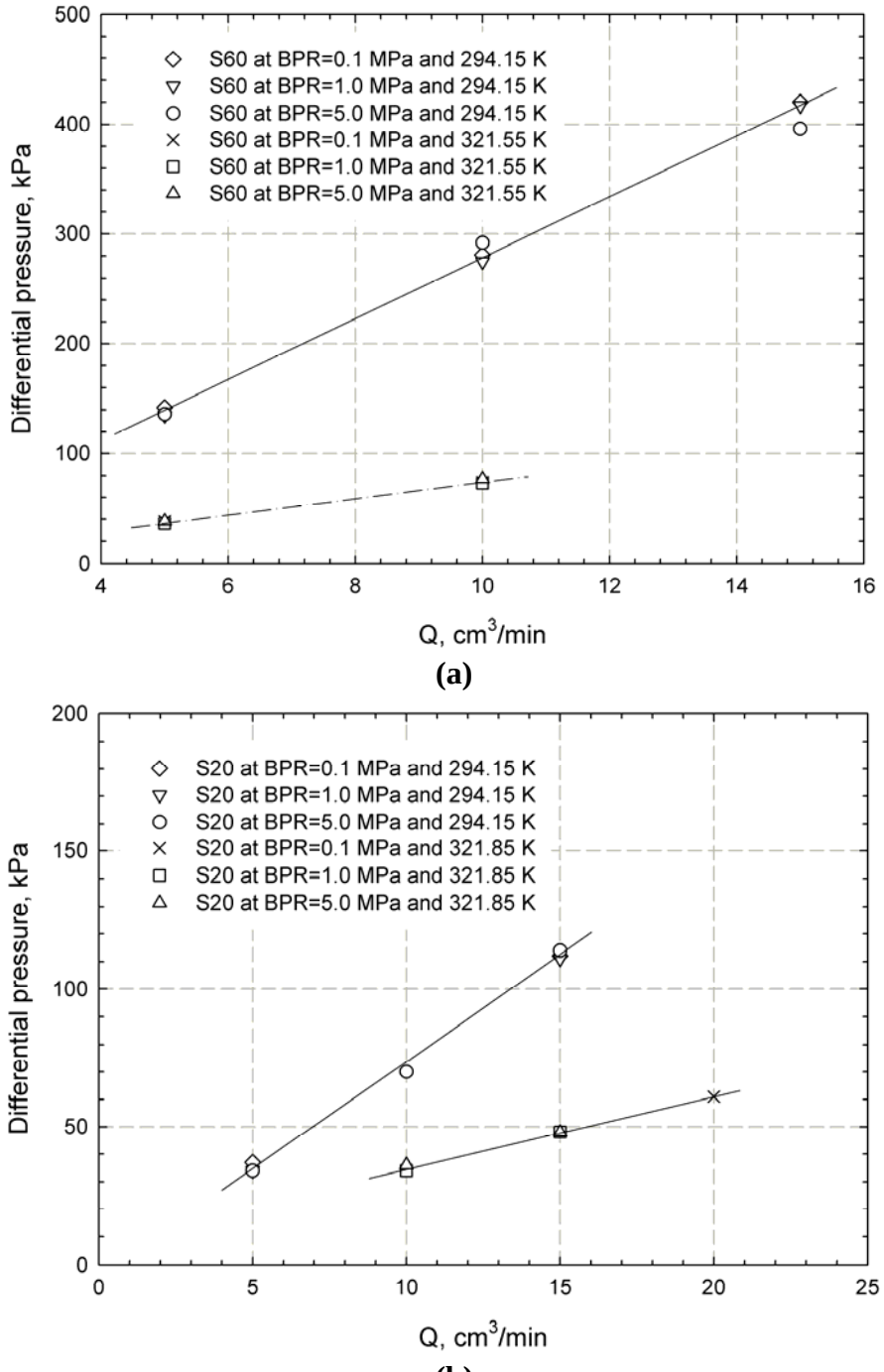

FIGURE 4-1: Effect of BPR pressure on the measured differential pressures across the capillary viscometer at different flow rates for (a) viscosity standard S60; and (b) viscosity standard S20

kPa to 5000.0 kPa at a given temperature, and pressures in the range of 101.3 kPa to 5000.0 kPa have a minor effect on the viscosity of liquid materials.

In practice, at a relatively low pressure, which is often lower than 10000.0 kPa for heavy oil applications, change of pressure in the range of 101.3 kPa to 10000.0 kPa on the single-phase liquid materials imposes a minor effect on the viscosity (Nagashima, 1977; Vogel *et al.*, 1998; Younglove and Ely, 1987). FIGURE 4-2 shows effect of pressure on the water viscosity and C_3H_8 viscosity at different temperatures, respectively. As can be seen from FIGURE 4-2, at pressures lower than 30000.0 kPa, change of pressure shows only a minor effect on the measured viscosity. Again, although the viscosity data for S60 and S20 at high pressures are not available, it is reasonable to consider that the effect of pressure change in the range of 101.3 kPa to10000.0 kPa on the liquid-phase S60 and S20 can be neglected.

FIGURE 4-3 shows effect of temperature on the calculated *k* constant of the capillary viscometer. It can be seen that the *k* constant is slightly reduced at a higher temperature. The degree of reduction for viscosity standard S60 is smaller than that for viscosity standard S20. A linear regression of *k* values as a function of temperature is applied by taking into account all the measured *k* values at different temperatures and pressures for S60 and S20. The following simplified Poiseuille equation is obtained for the capillary tube used in this study,

$$\mu = k\frac{\Delta P}{Q} = \left(14.3671 - 0.0324T\right)\frac{\Delta P}{Q} \qquad [4\text{-}2]$$

where *k* is a temperature-dependant characteristic factor, ΔP is differential pressure in kPa, and *Q* is flow rate in cm^3/min. The capillary viscometer has an overall accuracy of ±6.0%.

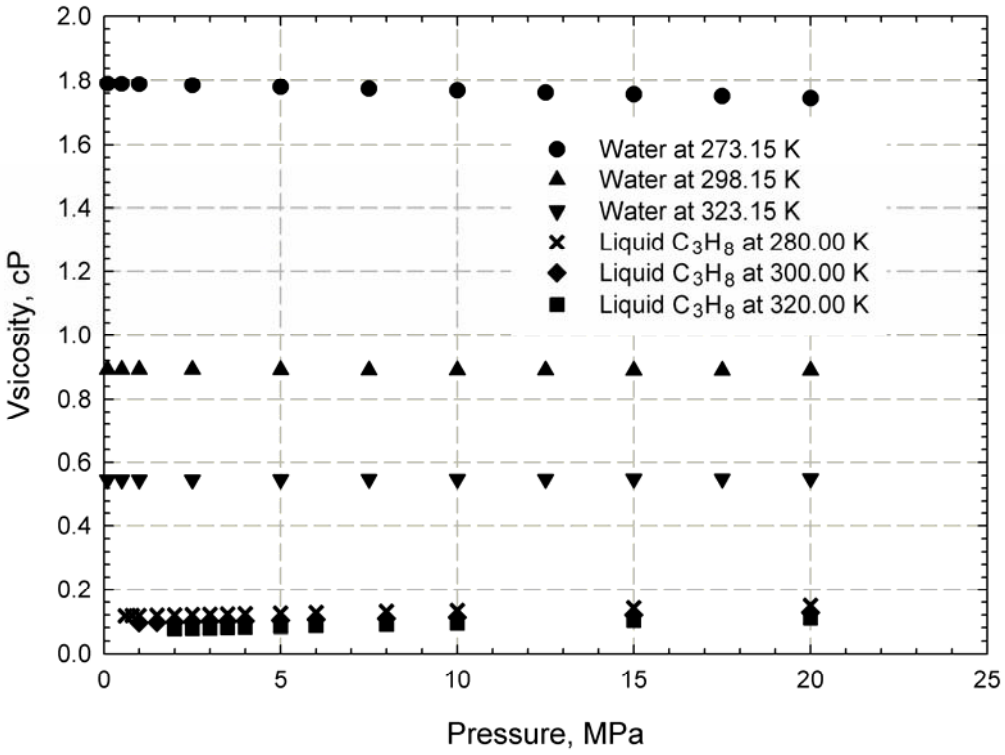

FIGURE 4-2: Effect of pressure on the water viscosity and C_3H_8 viscosity at different temperatures, respectively (Nagashima, 1977; Vogel *et al.*, 1998; Younglove and Ely, 1987)

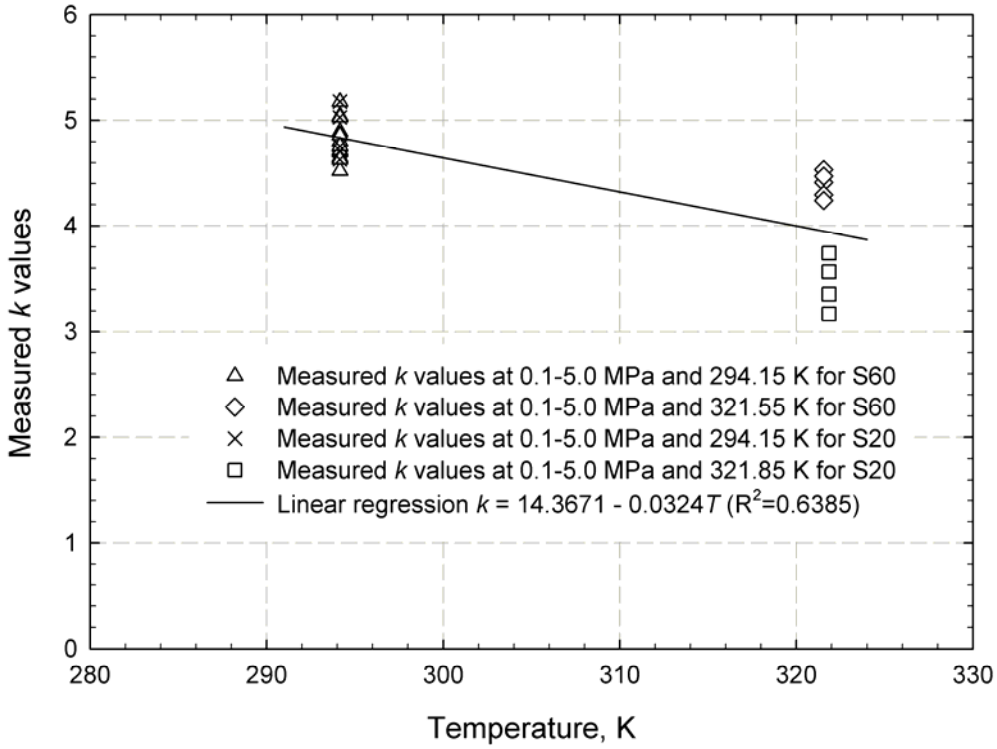

FIGURE 4-3: Effect of temperature on the calculated *k* constant of the capillary viscometer

As for the PVT measurements, viscosity of saturated CO_2, C_3H_8 and n-C_4H_{10} can be determined from correlations in the following form (Yaws, 2003), respectively.

$$\log_{10}(\mu_s) = d + \frac{e}{T} + fT + gT^2 \qquad [4\text{-}3]$$

where μ_s is the viscosity of the liquid solvent in cP, d, e, f and g are the coefficients with the corresponding values for CO_2, C_3H_8 and n-C_4H_{10} listed in TABLE 4-4. It should be noted that Equation [4-3] is only valid at temperatures below the critical value for a given solvent.

4.2.3. Density measurements

Densities of the heavy oil at a pressure range of 600.0 to 12600.0 kPa and a temperature range of 298.15 K to 348.15 K are measured by using a densitometer (DMA512P, Anton Paar, USA) with a repeatability of 1×10^{-5} g/cm^3. Prior to density measurement, the densitometer needs to be calibrated within the temperature and pressure range of interest. The densitometer has been calibrated by using deionized water as the test medium in a temperature range of 298.15 K to 348.15 K and a pressure range of 600.0-12600.0 kPa, respectively. At a given temperature and pressure, the oscillation period of density sensor can be recorded. The reference densities of water at various temperatures and pressures are found from the property tables summarized by Wagner and Pruß (2002). Then a calibration formula which correlates water density with pressure, temperature and oscillation period can be developed. Hence, density of a heavy oil sample can be calculated via the calibration equation by reading the oscillation period from the densitometer at a given temperature and a specified pressure.

TABLE 4-4: The coefficient values in Equations [4-3] and [4-6]

Gas	***d***	***e***	***f***	***g***	***h***	***l***	***n***
CO_2	-19.4920	1594.8000	0.0793	-1.2025E-04	0.4638	0.2616	0.2903
C_3H_8	-3.1759	297.1200	0.0095	-1.8781E-05	0.2215	0.2774	0.2870
n-C_4H_{10}	-6.8590	673.9300	0.0220	-3.0686E-05	0.2283	0.2724	0.2863

A high-precision syringe pump (500HP, ISCO Inc., USA) applies a given pressure to the cylinder that contains the Lloydminster heavy oil sample. The heated circulating water bath (Haake DC10, Thermo Electron Corporation, USA) is also used to maintain a constant temperature environment for the densitometer. In this study, the well-known Tait equation is used to reproduce the measured heavy oil density data (Goncalves *et al.*, 2010),

$$\rho_o(T,P) = \frac{\rho_0(T,P_0)}{1-\beta \ln\left(\frac{B+0.001P}{B+0.1}\right)} \quad [4\text{-}4]$$

where

$$\rho_0(T,P_0) = 784.0044 + 1.7217T - 3.3752\times10^{-3}T^2 \quad [4\text{-}5a]$$

$$\beta = \left(-6.1774 + 0.0213T\right) \quad [4\text{-}5b]$$

$$B = 3.7614\times10^4 - 1.8009\times10^7 T^{-1} + 2.0605\times10^9 T^{-2} \quad [4\text{-}5c]$$

where ρ is the heavy oil density in kg/m^3 and P is pressure in kPa. The values of the coefficients in the above equations are determined by regressing the heavy oil density data. The fit is accurate with a correlation coefficient of R^2=0.9999. FIGURE 4-4 shows the comparison of the measured and calculated density of Lloydminster heavy oil.

Density of the saturated CO_2, C_3H_8 and n-C_4H_{10} can be determined from correlations in the following form (Yaws, 2003), respectively.

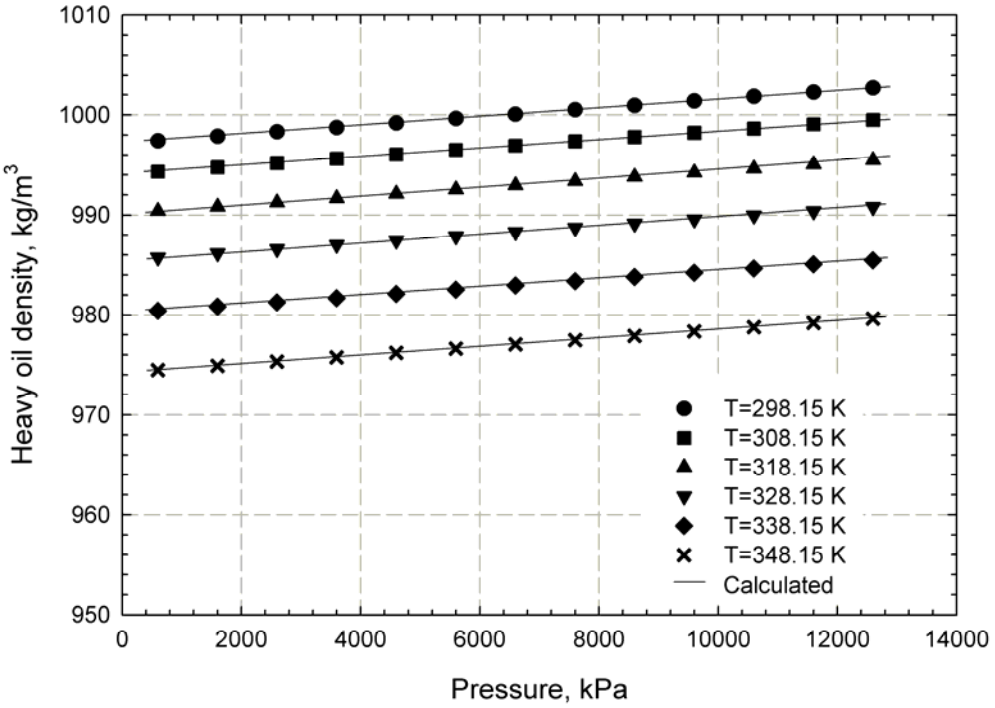

FIGURE 4-4: Comparison of the measured and calculated density of Lloydminster heavy oil

$$\log_{10}\left(\frac{\rho_s}{1000}\right) = \log_{10}(h) - \log_{10}(l)\left(1-\frac{T}{T_c}\right)^n \qquad [4\text{-}6]$$

where ρ_s is the density of the liquid solvent in kg/m^3, T_c is the critical temperature of the solvent, h, l and n are the coefficients with the corresponding values for CO_2, C_3H_8 and n-C_4H_{10} listed in TABLE 4-4. It should be noted that Equation [4-6] is only valid at temperatures below the critical value for a given solvent. Comparison of the calculated saturated-densities and viscosities for CO_2, C_3H_8 and n-C_4H_{10} via Equations [4-3] and [4-6] and the measured data in the literature (Younglove and Ely, 1987) indicates an excellent agreement (See FIGURE 4-5), justifying the use of Equations [4-3] and [4-6].

4.2.4. PVT measurements

In this study, the saturation pressures and swelling factors of 12 solvent(s)-CO_2-heavy oil systems have been experimentally measured by using the PVT system. The compositions of these 12 feeds are displayed in TABLE 4-5. All the PVT measurements for the solvent(s)-CO_2-heavy oil systems are performed by using a mercury-free DBR PVT system (PVT-0150-100-200-316-155, DBR, Canada). FIGURE 4-6 is a schematic diagram of the DBR PVT system together with a customized capillary viscometer. The major component of this system is a visual, high-pressure PVT cell, where fluid samples are encapsulated inside a glass tube. The glass tube has an inner diameter of 3.177 cm and a total length of 20.320 cm. In addition to the Heise pressure gauge used in the PVT system, a high-precision test gauge (2089, Ashcroft, USA) with an accuracy of 0.05% full scale of 13789.5 kPa (2000 psia), as indicated in FIGURE 4-6, is attached to the inlet tubing of the PVT cell for more accurate reading of the cell pressure.

The PVT cell has a maximum sample volume of 130 cm^3, while it can sustain

TABLE 4-5: Compositions of the C_3H_8-*n*-C_4H_{10}-CO_2-heavy oil mixtures tested

	Composition, wt%				Composition, mol%			
Feed No.	**C_3H_8**	***n*-C_4H_{10}**	**CO_2**	**Heavy oil**	**C_3H_8**	***n*-C_4H_{10}**	**CO_2**	**Heavy oil**
1	11.5	0.0	0.0	88.5	58.8	0.0	0.0	41.2
2	14.8	0.0	0.0	85.2	65.6	0.0	0.0	34.4
3	20.9	0.0	0.0	79.1	74.4	0.0	0.0	25.6
4	11.4	0.0	0.0	88.6	58.5	0.0	0.0	41.5
5	19.8	0.0	0.0	80.2	73.0	0.0	0.0	27.0
6	29.3	0.0	0.0	70.7	81.9	0.0	0.0	18.1
7	15.8	0.0	0.0	84.2	67.3	0.0	0.0	32.7
8	0.0	16.4	0.0	83.6	0.0	62.0	0.0	38.0
9	0.0	36.2	0.0	63.8	0.0	82.5	0.0	17.5
10	14.2	5.3	0.0	80.5	55.4	15.8	0.0	28.8
11	10.3	0.0	11.0	78.7	36.2	0.0	38.6	25.2
12	0.0	10.1	7.0	82.9	0.0	34.3	31.7	34.0

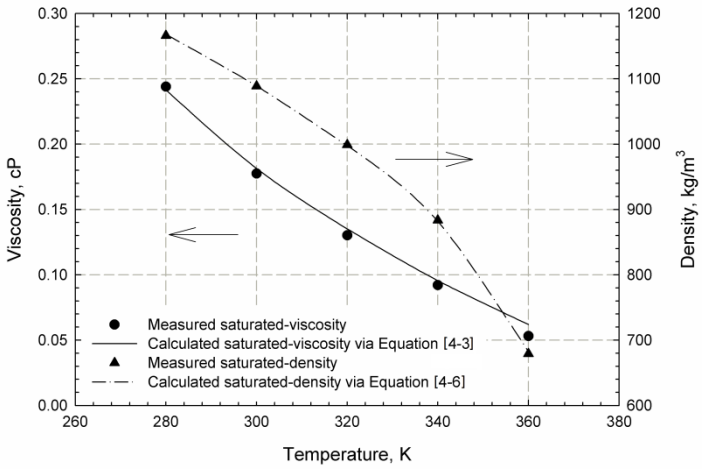

(a)

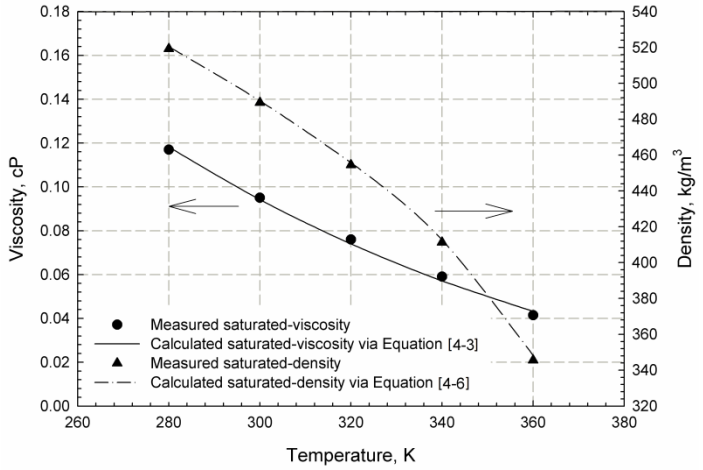

(b)

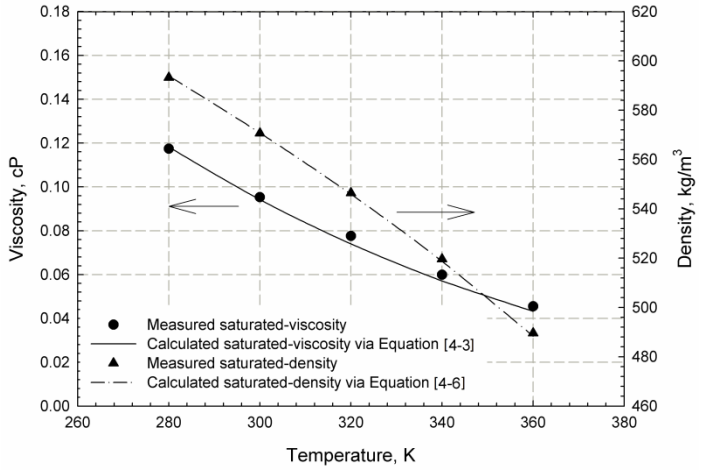

(c)

FIGURE 4-5: Comparison of the calculated saturated-densities and viscosities via Equations [4-3] and [4-6] and the measured data (Younglove and Ely, 1987; Vesovic *et al.*, 1990; Span and Wagner, 1996) for (a) CO_2, (b) C_3H_8 and (c) *n*-C_4H_{10}, respectively

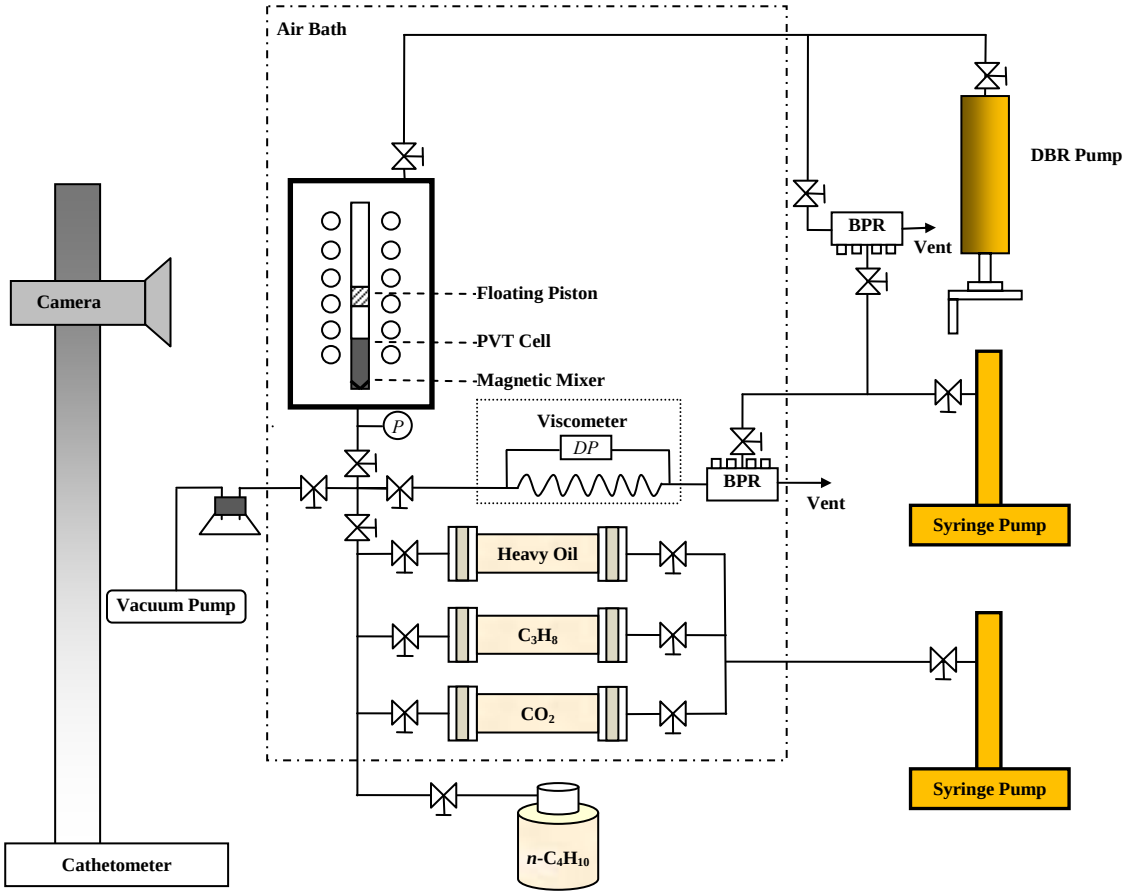

FIGURE 4-6: Schematic diagram of experimental setup for conducting the PVT measurements for solvent(s)-CO_2-heavy oil systems

pressures up to 69000.0 kPa and its working temperature ranges from 238.15 K to 473.15 K. Inside the glass tube, the fluid samples are isolated from the hydraulic oil by a moveable isolation piston. The cell pressure can be readily varied by using a high-pressure automatic positive-displacement pump (PMP-0500-1-10-MB-316-M4-C0, DBR, Canada) so as to move the floating piston downward or upward. A video-based digital cathetometer with a measurement resolution of 0.002 cm allows direct and accurate measurements of the cell volume. The PVT cell is also equipped with a magnetically coupled mixer, which can be used to effectively mix the fluid system when the fluid viscosity is lower than 100 cP at 298.15 K. The PVT cell and three sample cylinders used to pressurize heavy oil, CO_2 and C_3H_8, respectively, are housed inside a constant-temperature air bath. The air bath temperature is controlled to be accurate within ±0.1 K by using a microprocessor-based controller in conjunction with a resistance temperature device (RTD) sensor.

A fairly high pressure is required when injecting heavy oil sample from the cylinder into the PVT cell due to the long tubing used in the original DBR PVT system. It also needs strenuous effort to cleanse the heavy oil left in the long tubing. In order to enable the PVT system to more easily handle heavy oil sample, a customized-injection tubing assembly with a minimized length is adopted in this study (See FIGURE 4-6).

Saturation pressure and swelling factor: Prior to each test, the PVT cell and fluid handling tubing are thoroughly cleaned with kerosene, flushed with air and finally evacuated to remove any traces of the kerosene and air. Prior to each measurement, the temperature of the air bath is set to the desired value for 12 h so that the sample cylinders and the PVT cell are able to reach the preset constant temperature.

In order to expedite the mass transfer process between gas solvent and heavy oil, solvents (i.e., CO_2 and C_3H_8) are firstly compressed into liquid phase in the transfer cylinders, while liquid *n*-C_4H_{10} can be directly released from the gas cylinder. As for pure solvent-heavy oil systems, the experimental procedure is briefly described as follows.

The density of a liquid solvent in the PVT cell is calculated via Equation [4-6], while the volume of the liquid solvent is measured by using the cathetometer. Consequently, the mass of solvent injected can be obtained. The magnetic mixer is turned on after solvent injection. A certain amount of heavy oil is then added to the PVT cell by maintaining a constant pressure inside the PVT cell, ensuring the mixture is in the liquid phase. The volume of heavy oil added is determined to be the total volume reading from the cathetometer minus the solvent volume, assuming that there is no volume change due to the mixing of solvent and heavy oil since the volume measurement is conducted right after the heavy oil is injected into the PVT cell. The mass of heavy oil added can be then determined by calculating its density via Equation [4-6]. The solvent-heavy oil mixture is vigorously stirred for 6 h prior to any further measurement.

As for solvent mixture and heavy oil systems, the liquefied solvent with a lower vapour pressure is firstly introduced into the PVT cell. Then another liquefied solvent with a higher vapour pressure is injected into the PVT cell with a pressure just over its vapour pressure. The mass of the second solvent injected can be determined from the volume reading and density equation again. Subsequently, measurement of the bubble-point pressure for the mixture is further conducted to examine the accuracy of the solvent mixture composition. In this study, there exists a good agreement between the measured bubble-point pressure and the value calculated by using PR EOS. Heavy oil is finally

added to the solvent mixture with the pressure maintained just above the saturation pressure of the solvent mixture so that the expected overall composition can be achieved (Badamchi-Zadeh *et al.*, 2009b).

In general, two methods have been made available for determining the saturation pressure of solvent-heavy oil systems, i.e., continuous depressurization method (Badamchi-Zadeh *et al.*, 2009a; Memon *et al.*, 2010) and discrete depressurization method (Badamchi-Zadeh *et al.*, 2009a). A pressure-volume relationship curve can be obtained for either of the two methods. The saturation pressure is conventionally determined by locating the transitioning point on the pressure-volume curve. It is worth noting that, as for both methods, the magnetic stirrer is always kept on to rigorously stir the solvent and heavy oil mixtures in order to significantly shorten the time for the mixture to reach its equilibrium state.

As for the continuous depressurization method, the solvent(s)-heavy oil mixture is depressurized starting from liquid state at a low-enough withdrawal rate while keeping the magnetic mixer on. As for the discrete depressurization method, prior to any volume and pressure readings, the mixture is depressurized step by step while keeping the magnetic mixer on. Long-enough equilibration time is allowed for each step until the pressure inside the PVT cell reaches a stable value. The discrete depressurization method is considered to be more accurate since it can mitigate the supersaturation phenomenon that would otherwise occur in the continuous depressurization method (Badamchi-Zadeh *et al.*, 2009a). In this study, both methods are tested and compared. For the continuous depressurization method, a withdrawal rate of 3 cm^3/h is used, while for the discrete depressurization method, 12 h are found to be adequate for the system pressure to reach a

stable value and hence allotted to each step. It is worthwhile noting that both the saturation pressure and the mixture volume at the saturation pressure can be read from the transitioning point on the pressure-volume curve. Consequently, the swelling factor of the heavy oil at a given temperature can be determined to be the mixture volume at saturation point divided by the volume of heavy oil at atmospheric pressure and the given temperature.

Viscosity of the solvent(s)-saturated heavy oil: Prior to each viscosity measurement, the capillary tubing is cleaned with kerosene, flushed with air for 4 h, and finally vacuumed. The whole capillary viscometer setup is also placed in the PVT air bath to ensure it has the same temperature as the PVT cell. The BPR pressure is set at a pre-specified value which is well above the measured saturation pressure of a given solvent(s)-heavy oil mixture to prevent the occurrence of gas-liquid two-phase flow in the capillary tube. A high-accuracy syringe pump (500HP, Teledyne ISCO Inc., USA) is used to apply pressure on the BPR. After each saturation pressure measurement, the solvent(s)-saturated heavy oil is displaced into the capillary tubing by using the automatic displacement pump at a given flow rate. The differential pressure reading is recorded once it reaches a stable value. Then Equation [4-2] is then used to determine the viscosity of the solvent(s)-saturated heavy oil. In this study, the viscosity measurements are performed for the C_3H_8-heavy oil system, *n*-C_4H_{10}-heavy oil system, and *n*-C_4H_{10}-CO_2-heavy oil system at 298.85 K, and the C_3H_8-CO_2-heavy oil system at 318.75 K, respectively.

In this study, the pressure measurement, volume measurement, temperature measurement, determination of mixture composition, and viscosity measurement have uncertainties of ±6.9 kPa, $\pm 1.59\times10^{-2}$ cm^3, ±0.1 K, ±3.0 wt%, and ±6.0%, respectively.

4.3 Mathematical Formulation

4.3.1. PR EOS model

Due to its wide application in the petroleum and chemical industries, the PR EOS is chosen as the equation of state for describing phase behaviour of solvent(s)-CO_2-heavy oil systems. The detailed expressions of the PR EOS can be found in CHAPTER 3 of this dissertation. The new alpha function for the PR EOS is used to more accurately predict the low vapour pressures for heavy hydrocarbons. The new alpha function is expressed by,

$$\alpha = \exp\left\{\begin{array}{l}\left(0.13280-0.05052\omega+0.25948\omega^2\right)\left(1-T_{\mathrm{r}}\right)+\\ 0.81769\ln\left[1+\left(0.31355+1.86745\omega-0.52604\omega^2\right)\left(1-\sqrt{T_{\mathrm{r}}}\right)\right]^2\end{array}\right\} \qquad [4\text{-}7]$$

For a mixture system, the following van der Waals mixing rule is used,

$$a=\sum_{i=1}^{nc}\sum_{j=1}^{nc}x_i x_j\left(1-\delta_{ij}\right)\sqrt{a_i a_j} \qquad [4\text{-}8]$$

$$b=\sum_{i=1}^{nc}x_i b_i \qquad [4\text{-}9]$$

where nc is number of components in the mixture, x_i is mole fraction of the ith component in the mixture, a_i and b_i are calculated from Equations [3-2] and [3-4] for the ith component, respectively, and δ_{ij} is BIP between the ith component and the jth component.

In this study, molar volume of the liquid or vapour phase is calculated with a volume-translation strategy. In a volume-translated PR EOS framework, the corrected molar volume is simply related to the EOS-calculated molar volume by (Peneloux *et al.*, 1982),

$$V_{\text{corrected}} = V - C \qquad [4\text{-}10]$$

where $V_{\text{corrected}}$ is corrected molar volume, V is original molar volume calculated by the PR EOS, and C is a component-specific correction factor. The correction factor of a pure component is given as follows (Peneloux *et al.*, 1982),

$$C = 0.40768\left(\frac{RT_{\text{c}}}{P_{\text{c}}}\right)\left(0.29441 - Z_{\text{RA}}\right) \qquad [4\text{-}11]$$

where Z_{RA} is Rackett parameter that is a constant for a given substance. The Rackett parameter of a heavy oil sample can be calculated by applying the following equation at 60°F (Spencer and Danner, 1972),

$$V^* = \frac{RT_{\text{c}}}{P_{\text{c}}} Z_{\text{RA}}^{\left[1+\left(1-T_{\text{r}}^*\right)^{2/7}\right]} = \frac{MW}{SG} \qquad [4\text{-}12]$$

where V^* is molar volume of heavy oil at 60°F, and T_r^* is reduced temperature evaluated at 60°F. Solving Z_{RA} from Equation [4-12] results in the Rackett parameter for heavy oil,

$$Z_{\text{RA}} = \left(\frac{MW \cdot P_{\text{c}}}{RT_{\text{c}} \cdot SG}\right)^{\frac{1}{\left[1+\left(1-T_{\text{r}}^*\right)^{2/7}\right]}} \qquad [4\text{-}13]$$

Peneloux *et al.* (1982) extended Equation [4-10] to a multicomponent mixture by using the following mole-composition based mixing rule,

$$V_{\text{corrected}} = V - \sum_{i=1}^{nc} x_i C_i \qquad [4\text{-}14]$$

By treating each crude oil as a single pseudocomponent and characterizing it with specific gravity and normal boiling point or Watson factor, Mullken and Sandler (1980) proposed a CO_2-heavy oil BIP correlation with a better accuracy for determining both CO_2 solubility and swelling factor of the CO_2-saturated oil. It should be pointed out that normal boiling point or Watson factor is usually unavailable for heavy oil samples. However, molecular weight is a more accessible parameter for heavy oils that are documented in the literature than either normal boiling point or Watson factor.

In this study, each heavy oil sample is also treated as a single pseudocomponent, while specific gravity and molecular weight are used as the two parameters that characterize each heavy oil sample. As recommended by Whitson and Brule (2000), the Soreide correlation (Soreide, 1989) is used to calculate normal boiling point of heavy oil from molecular weight and specific gravity, while the commonly used Kesler-Lee correlations (Lee and Kesler, 1975; Kesler and Lee, 1976) are used to calculate critical properties of heavy oil based on normal boiling point and specific gravity. In addition, more solubility data for CO_2-heavy oil and C_3H_8-heavy oil systems are included in the database for developing the BIP correlations. One reason to characterize heavy oil as one pseudocomponent is to make the model presented in this work predictive in nature.

4.3.2. BIP correlations

Once the heavy oil is characterized by its critical properties, the BIP matrix (δ) remains to be a single parameter that is needed in the PR EOS to model the phase behaviour of solvent(s)-heavy oil systems at given conditions. Three solvents (i.e., CO_2, C_3H_8, and *n*-C_4H_{10}) are used in this study. For the purpose of convenience, CO_2, C_3H_8, *n*-C_4H_{10} and heavy oil are designated as Components #1, #2, #3 and #4, respectively.

TABLE 4-6 shows the BIP matrix for a four-component fluid system which is comprised of CO_2, C_3H_8, n-C_4H_{10} and heavy oil. The fixed δ_{12} for CO_2-C_3H_8 binary and δ_{13} for CO_2-n-C_4H_{10} binary are rigorously reviewed values retrieved from a commercial simulator (Computer Modelling Group, 2009). δ_{23} for C_3H_8-n-C_4H_{10} binary is calculated to be 0.00087 by using a hydrocarbon-hydrocarbon BIP correlation (Mehra, 1981).

TABLE 4-7 lists the phase behaviour database for binary CO_2-heavy oil system used for developing δ_{14} correlation, while TABLE 4-8 shows the database for C_3H_8-heavy oil system used for developing δ_{24} correlation. The δ_{34} correlation for n-C_4H_{10}-Lloydminster heavy oil system is developed based on the experimental data measured in this study. The heavy oils that have both specific gravity and molecular weight available are included in the database. The calculated critical properties of each oil sample are also provided in TABLEs 4-7 and 4-8, respectively. For each isotherm solubility data set, the BIP is optimized by minimizing the root-mean-squared relative error (*RMSRE*) between the measured and calculated solvent solubility in heavy oil,

$$RMSRE_X = \sqrt{\frac{1}{N}\sum_{i=1}^{N}\left[\frac{X_i^{\text{cal}} - X_i^{\text{exp}}}{X_i^{\text{exp}}}\right]^2} \qquad [4\text{-}15]$$

where X_i^{cal} is the calculated solvent solubility in heavy oil, X_i^{exp} is the measured solvent solubility in heavy oil, and N is number of data point along each isotherm. Once all the optimum BIPs are obtained for every isotherm of each oil sample, the optimum BIPs are correlated with the following linear equation (Mullken and Sandler, 1980),

$$\delta = F - G \cdot T_{\text{r}} - H \cdot SG - K \cdot \omega \qquad [4\text{-}16]$$

where F, G, H, and K are coefficients. The swelling factor of solvent-saturated heavy oil can be calculated via the following equation (Teja and Sandler, 1980),

TABLE 4-6: BIP matrix for the *n*-C_4H_{10}-C_3H_8-CO_2-heavy oil system

Component	**CO_2**	**C_3H_8**	***n*-C_4H_{10}**	**Heavy oil**
CO_2	0	0.13500	0.13000	δ_{14}
C_3H_8	0.13500	0	0.00087	δ_{24}
n-C_4H_{10}	0.13000	0.00087	0	δ_{34}
Heavy oil	δ_{14}	δ_{24}	δ_{34}	0

TABLE 4-7: Database for developing the BIP correlation for CO_2-heavy oil systems

Oil	MW	SG @ 60ºF	T_c, K	P_c, kPa	ω	Swelling factor	Reference
Senlac heavy oil	440	0.9718	908.16	1250.17	1.0095	Yes	Strivastava *et al.*, 1999
A	350	0.9509	861.00	1472.77	0.8831	Yes	Simon and Graue, 1965
B[a]	236	0.8586	753.01	1689.54	0.7168	Yes	Simon and Graue, 1965
C[a]	345	0.8586	824.42	1041.61	1.0251	Yes	Simon and Graue, 1965
D	358	0.9446	862.28	1408.55	0.9100	Yes	Simon and Graue, 1965
E	463	0.9759	918.26	1203.77	1.0374	Yes	Simon and Graue, 1965
F	330	0.9854	866.57	1721.62	0.7954	Yes	Simon and Graue, 1965
G[a]	373	0.8996	852.76	1130.91	1.0164	Yes	Simon and Graue, 1965
H	458	0.9868	920.44	1268.55	1.0095	Yes	Simon and Graue, 1965
I	370	0.9452	868.24	1362.96	0.9340	Yes	Simon and Graue, 1965
Athabasca bitumen	552	1.0070	958.33	1139.11	1.0936	No	Mehrotra and Svrcek, 1982; Mehrotra and Svrcek, 1985a; Fu *et al.*, 1985
Wabasca bitumen	446.5	1.0070	924.07	1396.28	0.9589	No	Mehrotra and Svrcek, 1985a
Saskatchewan oil	423	0.9653[b]	899.02	1271.37	0.9938	Yes	Jha, 1986
Cold lake bitumen	533	1.0484	967.49	1373.82	0.9933	No	Mehrotra and Svrcek, 1988; Yu *et al.*, 1989
Peace river bitumen	542	0.9974[c]	952.09	1115.30	1.1016	No	Svrcek and Mehrotra, 1989
Lindbergh heavy oil	490	0.9678	925.07	1096.63	1.0930	No	Sayegh *et al.*, 1990
Suffield heavy oil[d]	358	0.9533	865.82	1450.10	0.8959	Yes	Kodal and Sayegh, 1992
West Sask. oil #1	330	0.9433	847.74	1526.89	0.8535	No	DeRuiter *et al.*, 1994
West Sask. oil #2	446	0.9725	910.70	1235.70	1.0177	No	DeRuiter *et al.*, 1994

Note:
[a] These oil are dead oils with a vapour pressure lower than 1 atm.
[b] The SG is reported at 68ºF.
[c] The SG is averaged from the SGs of pseudocomponents reported in the corresponding literature.
[d] Solubility data are based on the average of reported data at the top and bottom of mixture.

TABLE 4-8: Database for developing the BIP correlation for C_3H_8-heavy oil systems

Oil	MW	SG @ 60°F	T_c, K	P_c, kPa	ω	Swelling factor	Reference
Athabasca bitumen	552	1.0070	958.33	1139.11	1.0936	No	Badamchi-Zadeh *et al.*, 2009a
Peace river bitumen	542	0.9974	952.09	1115.30	1.1016	No	Das and Butler, 1996
Winter heavy oil	412	0.9730	897.51	1343.27	0.9654	No	Freitag *et al.*, 2005
Lloydminster heavy oil	432.33[a]	0.9880	911.38	1349.27	0.9725	Yes	Luo *et al.*, 2007; Luo and Gu, 2007

Note:
[a] The MW is averaged from the MWs of pseudocomponents reported in the literature.

$$SF = \frac{V_{s2}}{V_{s1}} \times \frac{1}{1-X} \qquad [4\text{-}17]$$

where SF is swelling factor, V_{s1} is molar volume of heavy oil at atmospheric pressure and saturation temperature, V_{s2} is molar volume of solvent-saturated heavy oil at saturation pressure and saturation temperature, and X is solvent solubility in mole fraction.

CO_2-heavy oil systems: The following BIP correlation is obtained for CO_2-heavy oil systems,

$$\delta_{14} = -0.5462 T/T_c - 0.4596 SG - 0.0238\omega + 0.7523 \qquad [4\text{-}18]$$

where SG, and ω are specific gravity and acentric factor of heavy oil, respectively. The standard errors of the coefficients in Equation [4-18] are 0.0458, 0.0565, 0.0192 and 0.0626, respectively. Equation [4-18] indicates that the BIP between CO_2 and heavy oil has a negative dependence on the reduced temperature. FIGURE 4-7a shows the parity chart of the measured and calculated CO_2 solubility by using Equation [4-18]. There exists a good agreement between the measured and calculated CO_2 solubility with a percentage absolute average deviation (%AAD) of 7.00% for the 208 solubility data points. In addition, the PR EOS with Equation [4-18] has been applied to predict the swelling factor of the CO_2-saturated oils. FIGURE 4-7b shows the parity chart of the measured and calculated swelling factor. As can be seen from FIGURE 4-7b, a very accurate prediction of the swelling factor is achieved with a %AAD of only 1.80% for the 53 data points.

C_3H_8-heavy oil systems: As for the C_3H_8-heavy oil system, it is found that the BIP shows a weak dependence on specific gravity and acentric factor, but a strong dependence on the reduced temperature. Hence, the following BIP correlation for C_3H_8-

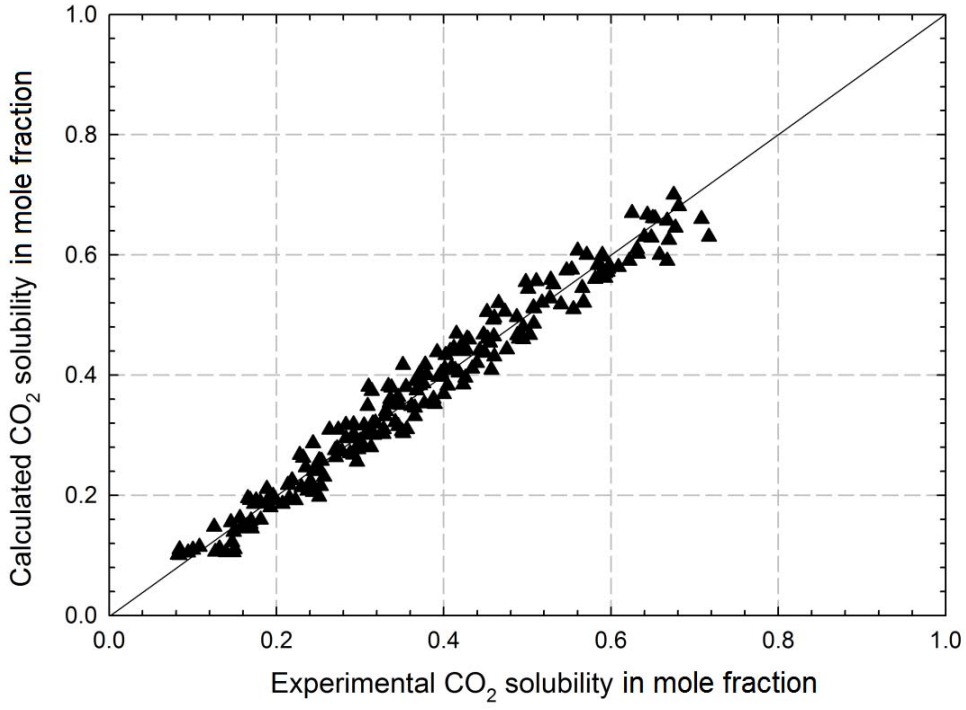

(a)

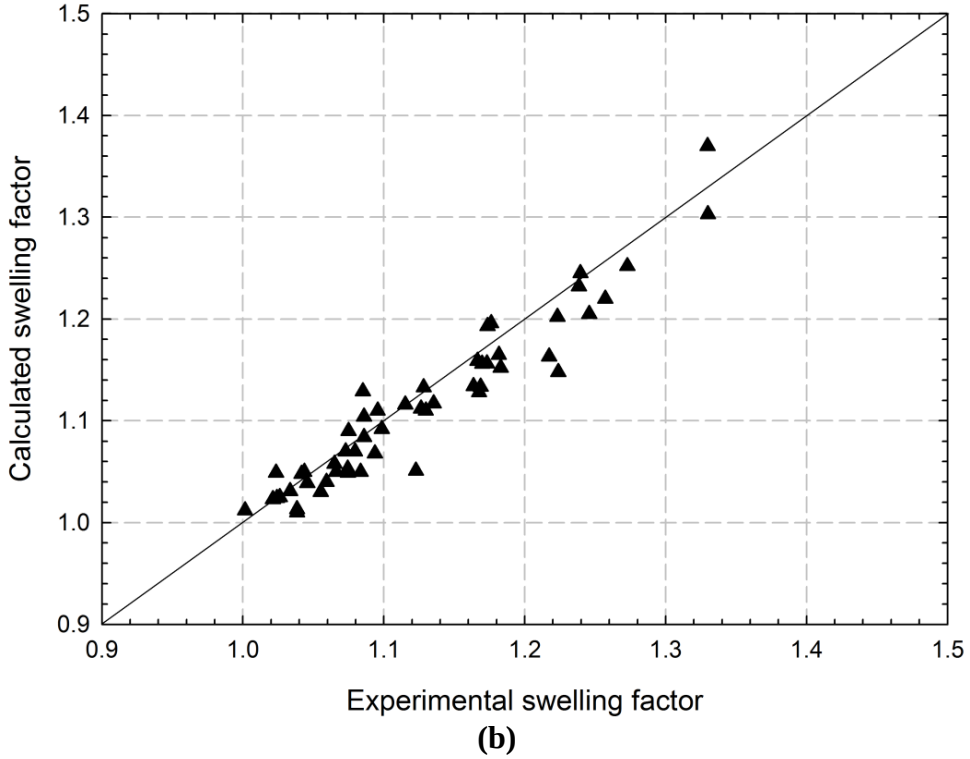

(b)

FIGURE 4-7: Parity chart of the measured and calculated phase behaviour data for CO_2-heavy oil systems by using the PR EOS with Equations [4-7] and [4-18]: (a) CO_2 solubility; and (b) swelling factor of CO_2-saturated heavy oil

heavy oil systems is obtained,

$$\delta_{24} = -0.4560\, T/T_c + 0.1817 \qquad [4\text{-}19]$$

The standard errors of the coefficients in Equation [4-19] are 0.1680 and 0.0539, respectively. FIGURE 4-8a shows the parity chart of the measured and calculated C_3H_8 solubility by using Equation [4-19]. A good agreement exists between the measured and calculated C_3H_8 solubility with a %AAD of 7.30% for the 65 solubility data points. The PR EOS with Equation [4-19] is also used to predict the swelling factor of the C_3H_8-saturated heavy oil (Luo *et al.*, 2007; Luo and Gu, 2009). Comparison between the measured and predicted swelling factor (See FIGURE 4-8b) shows that, in general, the swelling factor increases with an increased equilibrium pressure at a given temperature and decreases with temperature at a given equilibrium pressure. This is mainly attributed to the increased C_3H_8 solubility at a higher pressure or a lower temperature. Meanwhile, a very accurate prediction of the swelling factor of the C_3H_8-saturated heavy oil is also achieved with a %AAD of only 1.70% for the 9 data points.

***n*-C_4H_{10}-heavy oil systems**: FIGURE 4-9 shows the optimized BIP for the binary *n*-C_4H_{10}-heavy oil systems (Feeds #8 and #9) as a function of temperature. In general, the optimized BIP shows a negative dependence on temperature. A BIP correlation similar to Equation [4-19] is also obtained for the *n*-C_4H_{10}-heavy oil binary based on the phase behaviour data measured in this study,

$$\delta_{34} = -0.2331\, T/T_c + 0.1198 \qquad [4\text{-}20]$$

where δ_{34} is the BIP between *n*-C_4H_{10} and heavy oil. The fit is generally good with a correlation coefficient of 0.6103. The standard errors of two coefficients in Equation

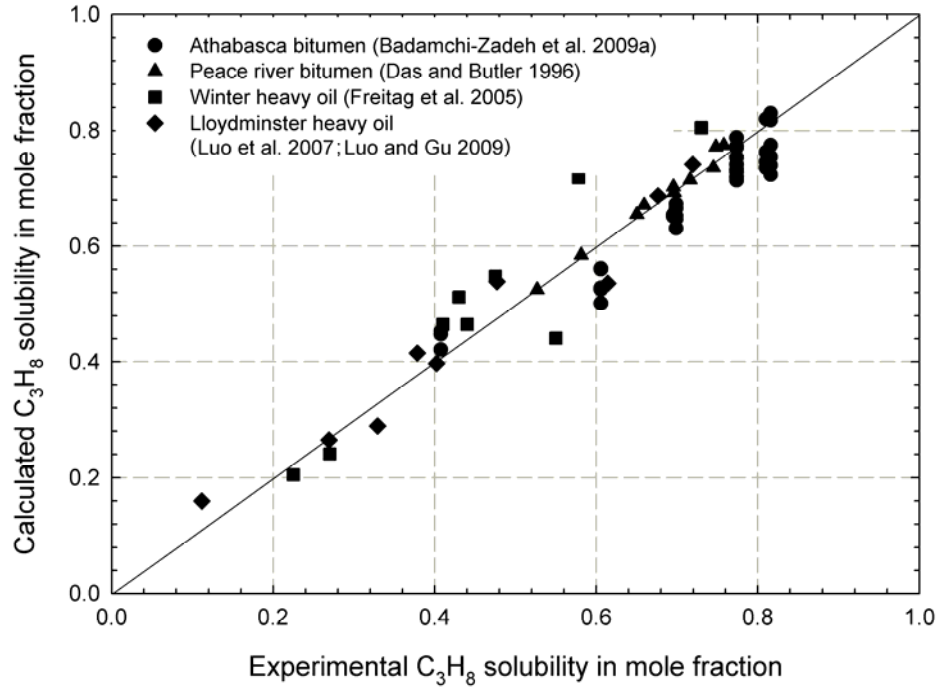

(a)

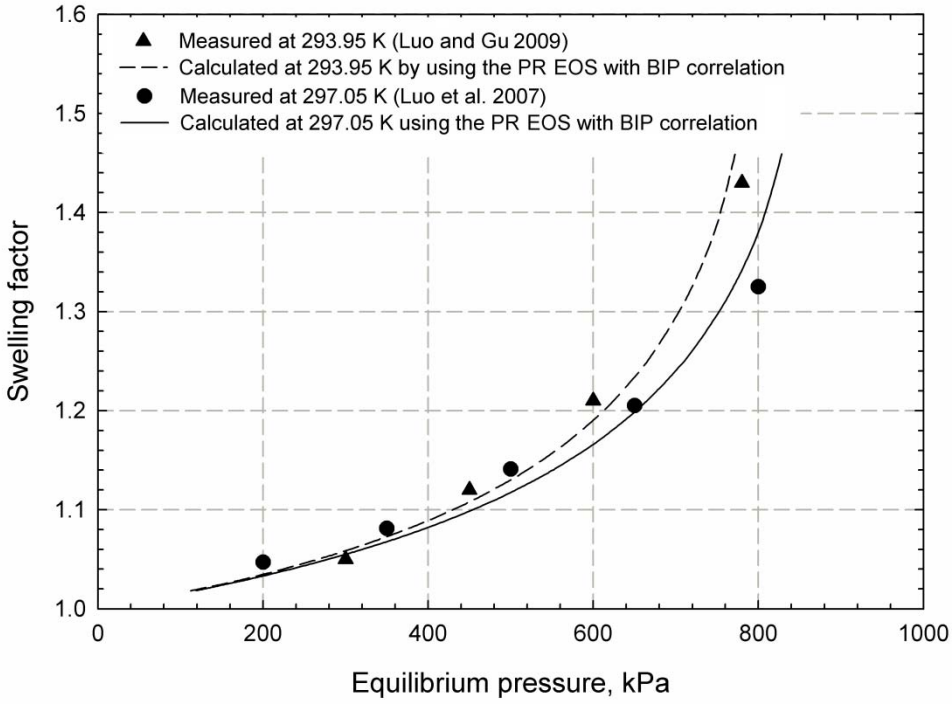

(b)

FIGURE 4-8: Comparison of the measured and calculated phase behaviour data for C_3H_8-heavy oil systems by using PR EOS with Equations [4-7] and [4-19]: (a) C_3H_8 solubility; and (b) swelling factor of C_3H_8-saturated heavy oil

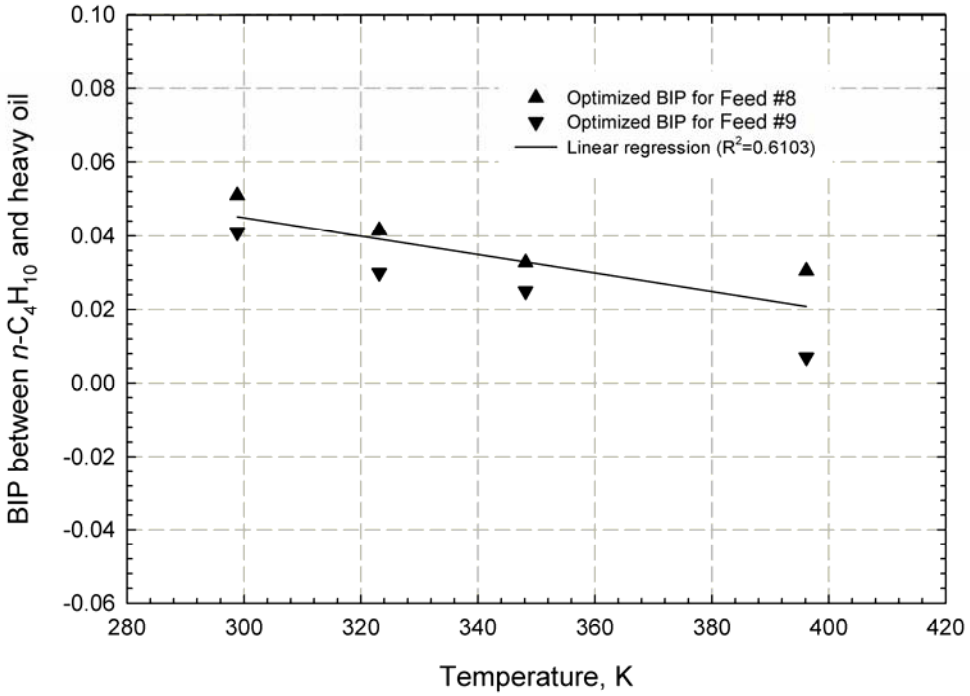

FIGURE 4-9: The experimentally optimized BIPs and the linearly regressed values for the n-C_4H_{10}-heavy oil binaries (Feeds #8 and #9) as a function of temperature

[4-20] are 0.0589 and 0.0217, respectively. It is noted that Equation [4-20] may be also applicable for other heavy oils, though it has not been tested in this study.

4.3.3. Mixing rules for mixture viscosity

Viscosity of solvent-heavy oil mixtures at a given temperature depends on mixture composition and viscosity of each component. Since it is extremely difficult to quantify the individual contribution of each component in heavy oil to the viscosity of the mixture, heavy oil is usually treated as a single pseudocomponent. Several mixing rules have been developed for estimating the viscosity of solvent-solute mixture. One classical mixing rule (i.e., the log-type mixing rule) is first examined in this study (Yazdani and Maini, 2010). The log-type mixing rule is given as,

$$\log_{10}(\mu_{\mathrm{m}}) = \phi_{\mathrm{s}} \log_{10}(\mu_{\mathrm{s}}) + \phi_{\mathrm{o}} \log_{10}(\mu_{\mathrm{o}}) \qquad [4\text{-}21]$$

where μ_m is the mixture viscosity, ϕ_s is the volume fraction of solvent, μ_s is the solvent viscosity, ϕ_o is the volume fraction of oil, and μ_c is the oil viscosity.

Cragoe (1933) developed a widely used method for predicting the liquid mixture viscosity based on the fact that the mixture viscosity is not a simply linear function of the solvent fraction. Mixing rules are used in their model to combine the "Liquidity" L of the solvent and solute. Liquidity is expressed as,

$$L = \frac{1000 \ln 20}{\ln \mu - \ln\left(5 \times 10^{-4}\right)} \qquad [4\text{-}22a]$$

where μ is viscosity of the solvent or oil. The mixture liquidity is calculated from the following mixing rule,

$$L_m = w_{\mathrm{s}} L_{\mathrm{s}} + w_{\mathrm{o}} L_{\mathrm{o}} \qquad [4\text{-}22b]$$

where L_m is the mixture liquidity, w_s is the weight fraction of solvent, w_o is the weight fraction of oil, and L_s and L_o are the liquidity of solvent and oil, respectively.

Lederer (1933) presented a modified form of the classic Arrhenius expression,

$$\ln \mu_{\mathrm{m}} = \frac{\phi_{\mathrm{s}}}{\alpha'\phi_{\mathrm{s}} + \phi_{\mathrm{o}}} \ln \mu_{\mathrm{s}} + \left(1 - \frac{\phi_{\mathrm{s}}}{\alpha'\phi_{\mathrm{s}} + \phi_{\mathrm{o}}}\right) \ln \mu_{\mathrm{o}} \qquad [4\text{-}23a]$$

where α' is an empirical constant with a value between 0 and 1. Shu (1984) extended the Lederer equation to higher viscosity ratios by using a generalized expression for the empirical constant α',

$$\alpha' = \frac{17.04\left(\rho_{\mathrm{o}} - \rho_{\mathrm{s}}\right)^{0.5237} \rho_{\mathrm{o}}^{3.2745} \rho_{\mathrm{s}}^{1.6316}}{\ln\left(\mu_{\mathrm{o}} / \mu_{\mathrm{s}}\right)} \qquad [4\text{-}23b]$$

where ρ_s and ρ_o are specific gravity of the solvent and heavy oil, respectively. This correlation is tested with heavy oil/bitumen-solvent blending data and provides an excellent prediction of the mixture viscosities. However, the correlation developed by Shu is based on organic solvents (e.g., kerosene) and may be not appropriate for CO_2-heavy oil systems where CO_2 density is higher than that of heavy oil at certain high pressures (Chung *et al.*, 1988). Chung *et al.* (1988) obtained a modified α' correlation for determining CO_2-heavy oil mixture viscosity,

$$\alpha' = 0.255 SG^{-4.16} \left(\frac{1.8T}{547.57}\right)^{1.85} \left[\frac{e^{7.36} - e^{7.36\left(1 - P/7384\right)}}{e^{7.36} - 1}\right] \qquad [4\text{-}23c]$$

The following Lobe's mixing rule is also examined for calculating the viscosity of solvent-diluted crude oil (Lobe, 1973),

$$v_{\mathrm{m}} = \phi_{\mathrm{s}} v_{\mathrm{s}} \exp\left(\phi_{\mathrm{o}} \alpha_{\mathrm{o}}\right) + \phi_{\mathrm{o}} v_{\mathrm{o}} \exp\left(\phi_{\mathrm{s}} \alpha_{\mathrm{s}}\right) \qquad [4\text{-}24a]$$

where

$$\alpha_o = 0.27 \ln\left(\frac{v_o}{v_s}\right) + \left[1.3 \ln\left(\frac{v_o}{v_s}\right)\right]^{0.5} \quad [4\text{-}24b]$$

$$\alpha_s = -1.7 \ln\left(\frac{v_o}{v_s}\right) \quad [4\text{-}24c]$$

where v is the kinematic viscosity which is related to the dynamic viscosity by $\mu = \rho v$.

4.4 Results and Discussion

4.4.1. Validation of the BIP correlations

In order to validate the predictive capability of the proposed BIP correlations, these correlations are tested with the recently published phase behaviour data on three C_3H_8-CO_2-Athabasca bitumen mixtures (Badamchi-Zadeh *et al.*, 2009b). It should be pointed out that the phase behaviour data for the three mixtures are not included in the database for developing the BIP correlations. The BIP between CO_2 and C_3H_8 is set as 0.13500, while those for CO_2-heavy oil binary and C_3H_8-heavy oil binary at different temperatures are predicted with Equations [4-18] and [4-19], respectively.

The saturation pressures of the mixtures are calculated by following the procedure provided by Peterson and Christensen (2006). FIGURE 4-10 compares the measured and predicted saturation pressures of the two C_3H_8-CO_2-Athabasca bitumen mixtures with different methods. In general, the PR EOS with the BIPs calculated by the proposed correlations is able to accurately reproduce the saturation pressures for the two mixtures. The PR EOS model used in this study is also compared to the advanced PR EOS (APR EOS) model that was recently used by Díaz *et al.* (2011). It is interesting to note that the PR EOS model, which treats the bitumen as a single pseudocomponent, provides a

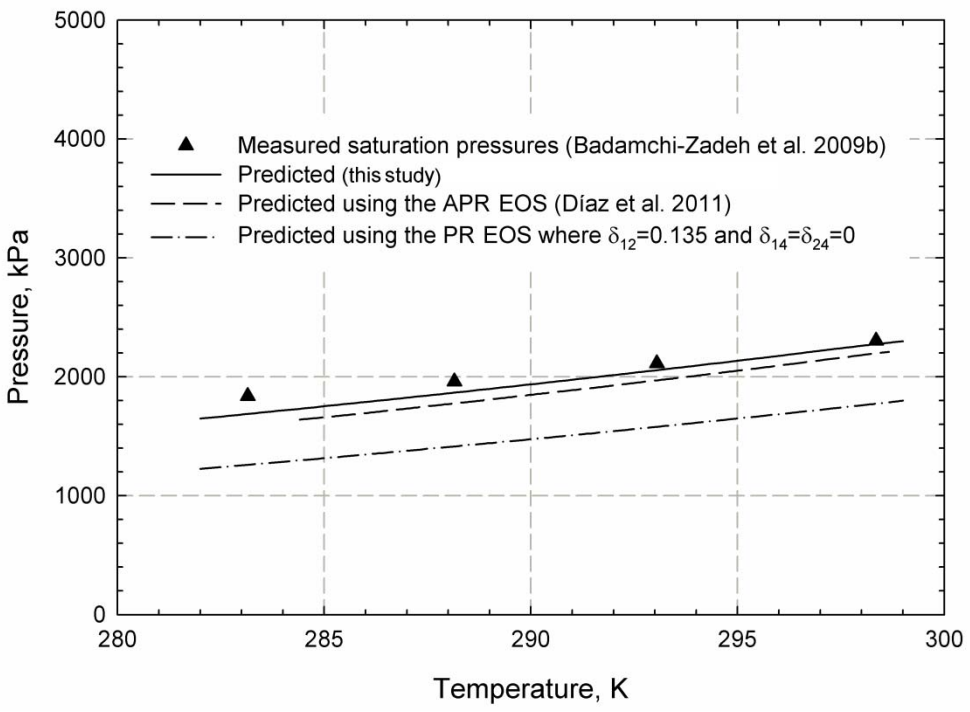

(a)

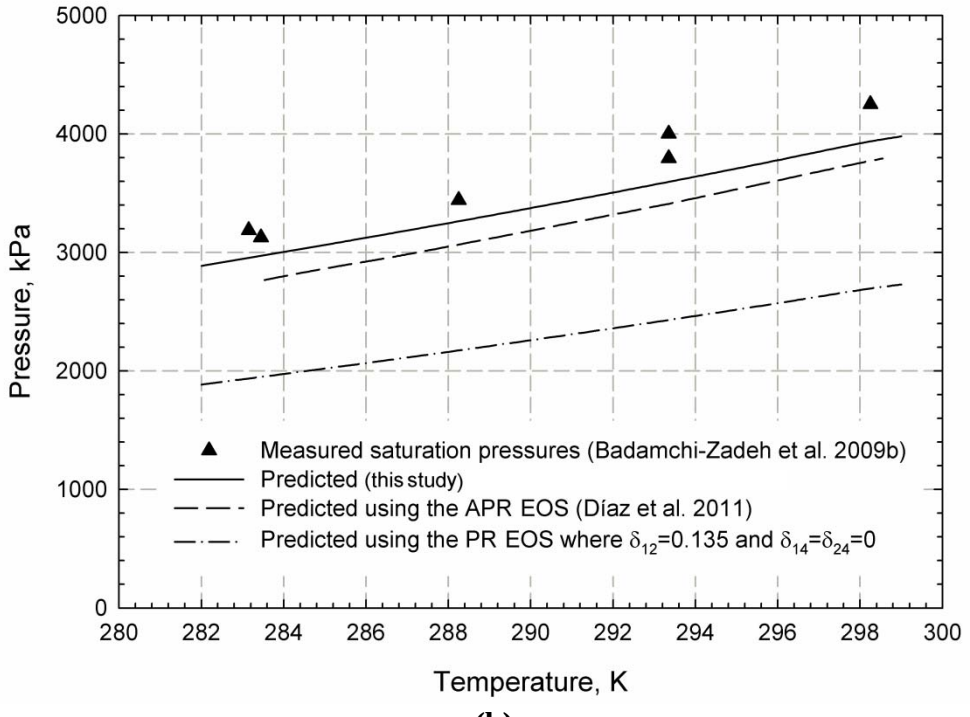

(b)

FIGURE 4-10: Comparison of the measured saturation pressures (Badamchi-Zadeh *et al.*, 2009b) and calculated values with different models for the ternary mixtures: (a) Mixture #1 (24.0 wt% C_3H_8, 6.2 wt% CO_2, 69.8 wt% bitumen); and (b) Mixture #2 (13.5 wt% C_3H_8, 11.0 wt% CO_2, 75.5 wt% bitumen)

slightly better prediction accuracy of the L_1V boundary as compared to the regressed APR EOS (Díaz *et al.*, 2011) model where the bitumen is treated as a mixture comprised of multi-pseudocomponents. In addition, it can be seen from FIGURE 4-10 that the use of zero BIPs for CO_2-bitumen pair and C_3H_8-bitumen pair cannot reproduce the saturation pressures correctly. This is ascribed to the fact that the BIP has a significant effect on performance of the PR EOS in predicting phase behaviours of heavy oil involved systems.

The L_1L_2V three phase boundaries of a mixture (13.1 wt% C_3H_8, 19.2 wt% CO_2, 67.7 wt% bitumen) were also reported recently (Badamchi-Zadeh *et al.*, 2009b). In principle, phase boundaries for a multicomponent system with a given feed can be detected by performing stability test and subsequent flash calculations. In this study, the Michelsen's stability test criteria are adopted to perform the stability test of a given multicomponent system (Michelsen, 1982). FIGURE 4-11 compares the measured three phase boundaries for the mixture with the predicted ones by using the PR EOS with the newly developed BIP correlations and Equation [4-7]. The PR EOS with the BIPs calculated by the newly proposed correlations reproduces well the three phase boundaries, though the PR EOS model used in this study generates a slightly larger error in comparison to the APR EOS model (Díaz *et al.*, 2011) (See FIGURE 4-11).

It should be pointed out herein that there is one underlying drawback that arises from characterizing the heavy oil as a single pseudocomponent in the PR EOS. According to Gibbs's phase rule, the L_1L_2V three phase boundaries will be predicted to be a line on the *P*-*T* diagram if the CO_2-heavy oil system is only characterized by two components, i.e., CO_2 and heavy oil. However, the L_1L_2V three phase boundary of some CO_2-heavy oil systems has been found to spread over a small area instead of a line (Kodal and

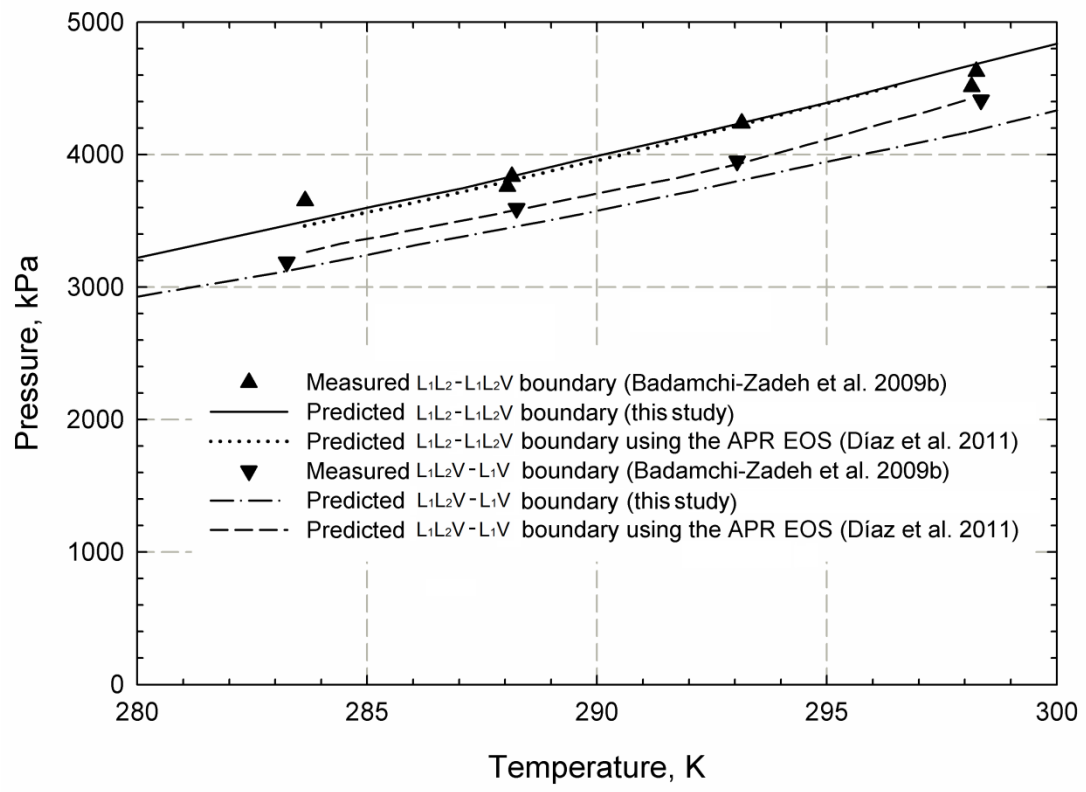

FIGURE 4-11: Comparison of the measured L_1L_2V boundaries (Badamchi-Zadeh *et al.*, 2009b) and calculated ones with the PR EOS used in this study and the APR EOS (Díaz *et al.*, 2011) for Mixture #3 (13.1 wt% C_3H_8, 19.2 wt% CO_2, 67.7 wt% bitumen)

Sayegh, 1992). Nonetheless, the newly proposed BIP correlations can still be of value as a tool to estimate the three phase boundary of CO_2-heavy oil systems due to the narrow span of the three phase boundary (Kodal and Sayegh, 1992).

4.4.2. Solvent(s)-Lloydminster heavy oil systems

C_3H_8-Lloydminster heavy oil system: Six C_3H_8-Lloydminster heavy oil systems have been tested in this study. FIGURE 4-12 shows the measured typical *P-V* relations by using the continuous depressurization method and discrete depressurization method for (a) Feed #3 (20.9 wt% C_3H_8, 79.1 wt% heavy oil) at 298.85 K and (b) Feed #4 (11.6 wt% C_3H_8, 88.4 wt% heavy oil) at 323.85 K, respectively. It can be seen from FIGURE 4-12 that there is a minor difference between the measured *P-V* curves by using the continuous depressurization method and discrete depressurization method. Badamchi-Zadeh *et al.* (2009a) also compared the measured *P-V* relations by using the above-mentioned methods for a C_3H_8-Athabasca bitumen system, though a larger discrepancy between them was observed. The minor difference caused by these two methods in this study is probably attributed to the lower viscosity of the Lloydminster heavy oil used, compared to that of the highly viscous Athabasca bitumen. In this study, the continuous depressurization method is subsequently used to perform the saturation pressure and swelling factor measurements for all the solvent(s)-CO_2-heavy oil systems. TABLE 4-9 summarizes the physical properties of CO_2, C_3H_8, *n*-C_4H_{10} and Lloydminster heavy oil which are used as inputs for the subsequent prediction of saturation pressures and swelling factors.

FIGURE 4-13 shows the measured and predicted saturation pressures and swelling factors for the C_3H_8-Lloydminster heavy oil systems with Feeds #1-3 at 298.85 K and

TABLE 4-9: Physical properties of CO_2, C_3H_8, n-C_4H_{10} and Lloydminster heavy oil

Component	P_c, **kPa**	T_c, **K**	ω	Z_{ra}	V_c, **m^3/kmol**
CO_2	7378	304.14	0.2238	0.2736	0.0940
C_3H_8	4246	369.80	0.1520	0.2763	0.2030
n-C_4H_{10}	3786	425.20	0.1930	0.2728	0.2550
Lloydminster heavy oil	1265	933.66	1.0288	0.2621	1.2460

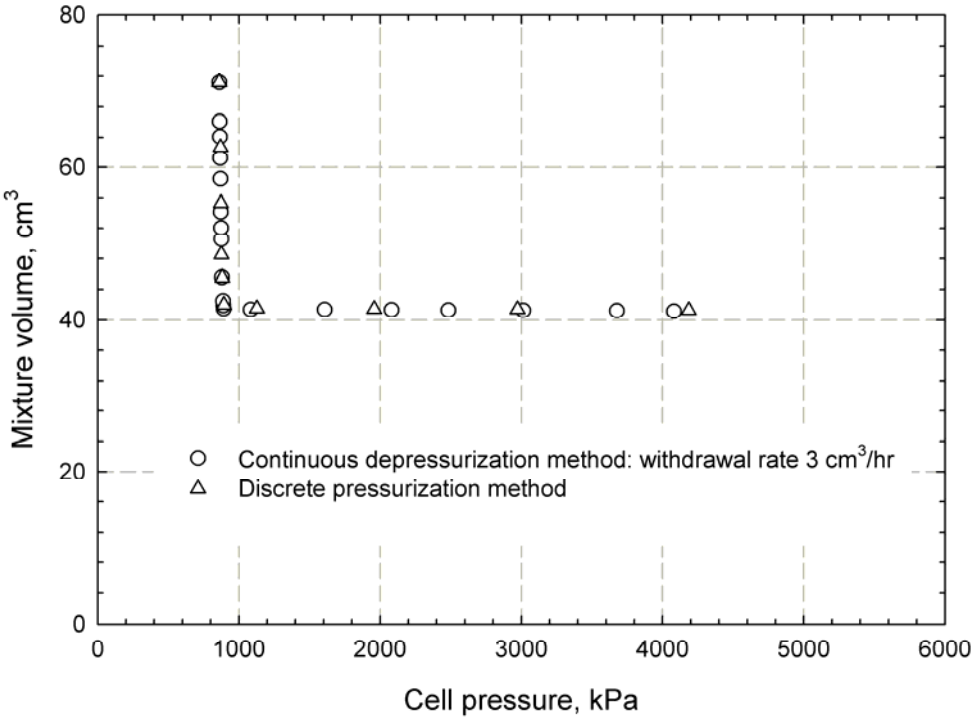

(a)

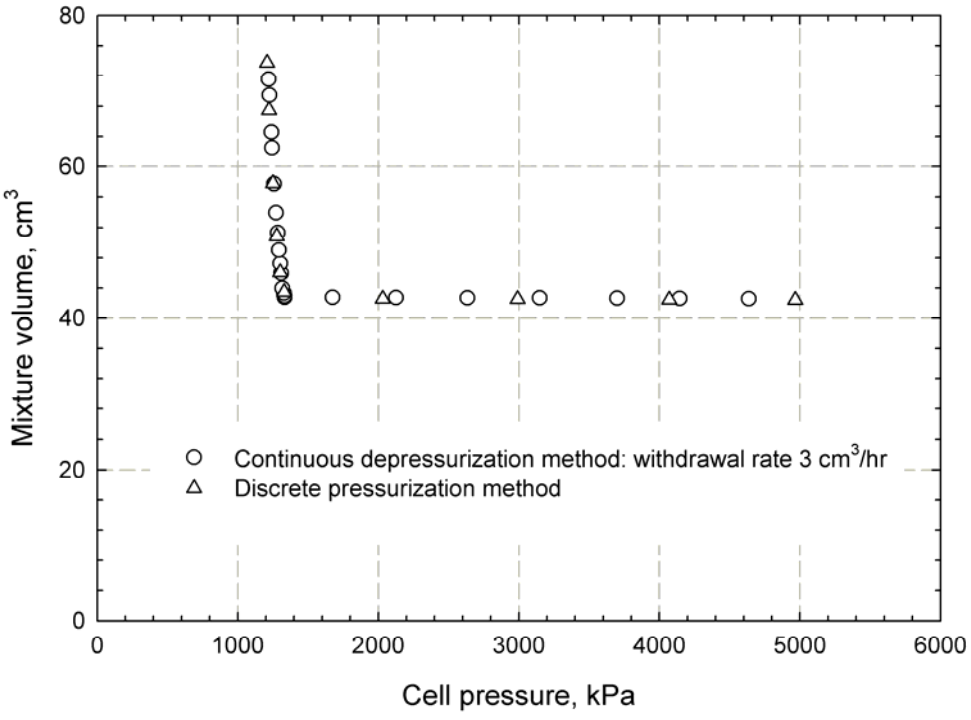

(b)

FIGURE 4-12: *P-V* relations measured by the continuous depressurization method and discrete depressurization method for (a) Feed #3 (20.9 wt% C_3H_8, 79.1 wt% heavy oil) at 298.85 K; and (b) Feed #4 (11.6 wt% C_3H_8, 88.4 wt% heavy oil) at 323.85 K

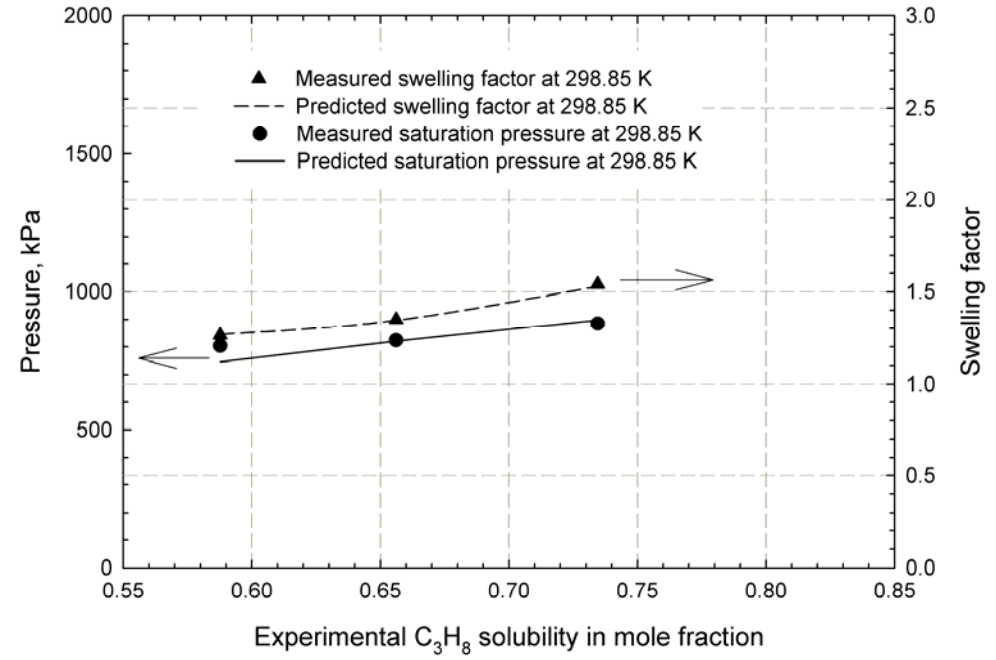

FIGURE 4-13: Measured and predicted saturation pressures and swelling factors for the C_3H_8-Lloydminster heavy oil system (a) Feeds #1-3 at 298.85 K; and (b) Feeds #4-6 at 323.85 K, respectively

with Feeds #4-6 at 323.85 K, respectively. It can be seen from FIGURE 4-13 that the saturation pressure increases as the solubility of C_3H_8 in heavy oil increases. The saturation pressure also increases with temperature for the same C_3H_8 solubility. It is worthwhile noting that dissolution of C_3H_8 leads to an enhanced swelling effect of the Lloydminster heavy oil. For example, the heavy oil swells around 1.50 times with dissolution of 74.4 mol% (20.9 wt%) of C_3H_8. A large swelling factor is particularly beneficial for achieving an improved recovery performance of solvent flooding processes. In addition, the PR EOS with Equations [4-7] and [4-19] is able to accurately predict the saturation pressures and swelling factors for the C_3H_8-Lloydminster heavy oil system.

FIGURE 4-14 compares the measured saturation pressures and swelling factors and their predicted values for the C_3H_8-Lloydminster heavy oil system: Feed #7. It can be seen from this figure that the saturation pressure increases with temperature. This implies that, at the same pressure, solubility of C_3H_8 at a higher temperature is smaller than that at a lower temperature. As can also be seen from FIGURE 4-14 the swelling factor for the C_3H_8-heavy oil binary maintains almost constant at different temperatures. It can be also seen from FIGURE 4-14 that, in general, there exists a generally good agreement between the measured and calculated saturation pressures, though the accuracy is somewhat compromised at a high temperature close to the critical temperature of C_3H_8. The reduced accuracy at a high temperature might be attributed to the fact that the PR EOS model is less accurate when used for modeling C_3H_8-heavy oil phase behaviour at temperatures close to the critical temperature of C_3H_8.

***n*-C_4H_{10}-Lloydminster heavy oil system**: Two *n*-C_4H_{10}-Lloydminster heavy oil systems have been tested in this study. FIGURE 4-15 compares the measured saturation

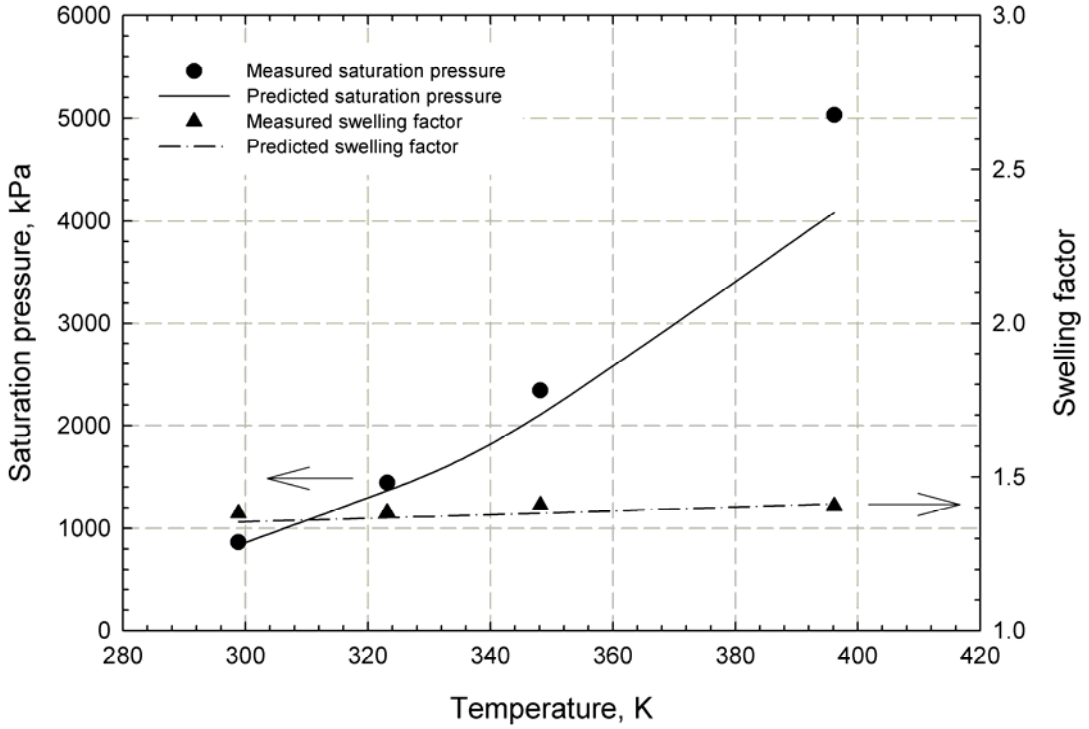

FIGURE 4-14: Comparison of the measured saturation pressures and swelling factors and their predicted values for the C_3H_8-Lloydminster heavy oil binary: Feed #7

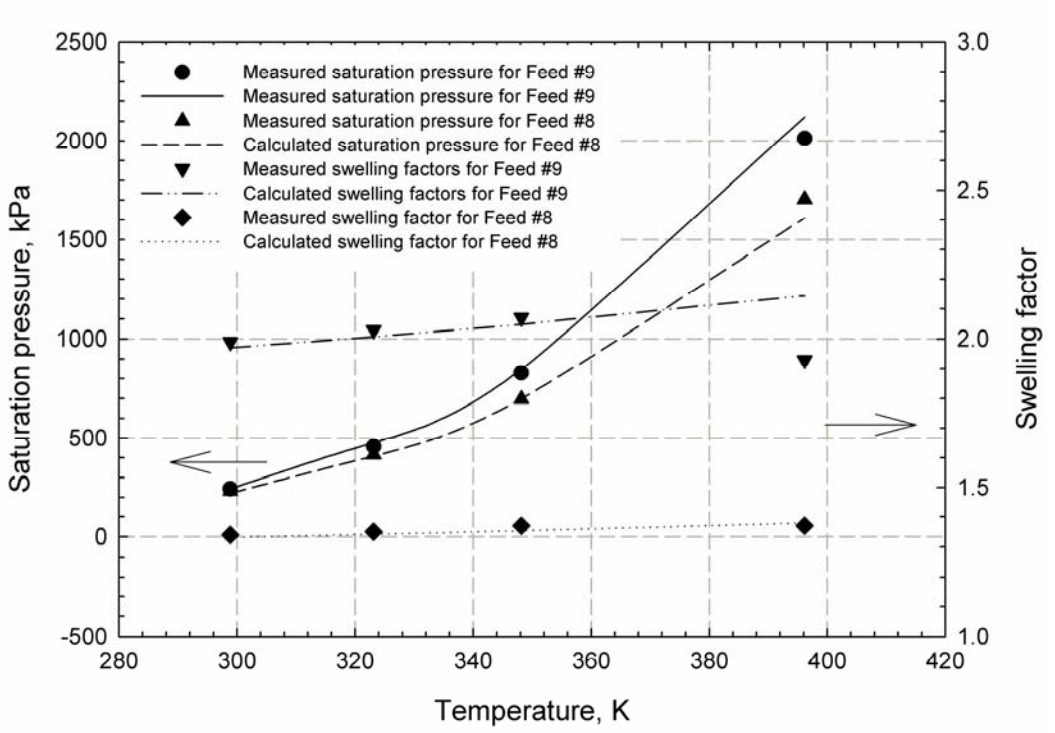

FIGURE 4-15: Comparison of the measured saturation pressures and swelling factors and their predicted values for the *n*-C_4H_{10}-Lloydminster heavy oil binaries: Feeds #8 and #9

pressures and swelling factors and their predicted values for the *n*-C_4H_{10}-Lloydminster heavy oil systems: Feeds #8 and #9. It can be found from FIGURE 4-15 that the saturation pressure increases with the operating temperature for a given feed. As more *n*-C_4H_{10} is present in the heavy oil (i.e., a larger *n*-C_4H_{10} solubility), the saturation pressure at a given temperature is also increased. This implies that, at the same pressure, the solubility of *n*-C_4H_{10} in heavy oil at a higher temperature is smaller than that at a lower temperature, while, at the same temperature, it increases with an increase in pressure. Overall, the measured swelling factor for a given *n*-C_4H_{10}-heavy oil system remains almost unchanged at different temperatures. One exception is given to Feed #9 at 396.15 K, for which the measured swelling factor is a little bit lower than the other three data points. The PR EOS together with Equations [4-7] is used to calculate the saturation pressure for Feeds #8 and #9, respectively. The BIPs between *n*-C_4H_{10} and heavy oil at different temperatures are calculated via Equation [4-20]. A generally good agreement between the measured and calculated saturation pressures has been achieved, though the accuracy is reduced at temperatures close to the critical temperature of *n*-C_4H_{10}. An accurate reproduction of the swelling factor of the *n*-C_4H_{10}-saturated heavy oil has also been obtained, except that the calculated swelling factor for Feed #9 at 396.15 K shows a relatively large deviation from the measured one.

C_3H_8-n-C_4H_{10}-Lloydminster heavy oil system: One C_3H_8-*n*-C_4H_{10}-Lloydminster heavy oil system is tested in this study. FIGURE 4-16 compares the measured saturation pressures and swelling factors together with their predicted values for the C_3H_8-*n*-C_4H_{10}-Lloydminster heavy oil system: Feed #10. It can be found from FIGURE 4-16 that the saturation pressure increases with the operating temperature for the ternary system tested.

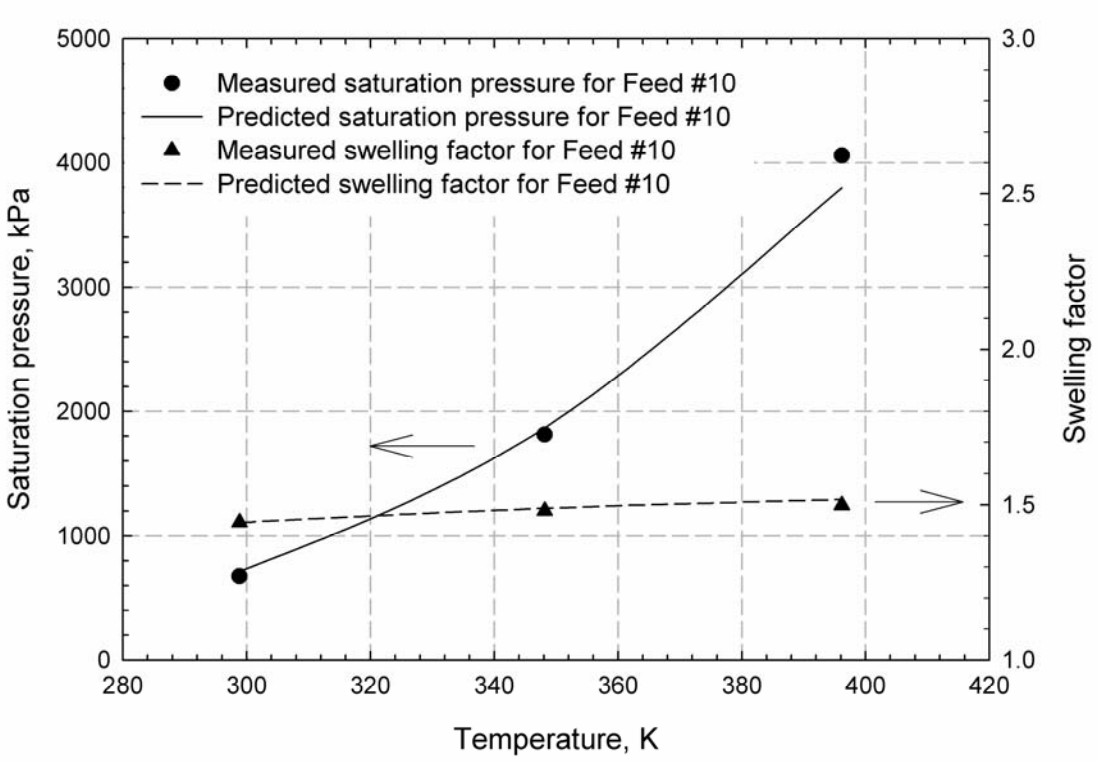

FIGURE 4-16: Comparison of the measured saturation pressures and swelling factors and their predicted values for the ternary C_3H_8-*n*-C_4H_{10}-Lloydminster heavy oil system: Feed #10

Similar to the CO_2-C_3H_8-heavy oil system, the swelling factor for the C_3H_8-*n*-C_4H_{10}-Lloydminster heavy oil mixture remains almost unchanged at different temperatures. The saturation pressures for Feed #10 are calculated by using the PR EOS enhanced with the modified alpha function. The BIPs for C_3H_8-heavy oil binary and *n*-C_4H_{10}-heavy oil binary at different temperatures are predicted via Equations [4-19] and [4-20], respectively. A good agreement exists between the measured and calculated saturation pressures throughout the tested temperature range. A very accurate prediction of the swelling factor of C_3H_8-*n*-C_4H_{10}-heavy oil mixture is also achieved.

Based on the generally good match between the measured and predicted data on saturation pressures and swelling factors from this work and the previous studies, it is proved that it is an effective and efficient methodology to model the saturation pressures and swelling factors of heavy oil with dissolution of various solvents (i.e., CO_2, C_3H_8 and *n*-C_4H_{10}) by treating heavy oil sample as a single pseudocomponent and utilizing the generalized BIP correlations developed in this study.

FIGURE 4-17 compares the measured viscosities of C_3H_8-saturated heavy oil by using the capillary viscometer at 298.85 K and predicted ones with different mixing rules. The C_3H_8 dissolution in heavy oil can significantly reduce the heavy oil viscosity (Luo *et al.*, 2007; Badamchi-Zadeh *et al.*, 2009a). For example, the heavy oil viscosity is reduced from 7812.32 cP down to 37.5 cP with dissolution of 14.8 wt% of C_3H_8 (i.e., the corresponding volume fraction of C_3H_8 is 26.1%) at 298.85 K. As can be seen from FIGURE 4-17, the Shu mixing rule, Chung mixing rule and Cragoe mixing rule provide similar prediction accuracies for the C_3H_8-saturated heavy oil viscosities, while the conventional log-type leads to the largest error. The Lobe mixing rule is found to be the

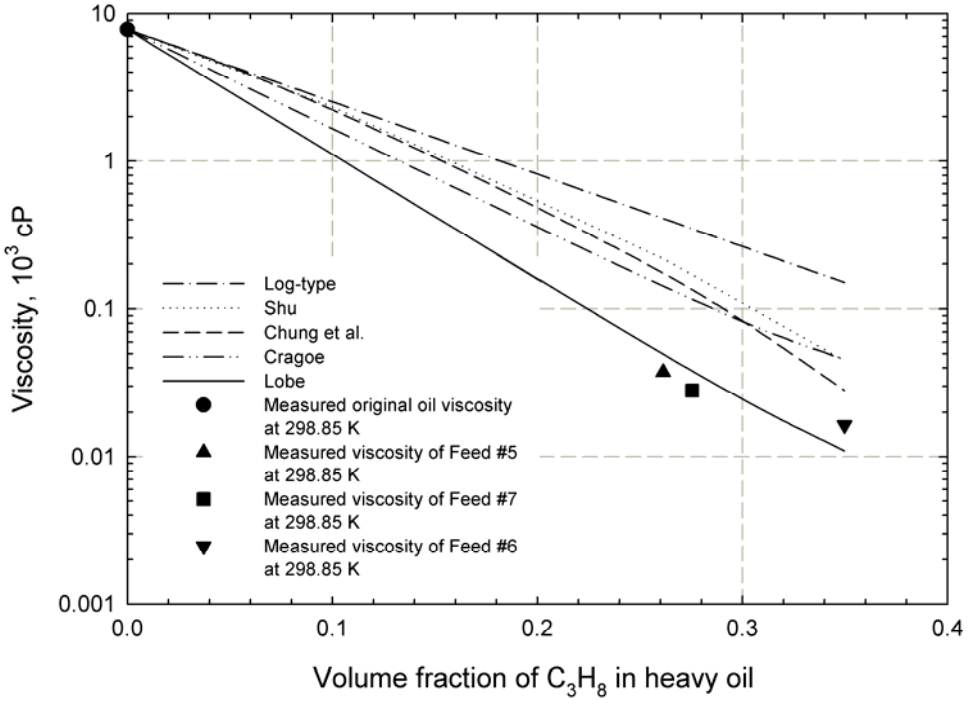

(a)

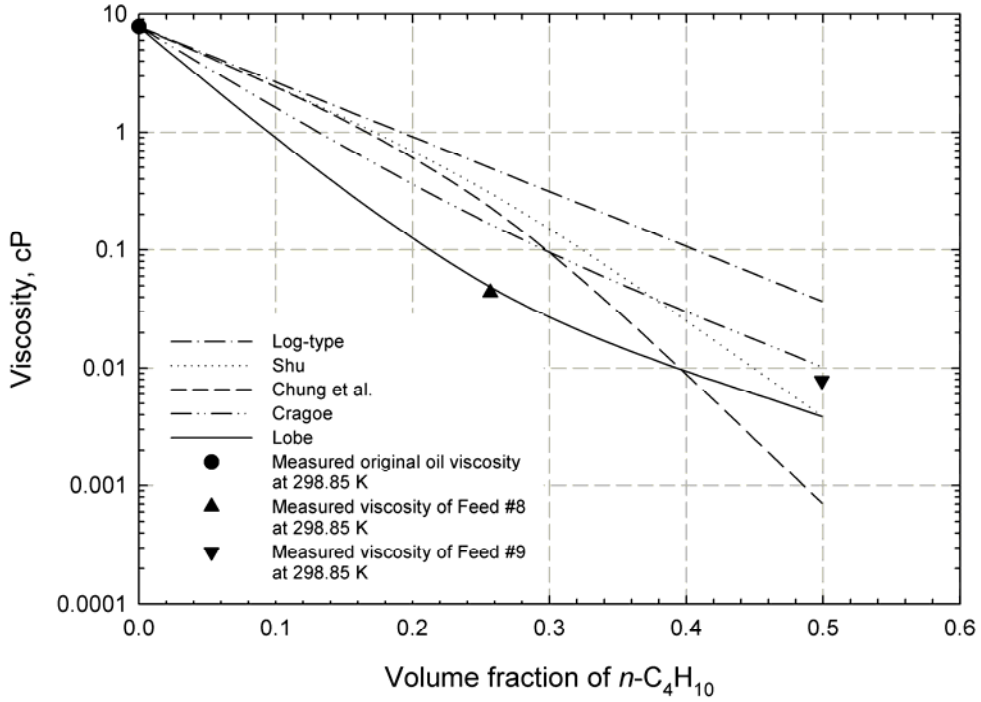

(b)

FIGURE 4-17: Measured viscosity and predicted viscosity by using different mixing rules for (a) C_3H_8-heavy oil mixtures at 298.85 K and (b) n-C_4H_{10}-heavy oil mixtures at 298.85 K

most accurate one among the mixing rules examined for the given heavy oil sample.

It is very likely to observe asphaltene precipitation at high C_3H_8 fractions. FIGURE 4-18 shows the precipitated asphaltene particles that are captured on the PVT cell wall for Feed #3 (29.3 wt% C_3H_8, 70.7 wt% heavy oil) at 1500 kPa and 323.85 K. The digital image is taken after the magnetic mixer is turned off. This implies that the asphaltene precipitation caused by C_3H_8 dissolution must be taken into account when injecting C_3H_8 at pressures close to its dew point pressure.

4.4.3. Solvent(s)-CO_2-Lloydminster heavy oil systems

PVT tests are also performed to measure the saturation pressures and swelling factors at different temperatures for a C_3H_8-CO_2-Lloydminster heavy oil system with Feed #11 and a *n*-C_4H_{10}-CO_2-Lloydminster heavy oil system with Feed #12. FIGURE 4-19 illustrates the measured and predicted saturation pressures and swelling factors for these two ternary mixtures at different temperatures. It can be seen from FIGURE 4-19 that, as for a solvent-CO_2-heavy oil mixture, the measured saturation pressure increases significantly with the temperature, while the measured swelling factor maintains a high value and only increases slightly with temperature. The BIPs for CO_2-heavy oil pair, C_3H_8-heavy oil pair, *n*-C_4H_{10}-heavy oil pair at different temperatures are calculated by using Equations [4-18], [4-19] and [4-20], respectively. Then the calculated BIPs are incorporated into the PR EOS together with Equation [4-7] to predict the saturation pressures and swelling factors for the two ternary mixtures. As can also be observed from FIGURE 4-19, there exists a generally good agreement between the measured and predicted saturation pressures and swelling factors. The viscosity of the ternary C_3H_8-

FIGURE 4-18: Asphaltene precipitation observed on the PVT cell wall for Feed #3 (29.3 wt% C_3H_8, 70.7 wt% heavy oil) at 1500.0 kPa and 323.85 K

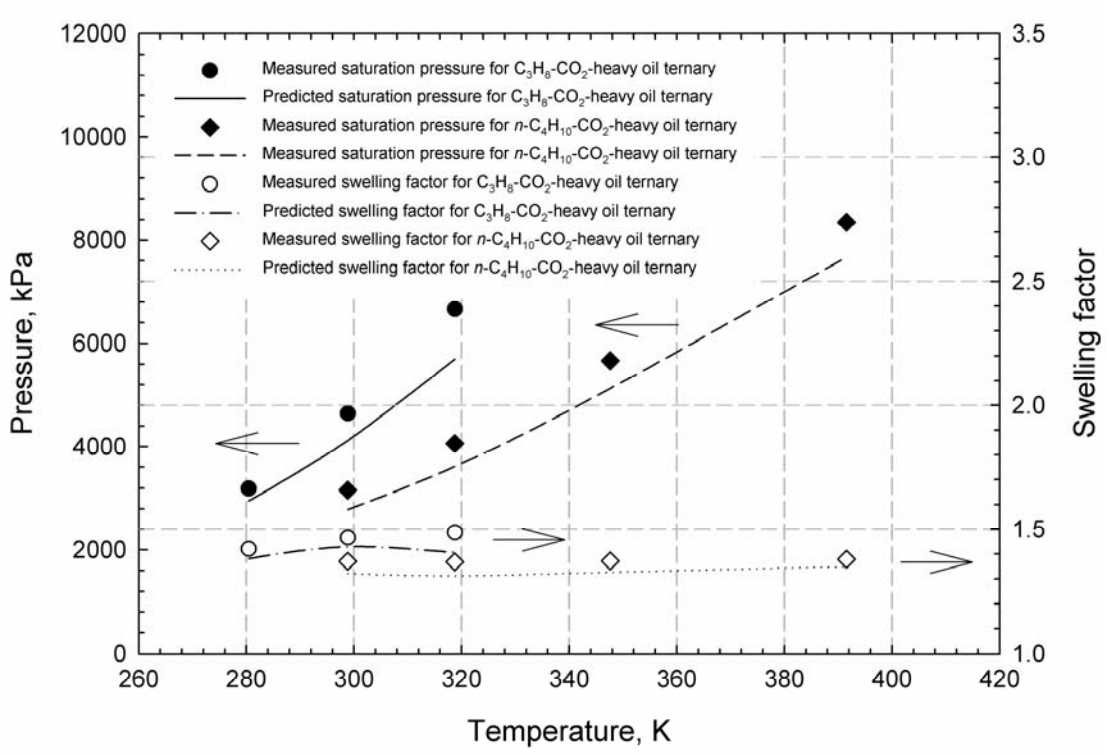

FIGURE 4-19: Measured and predicted saturation pressures and swelling factors for the C_3H_8-CO_2-heavy oil system with Feed #11 (10.3 wt% C_3H_8, 11.0 wt% CO_2, 78.7 wt% Lloydminster heavy oil) and the n-C_4H_{10}-CO_2-heavy oil system with Feed #12 (10.1 wt% n-C_4H_{10}, 7.1 wt% CO_2, 82.8 wt% Lloydminster heavy oil)

CO_2-Lloydminster heavy oil mixture at 318.75 K and saturation pressure of 6657.0 kPa is measured to be 12.1 cP, while the viscosity of the ternary *n*-C_4H_{10}-CO_2-Lloydminster heavy oil mixture at 298.85 K and saturation pressure of 3154.0 kPa is measured to be 34.4 cP.

In order to examine the effect of adding a solvent into CO_2 stream on the swelling factor and viscosity of CO_2-heavy oil system, the swelling factor of CO_2-saturated heavy oil at 298.85 K is calculated by using the PR EOS together with Equations [4-7] and [4-18] and by using a swelling factor correlation (Emera and Sarma 2008), respectively, while the viscosity of CO_2-saturated heavy oil at 298.85 K is calculated with a viscosity correlation (Emera and Sarma 2008) (See FIGURE 4-20). In addition to the predicted swelling factors and mixture viscosity for the CO_2-Lloydminster heavy oil system at 298.85 K, FIGURE 4-20 also presents the swelling factor of the ternary C_3H_8-CO_2-Lloydminster heavy oil mixture measured at 298.85 K and saturation pressure of 4642.0 kPa together with the swelling factor and viscosity of the *n*-C_4H_{10}-CO_2-Lloydminster heavy oil mixture measured at 298.85 K and saturation pressure of 3154.0 kPa.

By comparing FIGUREs 4-13 and 4-20, it can be found that, at the same saturation pressure, C_3H_8 is able to swell the heavy oil to a far larger degree than pure CO_2. Similarly, *n*-C_4H_{10} can swell heavy oil to a larger degree than pure CO_2 (Li and Yang 2012). This is mainly attributed to two aspects: 1) Solubility of C_3H_8 or *n*-C_4H_{10} in heavy oil is much higher than CO_2 under the same pressure; and 2) Density of liquid C_3H_8 or *n*-C_4H_{10} is smaller than that of liquid CO_2. As can be seen from FIGURE 4-20, at the same saturation pressure and temperature, addition of *n*-C_4H_{10} into CO_2 stream increases the swelling factor from 1.06 to 1.37, but decreases the viscosity from 426.9 cP to 34.4 cP.

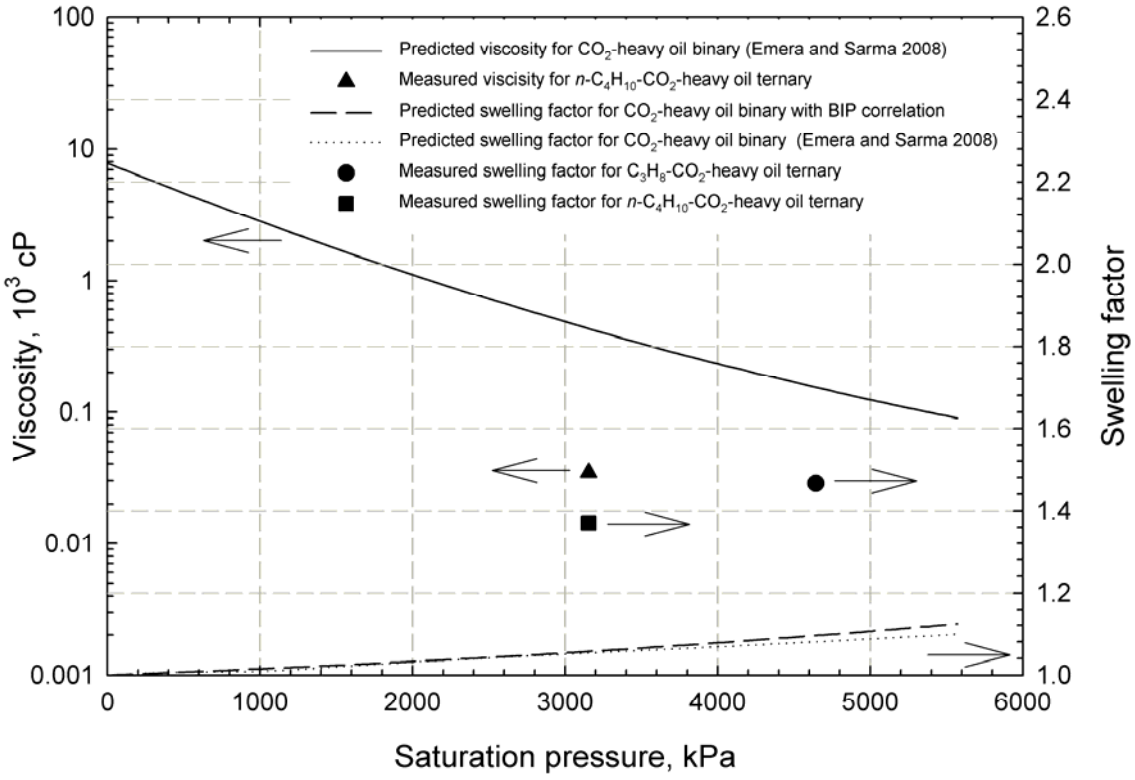

FIGURE 4-20: Predicted swelling factor and mixture viscosity for the CO_2-Lloydminster heavy oil system at 298.85 K, respectively. The swelling factor is predicted by using the PR EOS together with Equations [4-7] and [4-18] as well as a genetic algorithm-based swelling factor correlation (Emera and Sarma 2008), respectively, while the viscosity is calculated with a genetic algorithm-based viscosity correlation (Emera and Sarma 2008)

FIGURE 4-20 also shows that, at the same saturation pressure and temperature, a significantly larger swelling factor of 1.47 can be achieved by adding C_3H_8 into CO_2 stream compared to that of 1.10 for the CO_2-heavy oil system. The enhanced swelling factor and viscosity reduction effect is achieved mainly through the enhanced dissolution of the alkane solvent either C_3H_8 or *n*-C_4H_{10} into heavy oil.

4.4.4. Formation of foamy heavy oil

One interesting phenomenon is observed during all the PVT experiments for solvent(s)-CO_2-heavy oil systems. Foamy solvent-heavy oil mixture has been observed when the mixture is subjected to a sudden pressure decrease and released to the atmosphere. The foamy oil behaviour is a beneficial mechanism for the practical implementation of solvent-based processes for heavy oil recovery. FIGURE 4-21 illustrates a sequence of images of the C_3H_8-*n*-C_4H_{10}-heavy oil mixture which is released to the atmosphere from the PVT cell at saturation pressure and 298.85 K right after the viscosity measurements. The five digital images are taken in sequence when the mixture is released at 0 s, 30 s, 60 s, 90 s, and 120 s, respectively. It is observed from FIGURE 4-21 that the discharge process is terminated within a short time period of about 120 s. A subsequent check on the tubing and PVT cell shows that there is only little heavy oil or solvents remaining in the tubing and PVT cell. The high mobility and efficient self-cleaning phenomenon of the foamy heavy oil are mainly attributed to two aspects. Firstly, the emergence of gas bubbles in the heavy oil due to sudden pressure decrease acts as an efficient solution-gas-drive mechanism inside the tubing (Turta *et al.*, 2003; Kumar and Mahadevan, 2012). Secondly, C_3H_8-*n*-C_4H_{10} mixture in heavy oil is fairly soluble in

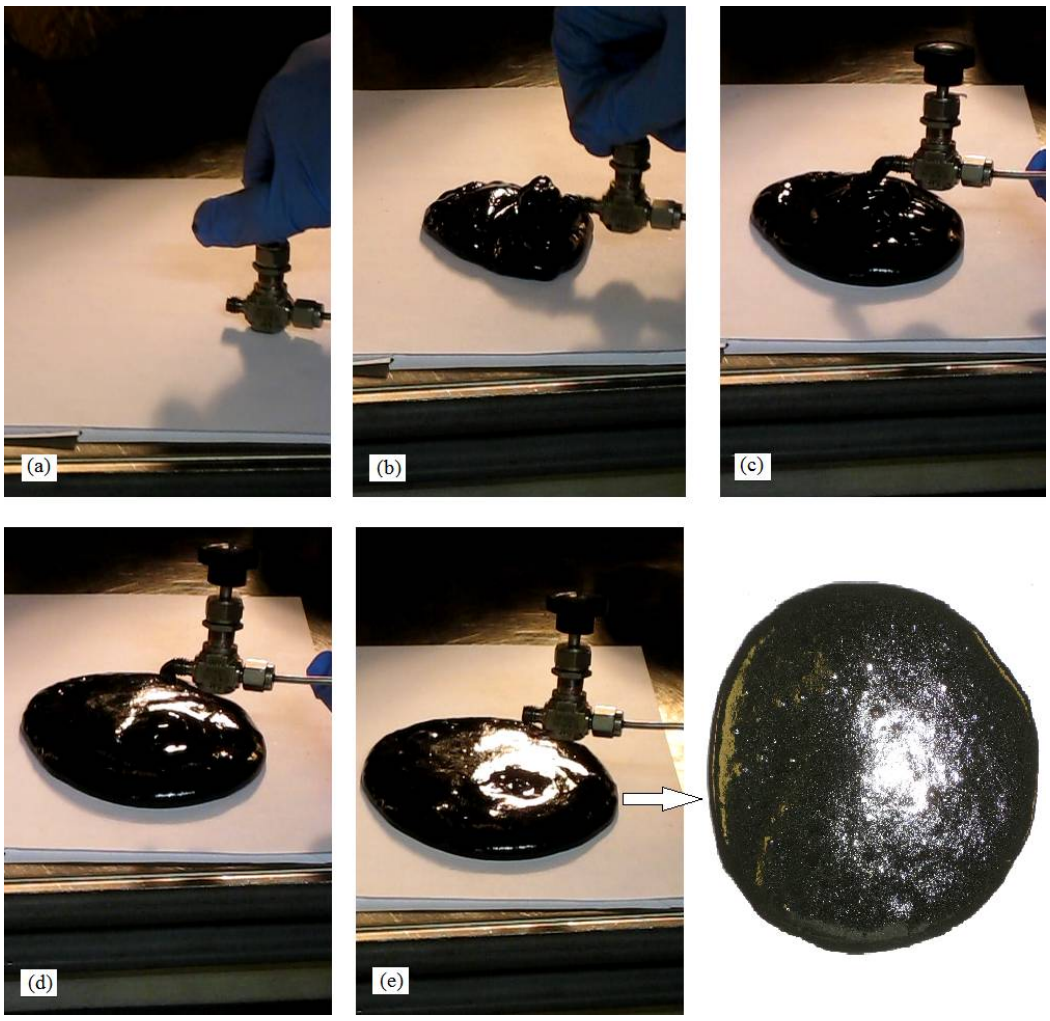

FIGURE 4-21: Sequential images of the foamy C_3H_8-*n*-C_4H_{10}-heavy oil system Feed #10 which is released to atmosphere from the PVT cell at saturation pressure and 298.85 K after the viscosity measurements at: (a) 0 s; (b) 30 s; (c) 60 s; (d) 90 s; and (e) 120 s. The total volume of the ternary mixture discharged is around 10 cm^3 at saturation conditions

heavy oil at atmospheric pressure. This means that the heavy oil is still able to preserve a low viscosity level even at atmospheric pressure, which facilitates swelling the heavy oil and carrying it by the gas solvents.

4.5 Summary

Techniques have been developed to experimentally and theoretically examine the enhanced swelling effect and viscosity reduction of CO_2-saturated heavy oil with addition of either C_3H_8 or *n*-C_4H_{10}. The newly developed three BIP correlations CO_2-heavy oil binaries, C_3H_8-heavy oil binaries and *n*-C_4H_{10}-heavy oil binaries in PR EOS together with Equation [4-7] are able to reproduce the experimental solubility data and predict the swelling factor with a good accuracy. The proposed BIP correlations are also validated with the recently published phase behaviour data, including saturation pressures and L_1L_2V three phase boundaries, for CO_2-C_3H_8-heavy oil systems. A good agreement between the experimental and calculated phase behaviour data is obtained.

PVT measurements on the saturation pressure, swelling factor and viscosity of the solvent(s)-CO_2-heavy oil system indicate that, under the same conditions, a significantly increased swelling effect of heavy oil can be obtained by adding either C_3H_8 or *n*-C_4H_{10} into CO_2 stream. An enhanced viscosity reduction of the CO_2-heavy oil system can be also achieved in the presence of either C_3H_8 or *n*-C_4H_{10}. The enhanced swelling effect and viscosity reduction caused by adding either C_3H_8 or *n*-C_4H_{10} into CO_2 stream implies that solvent(s)-enriched CO_2 flooding is a highly promising technique to recover heavy oil resources where other recovery techniques are not economically or efficiently available. The PR EOS together with the proposed BIP correlations is able to predict the

saturation pressures and swelling factors of solvent(s)-CO_2-heavy oil systems with a good accuracy. In addition, the Lobe's mixing rule is found to be generally superior to other mixing rules in evaluating solvent-saturated heavy oil viscosities.

CHAPTER 5 DETERMINATION OF EQUILIBRIUM INTERFACIAL TENSION FOR SOLVENT(S) -CO_2-HEAVY OIL SYSTEMS

5.1 Introduction

Immiscible CO_2 flooding is a non-thermal recovery method that has considerable potential for a large range of heavy oil reservoirs, where other enhanced oil recovery (EOR) techniques are not applicable (Tuzunoglu and Bagci, 2000). During the immiscible flooding process, CO_2 is injected into the formation to highly mobilize the contacted oil and displace it towards the production well once diluted and swollen. Oil mobility is improved due to solubility of CO_2 in the oil that causes both a reduction in the viscosity and an increase in oil volume (Al-Abri and Amin, 2010). Recovery mechanisms related to immiscible CO_2 flooding consist of viscosity reduction, oil swelling effect, IFT reduction, and blowdown recovery (Rojas and Farouq Ali, 1986). The dissolved CO_2 functions as a surface-active agent, which is responsible for the IFT reduction (Yang and Gu, 2006). Addition of rich solvents, such as C_3H_8 and/or *n*-C_4H_{10}, into CO_2 stream is a promising technique that can improve the performance of immiscible CO_2 processes in heavy oil reservoirs.

Experiments are first carried out, in this study, to examine the IFT reduction effect of CO_2-heavy oil system caused by addition of C_3H_8 and/or *n*-C_4H_{10}, which has not been covered previously. Due to the large uncertainty involved in characterization of heavy oils, it is extremely difficult to accurately model the equilibrium IFT for the solvent(s)-CO_2-heavy oil systems. In this study, a recently proposed mechanistic parachor model (Ayirala and Rao, 2006) is used to model the equilibrium IFT of solvent(s)-CO_2-heavy oil

systems. More specifically, the PR EOS (Peng and Robinson, 1976) together with the new alpha function Equation [4-7] is used to perform two-phase flash calculations. The flash calculation results are then used as inputs for the mechanistic parachor model (Ayirala and Rao, 2006). Both the parachor of the heavy oil and the mass transfer exponent in mechanistic parachor model are treated as two tuning parameters and optimized by minimizing the discrepancy between the measured and calculated equilibrium IFTs.

5.2 Experimental

An axisymmetric drop shape analysis (ADSA) system (Yang *et al.*, 2005) has been used to measure both the dynamic and equilibrium IFTs between the heavy oil and pure solvents (i.e., CO_2, C_3H_8, and *n*-C_4H_{10}) together with their mixtures (i.e., CO_2-C_3H_8, CO_2-*n*-C_4H_{10}, C_3H_8-*n*-C_4H_{10} and CO_2-C_3H_8-*n*-C_4H_{10}).

5.2.1. Materials

The heavy oil sample is collected from the Lloydminster area in Saskatchewan, Canada. The molar mass of the Lloydminster heavy oil is measured to be 482 g/mol with a freezing point depression method. The density of the Lloydminster heavy oil at 60°F is measured to be 999.7 kg/m^3 by using a densitometer (DMA512P, Anton Paar, USA). The compositional analysis results of the Lloydminster heavy oil are obtained by using the simulated distillation method and provided in TABLE 4-1.

The gas solvents, CO_2, C_3H_8, and *n*-C_4H_{10} (Praxair, Canada) used in the IFT measurements have purities of 99.998 mol%, 99.99 wt%, and 99.9 wt%, respectively.

The pure gases are also used to prepare seven gas mixtures for the IFT measurements. The seven gas mixtures are listed in TABLE 5-1.

5.2.2. IFT measurements

In this study, the axisymmetric drop shape analysis (ADSA) for the pendant drop case is employed to measure both the dynamic and equilibrium IFTs of the aforementioned three pure solvents and seven solvent mixtures with the Lloydminster heavy oil at different temperatures and pressures.

FIGURE 5-1 shows a schematic of the ADSA system for the pendant drop case used in this study. A major component of this system is a see-through-windowed high-pressure cell (IFT-10, Temco), which has a chamber volume of 41.5 cm^3. The maximum operating pressure and temperature of this pressure cell are 69000 kPa and 177.0°C, respectively. The temperature during the measurements is maintained by a heating tape (HT95504×1, Electrothermal) with the accuracy of ±0.1°C, which is connected to a stepless temperature controller (CN45515, Thermolyne). The pressure of the high-pressure cell is measured with a digital precision test gauge (Model 2089, Ashcroft) with an accuracy of 0.05% of full range, while the temperature is measured by using a thermocouple (JMQSS-125U-6, Omega) with an accuracy of 0.1°C. The light source and glass diffuser are used to provide a uniform illumination for the pendant oil drop. A MZ6 microscope camera (Leica, Germany) is used to capture the sequential digital images of the dynamic pendant drops. The entire experimental setup is positioned on a vibration-free table (RS4000, Newport). All the digital images of the pendant oil drop are stored in a desktop computer, subsequently digitized and computed.

TABLE 5-1: Compositions of seven solvent mixtures

Mixture No.	Composition
1	89.3 mol% CO_2, 10.7 mol% C_3H_8
2	76.0 mol% CO_2, 24.0 mol% C_3H_8
3	62.3 mol% CO_2, 37.7 mol% C_3H_8
4	81.5 mol% CO_2, 18.5 mol% *n*-C_4H_{10}
5	76.8 mol% C_3H_8, 23.2 mol% *n*-C_4H_{10}
6	61.4 mol% C_3H_8, 38.6 mol% *n*-C_4H_{10}
7	93.0 mol% CO_2, 5.9 mol% C_3H_8, 1.1 mol% *n*-C_4H_{10}

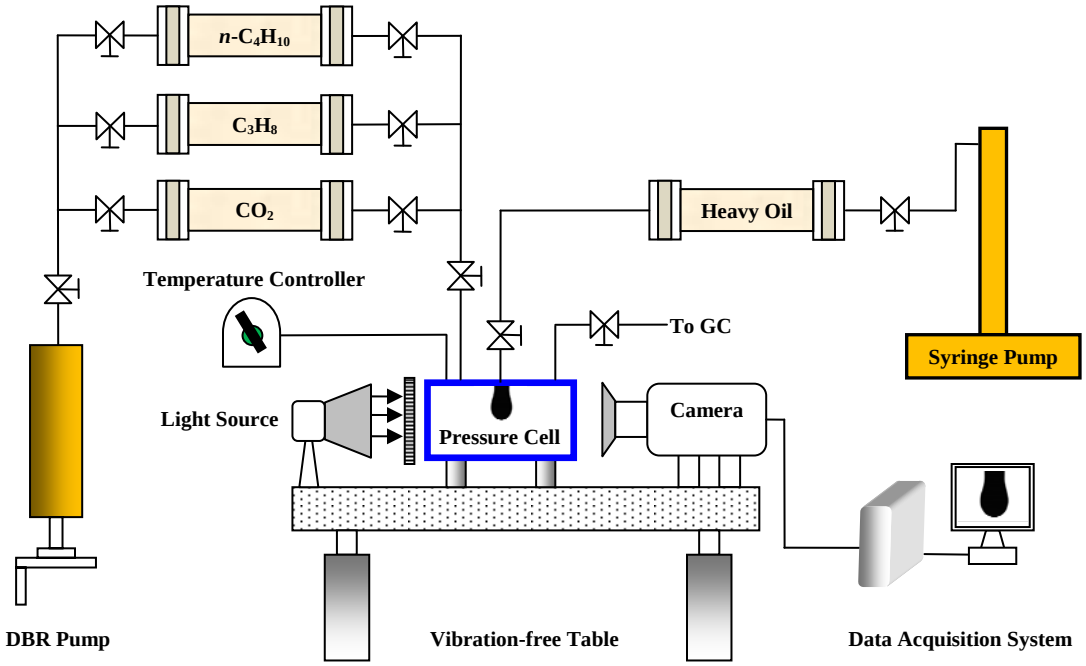

FIGURE 5-1: Schematic diagram of experimental setup for measuring the dynamic and equilibrium IFT of solvent(s)-CO_2-heavy oil systems by using the ADSA technique for the pendant drop case

The three gaseous solvents (CO_2, C_3H_8, and n-C_4H_{10}) are pressurized in three sample cylinders which are controlled by using a manual positive displacement pump (PMP-500-1-10-HB, DBR, Canada). The heavy oil sample is contained in a sample cylinder that is controlled by a syringe pump (500HP, ISCO Inc., USA). The IFT of the CO_2-heavy oil system is measured in the pressure ranges of 1101-15640 kPa at 21.0°C and 3190-11175 kPa at 44.0°C, respectively, C_3H_8-heavy oil system in the pressure ranges of 195-801 kPa at 21.0°C and 201-823 kPa at 46.1°C, respectively, and n-C_4H_{10}-heavy oil system in the pressure ranges of 123-213 kPa at 21.0°C and 116-219 kPa at 48.6°C, respectively. It should be noted that the dynamic and equilibrium IFTs of the solvent mixture-heavy oils systems are all measured below the dewpoint pressures of the respective solvent mixtures at 21.0°C.

Prior to each measurement between pure gas solvent and heavy oil, the high-pressure cell is thoroughly cleaned with ethanol and then flushed with the pure solvent. Then the pressure cell is filled with a pure gas solvent at a specified pressure and a constant temperature. As for the IFT measurements for a solvent mixture, one solvent is first injected into the pressure cell to pressurize the pressure cell to a certain pressure. Subsequently, another solvent is then injected into the pressure cell, resulting in a different pressure, until all the desired solvents are present in the pressure cell with their individual fraction. A sampler (Swagelok, Canada) with a volume of 10 cm^3 and a pressure rating of 1000 psi is used to collect the gas solvent sample inside the high pressure cell. Then the composition of the sample is determined by using a gas chromatography (GC) method. After the pressure and temperature inside the pressure cell are stabilized, the heavy oil is introduced from the sample cylinder to the pressure cell to

form a pendant oil drop at the syringe needle tip. Once a well-shaped pendant drop is formed, the sequential digital images of the dynamic pendant oil drop at different times are acquired and stored automatically in the desktop computer. It should be noted that the density of heavy oil and density of bulk gas phase are required inputs for implementing the ADSA program. In this study, the density of Lloydminster heavy oil at any temperature and pressure can be calculated by using the heavy oil density correlation presented elsewhere (Li *et al.*, 2011), while the density of the bulk solvent phase is calculated with the PR EOS. Thereafter, the ADSA program for the pendant drop case is executed to determine both the dynamic and equilibrium IFT by solving the Laplace equation of capillarity. Each IFT measurement is repeated three times to ensure the repeatability of the measurement.

5.3 Mathematical Formulation

5.3.1. PR EOS model

The PR EOS is chosen as the equation of state for describing phase behaviour of solvent(s)-CO_2-heavy oil systems. The detailed expressions of the PR EOS together with the new alpha function can be found in CHAPTER 3 of this dissertation. In this study, the heavy oil sample is treated as a single pseudocomponent, while the specific gravity and molar mass are used as the two characterization parameters. The characterization method for the heavy oil sample is provided in CHAPTER 4. Once the heavy oil is characterized by its critical properties, the BIP matrix (δ) remains the single parameter that is needed in PR EOS to model the phase behaviour of solvent(s)-CO_2-heavy oil systems at a given condition. The BIP matrix for a four-component fluid system which is comprised of CO_2,

C_3H_8, *n*-C_4H_{10} and heavy oil is shown in TABLE 4-6. The fixed δ_{12} and δ_{13} values for CO_2-C_3H_8 and CO_2-*n*-C_4H_{10} are rigorously reviewed data which are retrieved from a commercial phase behaviour simulator (Computer Modelling Group Ltd., 2009), while δ_{23} value for C_3H_8-*n*-C_4H_{10} is calculated to be 0.00087 by using the commonly used correlation for hydrocarbon-hydrocarbon binaries (Computer Modelling Group Ltd., 2009),

$$\delta_{ij} = 1 - \left[\frac{2\sqrt{V_{ci}^{1/3} V_{cj}^{1/3}}}{V_{ci}^{1/3} + V_{cj}^{1/3}} \right]^{1.2} \qquad [5\text{-}1]$$

Correlations for δ_{14} and δ_{24} have been developed by fitting experimental solubility data for CO_2-heavy oil systems and C_3H_8-heavy oil systems that are presented in CHAPTER 4 (See Equations [4-18] and [4-19]), respectively. The BIP between *n*-C_4H_{10} and the Lloydminster heavy oil is estimated by Equation [5-1].

5.3.2. Mechanistic parachor model for equilibrium IFT

Parachor model is a conventional IFT model that is widely used in petroleum industry for calculating IFT between two immiscible fluid systems. Macleod (1923) and Sudgen (1924) related surface tension of a pure compound to the molar density difference between the coexisting phases with,

$$\sigma^{1/4} = P_a \left(\rho^L - \rho^V \right) \qquad [5\text{-}2]$$

where σ is surface tension (mN/m), ρ^L and ρ^V are molar densities of the liquid and vapour phases (mol/cm^3), respectively, and P_a is known as the parachor.

The original parachor model for pure substances was extended to a multicomponent mixture by Weinaug and Katz (1943) as follows,

$$\gamma^{1/4} = \rho^{\mathrm{L}} \sum_{i=1}^{nc} x_i P_{\mathrm{a}i} - \rho^{\mathrm{V}} \sum_{i=1}^{nc} y_i P_{\mathrm{a}i} \qquad [5\text{-}3]$$

where γ is equilibrium IFT between the bulk liquid phase and vapour phase of the multicomponent mixture, x_i and y_i are mole percentages of the ith component in the bulk liquid phase and vapour phase, respectively, nc is number of components in the mixture, and $P_{\mathrm{a}i}$ is parachor of the ith component. Although many parachor correlations have been proposed to estimate the parachor of petroleum fraction (Firoozabadi *et al.*, 1988; Ahmed, 1989), there is no consensus on which correlation provides the most accurate estimation for heavy oil. In this study, the parachor of the Lloydminster heavy oil P_{ao} is treated as a tuning parameter in the parachor model.

The parachor model has found its successful application for predicting IFT of pure compounds and binary mixtures. However, this model provides a poor accuracy for predicting IFT of complex hydrocarbon mixtures, in particular, the ones involved with heavy oils. Ayirala and Rao (2006) recently proposed a mechanistic parachor model that took into account of mass transfer effect by introducing a ratio of diffusivity coefficients raised to an exponent. The mechanistic parachor model is given as (Ayirala and Rao, 2006),

$$\gamma^{1/4} = \left(\frac{D_{\mathrm{os}}}{D_{\mathrm{so}}} \right)^{n/4} \left(\rho^{\mathrm{L}} \sum_{i=1}^{nc} x_i P_{\mathrm{a}i} - \rho^{\mathrm{V}} \sum_{i=1}^{nc} y_i P_{\mathrm{a}i} \right) \qquad [5\text{-}4]$$

where D_{os} is diffusivity of oil in gas solvent, D_{so} is diffusivity of gas solvent in oil, and n denotes the exponent whose sign and value characterize the type and extent of the

governing mass transfer mechanism for fluid phase equilibria. As noted by Ayirala and Rao (2006), if n>0, vaporization of lighter components from the oil into the gas phase plays a dominant role in the governing mass transfer mechanism, whereas, if n<0, condensation of gas solvents into oil contributes more. A value of n equal to approximately zero indicates equal proportions of vaporizing and condensing mass transfer mechanisms. The empirical diffusivity correlation provided by Wilke and Chang (1995) is used to estimate the diffusivities in Equation [5-4],

$$D_{\mathrm{AB}} = \frac{117.3\times10^{-18}\left(kM_{\mathrm{B}}\right)^{0.5}T}{\mu V_{\mathrm{A}}^{0.6}} \qquad [5\text{-}5]$$

where D_{AB} is diffusivity of solute A in solvent B (m^2/s), M_{B} is molar mass of the solvent B (g/mol), T is temperature (K), μ is solution viscosity ($\mathrm{Pa}\cdot\mathrm{s}$), V_{A} is solute molar volume at normal boiling point (m^3/kmol), and k is association factor for solvent, which is equal to unity for unassociated solvents. The substances considered in this study, i.e., CO_2, C_3H_8, n-C_4H_{10}, and heavy oil, are assumed to be unassociated, resulting in $k=1$. Equation [5-5] is extended to multicomponent mixtures by using (Ayirala and Rao, 2006),

$$M_{\mathrm{B}} = \sum_{i=1}^{nc} x_{\mathrm{B}i} M_{\mathrm{B}i} \qquad [5\text{-}6]$$

$$V_{\mathrm{A}} = \sum_{i=1}^{nc} x_{\mathrm{A}i} V_{\mathrm{A}i} \qquad [5\text{-}7]$$

where $x_{\mathrm{B}i}$ is mole fraction of the ith component in the mixture, $M_{\mathrm{B}i}$ is molar mass of the ith component, and $V_{\mathrm{A}i}$ is molar volume of ith component at normal boiling point. In this study, the molar volumes of CO_2, C_3H_8, n-C_4H_{10}, and heavy oil at normal boiling point are calculated with the accurate Rackett equation of Spencer and Danner (1972),

$$V_{\mathrm{A}} = \frac{RT_c}{P_c} Z_{\mathrm{RA}}^{\left[1+(1-T_{\mathrm{br}})^{2/7}\right]} \qquad [5\text{-}8]$$

where T_{br} is the reduced temperature at normal boiling point, and Z_{RA} is Rackett parameter that is a constant for a given substance. The Rackett parameter of the heavy oil sample can be calculated with Equation [4-13], while the following correlation for the PR EOS is used to correct molar volume for pure substance (Twu and Chan, 2009),

$$C = 0.406501\left(\frac{RT_{\mathrm{C}}}{P_{\mathrm{C}}}\right)\left(0.260484 - Z_{\mathrm{RA}}\right) \qquad [5\text{-}9]$$

Once all the required input information for the mechanistic parachor model has been acquired, the parachor of the Lloydminster heavy oil and the exponent *n* in Equation [5-4] are optimized by minimizing the root-mean-squared relative error (*RMSRE*) between the measured and calculated IFT data,

$$RMSRE_{\mathrm{IFT}} = \sqrt{\frac{1}{N}\sum_{i=1}^{N}\left[\frac{IFT_i^{\mathrm{cal}} - IFT_i^{\mathrm{exp}}}{IFT_i^{\mathrm{exp}}}\right]^2} = f\left(n, P_{\mathrm{ao}}\right) \qquad [5\text{-}10]$$

where IFT^{cal} is the calculated IFT, IFT^{exp} is the measured IFT, and *N* is total number of data point.

5.4 Results and Discussion

5.4.1. Dynamic IFT of the solvent(s)-CO_2-heavy oil systems

The dynamic IFT of solvent(s)-heavy oil systems are measured as a function of time to examine the effect of mass transfer between solvent(s) and heavy oil on IFT. FIGURE 5-2 plots four typical measurements of dynamic IFT for three pure solvents (CO_2, C_3H_8, and *n*-C_4H_{10}) and a solvent mixture (62.3 mol% CO_2, 37.7 mol% C_3H_8) at 21.0°C. It can

be seen from FIGURE 5-2 that, for the CO_2-heavy oil system, the dynamic IFT remains almost constant as a function of time at P=1100 kPa and T=21.0°C. This means that the CO_2-heavy oil interface is able to quickly reach the equilibrium state, even though the dissolution process of CO_2 into the pendant heavy oil drop may take place for a long duration (Yang and Gu, 2005; 2006). As for the C_3H_8-heavy oil system at 195 kPa and 21.0°C and *n*-C_4H_{10}-heavy oil system at 215 kPa and 21.0°C, the dynamic IFT varies with a slightly larger degree at the initial stage of the mass transfer process compared to that of the CO_2-heavy oil system and remains almost a constant afterwards. The relatively large variation of the dynamic IFT for the C_3H_8-heavy oil and *n*-C_4H_{10}-heavy oil systems may be attributed to the fast and large swelling of the pendant heavy oil drop due to the dissolution of rich solvents (Yang and Gu, 2005).

The variation trend of the measured dynamic IFTs for the pure solvent-heavy oil systems are in a good agreement with those reported previously (Yang and Gu, 2005). For the solvent mixture (62.3 mol% CO_2, 37.7 mol% C_3H_8) and heavy oil system at 1600 kPa and 21.0°C, the measured dynamic IFTs fluctuate around 15 mN/m during the observation period. This may be due to the interplay of mass transfer processes of the three solvents present in the mixture into the pendant heavy oil drop. Overall, it is reasonable to consider that the dynamic IFT can reach its equilibrium value within a short period (600 s).

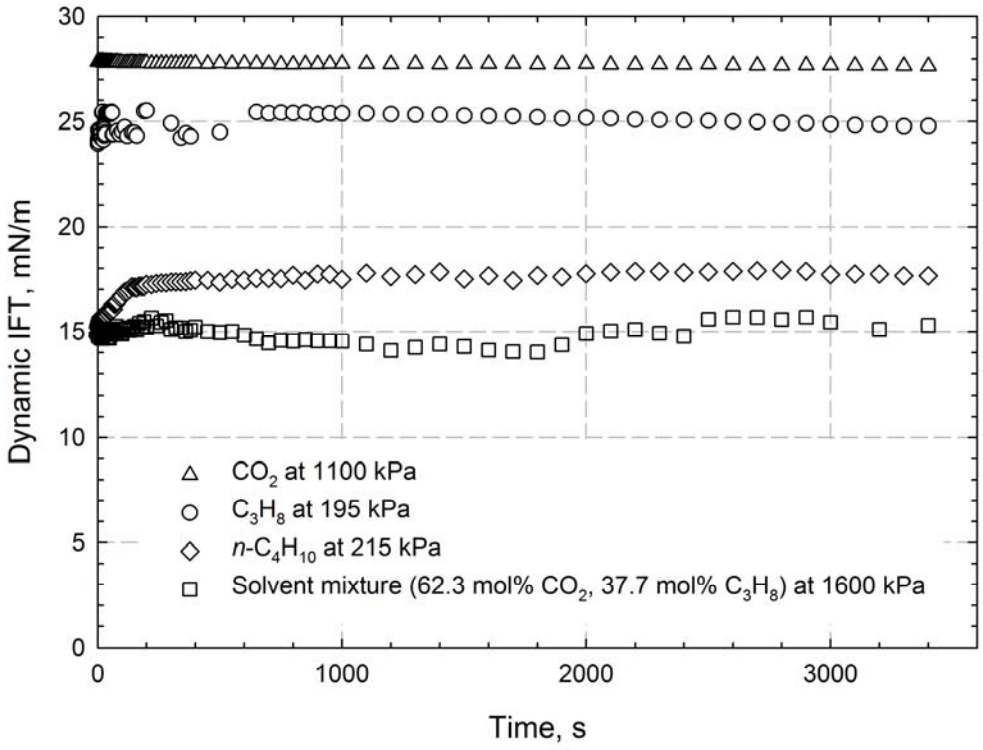

FIGURE 5-2: Measured dynamic IFT as a function of time between various solvents and heavy oil at 21.0°C

5.4.2. Equilibrium IFT of the solvent(s)-CO_2-heavy oil systems

In order to examine the effect of adding rich solvent(s) C_3H_8 and *n*-C_4H_{10} into CO_2 stream on the equilibrium IFT, the equilibrium IFT measurements have been also conducted between the Lloydminster heavy oil and seven solvent mixtures that are composed of CO_2, C_3H_8, and *n*-C_4H_{10} with varied fractions. All the equilibrium IFTs of solvent(s)-heavy oil systems are measured in the liquid-vapour phase region, except for the CO_2-heavy oil system. The conventional parachor model is found to significantly underestimate the measured equilibrium IFTs of the solvent(s)-heavy oil systems in the liquid-liquid or dense fluid-liquid (at supercritical conditions) phase region, though it can represent qualitatively the measured equilibrium IFTs of the solvent(s)-CO_2-heavy oil systems in the liquid-vapour phase region. Therefore, only the equilibrium IFT data for all the solvent(s)-CO_2-heavy oil systems measured in the liquid-vapour phase region are selected to optimize the parachor of Lloydminster heavy oil and mass transfer exponent in the mechanistic parachor model. TABLE 5-2 shows the basic physical properties of the solvents and Lloydminster heavy oil used in the mechanistic parachor model. The BIPs for CO_2-heavy oil pair and C_3H_8-heavy oil pair are predicted by using Equations [4-18] and [4-19], respectively, while BIP for *n*-C_4H_{10}-heavy oil pair is calculated with Equation [5-1].

FIGURE 5-3 shows variation of the objective function $RMSRE_{IFT}$ with the parachor of Lloydminster heavy oil and the mass transfer exponent in the mechanistic model. The optimum parachor of Lloydminster heavy oil and mass transfer exponent are found to be 835 and -0.448, respectively, which leads to the minimum $RMSRE_{IFT}$ of 0.1574. Hence,

TABLE 5-2: Physical properties of the three solvents and Lloydminster heavy oil used in the mechanistic parachor model

Component	P_C, **kPa**	T_C, **K**	ω	Z_{ra}	V_c, **m^3/kmol**	V_A, **m^3/kmol**	**Parachor**
CO_2	7378	304.14	0.2238	0.2736	0.0940	0.0356	78.0
C_3H_8	4246	369.80	0.1520	0.2763	0.2030	0.0757	150.0
n-C_4H_{10}	3786	425.20	0.1930	0.2728	0.2550	0.0967	189.9
Lloydminster heavy oil	1265	933.66	1.0288	0.2622	1.2460	0.6962	P_{ao}

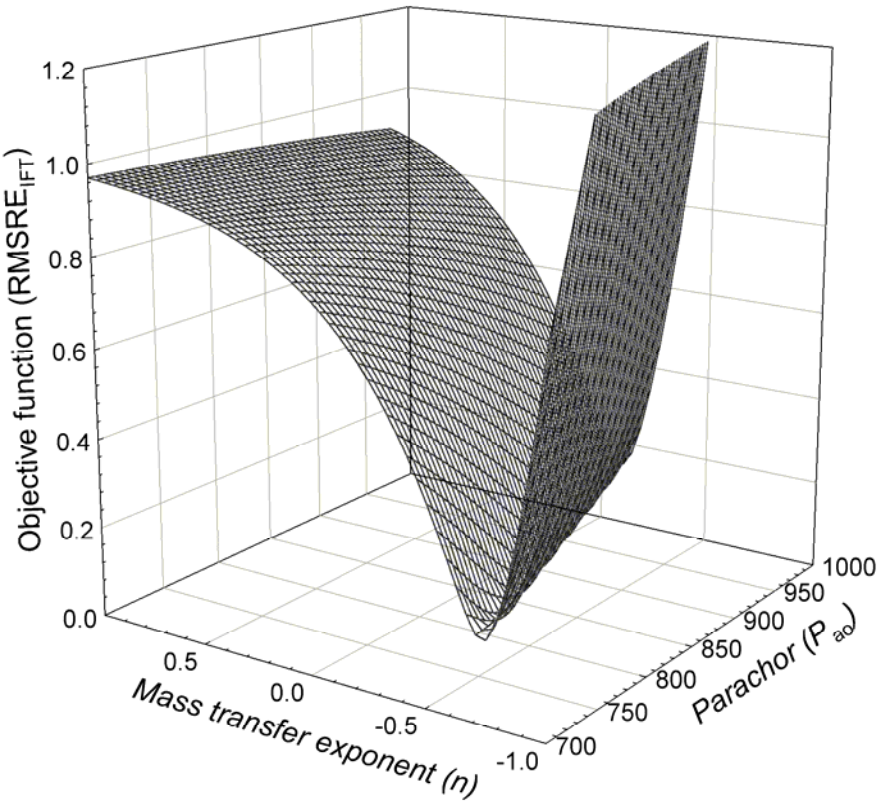

FIGURE 5-3: Variation of the objective function $RMSRE_{IFT}$ with the parachor of Lloydminster heavy oil P_{ao} and the mass transfer exponent n in the mechanistic model

the mechanistic parachor model for describing the equilibrium IFT of solvent(s)-CO_2-heavy oil systems is finalized as follows,

$$\gamma = \left(\frac{D_{os}}{D_{so}} \right)^{-0.448} \left(\rho^L \sum_{i=1}^{nc} x_i P_{ai} - \rho^V \sum_{i=1}^{nc} y_i P_{ai} \right)^4 \qquad [5\text{-}11]$$

Equation [5-11] results in a percentage average absolute deviation (%AAD) of 11.86% for reproducing the measured 56 liquid-vapour equilibrium IFT data points. It is worthwhile mentioning that the negativity of exponent *n* indicates that the condensation or dissolution of gas solvents into heavy oil is the controlling mass transfer process for the solvent(s)-heavy oil systems (Ayirala and Rao, 2006). It is reasonable to consider the fact that the Lloydminster heavy oil is mainly composed of heavy hydrocarbon components, and thus the extraction of light components from heavy oil by solvent(s) would be insignificant. This can be also confirmed by the calculated phase compositions. For example, for Mixture #7 (93.0 mol% CO_2, 5.9 mol% C_3H_8, 1.1 mol% *n*-C_4H_{10}), the calculated phase compositions for the feed (92.9 mol% CO_2, 5.9 mol% C_3H_8, 1.1 mol% *n*-C_4H_{10}, 0.1 mol% heavy oil) at 1101 kPa and 21.0°C are (14.0 mol% CO_2, 4.9 mol% C_3H_8, 2.8 mol% *n*-C_4H_{10}, 78.3 mol% heavy oil) for the liquid phase and (93.0 mol% CO_2, 5.9 mol% C_3H_8, 1.1 mol% *n*-C_4H_{10}, 0.0 mol% heavy oil) for the gas phase. It is apparent from the calculated phase compositions that the gas solvents CO_2, C_3H_8 and *n*-C_4H_{10} dissolve into heavy oil, while heavy oil is not noticeable in the gas phase. It is also valid for other solvents-CO_2-heavy oil systems where no heavy oil or only negligible trace of heavy oil is present in the gas phase.

***Pure solvent-heavy oil system*:** FIGURE 5-4a depicts the measured and calculated equilibrium IFTs for the CO_2-heavy oil system at 21.0°C and 44.0°C, respectively. In

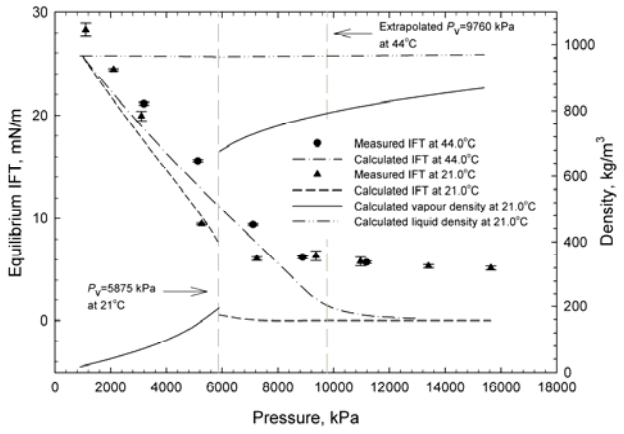

(a)

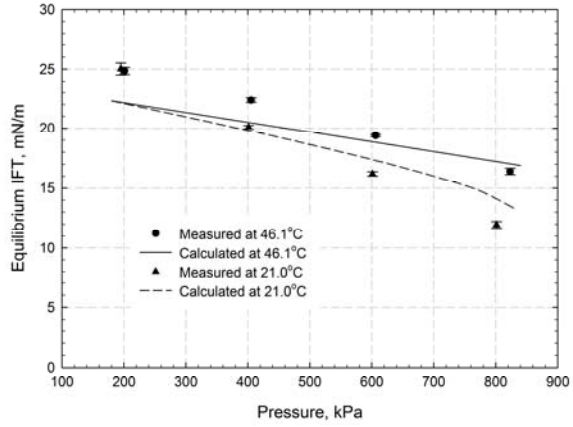

(b)

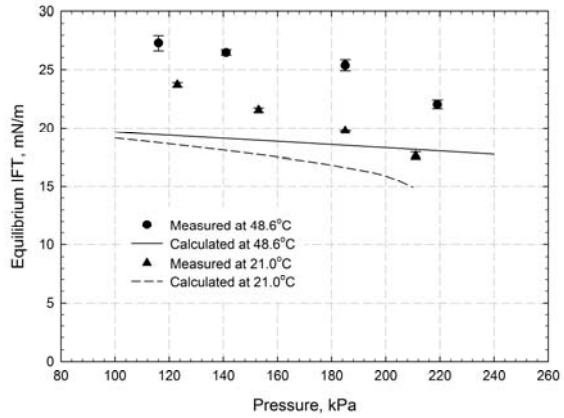

(c)

FIGURE 5-4: Comparison of the measured and calculated equilibrium IFT using the mechanistic model Equation [5-11] for the pure solvent-heavy oil systems: (a) CO_2-heavy oil system at 21.0°C and 44.0°C, respectively; (b) C_3H_8-heavy oil system at 21.0°C and 46.1°C, respectively; and (c) *n*-C_4H_{10}-heavy oil system at 21.0°C and 48.6°C, respectively

general, at a given temperature, it can be seen from FIGURE 5-4a that the equilibrium IFT of the CO_2-heavy oil system decreases significantly at the initial stage as pressure increases and then decreases slightly with the further increase of pressure. In addition, the IFT of the CO_2-heavy oil system at 44.0°C is found to be higher than that at 21.0°C. The similar variation trend of IFT with pressure and temperature has also been reported for a CO_2-light oil system (Yang and Gu, 2005). The variation trend of IFT with pressure and temperature is consistent with the change of CO_2 solubility with pressure and temperature. The CO_2 solubility at a higher temperature is lower than that at a lower temperature, resulting in a higher IFT (Simon and Graue, 1965).

At a given temperature, the initial dramatic reduction of IFT is mainly because of the increased solubility of CO_2 in heavy oil due to an increase in pressure (Simon and Graue, 1965). At some points where liquid-liquid two phase (subcritical for CO_2) or dense fluid-liquid (supercritical for CO_2) two phase appears, further increase of pressure will only lead to a slight increase of CO_2 solubility in heavy oil (Sayegh *et al.*, 1990), consequently, leading to only a slight decrease of the IFT. It is found that the transition pressure where the large IFT reduction terminates due to pressure increase can be approximated with the vapour pressure of CO_2 at subcritical temperatures or extrapolated vapour pressure of CO_2 at supercritical temperatures. The transition pressures for the CO_2-heavy oil system at 21.0°C (subcritical) and 44.0°C (supercritical) are estimated to be 5875 kPa and 9760 kPa (See FIGURE 5-4a), respectively. The calculated IFTs for the CO_2-heavy oil system by using the mechanistic model and the phase densities are also plotted in FIGURE 5-4a.

It can be seen that the mechanistic parachor model provides a qualitative agreement with the measured IFTs for the CO_2-heavy oil system at pressures lower than the

aforementioned transition pressure, but significantly underestimates the IFT at pressures beyond the transition pressure. At a higher pressure, the CO_2-dominant phase exists as either a liquid at subcritical temperatures (e.g., 21.0°C) or a liquid-like dense fluid at supercritical temperatures (e.g., 44.0°C). It can be found from FIGURE 5-4 the parachor model provides low IFTs for the liquid-liquid region or dense fluid-liquid region. This is partially attributed to a smaller density difference of the coexisting liquid phases as shown in FIGURE 5-4a compared to that of the liquid and vapour phase (See Equation [5-11]). In addition, it is the discontinuity of vapour phase density that causes the discontinuous change in the calculated IFT at 21.0°C.

FIGURE 5-5 shows the calculated *P-X* diagrams for CO_2-heavy oil system by using PR EOS with the modified alpha function at 21.0°C and at 44.0°C, respectively. It can be seen from FIGURE 5-4a that the transition pressure where the discontinuity of IFT data occurs at 21°C coincides with the L_1L_2V three-phase coexisting pressure, i.e., the vapour pressure of CO_2 in this case. FIGUREs 5-4b and c show the measured and calculated equilibrium IFT for the C_3H_8-heavy oil system at 21.0°C and 46.1°C, and *n*-C_4H_{10}-heavy oil system at 21.0°C and 48.6°C, respectively. Comparison of FIGUREs 5-4a, b and c shows that, at the same temperature and pressure, *n*-C_4H_{10} leads to the lowest IFT, while CO_2 has the highest IFT. This is because *n*-C_4H_{10} has the highest solubility in heavy oil, whereas CO_2 has the lowest solubility in heavy oil at the same temperature and pressure (Yang and Gu, 2006). It should be noted in FIGURE 5-4c that the mechanistic parachor model leads to a fairly underestimated equilibrium IFT for the *n*-C_4H_{10}-heavy oil system.

Solvent(s)-CO_2-heavy oil system: FIGURE 5-6 compares the measured and calculated equilibrium IFTs for the CO_2-heavy oil system, CO_2-C_3H_8-heavy oil system,

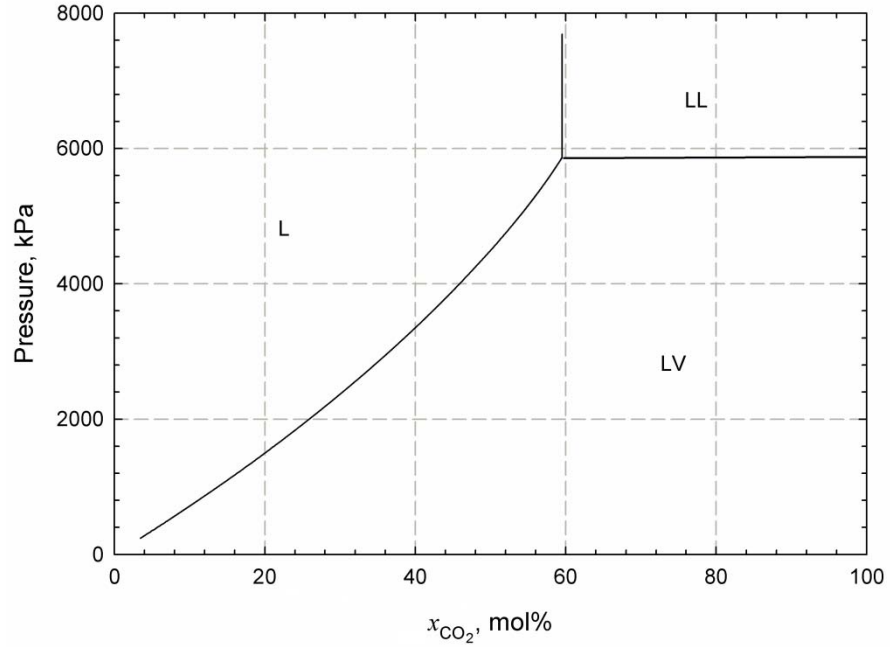

(a)

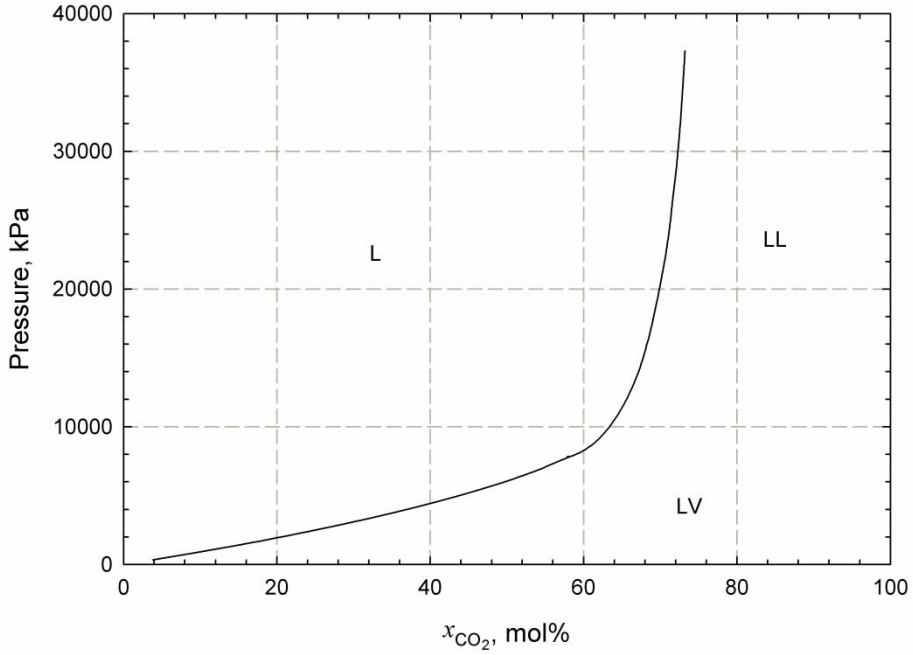

(b)

FIGURE 5-5: Calculated *P-X* diagrams for CO_2-heavy oil system by using PR EOS with the modified alpha function: (a) at 21.0°C and (b) at 44.0°C, respectively

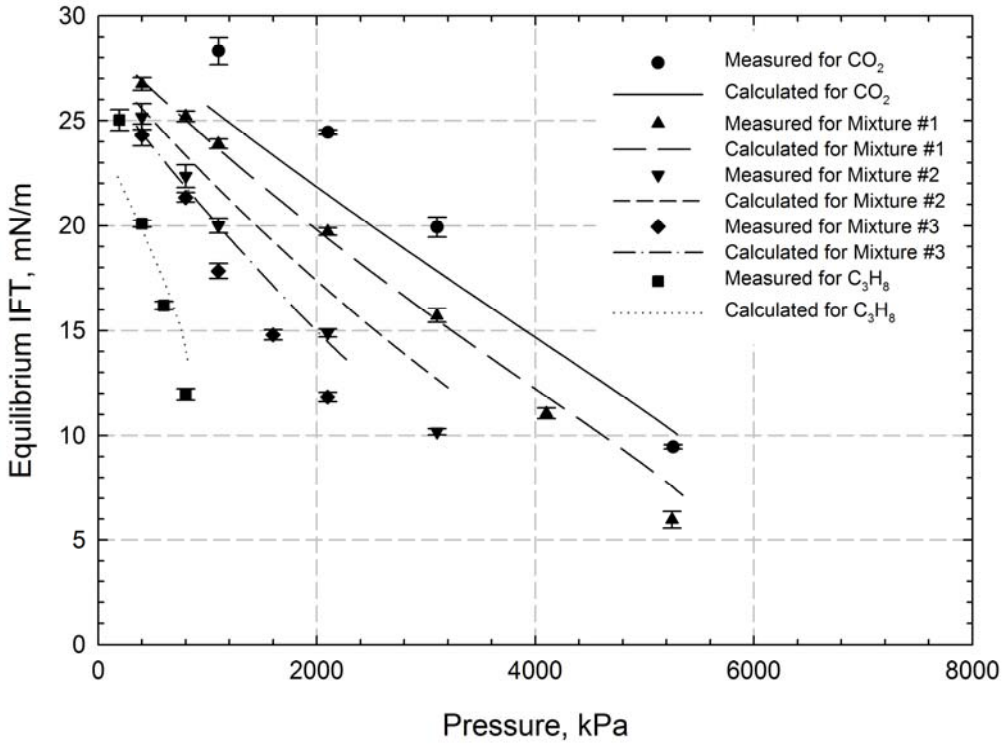

FIGURE 5-6: Comparison of the measured and calculated equilibrium IFT using Equation [5-11] for the CO_2-heavy oil system, CO_2-C_3H_8-heavy oil system (i.e., Mixtures #1, #2 and #3), and C_3H_8-heavy oil system at 21.0°C, respectively. The compositions of Mixtures #1, #2 and #3 are (89.3 mol% CO_2, 10.7 mol% C_3H_8), (76.0 mol% CO_2, 24.0 mol% C_3H_8), and (62.3 mol% CO_2, 37.7 mol% C_3H_8), respectively

and C_3H_8-heavy oil system at 21.0°C, respectively. It is interesting to find from FIGURE 5-6 that addition of C_3H_8 into CO_2 stream is able to significantly reduce the IFT between CO_2 and heavy oil. For example, the IFT of the CO_2-heavy oil system at 3101 kPa and 21.0°C is reduced from 19.92 mN/m to 10.18 mN/m by adding 24.0 mol% C_3H_8 into the CO_2 stream. A greater reduction of IFT is achieved with a larger mole fraction of C_3H_8 that is present in the CO_2-C_3H_8 mixture.

The IFT reduction effect caused by addition of C_3H_8 can be mainly attributed to two factors. Firstly, the addition of C_3H_8 into the CO_2 increased the solubility of gas solvents in the heavy oil. Secondly, the parachor difference between C_3H_8 and heavy oil is smaller than that between CO_2 and heavy oil, which tends to result in a lower IFT according to Equation [5-16]. The mechanistic parachor model provides a reasonably accurate prediction of the IFT for the CO_2-C_3H_8-heavy oil systems.

The measured and calculated equilibrium IFTs for the CO_2-*n*-C_4H_{10}-heavy oil system are shown in FIGURE 5-7. As can be seen from FIGURE 5-7, a significant reduction of IFT can be achieved by adding *n*-C_4H_{10} into CO_2. For example, the IFT between CO_2 and heavy oil at 1101 kPa and 21.0°C is reduced from 28.31 mN/m to 16.07 mN/m by adding 18.5 mol% *n*-C_4H_{10} into the CO_2 stream. The mechanistic parachor model is able to predict the equilibrium IFT for the CO_2-*n*-C_4H_{10}-heavy oil system with a good accuracy.

FIGURE 5-8 compares the measured and calculated equilibrium IFTs for the C_3H_8-*n*-C_4H_{10}-heavy oil system. The addition of *n*-C_4H_{10} into C_3H_8 leads to a reduction of the equilibrium IFT for the C_3H_8-heavy oil system, though the reduction effect is not as significant as that for CO_2-heavy oil system. For example, the IFT of the C_3H_8-heavy oil system at 401 kPa and 21.0°C is reduced from 20.09 mN/m to 17.99 mN/m by adding

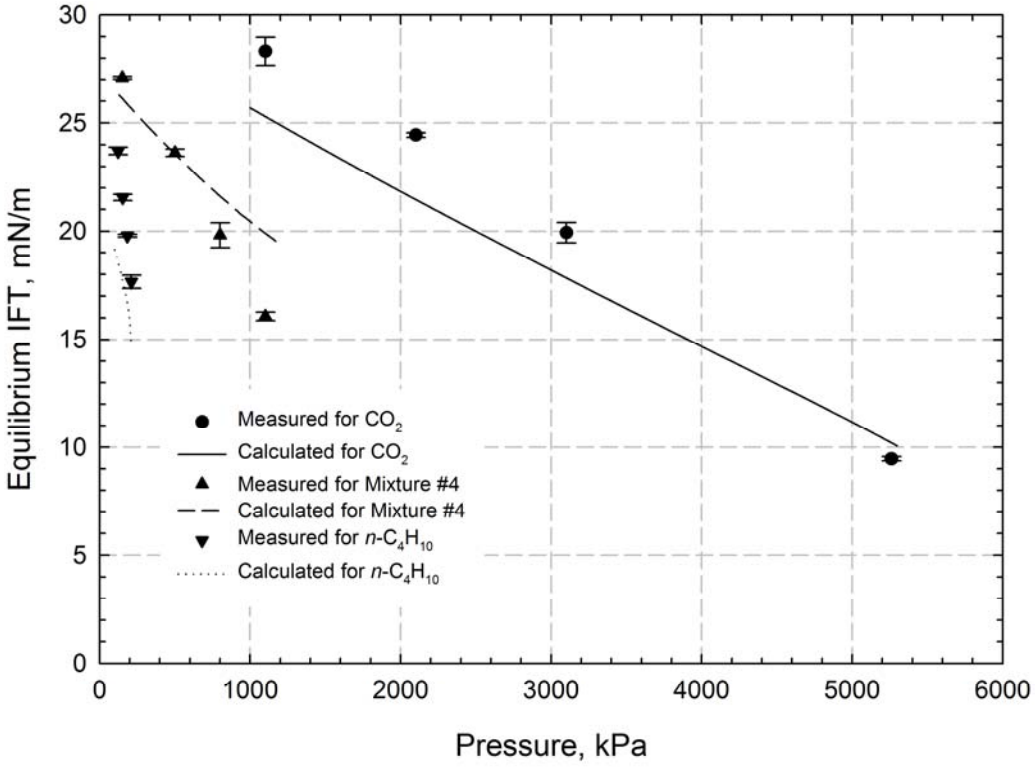

FIGURE 5-7: Comparison of the measured and calculated equilibrium IFT using Equation [5-11] for the CO_2-heavy oil system, CO_2-*n*-C_4H_{10}-heavy oil system (i.e., Mixture #4), and *n*-C_4H_{10}-heavy oil system at 21.0°C, respectively. The composition of Mixture #4 is (81.5 mol% CO_2, 18.5 mol% *n*-C_4H_{10})

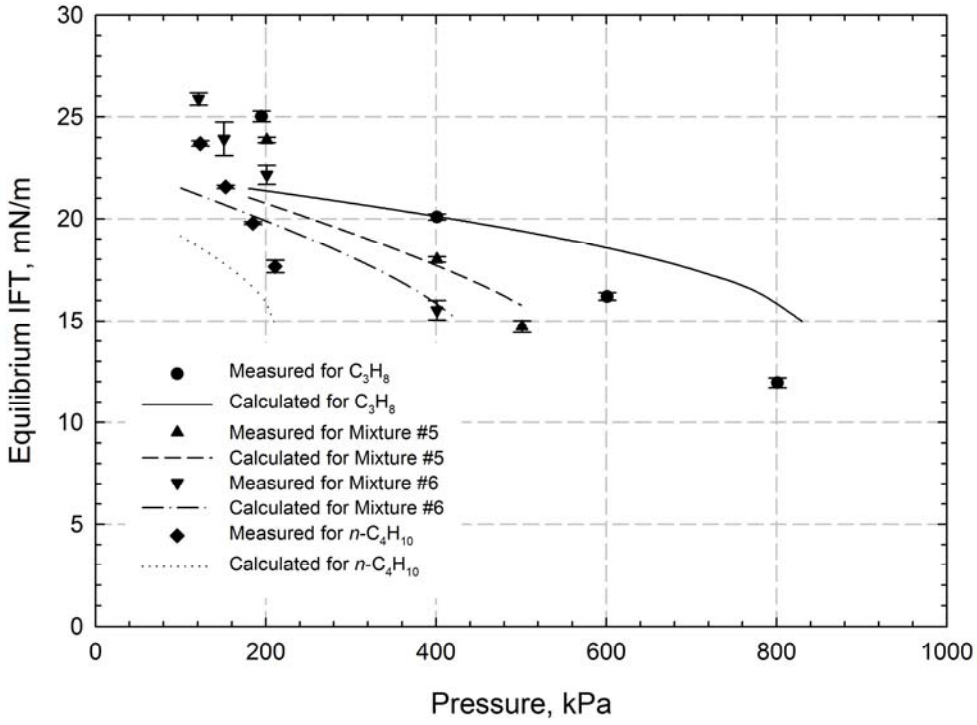

FIGURE 5-8: Comparison of the measured and calculated equilibrium IFT using Equation [5-11] for the C_3H_8-heavy oil system, C_3H_8-n-C_4H_{10}-heavy oil system (i.e., Mixtures #5 and #6), and n-C_4H_{10}-heavy oil system at 21.0°C, respectively. The compositions of Mixtures #5 and #6 are (76.8 mol% C_3H_8, 23.2 mol% n-C_4H_{10}) and (61.4 mol% C_3H_8, 38.6 mol% n-C_4H_{10}), respectively

23.2 mol% *n*-C_4H_{10} into the C_3H_8 stream. A greater reduction of IFT is achieved with a larger fraction of *n*-C_4H_{10}. The mechanistic parachor model cannot accurately reproduce the measured equilibrium IFTs for the C_3H_8-*n*-C_4H_{10}-heavy oil system. This is probably because the mechanistic parachor model provides fairly underestimated equilibrium IFTs for the *n*-C_4H_{10}-heavy oil system.

FIGURE 5-9 shows the measured and calculated equilibrium IFTs between heavy oil and Mixture #7 (93.0 mol% CO_2, 5.9 mol% C_3H_8, 1.1 mol% *n*-C_4H_{10}). Compared to the pure CO_2 case, the solvent mixture leads to a reduced IFT due to the presence of the rich solvents of C_3H_8 and *n*-C_4H_{10}. For example, the IFT of the CO_2-heavy oil system at 3101 kPa and 21.0°C is reduced from 19.92 mN/m to 15.28 mN/m by adding 5.9 mol% C_3H_8 and 1.1 mol% *n*-C_4H_{10} into the CO_2 stream. It can be seen from FIGURE 5-9 that there exists a good agreement between the measured and calculated IFT for Mixture #7. It is worthwhile mentioning that another effect of adding rich solvents into CO_2 is reduction of the dewpoint pressure of the gas phase. *n*-C_4H_{10} shows a larger reduction effect compared to C_3H_8. In practice, it is more desirable to keep the injected solvents at gaseous state other than liquid state in a solvent processes for heavy oil recovery from the pressure maintenance point of view (Upreti *et al.*, 2007; Pathak *et al.*, 2011). Therefore, the type and amount of the added rich solvents must be carefully determined in a solvent recovery process according to the specific reservoir temperature and pressure in order to avoid the occurrence of liquid solvent phase.

It has been demonstrated previously that addition of C_3H_8 and/or *n*-C_4H_{10} into CO_2 results in an obvious reduction of equilibrium IFT between CO_2 and heavy oil. Such reduced IFT is favourable for achieving an improved recovery performance in an

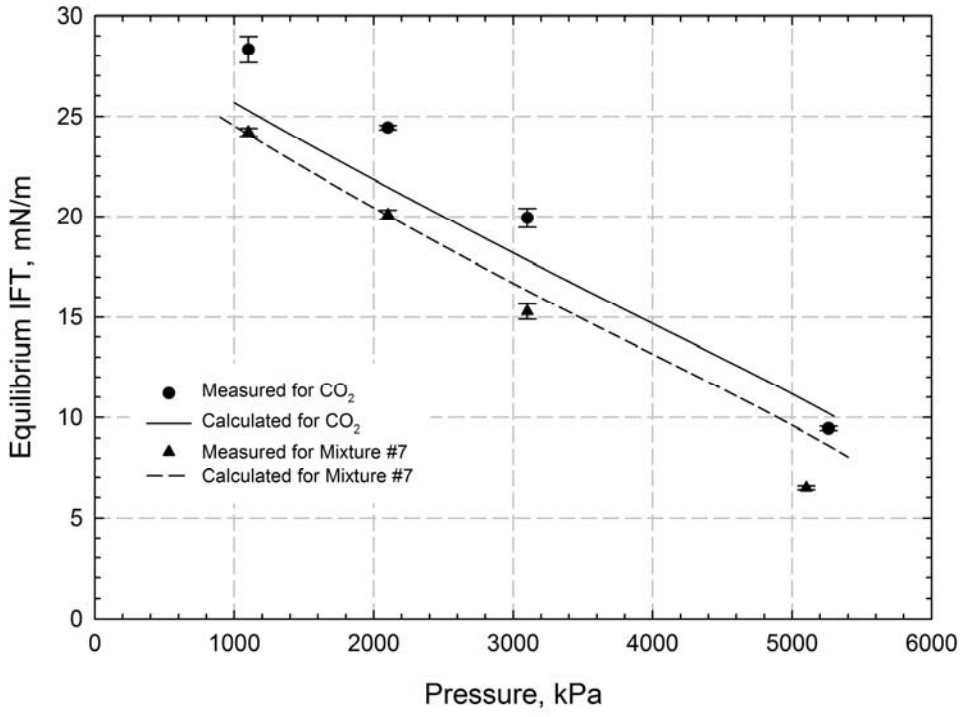

FIGURE 5-9: Comparison of the measured and calculated equilibrium IFT using Equation [5-11] for the CO_2-heavy oil system and CO_2-C_3H_8-*n*-C_4H_{10}-heavy oil system (i.e., Mixture #7) at 21.0°C, respectively. The composition of Mixture #7 is (93.0 mol% CO_2, 5.9 mol% C_3H_8, 1.1 mol% *n*-C_4H_{10})

immiscible CO_2 flooding process because the reduced IFT will result in an increased ratio of viscous to capillary forces, i.e., capillary number. A higher recovery factor of heavy oil can be expected since the recovery factor generally increases with the capillary number (Nobakht *et al.*, 2007).

5.5 Summary

Experimental measurements of the equilibrium IFT for CO_2-, C_3H_8- and *n*-C_4H_{10}-heavy oil systems indicate that, at the same temperature and pressure, *n*-C_4H_{10} leads to the lowest IFT while CO_2 results in the highest IFT. Addition of rich solvent(s) C_3H_8 and/or *n*-C_4H_{10} into CO_2 stream leads to an obvious reduction of IFT between CO_2 and the Lloydminster heavy oil, though the degree of IFT reduction is dependent on the amount of the rich solvent(s) added. The IFT reduction of CO_2-heavy oil system due to addition of rich solvent(s) results in an increased capillary number, which is beneficial for achieving a higher heavy oil recovery.

The PR EOS together with the new alpha function is incorporated into a mechanistic parachor model to determine the equilibrium IFT of solvent(s)-CO_2-heavy oils systems. It is found that the mechanistic parachor model with the optimized parachor of Lloydminster heavy oil and mass transfer exponent can be used to qualitatively reproduce the measured IFTs between solvent(s) and heavy oil in the liquid-vapour phase region.

CHAPTER 6 DETERMINATION OF THREE-PHASE BOUNDARIES OF SOLVENT(S)-CO_2-HEAVY OIL SYSTEMS UNDER RESERVIOR CONDITIONS

6.1 Introduction

Previous studies indicate that, in addition to the normally observed L_1V phase equilibria and L_1L_2 phase equilibria, L_1L_2V phase equilibria may also occur in the solvent(s)-CO_2-heavy oil systems under reservoir conditions (Shaw and Zou, 2007; Talbi and Maini, 2008; Badamchi-Zadeh *et al.*, 2009b). In a typical L_1L_2V phase equilibrium for solvent(s)-CO_2-heavy oil systems, the L_1 phase refers to the high-density liquid phase which contains significant amount of both solvents and heavy oil. The L_2 phase refers to the low-density liquid phase which is mainly composed of liquid solvents, while the V phase refers to the vapour phase which is mainly composed of gaseous solvents. Numerous efforts have been made available to study the three-phase behaviour in CO_2-light oil systems, in which high displacement efficiency can be achieved due to the presence of L_1L_2V phase behaviour (Orr *et al*., 1981; Orr *et al*., 1983; Okuno *et al.*, 2011). However, few efforts have been made available to determine the L_1L_2V three-phase boundary of solvent(s)-CO_2-heavy oil systems under reservoir conditions (Badamchi-Zadeh *et al.*, 2009b).

In this chapter, the L_1L_2V phase boundaries of one CO_2-heavy oil mixture, one *n*-C_4H_{10}-CO_2-heavy oil mixture and one C_3H_8-CO_2-heavy oil mixture in the pressure-temperature (*P*-*T*) diagram are determined by using a pressure-volume-temperature (PVT) setup. The PR EOS model with a modified alpha function and three previously developed

BIP correlations is employed to predict the L_1L_2V phase boundaries for the aforementioned systems. Subsequently, the measured and predicted L_1L_2V phase boundaries have been presented, analyzed, and discussed.

6.2 Experimental

6.2.1. Materials

The heavy oil sample, collected from the Lloydminster area in Saskatchewan, Canada, has molecular weight of 482 g/mol and specific gravity of 0.9997 g/cm^3. The compositional analysis result of the Lloydminster heavy oil is provided in TABLE 4-1. The viscosity equation of the heavy oil sample is given by Equation [4-1], while its density equation is given by Equations [4-4] and [4-5]. The gas solvents, CO_2, C_3H_8 and *n*-C_4H_{10} (Praxair, Canada), used in the measurements have purities of 99.998 mol%, 99.99 wt%, and 99.5 wt%, respectively. The densities of saturated gas solvents can be calculated with Equation [4-6].

6.2.2. Experimental setup

As shown in FIGURE 4-2, all the PVT measurements for the solvent(s)-CO_2-heavy oil systems are performed by using a mercury-free DBR PVT system (PVT-0150-100-200-316-155, DBR, Canada). The detailed description regarding the DBR PVT system can be found in CHAPTER 4.

6.2.3. Experimental procedures

In this study, one CO_2-heavy oil mixture (Feed #13), one C_3H_8-CO_2-heavy oil mixture (Feed #14), and one *n*-C_4H_{10}-CO_2-heavy oil mixture (Feed #15) have been

prepared and tested, respectively. TABLE 6-1 lists the detailed compositions of these three mixtures. Prior to each test, the PVT cell and the inlet tubing are thoroughly cleaned with kerosene, flushed with the gas solvent that will be injected and finally evacuated by using a vacuum pump. Sufficient liquefied CO_2 and C_3H_8 are first stored in the transfer cylinders that are connected to the inlet tubing of the PVT cell. Then the air bath temperature is set to the pre-specified point for at least 12 h to ensure that the transfer cylinders and the PVT cell reach the same temperature. The *n*-C_4H_{10} cylinder, which allows for direct withdrawal of liquid *n*-C_4H_{10} from the cylinder, is also connected to the inlet tubing of the PVT cell.

As for the measurements of CO_2-heavy oil system (i.e., Feed #13), a large amount of liquid CO_2 is injected into the PVT cell just above its vapour pressure using a high-pressure syringe pump (500HP, Teledyne ISCO Inc., USA). The mass of the liquid CO_2 injected can be determined according to its density and its volume measured by the accurate cathetometer. The magnetic stirrer is turned on just after CO_2 injection. Then heavy oil is added to the PVT cell to constitute the composition of Feed #13. The volume of heavy oil injected can be determined to be the total volume minus the liquid solvent volume. No volume change can be assumed since the volume measurement is conducted right after the heavy oil is injected into the PVT cell. Then the mass of heavy oil added can also be determined. The magnetic stirrer is found to be able to work properly because of the presence of excessive CO_2 in the CO_2-heavy oil mixture. The CO_2-heavy oil mixture is vigorously stirred for 6 h prior to any further measurement.

The experimental procedure for measuring the L_1L_2V phase boundary for Feed #13 is briefly described as follows. Starting from a high pressure at which L_1L_2 phase

TABLE 6-1: Compositions of solvent(s)-CO_2-heavy oil systems examined in this study

Feed No.	Composition, wt%				Composition, mol%			
	C_3H_8	*n*-C_4H_{10}	CO_2	Heavy oil	C_3H_8	*n*-C_4H_{10}	CO_2	Heavy oil
13	0.0	0.0	60.4	39.6	0.0	0.0	94.4	5.6
14	12.3	0.0	35.1	52.6	23.6	0.0	67.2	9.2
15	0.0	10.1	54.2	35.7	0.0	11.8	83.2	5.0

equilibrium exists, the system pressure is reduced in a discrete manner by using a high-pressure automatic positive-displacement pump (PMP-0500-1-10-MB-316-M4-C0, DBR, Canada). For each pressure step, the magnetic stirrer is kept on to rigorously stir the CO_2-heavy oil mixture. It is experimentally found that 12 h is sufficient for the cell pressure to reach a stabilized value for each step. A moment after the stirrer is turned off, the equilibrium state of the mixture (e.g., L_1L_2 equilibrium, L_1L_2V equilibrium or L_1V equilibrium) can be determined based on visual observations made upon the mixture.

Once all the measurements for Feed #13 have been completed, a certain amount of liquid *n*-C_4H_{10} is added into Feed #13 to constitute the composition of the *n*-C_4H_{10}-CO_2-heavy oil system (i.e., Feed #15). As for Feed #14, liquid C_3H_8 is first discharged into the PVT cell, followed by adding liquid CO_2 into the PVT cell. Afterwards, a certain amount of heavy oil is added into the PVT cell to achieve the composition of Feed #14. Similarly, the same procedure, used for determining the L_1L_2V phase boundary for Feed #13 at the L_1L_2V-L_1L_2 boundary, is also applied for Feed #14 and #15, respectively. In this study, the pressure measurement, volume measurement, temperature measurement, and determination of mixture composition have uncertainties of ±3.5 kPa, $\pm 1.59\times10^{-2}$ cm^3, ±0.1 K, and ±3.0 wt%, respectively.

6.3 Mathematical Formulation

6.3.1. PR EOS model

The PR EOS together with the new alpha function is used to describe the phase behaviour of solvent(s)-CO_2-heavy oil systems. The detailed expressions of the PR EOS together with the modified alpha function Equation [3-21] can be found in CHAPTER 3.

In this study, the heavy oil sample is treated as a single pseudocomponent, while the specific gravity and molar mass are used as the two characterization parameters. The characterization method for the heavy oil sample is provided in CHAPTER 4. The critical properties of CO_2, C_3H_8, *n*-C_4H_{10} and heavy oil can be found in TABLE 4-9. The BIP for a four-component fluid system which is comprised of CO_2, C_3H_8, *n*-C_4H_{10} and heavy oil is shown in TABLE 4-6. The BIP Equations [4-18], [4-19] and [4-20] are used to calculate the BIPs for CO_2-heavy oil binary, C_3H_8-heavy oil binary, and *n*-C_4H_{10}-heavy oil binary, respectively at a given temperature.

6.3.2. Determination of the L_1L_2V phase boundaries

In general, the L_1L_2V phase boundaries for a multi-component system can be determined by using stability analysis in conjunction with two phase flash calculations. The multi-component system with a given feed will be split into two phases if the minimum tangent plane distance function (TPDF) is calculated to be negative (Baker *et al.*, 1982). It has been shown that the traditional gradient-based method may fail in some cases due to the existence of multiple stationary points for the TPDF (Saber and Shaw, 2008).

In this chapter, the robust global optimization algorithm Dividing RECTangles approach (DIRECT) is used to perform the stability analysis (Saber and Shaw, 2008). Once stability results show that the feed is unstable, two-phase flash calculations will be executed. Stability analysis is again performed for the two phases resulted from the two phase flash calculations. It should be noted that it is only necessary to perform one run of stability analysis for any one of the two equilibrium phases (Li and Firoozabadi, 2010).

Similarly, the three-phase flash calculations are initiated once the stability analysis shows that the multi-component system is unstable in the two-phase state.

At a constant temperature for a given feed, the L_1L_2V-L_2V phase boundary and L_1L_2V-L_1L_2 boundary in *P*-*T* phase diagram can be determined by performing stability analysis and two phase flash calculation with the pressure varying along the isothermal line. Subsequently, the temperature is changed to another point at which the BIPs are recalculated, while stability analysis, two-phase flash calculation and possible three-phase flash calculation are repeated.

6.4 Results and Discussion

The measured three-phase boundary pressures for Feeds #13-15 are tabulated in TABLE 6-2. FIGURE 6-1 shows digital images of the typical phase equilibria captured for the C_3H_8-CO_2-heavy oil system (Feed #14) at 298.55 K. As can be clearly seen from FIGURE 6-1, at the constant temperature of 298.55 K, the ternary C_3H_8-CO_2-heavy oil mixture has experienced L_1V phase equilibrium, L_1L_2V phase equilibrium, and L_1L_2 phase equilibrium in a sequential order with an gradual increase in system pressure. As for a typical L_1L_2V phase equilibrium shown in FIGURE 6-1b, the L_1 phase refers to the high-density liquid phase which contains significant amount of both solvents (i.e., C_3H_8 and CO_2) and heavy oil. The L_2 phase, i.e., the low-density liquid phase, mainly contains liquid solvents (i.e., C_3H_8 and CO_2), while the V phase is mainly composed of gaseous solvents (i.e., C_3H_8 and CO_2).

TABLE 6-2: Raw experimental data obtained in this study

Systems	Temperature, K	L_1L_2V-L_1L_2 boundary pressure, kPa	L_1L_2V-L_1V boundary pressure, kPa
Feed #13	288.65	5175	5097
	298.65	6508	6487
	304.95	Not detected	Not detected
Feed #14	288.95	4640	4305
	298.55	5610	5328
	309.55	Not detected	Not detected
Feed #15	288.65	4595	3754
	298.65	5560	4750
	308.55	6718	5941

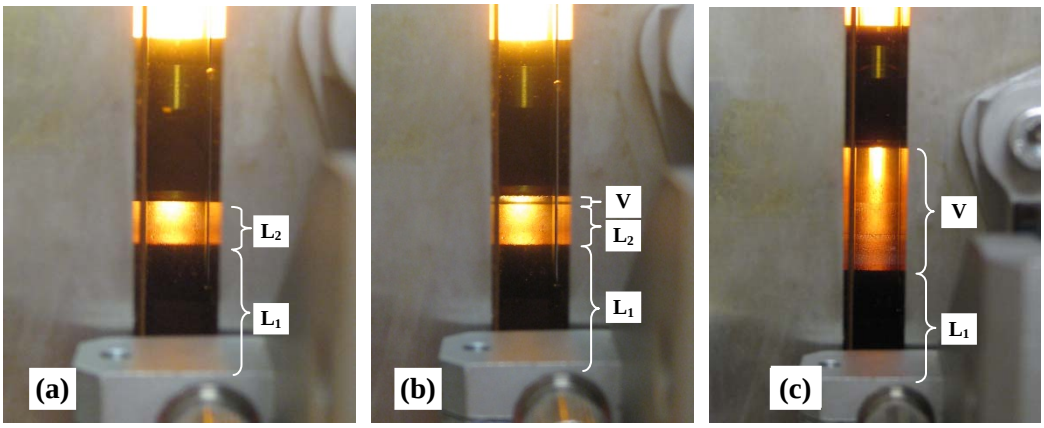

FIGURE 6-1: Digital images of typical phase equilibria captured for the C_3H_8-CO_2-heavy oil system (Feed #14): (a) L_1L_2 phase equilibrium at 298.55 K and 6501.0 kPa; (b) L_1L_2V phase equilibrium at 298.55 K and 5538.0 kPa; and (c) L_1V phase equilibrium at 298.55 K and 5306.0 kPa

6.4.1. CO_2-heavy oil system

FIGURE 6-2 shows the measured L_1L_2V phase boundary together with the calculated one by using PR EOS with Equations [4-7] and [4-18] for CO_2-heavy oil binary: Feed #13. FIGURE 6-2 also includes the measured *K* points (where the L_2 phase and V phase becomes identical) for four CO_2-heavy alkane binaries, i.e., CO_2-*n*-$C_{14}H_{30}$ binary, CO_2-$C_{15}H_{32}$ binary, CO_2-*n*-$C_{19}H_{40}$ binary and CO_2-*n*-$C_{21}H_{44}$ binary (Miller and Luks, 1989). Similar to the CO_2-heavy alkane binaries, emergence of three-phase coexistence in a CO_2-heavy oil binary is attributed to the presence of excessive CO_2 concentration in the binary mixture. It can be seen from FIGURE 6-2 that the L_1L_2V phase boundary of CO_2-heavy oil binary spans within a narrow region on the *P*-*T* phase diagram which is close to the vapour pressure line of pure CO_2. For example, there is only a pressure difference of 78.0 kPa between the L_1L_2V-L_1L_2 phase boundary and the L_1L_2V-L_1V phase boundary at 288.65 K. This small span is consistent with the findings in the literature (Kodal and Sayegh, 1992). Also, the L_1L_2V phase boundary becomes narrower with an increase in temperature.

It can also be found from FIGURE 6-2 that the L_1L_2V phase boundary is predicted to be a line, instead of a narrow area measured by the experiments (Sayegh *et al.*, 1990; Kodal and Sayegh, 1992) by using the PR EOS with Equations [4-7] and [4-18]. This is because the heavy oil is characterized with only a single pseudocomponent in this study. The predicted L_1L_2V phase boundary, however, is close to the experimentally measured boundaries. The predicted ending point of the L_1L_2V phase boundary, i.e., the *K* point, is also shown in FIGURE 6-2. The predicted *K* point for the CO_2-heavy oil binary is found to exist at a lower temperature than those measured *K* points for the CO_2-heavy alkane

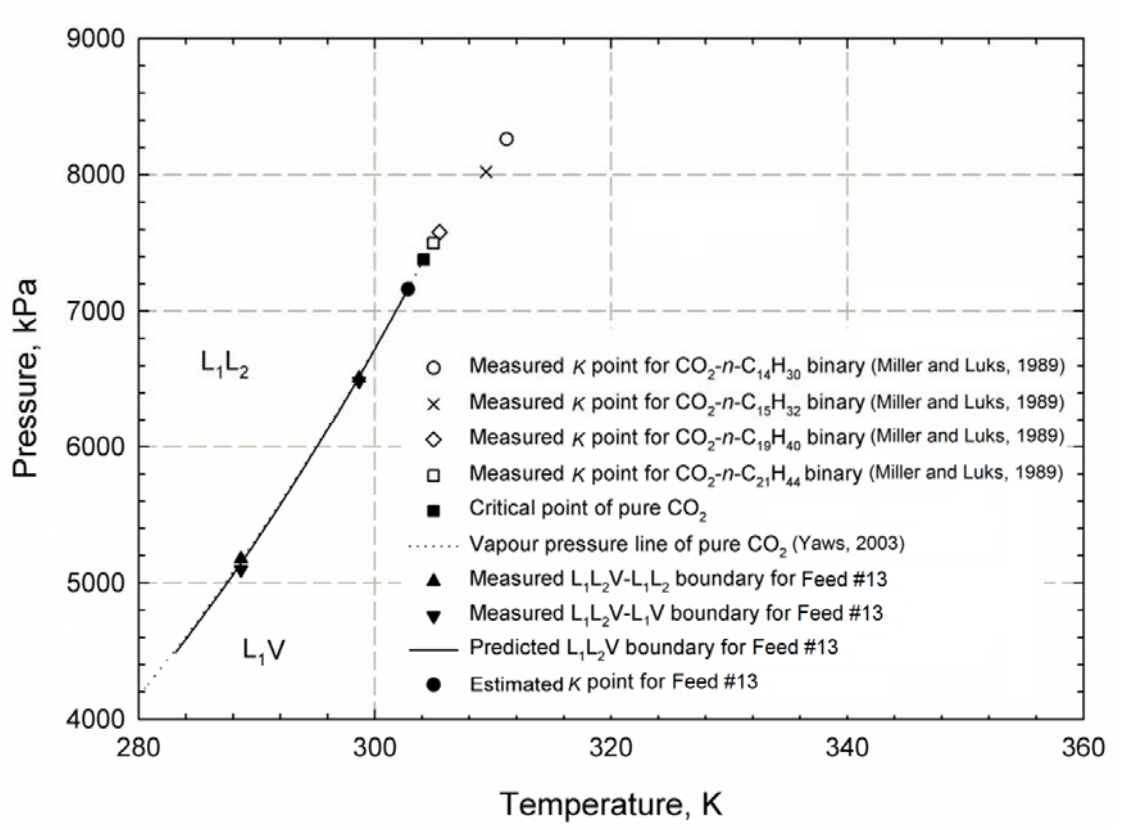

FIGURE 6-2: Comparison of the measured L_1L_2V phase boundary and the predicted L_1L_2V phase boundary by using the PR EOS with Equations [4-7] and [4-18] for the general CO_2-heavy oil system: Feed #13

binaries. This is reasonable because the molecular weight of the heavy oil sample used in this study is larger than that of *n*-$C_{21}H_{44}$, while the measured *K* point occurs at a lower temperature for a binary mixture containing CO_2 and a heavier alkane (Miller and Luks, 1989).

6.4.2. C_3H_8-CO_2-heavy oil system

FIGURE 6-3 compares the measured L_1L_2V phase boundary and the predicted L_1L_2V phase boundary with Equations [4-7], [4-18] and [4-19] for the ternary C_3H_8-CO_2-heavy oil system: Feed #14. It can be apparently observed from FIGURE 6-3 that, at the same temperature, the measured L_1L_2V phase equilibria of the ternary C_3H_8-CO_2-heavy oil system occur at a lower pressure compared to those of the CO_2-heavy oil system. The pressure range of the measured L_1L_2V phase boundary of the ternary C_3H_8-CO_2-heavy oil system spans within a wider area compared to that of the binary CO_2-heavy oil system.

In general, the L_1L_2V phase boundary of the C_3H_8-CO_2-heavy oil system is inclined to move to the higher-temperature and lower-pressure side of the *P*-*T* diagram if the L_1L_2V phase boundary of CO_2-heavy oil system is considered as the reference for comparison. Such an observation is consistent with the three-phase boundary measurements made on a C_3H_8-CO_2-Athabasca bitumen system in the literature (Badamchi-Zadeh *et al.*, 2009b).

It can be also found from FIGURE 6-3 that the measured L_1L_2V-L_1L_2 phase boundary for the ternary C_3H_8-CO_2-heavy oil system agrees well with the predicted L_1L_2V-L_1L_2 phase boundary, though the predicted L_1L_2V-L_1V phase boundary is slightly lower than its measured boundary. The predicted three-phase envelope for the ternary C_3H_8-CO_2-heavy oil system also shrinks with an increase in temperature and terminates

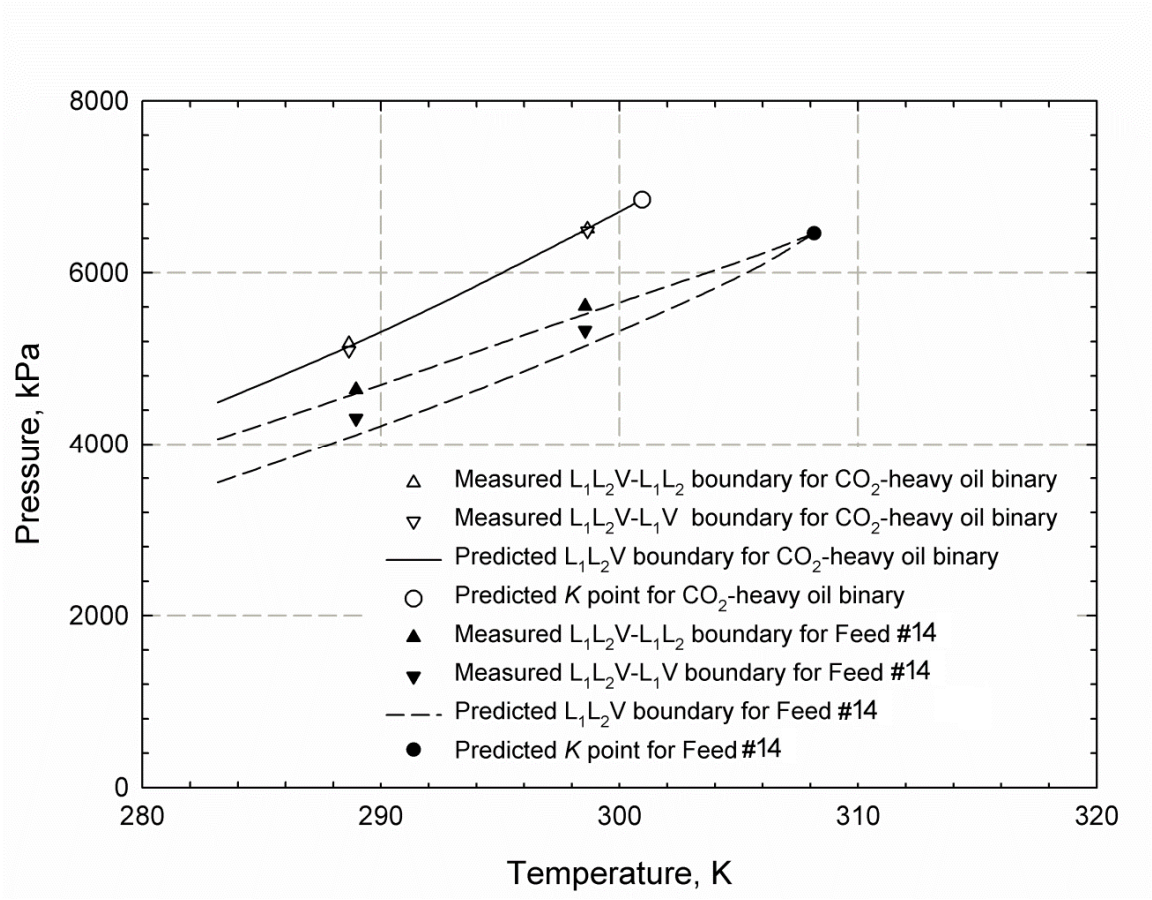

FIGURE 6-3: Comparison of the measured L_1L_2V phase boundary and the predicted L_1L_2V phase boundary with Equations [4-7], [4-18] and [4-19] for the ternary C_3H_8-CO_2-heavy oil system: Feed #14

at the *K* point, where the L_2 phase and V phase become identical and coexist with the L_1 phase. The effect of adding C_3H_8 to CO_2 stream on the L_1L_2V phase equilibria is in good agreement with the observed effect of adding C_3H_8 to CO_2 stream on the three-phase L_1L_2V immiscibility of CO_2-*n*-$C_{19}H_{40}$ feed (Fall and Luks, 1986). The measured L_1L_2V equilibria of C_3H_8-CO_2-*n*-$C_{19}H_{40}$ mixture also tend to move to the high-temperature and lower-pressure side of the *P-T* diagram and cover a larger area compared to the L_1L_2V equilibria of CO_2-*n*-$C_{19}H_{40}$ mixture. This effect is mainly attributed to the fact that C_3H_8 is highly soluble in both CO_2 and *n*-$C_{19}H_{40}$, leading to the partition of L_1L_2V three phases at the extended temperature and pressure ranges (Saber and Shaw, 2009).

6.4.3. *n*-C_4H_{10}-CO_2-heavy oil system

FIGURE 6-4 compares the measured L_1L_2V phase boundary and the predicted L_1L_2V phase boundary by using the PR EOS with Equations [4-7] [4-18] and [4-20] for the ternary *n*-C_4H_{10}-CO_2-heavy oil system: Feed #15. Again, the pressure range of the measured L_1L_2V phase boundary of the ternary *n*-C_4H_{10}-CO_2-heavy oil system spans within a wider area compared to that of the binary CO_2-heavy oil system. The L_1L_2V phase boundary of the *n*-C_4H_{10}-CO_2-heavy oil system is also located at the higher-temperature and lower-pressure side of the *P-T* diagram compared to the L_1L_2V phase boundary of CO_2-heavy oil system. FIGURE 6-4 demonstrates that there exists a generally good agreement between the measured L_1L_2V phase boundary and the predicted L_1L_2V phase boundary by using the PR EOS with the Equations [4-7], [4-18] and [4-20] for the ternary *n*-C_4H_{10}-CO_2-heavy oil system. It can be also seen from FIGURE 6-4 that the predicted three-phase envelope shrinks with an increase in

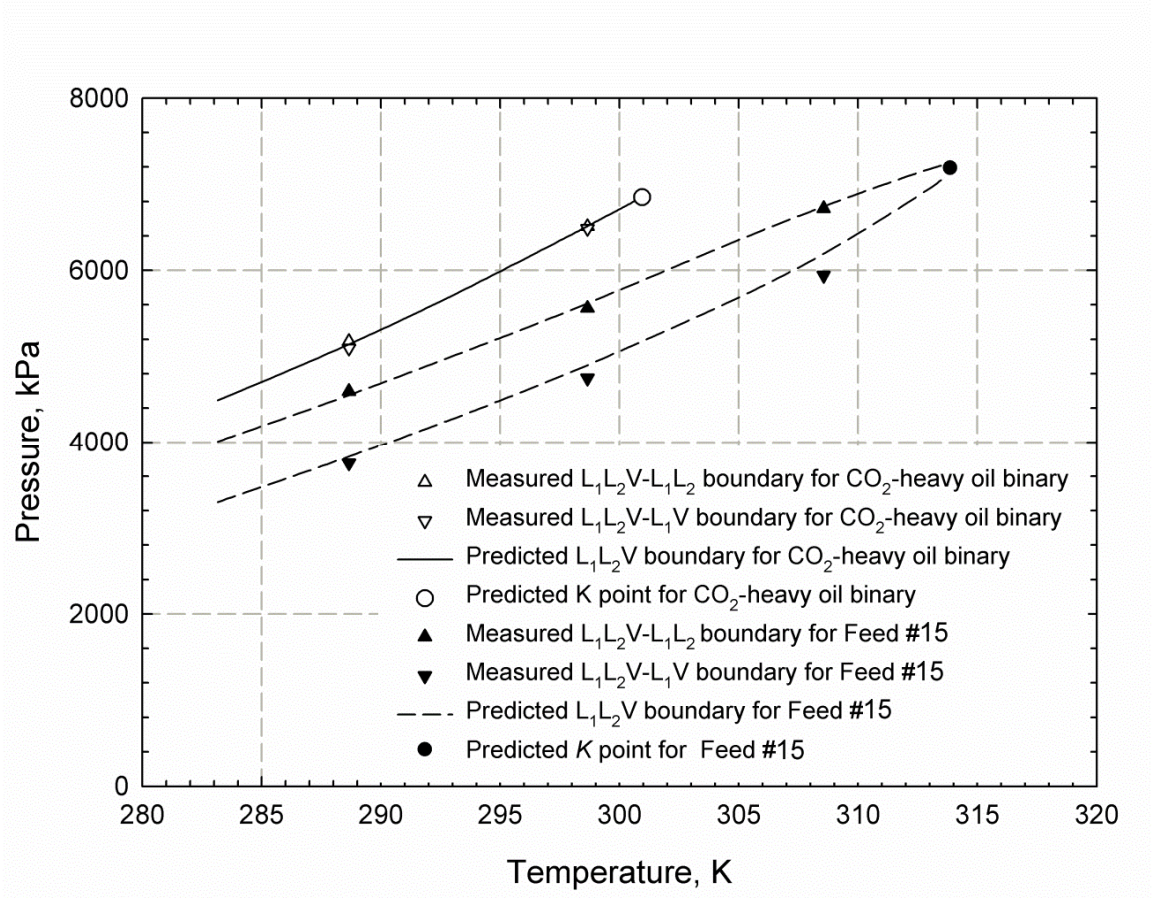

FIGURE 6-4: Comparison of the measured L_1L_2V phase boundary and the predicted L_1L_2V phase boundary by using the PR EOS with Equations [4-7], [4-18] and [4-20] for the ternary *n*-C_4H_{10}-CO_2-heavy oil system: Feed #15

temperature and finally disappears at the *K* point, where the L_2 phase and V phase become identical and coexist with the L_1 phase.

FIGURE 6-5 shows the calculated phase volumes and phase compositions for 1 mole feed with the composition of Feed #15 as a function of pressure at 298.65 K. The phase stability, two-phase flash and three-phase flash calculations are performed by using the volume-translated PR EOS with Equations [4-7], [4-18] and [4-20] for the ternary *n*-C_4H_{10}-CO_2-heavy oil system. As can be clearly seen from FIGURE 6-5a, the L_2 phase emerges at the L_1L_2V-L_1V boundary pressure, while the V phase disappears at the L_1L_2V-L_1L_2 boundary pressure. This is consistent with the visual observations during the measurements. In addition, the phase compositions shown in FIGUREs 6b, c, and d, indicate that, if three phases are coexisting, only trace of heavy oil is present in the V phase and L_2 phase, while a significant amount of CO_2 and *n*-C_4H_{10} is dissolved in heavy oil in the L_1 phase.

Overall, it can be concluded from above discussion that addition of an alkane solvent, either C_3H_8 or *n*-C_4H_{10}, can lead to the existence of three-phase L_1L_2V equilibria over an extended temperature and pressure ranges. These temperature and pressure conditions are close to the *in-situ* conditions of typical heavy oil reservoirs. This implies that, when a solvent mixture composed of an alkane solvent and CO_2 is injected into heavy oil formations, three-phase L_1L_2V phase equilibria are highly likely to occur under reservoir conditions (Talbi and Maini, 2008). Such occurred three-phase equilibria should be taken into account when injection of solvent(s)-CO_2 mixture is considered for recovering heavy oil in hydrocarbon reservoirs.

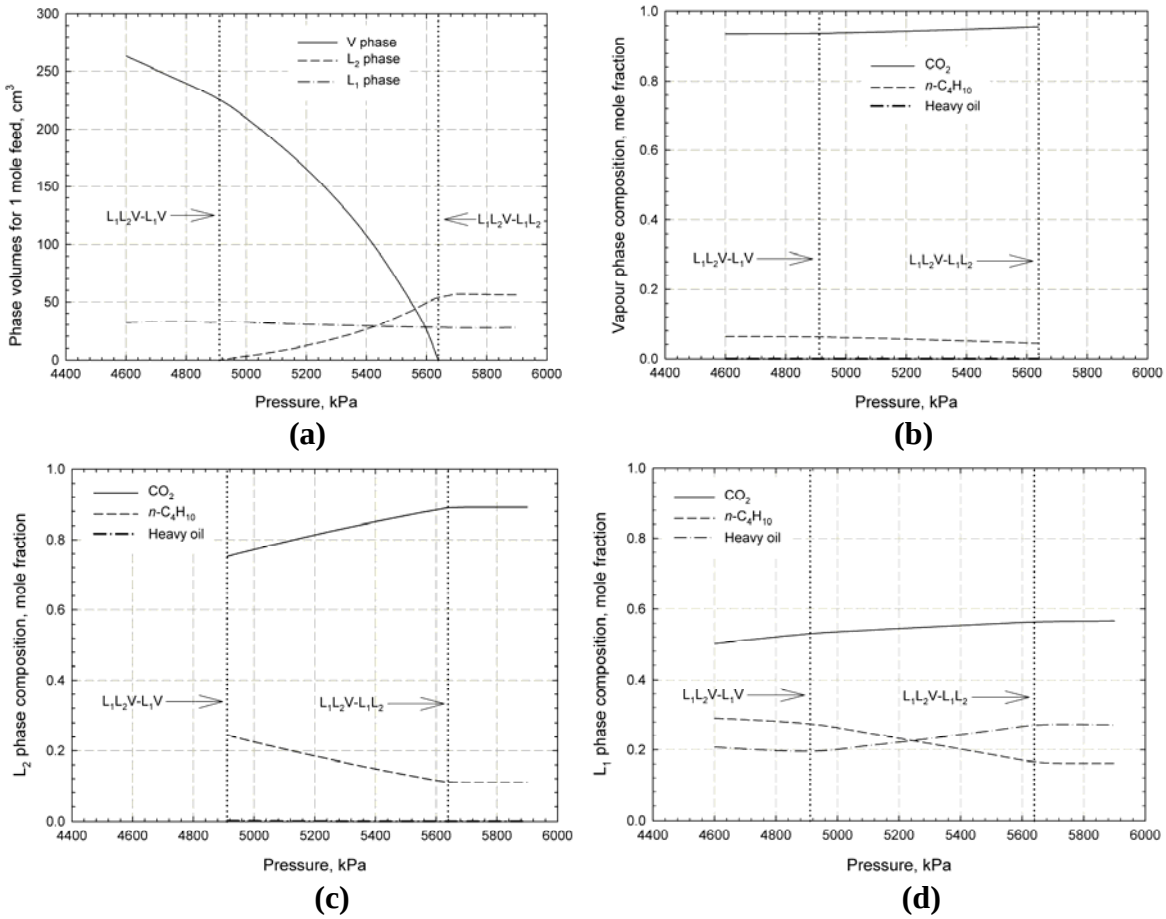

FIGURE 6-5: (a) Calculated phase volumes for 1 mole of Feed #15 as a function of pressure at 298.65 K; Correspondingly calculated phase compositions as a function of pressure at 298.65 K; (b) V phase; (c) L_2 phase; and (d) L_1 phase. The phase behaviour calculations are performed by using the volume-translated PR EOS (Peneloux *et al.*, 1982) with Equations [4-7], [4-18] and [4-20] for the ternary *n*-C_4H_{10}-CO_2-heavy oil system

Recent studies prove that adding alkane solvent C_3H_8 into CO_2 stream is able to significantly improve the recovery performance of CO_2 flooding in heavy oil formations (Talbi and Maini, 2008; Luo *et al.*, 2012). Such an improvement is achieved based on several important mechanisms which mainly encompass the enhanced swelling effect and viscosity reduction of heavy oil, and IFT reduction between gas mixture and heavy oil. In addition to these established mechanisms, it is possible that the observed three-phase L_1L_2V equilibria of the solvent(s)-CO_2-heavy oil systems may also play an important role in improving the heavy oil recovery performance of solvent-enriched CO_2 flooding processes (Okuno *et al.*, 2011; Feizabadi *et al.*, 2012).

6.5 Summary

The L_1L_2V three-phase boundaries of one CO_2-heavy oil mixture, one *n*-C_4H_{10}-CO_2-heavy oil mixture and one C_3H_8-CO_2-heavy oil mixture are experimentally and theoretically determined under reservoir conditions. It is found that L_1L_2V phase equilibria occur in the CO_2-heavy oil system due mainly to the presence of excessive CO_2. It is found that adding an alkane solvent, either C_3H_8 or *n*-C_4H_{10}, to the CO_2-heavy oil system tends to expand the pressure span of the L_1L_2V phase boundary. Also, the measured L_1L_2V phase boundaries of the solvent(s)-CO_2-heavy oil system is found to be located at the higher-temperature and lower-pressure side of the *P*-*T* diagram compared to the measured L_1L_2V phase boundary of CO_2-heavy oil system.

The extended span of L_1L_2V phase boundary observed for the solvent(s)-CO_2-heavy oil system indicates that three phase behaviour may occur over a wide range of temperature and pressure conditions when solvent(s)-CO_2 mixture is injected into heavy

oil reservoirs. The PR EOS with the modified alpha function and the BIP correlations, previously developed for CO_2-heavy oil binary, C_3H_8-heavy oil binary, and *n*-C_4H_{10}-heavy oil binary, respectively, is able to provide a generally good prediction of the measured L_1L_2V phase boundaries of the solvent(s)-CO_2-heavy oil systems under reservoir conditions.

CHAPTER 7 DETERMINATION OF MOLECULAR DIFFUSION COEFFICIENTS OF SOLVENT(S)-CO_2 MIXTURES IN HEAVY OIL

7.1 Introduction

Phase behaviour of solvent(s)-CO_2-heavy oil systems needs to be studied at equilibrium conditions. Intrusive forces can be applied in laboratory experiments to significantly accelerate the mass transfer between solvent(s)-CO_2 mixture and heavy oil. These intrusive forces are normally not available in the reservoir. The *in-situ* mass transfer between gas mixture and heavy oil under reservoir conditions are dominated by molecular diffusion and dispersion (Sayegh and Maini, 1984; Knorr and Imran, 2011). The magnitude of molecular diffusion coefficients affects the time for the heavy oil to achieve desirable viscosity reduction and swelling effect, thus influencing the oil production response (Boustani and Maini, 2001; Frauenfeld *et al.*, 2006). It is of fundamental and practical importance to determine the molecular diffusion coefficients of the solvent(s)-CO_2 mixture in heavy oil, allowing for accurate reservoir simulation and sound field development design.

In this study, a PVT experimental setup is used to conduct molecular diffusion tests to determine the individual molecular diffusion coefficient of each component in a gas mixture in heavy oil under reservoir conditions. During the diffusion tests, the gas mixture is allowed to naturally diffuse into heavy oil. Both the pressure- and volume-history of either gas or liquid phase are simultaneously recorded. Compositions of the gas

phase are measured before and after the diffusion test, respectively. Such determined molecular diffusion coefficients allow for more accurate determination of the rate and amount of solvent(s)-CO_2 mixture to be used in the huff cycle of a huff-*n*-puff process.

7.2 Experimental

7.2.1. Materials

The Lloydminster heavy oil sample has molecular weight of 482 g/mol and specific gravity of 999.7 kg/m^3. TABLE 4-1 shows the compositional analysis result of the Lloydminster heavy oil. The viscosity and density of the heavy oil sample are given by Equation [4-1] and [4-4], respectively. The viscosity of the Lloydminster heavy oil is 12854 cP at the test temperature of 294.55 K according to Equation [4-1]. The three gases, i.e., CO_2, C_3H_8 and *n*-C_4H_{10} (Praxair, Canada), have purities of 99.998 mol%, 99.99 wt%, and 99.5 wt%, respectively.

7.2.2. Experimental setup

As shown in FIGURE 7-1, the molecular diffusion tests for the solvent(s)-CO_2-heavy oil systems are performed by using a DBR PVT system (PVT-0150-100-200-316-155, DBR, Canada). Detailed descriptions regarding the DBR PVT system can be found in CHAPTER 4.

7.2.3. Experimental procedures

Molecular diffusion tests have been performed for one pure CO_2-heavy oil system, one C_3H_8-CO_2-heavy oil system, and one *n*-C_4H_{10}-CO_2-heavy oil system, respectively.

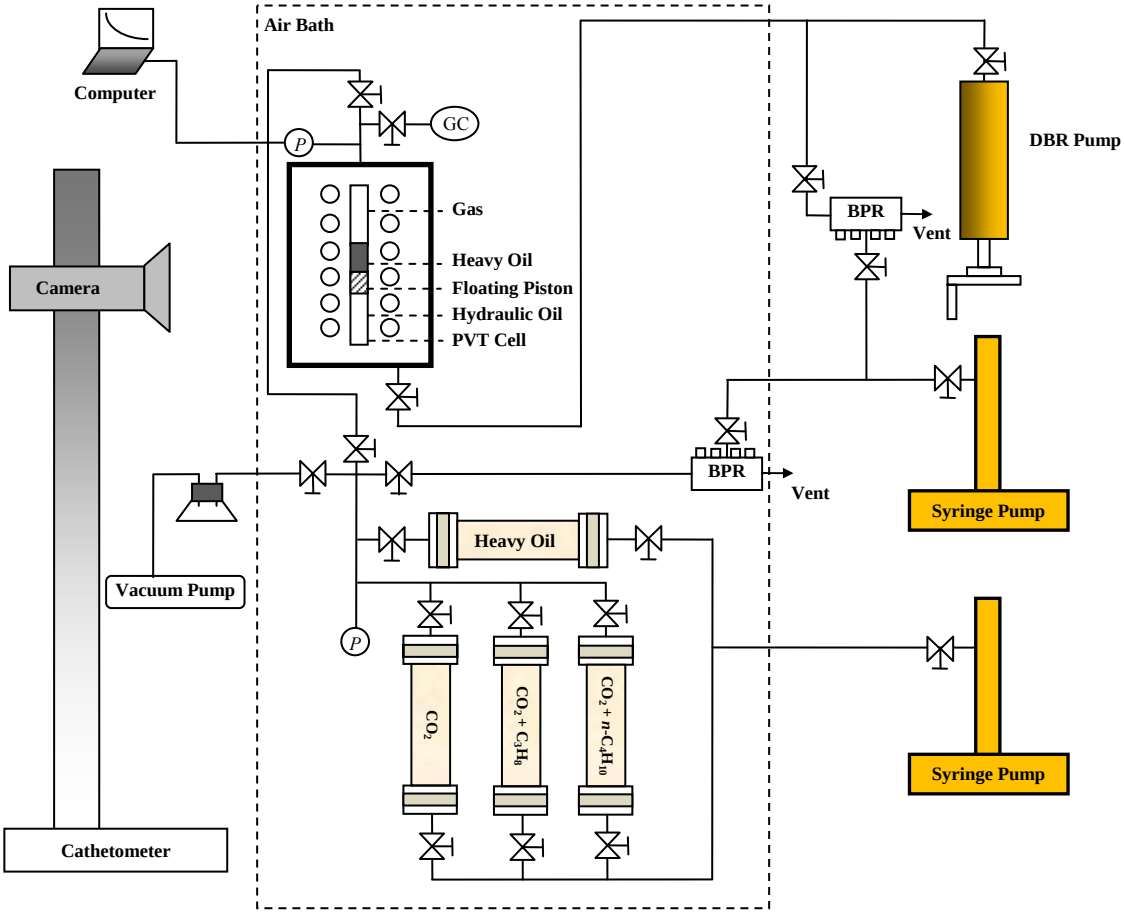

FIGURE 7-1: Schematic of PVT system for conducting molecular diffusion experiments

TABLE 7-1 shows the overall composition of these three systems together with the initial conditions of the molecular diffusion test. The first two tests are performed at similar pressures for comparison purpose.

The following section briefly describes the experimental procedure for the pure CO_2-heavy oil system. As shown in FIGURE 7-1, the isolation piston is first placed closer to the bottom of PVT cell, while the inlet valve of the PVT cell close to the hydraulic side is closed. Prior to each diffusion test, the PVT cell is tested for leakage with high-pressure nitrogen. The PVT cell and inlet tubing are then thoroughly cleaned with kerosene and flushed with air. A certain amount of heavy oil is gently introduced into the PVT cell. After the injection of heavy oil, it is necessary to increase the temperature to 338.15 K for 12 hours, allowing the heavy oil which is previously adhered to its wall for completely slipping downwards to the bulk heavy oil phase inside the PVT cell. Subsequently, the air-bath temperature is set to the test temperature of 294.55 K for at least 12 hours.

The PVT cell and tubing is vacuumed with the vacuum pump down to -60 kPa (gauge pressure) only to avoid possible upward movement of the piston. Once completed, the valve connected to the vacuum pump is closed and pure CO_2 is introduced directly from the transfer cylinder into the PVT cell. When the inlet valve is closed, pressure inside the PVT cell is recorded continuously using a high-precision pressure sensor (PM Series, 5000 psia, Heise, USA) with a full-scale accuracy of 0.025%. Meanwhile, the gas-phase volume and liquid-phase volume are measured simultaneously by tracking the upper gas-oil interface and the lower piston-hydraulic-oil interface. The test is terminated after 168 hours.

As for the experimental procedure for the C_3H_8-CO_2-heavy oil system, the C_3H_8-CO_2

TABLE 7-1: Overall compositions for the three feeds and initial conditions of the three diffusion tests

Feed No.	System	Initial pressure, kPa	Temperature, K	Composition	Initial phase volume, cm^3
16	CO_2-heavy oil	3741	294.55	(74.05 mol% CO_2, 25.95 mol% heavy oil)	(79.1144cm^3 CO_2, 27.2540 cm^3 heavy oil)
17	C_3H_8-CO_2-heavy oil	3799	294.55	(11.28 mol% C_3H_8, 60.94 mol% CO_2, 27.78 mol% heavy oil)	(54.3416 cm^3 C_3H_8+CO_2, 22.6324 cm^3 heavy oil)
18	*n*-C_4H_{10}-CO_2-heavy oil	1128	294.55	(4.71 mol% *n*-C_4H_{10}, 35.67 mol% CO_2, 59.62 mol% heavy oil)	(77.8826 cm^3 *n*-C_4H_{10}+ CO_2, 27.9041 cm^3 heavy oil)

transfer cylinder is placed vertically prior to the mixing. Firstly, C_3H_8 fills the vacuumed transfer cylinder by pushing the floating piston downward, resulting in a certain pressure. Next, CO_2 is released into the cylinder to mix with C_3H_8 that is already contained in the cylinder, resulting in a higher pressure. With a sufficient duration of static mixing for 12 hours, the top valve of the transfer cylinder is opened. The C_3H_8-CO_2 mixture then flows into the vacuumed PVT cell and a 10 cm^3 sampler (Swagelok, Canada, 1000 psi) simultaneously. When the inlet valve of the PVT cell is closed, the sampler is detached for gas-composition analysis with a high-precision gas chromatography (GC) analyzer (Model No.: 6890N, Agilent). Once the diffusion test is finished, the gas mixture in the PVT cell is sampled again for the compositional analysis. The sampling of the gas mixture from the beginning to the end of the test is able to quantitatively reflect the change in gas-phase composition during the diffusion test. The same experimental procedure is followed for the *n*-C_4H_{10}-CO_2-heavy oil system.

7.3 Mathematical Formulation

7.3.1. Mass transfer model

FIGURE 7-2 shows a schematic of molecular diffusion of a gas into heavy oil in a closed cell. The following assumptions are considered for the mass transfer model in this study: 1) The whole diffusion test can be considered an isothermal process since the environment temperature is controlled within the accuracy of ±0.1 K; 2) one-dimensional and one-way diffusion from gas phase to heavy oil (Jamialahmadi *et al.*, 2006; Tharanivasan *et al.*, 2006); and 3) the quasi-equilibrium boundary condition exists at the gas-liquid interface at a given pressure and temperature (Tharanivasan *et al.*, 2006).

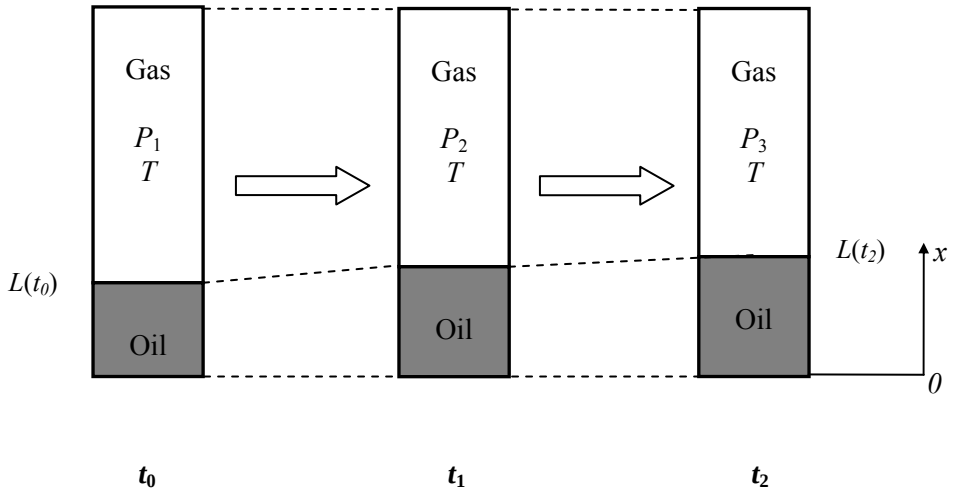

FIGURE 7-2: Schematic of dynamic process of molecular diffusion of the solvent(s)-CO_2 mixture into heavy oil in a closed PVT cell at a constant temperature

Based on the Fick's second law, the mass transfer from the *i*th solvent component in a mixture to heavy oil is described by,

$$\frac{\partial c_i}{\partial t} = D_i \frac{\partial^2 c_i}{\partial x^2} \qquad [7\text{-}1]$$

where c_i is concentration of the *i*th solvent component in heavy oil in mole fraction, D_i is the individual molecular diffusion coefficient of the *i*th component in heavy oil, t is time, and x is distance from the bottom of the diffusion cell as shown in FIGURE 7-2. The molecular diffusion coefficients are assumed to be constant, considering that the duration of each molecular diffusion test is relatively short (i.e., 168 hours) and the solvent(s)-CO_2 concentration in heavy oil is relatively low. Assuming constant molecular diffusion coefficients also facilitates easier comparison with the published data.

Since no solvent is dissolved in heavy oil at the beginning, the initial condition is,

$$c_i = 0,\ 0 \le x \le L_0,\ t = 0 \qquad [7\text{-}2a]$$

where L_0 is initial height of heavy oil. The Neumann boundary condition can be applied at the impermeable bottom,

$$\frac{\partial c_i}{\partial x} = 0,\ x = 0,\ t > 0 \qquad [7\text{-}2b]$$

The Dirichlet quasi-equilibrium boundary condition at the gas-liquid interface is given by,

$$c_i = c_{i,\,\mathrm{sat}}\left[P(t)\right],\ x = L(t),\ t > 0 \qquad [7\text{-}2c]$$

where $c_{i,\,\mathrm{sat}}$ is saturation concentration of the *i*th gas component in heavy oil at current pressure $P(t)$ and temperature, and $L(t)$ is the height of the gas-diluted heavy oil at a given time. The saturation concentrations at the gas-liquid boundary can be determined

by performing two-phase flash calculations for the overall feed at a given pressure and temperature. It should be noted that this statement is only valid when the feed is found to be unstable and phase split calculation is required (Baker *et al*., 1982). This is the case for all the three diffusion tests in this study. The two-phase flash calculations are performed with the volume-translated PR EOS. As for the Lloydminster heavy oil sample examined in this study, the PR EOS and BIP correlations described by Equations [3-1]-[3-4] in CHAPTER 3 and Equations [4-7]-[4-20] in CHAPTER 4 are able to provide reliable estimates of the saturation concentration at the interface because these BIP correlations have been validated with the measured phase behaviour data. The BIP matrix used is shown in TABLE 4-6.

The mole fraction of each component x_i in the liquid phase can be determined by integrating the concentration along the diffusion direction,

$$x_i = \frac{1}{L(t)} \int_0^{L(t)} c_i dx \qquad [7\text{-}3]$$

Once the liquid-phase molar volume is obtained, its height can be updated for the next iteration by,

$$L(t) = V_{\text{corrected}} \sum_{j=1}^{nc} n_j / A \qquad [7\text{-}4]$$

where n_j is molar mass of the jth component in liquid phase, which is calculated via the volume-translated PR EOS model. A is cross-sectional area of the diffusion cell.

The swelling effect of heavy oil due to solvent dissolution can be quantified by swelling factor. Similar to the definitions in the literature (Teja and Sandler, 1980), the swelling factor in this study can be redefined as,

$$SF(t) = \frac{V(t)}{V_0} \times \frac{1}{1 - X(t)} = \frac{V(t)}{V_0} \times \frac{1}{1 - \sum_{i=1}^{ng} x_i(t)} \quad [7\text{-}5]$$

where V_0 is molar volume of heavy oil at the beginning of the pressure decay experiment, $V(t)$ is molar volume of solvent-diluted heavy oil at a given pressure and temperature, and $X(t)$ is mole fraction of gas solvent in heavy oil. V_1 and $V(t)$ are updated with the volume-translated PR EOS.

7.3.2. Determination of molecular diffusion coefficients

Numerical calculation is performed to determine the individual molecular diffusion coefficient of each component of a gas mixture in heavy oil. FIGURE 7-3 shows a schematic for domain discretization, where $c_{m,n}$ at the *m*th node and *n*th time step in the centre of the control domain (dashed area) is considered to be the characteristic mean value of this control domain.

The temporal term in Equation [7-1] is discretized with the first-order forward difference method,

$$\left.\frac{\partial c}{\partial t}\right|_{m,n} = \frac{c_m^{n+1} - c_m^n}{\Delta t} \quad [7\text{-}6]$$

The diffusion term in Equation [7-1] is discretized with the second-order central difference method,

$$\left.\frac{\partial^2 c}{\partial x^2}\right|_{m,n} = \frac{c_{m+1}^n - 2c_m^n + c_{m-1}^n}{\Delta x^2} \quad [7\text{-}7]$$

where *m* is the *m*th node along *x* direction, and *n* is the *n*th time step.

FIGURE 7-4 shows the procedure for determining the individual molecular diffusion

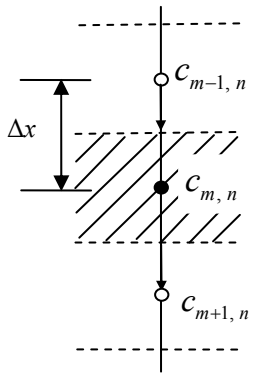

FIGURE 7-3: Schematic of domain discretization

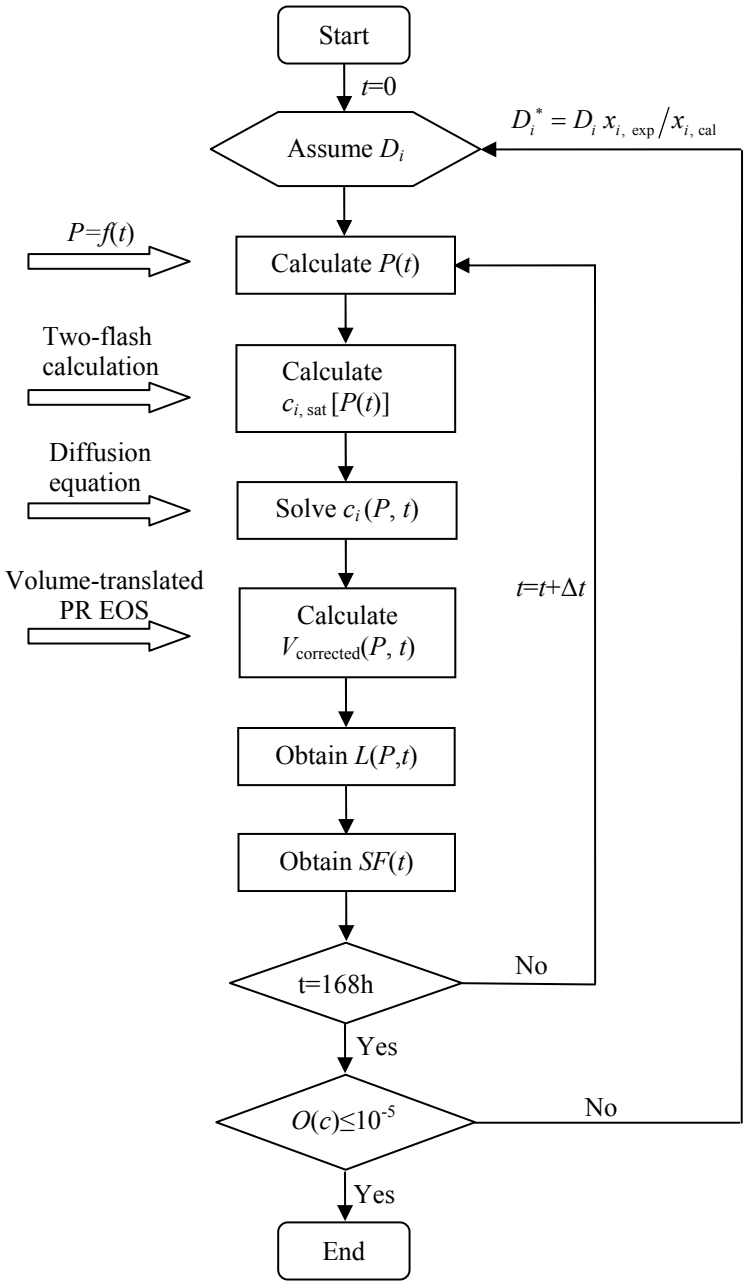

FIGURE 7-4: Flowchart of determining the individual molecular diffusion coefficients

coefficients of each component in a gas mixture in heavy oil. The detailed procedure is described as follows:

1) Assume an initial molecular diffusion coefficient for each component in the gas mixture;
2) Based on the measured decaying pressure versus time, develop an accurate correlation between the decaying pressure and time, which will be used to determine the current pressure and then calculate the interface saturation concentration of each component at this pressure by performing two-phase flash calculation;
3) Solve the concentration of each component along x direction with Equations [7-1]-[7-2c];
4) Use the volume-translated PR EOS model to update the molar volume of the solvent-diluted heavy oil by using Equations [3-1]-[3-4] and [4-7]-[4-14];
5) Update the liquid-phase height with Equation [7-4];
6) Calculate the swelling factor with Equation [7-5];
7) Repeat Steps #2-6 by using the updated data;
8) At the end of the diffusion test at t=168 h, the following objective function $O(c)$ is evaluated with the assumed diffusion coefficients. The objective function for both pure gas-heavy oil system and gas mixture-heavy oil system can be expressed by,

$$O(c)=\sqrt{\frac{1}{ng}\sum_{i=1}^{ng}\left|x_i^{\mathrm{cal}}-x_i^{\mathrm{exp}}\right|^2} \qquad [7\text{-}8]$$

where *ng* is the number of gas-phase components, x_i^{cal} and x_i^{exp} are the calculated and measured mole fraction of the *i*th component in liquid phase at the end of the diffusion test, respectively;

9) If $O(c) \le 10^{-5}$, terminate the calculation and consider the current diffusion coefficients as the optimum one for each component. If $O(c) > 10^{-5}$, another set of molecular diffusion coefficients should be assumed for next iteration by repeating Steps #2-8. The new molecular diffusion coefficients can be updated by the following successive substitution,

$$D_i^* = D_i \frac{x_i^{\text{exp}}}{x_i^{\text{cal}}} \qquad [7\text{-}9]$$

10) After the individual molecular diffusion coefficients are obtained, repeat Steps #2-7 to calculate the swelling factor of heavy oil as a function of time.

The apparent molecular diffusion coefficient of a gas mixture can be obtained by assuming $D = D_1 = D_2$ for the two components in the gas mixture. In this study, the above procedure is then used to determine the apparent molecular diffusion coefficient unless Step #9 is changed to conduct one-dimensional exhaustive search of *D* to achieve the minimum of Equation [7-8].

7.4 Results and Discussion

Before directly going to the measurement results, it is necessary to justify why an extremely long test is not required in this study to determine the molecular diffusion coefficients for a gas-mixture-heavy oil system. First of all, the soaking period during the

field application of solvent-based huff-*n*-puff processes is not extremely long, normally falling in the range of several hours to several days (Monger and Coma, 1988; Olenick *et al.*, 1992). Thus, the molecular coefficients determined from an extremely long test might not be appropriate to be used for field huff-*n*-puff processes. In a traditional pressure-decay test, the system pressure experiences a long duration before reaching the so-called equilibrium pressure. However, there is no need to measure the decaying pressure data over an extremely long time if the experimental phase behaviour data, e.g., pressure versus solubility for a pure-gas-heavy oil system, are available (Tharanivasan *et al.*, 2006). In addition, the measurement of the volume decay and gas-phase composition in this study, even during a short period, allows for more detailed understanding of the mass transfer mechanisms between gas phase and liquid phase.

In the case of a gas-mixture-heavy oil system, only two-phase flash calculation via an EOS model can provide the equilibrium saturation concentration in liquid phase at a given pressure because pressure-solubility relationship curve cannot be measured for a gas-mixture-heavy oil system. This is not the same as the case of a pure-gas-heavy oil system, in which, the solubility of pure gas in heavy oil can be measured as a function pressure. In this study, the PR EOS with the three BIP correlations has been validated with the measured phase behaviour data of solvent(s)-CO_2-heavy-oil systems in CHAPTER 4. Therefore, the PR EOS model is able to provide reliable saturation-concentration calculations for the liquid phase that is required by the quasi-equilibrium boundary condition.

7.4.1. Diffusion profiles

Pressure-decay profile: FIGUREs 7-5, 7-6 and 7-7 display the measure pressure-decay history for the pure CO_2-heavy oil system, C_3H_8-CO_2-heavy oil system, and *n*-C_4H_{10}-CO_2-heavy oil system, respectively.

The pressure-decay history can be explicitly expressed as an exponential function of time with the following form (Zhang *et al.*, 2000; Tharanivasan *et al.*, 2006),

$$P(t) = m_1 e^{-t/k_1} + m_2 e^{-t/k_2} + P_{eq} \qquad [7\text{-}10]$$

As for the pure CO_2-heavy oil system, C_3H_8-CO_2-heavy oil system, CO_2-*n*-C_4H_{10}-heavy oil system, the decaying pressure can be well described with the following fits with R^2=0.9997, R^2=0.9998 and R^2=0.9978, respectively,

$$P(t)_{CO_2} = 81.7014e^{-t/19558.7545} + 367.8442e^{-t/455580.8656} + 3276.3647 \qquad [7\text{-}11a]$$

$$P(t)_{CO_2\text{-}C_3H_8} = 397.7363e^{-t/384911.4704} + 128.5204e^{-t/27765.4376} + 3268.1042 \qquad [7\text{-}11b]$$

$$P(t)_{CO_2\text{-}n\text{-}C_4H_{10}} = 25.4486e^{-t/5000.0000} + 142.1509e^{-t/422083.4037} + 948.4474 \qquad [7\text{-}11c]$$

where *t* is the diffusion time in s. The correlation coefficients of the three fits are all close to unity, indicating that Equation [7-10] is able to provide an excellent approximation for both the pure CO_2-heavy oil systems and for the solvent(s)-CO_2-heavy oil systems.

Gas-phase volume-decay profile: FIGURE 7-8 shows the measured gas-phase volume-decay profiles as a function of diffusion time for the three tests. It can be seen from FIGURE 7-8 that the gas-phase volume decreases slightly as diffusion proceeds for all the three tests, which is caused by the swelling of the heavy oil due to the gas dissolution. Apparently, the gas-phase volume-decaying history shown in FIGURE 7-8 appears to be much less obvious in comparison with the pressure-decaying profiles in FIGUREs 7-5 to 7-7.

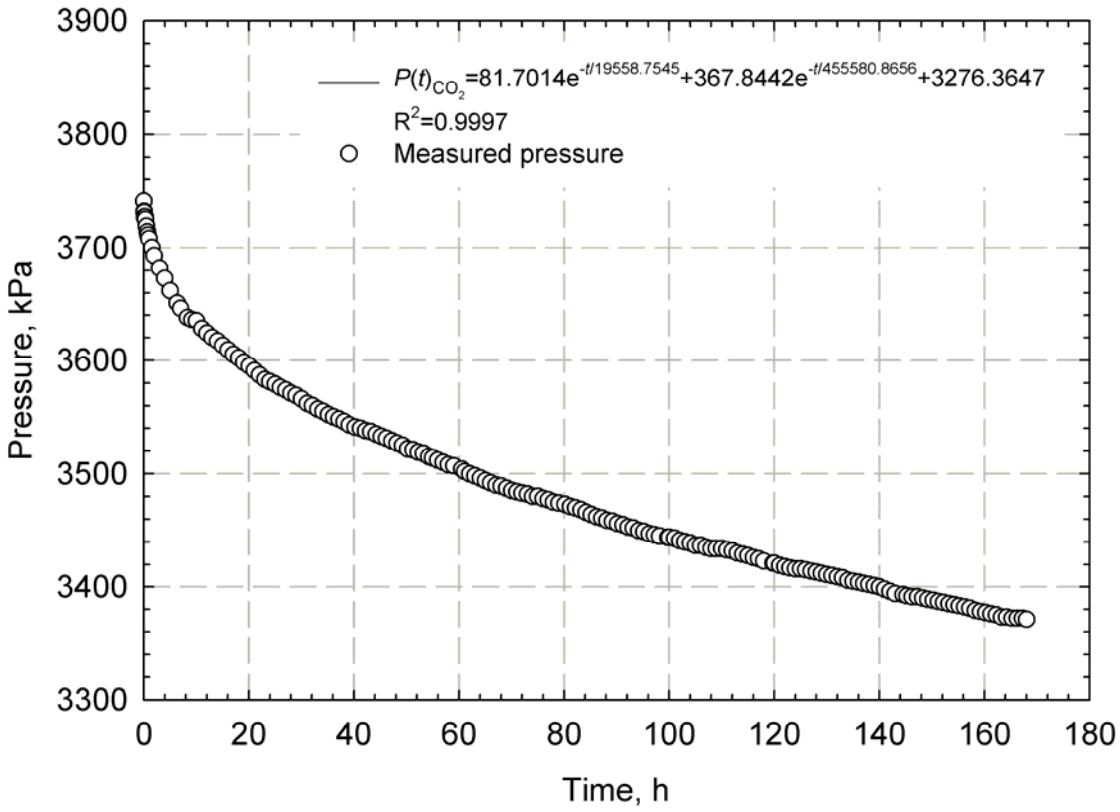

FIGURE 7-5: Measured and correlated pressure-decay profile as a function of time for the CO_2-heavy oil system

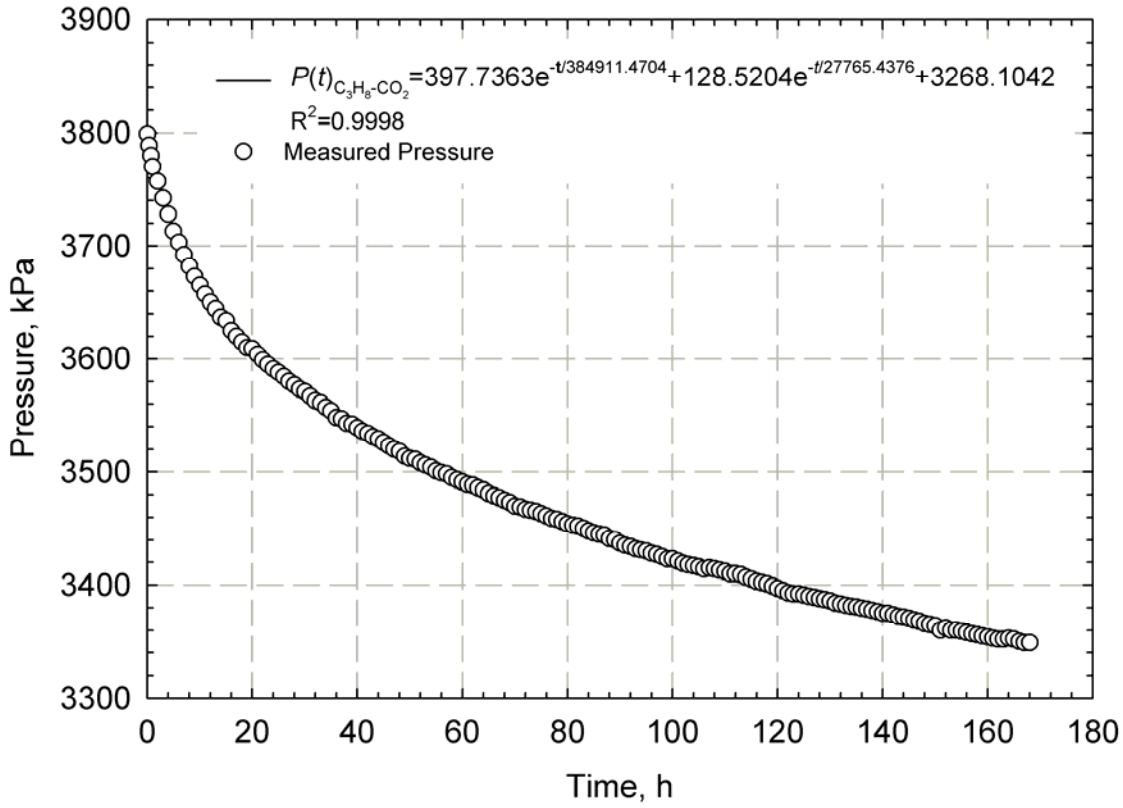

FIGURE 7-6: Measured and correlated pressure-decay profile as a function of time for the C_3H_8-CO_2-heavy oil system

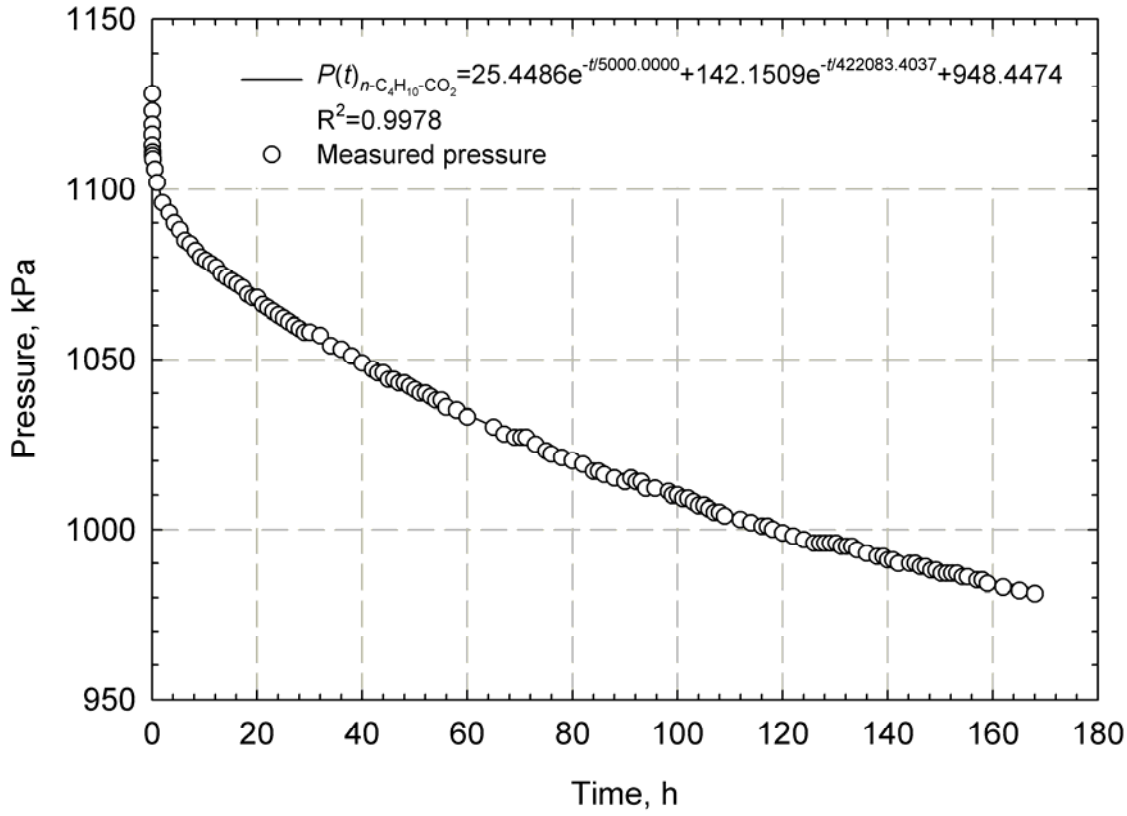

FIGURE 7-7: Measured and correlated pressure decay profile as a function of time for the *n*-C_4H_{10}-CO_2-heavy oil system

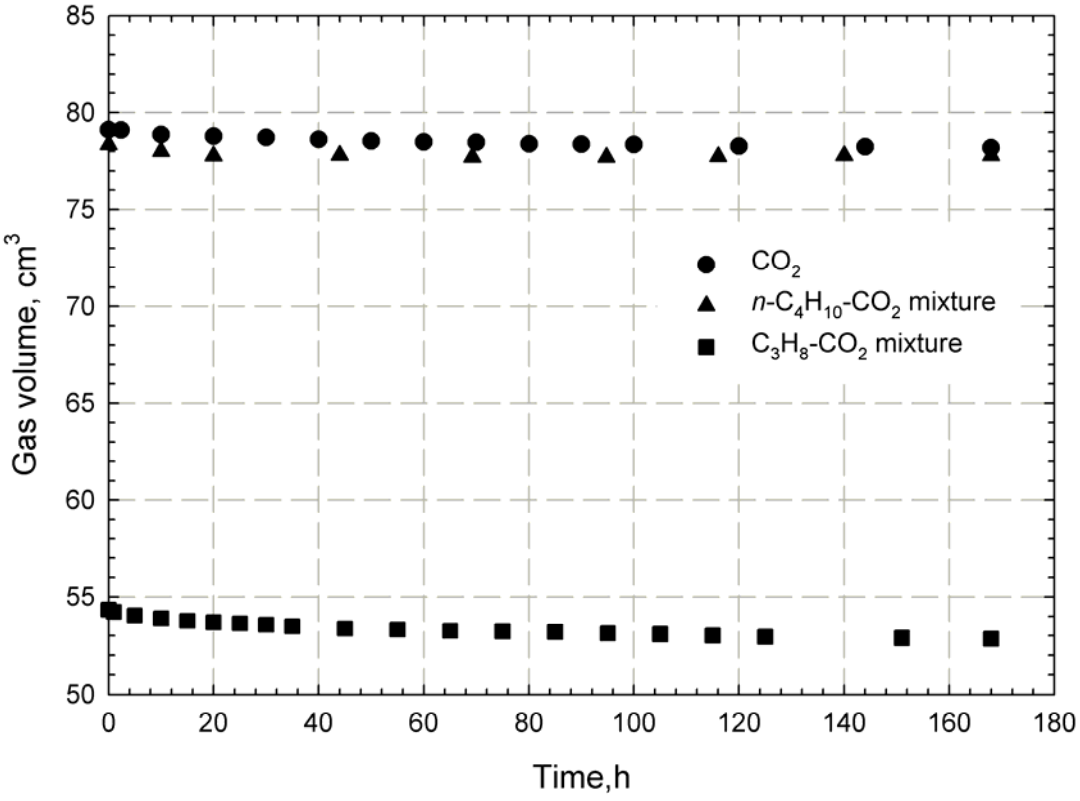

FIGURE 7-8: Gas-phase volume-decay profiles as a function of time for the three diffusion tests

Gas-phase compositional changes: Although continuous monitoring of gas-phase composition has not been made possible in this study, the gas-phase compositions measured at the beginning and the end of the diffusion test are able to generally indicate the compositional change in the gas phase during the diffusion.

TABLE 7-2 shows the compositions of C_3H_8-CO_2 mixture and *n*-C_4H_{10}-CO_2 mixture measured at the beginning and the end of the diffusion test. The GC-analysis results indicate that no heavy hydrocarbon is detected in the gas phase after 168 hours of the diffusion test, confirming the one-dimensional and one-way diffusion assumed in this study. It can be also found from TABLE 7-2 that the concentration of gas solvent C_3H_8 or *n*-C_4H_{10} shows a large decrease at the end of the diffusion test, compared to their initial values. Accordingly, CO_2 concentration increases at the end of the diffusion test. As for the C_3H_8-CO_2-heavy oil system, C_3H_8 concentration decreases from 15.62 mol% to 9.96 mol% after 168 hours of diffusion, while CO_2 concentration increases from 84.38 mol% to 90.04 mol%. Similarly, with regard to the *n*-C_4H_{10}-CO_2-heavy oil system, the *n*-C_4H_{10} concentration decreases from 11.67 mol% to 4.79 mol% after 168 hours of diffusion, whereas the CO_2 concentration increases from 88.33 mol% to 95.21 mol%.

7.4.2. Molecular diffusion coefficients

Based on the multi-component diffusion model as described by Equation [7-1], the molecular diffusion coefficients for a pure gas or a gas mixture can be determined by minimizing the objective function Equation [7-8].

TABLE 7-3 shows the molecular coefficient of pure CO_2 in heavy oil at 294.55 K, the individual molecular diffusion coefficients of C_3H_8 and CO_2 in heavy oil, and the individual molecular diffusion coefficients of *n*-C_4H_{10} and CO_2 in heavy oil, respectively.

TABLE 7-2: Compositional analysis results of C_3H_8-CO_2 mixture and *n*-C_4H_{10}-CO_2 mixture measured at the beginning and the end of the diffusion tests

System	Beginning		End	
C_3H_8-CO_2 mixture	H_2	<0.01 mol%	H_2	<0.01 mol%
	CO	<0.01 mol%	CO	<0.01 mol%
	N_2	0.08 mol%	N_2	<0.01 mol%
	O_2	<0.01 mol%	O_2	<0.01 mol%
	CO_2	84.25 mol%	CO_2	90.04 mol%
	CH_4	0.06 mol%	CH_4	<0.01 mol%
	C_2H_4	<0.01 mol%	C_2H_4	<0.01 mol%
	C_2H_6	<0.01 mol%	C_2H_6	<0.01 mol%
	C_3H_6	<0.01 mol%	C_3H_6	<0.01 mol%
	C_3H_8	15.60 mol%	C_3H_8	9.96 mol%
	i-C_4H_{10}	<0.01 mol%	*i*-C_4H_{10}	<0.01 mol%
	n-C_4H_{10}	<0.01 mol%	*n*-C_4H_{10}	<0.01 mol%
	C_{5+}	<0.01 mol%	C_{5+}	<0.01 mol%
	C_{6+}	<0.01 mol%	C_{6+}	<0.01 mol%
Rounded C_3H_8-CO_2 composition	(15.62 mol% C_3H_8, 84.38 mol% CO_2)		(9.96 mol% C_3H_8, 90.04 mol% CO_2)	
***n*-C_4H_{10}-CO_2 mixture**	H_2	<0.01 mol%	H_2	<0.01 mol%
	CO	<0.01 mol%	CO	<0.01 mol%
	N_2	0.23 mol%	N_2	<0.01 mol%
	O_2	<0.01 mol%	O_2	<0.01 mol%
	CO_2	88.10 mol%	CO_2	95.06 mol%
	CH_4	<0.01 mol%	CH_4	<0.01 mol%
	C_2H_4	<0.01 mol%	C_2H_4	<0.01 mol%
	C_2H_6	<0.01 mol%	C_2H_6	<0.01 mol%
	C_3H_6	0.02 mol%	C_3H_6	<0.01 mol%
	C_3H_8	0.01 mol%	C_3H_8	0.16 mol%
	i-C_4H_{10}	<0.01 mol%	*i*-C_4H_{10}	<0.01 mol%
	n-C_4H_{10}	11.64 mol%	*n*-C_4H_{10}	4.78 mol%
	C_{5+}	<0.01 mol%	C_{5+}	<0.01 mol%
	C_{6+}	<0.01 mol%	C_{6+}	<0.01 mol%
Rounded *n*-C_4H_{10}-CO_2 composition	(11.67 mol% *n*-C_4H_{10}, 88.33 mol% CO_2)		(4.79 mol% *n*-C_4H_{10}, 95.21 mol% CO_2)	

TABLE 7-3: Comparison of the measured molecular diffusion coefficients in different oils

Gas system		Heavy oil	Viscosity cP	Pressure kPa	Temperature K	Molecular diffusion Coefficient 10^{-10} m^2/s
Pure gas	CO_2 (this study)	Lloydminster heavy oil	12854 @ 294.55 K	3741-3371	294.55	8.24
	CO_2 (Yang and Gu, 2006b)	Lloydminster heavy oil	23000 @ 297.05 K	2000-6000	297.05	2.00-5.50
	CO_2 (Upreti and Mehrotra, 2000)	Athabasca bitumen	767 @ 353.15 K	3100-4100	298.15	1.60-2.20
	CO_2 (Upreti and Mehrotra, 2002)	Athabasca bitumen	821000 @ 298.15 K	4000	298.15	1.20-2.00
	CO_2 (Rasmussen and Civan, 2009)	Athabasca bitumen	106000 @ 313.15 K	4000-3240	348.15	5.03
	CO_2 (Fadaei *et al.*, 2011)	Athabasca bitumen	~2000000 @ 294 K	3100-5600	294.15	1.20-2.40
	C_3H_8 (Luo *et al.*, 2007)	Lloydminster heavy oil	24137 @ 297.05	200-800	297.05	0.53-4.90
	C_3H_8 (Yang and Gu, 2006b)	Lloydminster heavy oil	23000 @ 297.05 K	400-900	297.05	0.90-6.80
	C_3H_8 (Ganapathi, 2009)	Lloydminster heavy oil	13144 @ 290 K	400-600	298	2.12-3.59
	n-C_4H_{10} (Ganapathi, 2009)	Lloydminster heavy oil	13144 @ 290 K	100-150	298	1.10-1.84
Gas mixture	(84.38 mol% CO_2, 15.62 mol% C_3H_8) (this study)	Lloydminster heavy oil	12854 cP @ 294.55 K	3799-3349	294.55	4.06 (CO_2) 13.34 (C_3H_8)
						4.63*
	(88.33 mol% CO_2, 11.7 mol% *n*-C_4H_{10}) (this study)	Lloydminster heavy oil	12854 cP @ 294.55 K	1128-982	294.55	1.92 (CO_2) 13.41 (*n*-C_4H_{10})
						2.88*
	(70 mol% CO_2, 30 mol% C_3H_8) (Yang and Gu, 2006b)	Lloydminster heavy oil	23000 @ 297.05 K	1003-3005	297.05	0.82-8.20*

*Note: Apparent molecular diffusion coefficients of the gas mixture.

TABLE 7-3 also presents the molecular diffusion coefficients for pure CO_2, pure C_3H_8, pure *n*-C_4H_{10} and one CO_2-C_3H_8 mixture in different heavy oils that are documented in the literature for comparison purpose. The molecular diffusion coefficient of pure CO_2 in heavy oil at the starting pressure of 3741 kPa and 294.55 K is measured to be 8.24×10^{-10} m^2/s. This value is higher than the other literature values shown in TABLE 7-3 at similar conditions due probably to the lower viscosity of the Lloydminster heavy oil used in this study compared to the other oil samples in the literature.

As can be seen from TABLE 7-3, the individual molecular diffusion coefficients of CO_2 and C_3H_8 in heavy oil are determined to be 4.06×10^{-10} m^2/s and 13.34×10^{-10} m^2/s, respectively. Obviously, under the same pressure and temperature, C_3H_8 in the C_3H_8-CO_2 mixture diffuses faster into heavy oil than CO_2. Furthermore, it is interesting to note that the diffusivity of C_3H_8 (13.34×10^{-10} m^2/s) measured at 294.55 K in this study is significantly larger than those measured in the literature at similar temperatures, e.g., 0.90×10^{-10}-6.80×10^{-10} m^2/s at pressure range of 400-900 kPa and 297.05 K (Yang and Gu, 2006b). The larger diffusivity of C_3H_8 measured in this study can be attributed to a higher pressure of the CO_2-C_3H_8 mixture used. It is well recognized in the literature that, at the same temperature, a higher pressure but lower than its dew point pressure leads to a higher diffusivity of C_3H_8 in heavy oil (Yang and Gu, 2006b; Luo *et al.*, 2007). The starting pressure of 3799 kPa at 294.55 K in this study is greatly larger than the pressures at 297.05 K tested in the literature (Yang and Gu, 2006b; Luo *et al.*, 2007), leading to a higher diffusivity of C_3H_8 in heavy oil. This implies one of the beneficial effects for using CO_2-C_3H_8 mixture instead of only C_3H_8. The presence of CO_2 in the CO_2-C_3H_8 mixture can make the dew point pressure of the CO_2-C_3H_8 significantly larger than that of pure

C_3H_8, allowing for a faster dissolution of solvent C_3H_8 into heavy oil. It can also be noted from TABLE 7-4 that, at the end of the diffusion test, a total of 35.92 mol% of C_3H_8-CO_2 mixture is dissolved in heavy oil, while a smaller fraction, 28.92 mol% of CO_2, is present in heavy oil. A larger fraction of gas components in heavy oil is able to provide larger swelling effect and viscosity reduction of heavy oil.

The individual molecular diffusion coefficients of CO_2 and *n*-C_4H_{10} in heavy oil are determined to be 1.92×10^{-10} m^2/s and 13.41×10^{-10} m^2/s, respectively. Similarly, it is found that *n*-C_4H_{10} in the *n*-C_4H_{10}-CO_2 mixture diffuses faster into heavy oil than CO_2. Compared to the literature data (Ganapathi, 2009), the larger diffusivity of *n*-C_4H_{10} measured in this study can also be ascribed to a higher pressure of the CO_2-*n*-C_4H_{10} mixture used in the diffusion test. However, one effect must be taken into account when adding *n*-C_4H_{10} into CO_2 stream. Due to the low dew point pressure of *n*-C_4H_{10}, addition of *n*-C_4H_{10} into CO_2 stream can significantly reduce the dew point pressure of *n*-C_4H_{10}-CO_2 mixture, and therefore induce the formation of liquid *n*-C_4H_{10}-CO_2 mixture under reservoir conditions.

As mentioned earlier, the apparent molecular diffusion coefficients can also be determined by minimizing the discrepancy between the measured and calculated mole fractions of solvent(s)-CO_2 mixture in heavy oil (See TABLE 7-3). TABLE 7-4 shows the measured and calculated mole fractions of solvent(s)-CO_2 mixture in heavy oil at the end of diffusion tests by both using the individual and apparent molecular diffusion coefficients. It can be seen from TABLE 7-4 that the individual molecular diffusion coefficients are able to provide far more accurate prediction of the mole fractions of solvent(s)-CO_2 in heavy oil at the end of diffusion tests. This is exactly the reason why

TABLE 7-4: Measured and calculated mole fractions of solvent(s)-CO_2 in heavy oil at the end of diffusion tests

System	Measured*	Calculated	
		Using individual diffusion coefficients	**Using apparent diffusion coefficient for gas mixture**
Pure CO_2 in heavy oil	28.92 mol% CO_2	28.92 mol% CO_2	---
C_3H_8-CO_2 mixture in heavy oil	(13.01 mol% C_3H_8, 22.91 mol% CO_2)	(13.01 mol% C_3H_8, 22.92 mol% CO_2)	(9.15 mol% C_3H_8, 24.36 mol% CO_2)
n-C_4H_{10}-CO_2 mixture in heavy oil	(4.55 mol% *n*-C_4H_{10}, 4.71 mol% CO_2)	(4.55 mol% *n*-C_4H_{10}, 4.71 mol% CO_2)	(2.37 mol% *n*-C_4H_{10}, 5.59 mol% CO_2)

***Note:** The mole fractions of solvent(s) and CO_2 in heavy oil are determined based on the composition change at the beginning and the end of the diffusion tests as shown in TABLE 7-2

the molecular diffusion coefficient of each component in the mixture must be treated separately in the numerical model to generate a good match with the measured composition change during the diffusion test.

7.4.3. Swelling factor

Swelling effect is an important physical phenomenon when using a solvent(s)-CO_2 mixture in heavy-oil recovery processes. FIGURE 7-9 shows the measured and calculated swelling factor as a function of diffusion time for the CO_2-heavy oil system, C_3H_8-CO_2-heavy oil system, and *n*-C_4H_{10}-CO_2-heavy oil system, respectively. The calculated swelling factors are in generally good agreement with the measured ones. It can be seen from FIGURE 7-9 that, at the similar starting pressures, the C_3H_8-CO_2-heavy oil system is able to provide a significantly larger swelling factor along the diffusion process in comparison with the CO_2-heavy oil system.

The molecular diffusion of C_3H_8-CO_2 mixture into heavy oil tends to accelerate the swelling of heavy oil, leading to a larger degree of swelling effect at the same diffusion time. The swelling factors of the C_3H_8-CO_2-heavy oil system and the CO_2-heavy oil system are measured to be 1.058 and 1.031 at the end of the diffusion test. Such enhanced swelling effect of the C_3H_8-CO_2-heavy oil system is attributed to the fact that C_3H_8 diffuses faster into heavy oil than CO_2 and that C_3H_8 is able to generate a larger swelling effect than CO_2 when the same mole fractions of CO_2 or C_3H_8 is dissolved in heavy oil (Yang and Gu, 2006b; Li *et al.*, 2011). The swelling factor of the *n*-C_4H_{10}-CO_2-heavy oil system is measured to be only 1.015 at the end of the diffusion test. This is ascribed to the fact that a low pressure of the *n*-C_4H_{10}-CO_2 mixture used in the diffusion test can only lead to a small solubility of such a mixture in heavy oil even at equilibrium

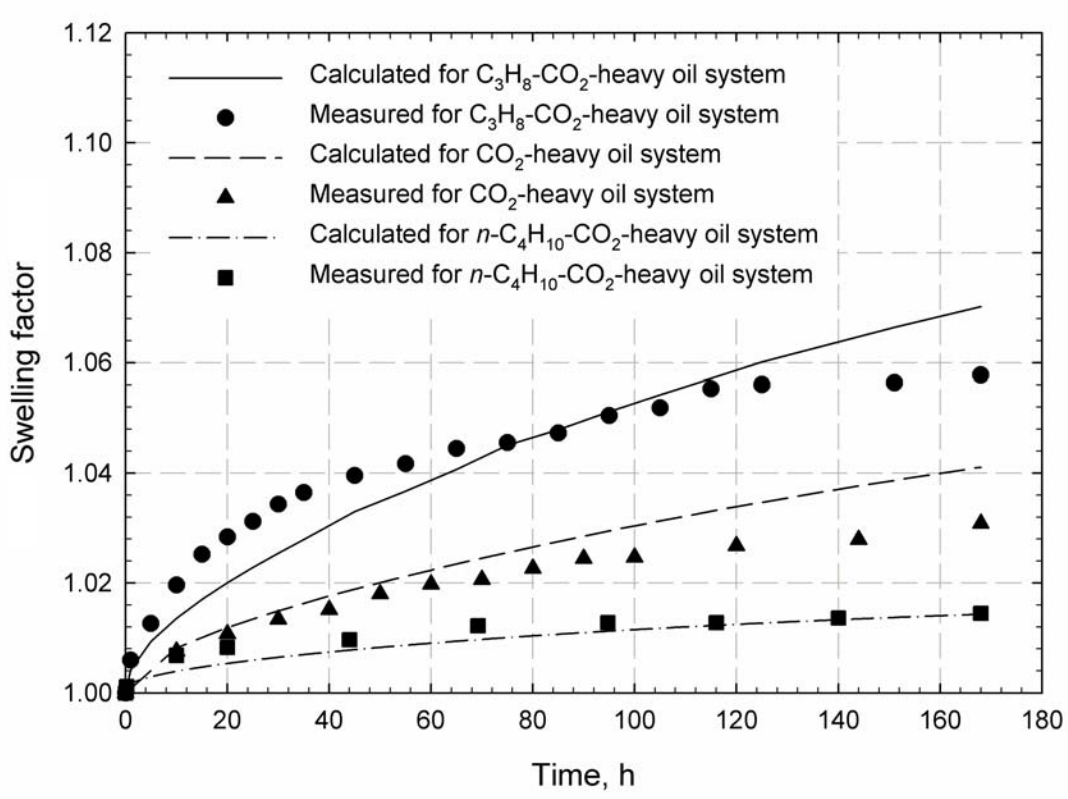

FIGURE 7-9: Measured and calculated swelling factor based on the individual molecular diffusion coefficients for the CO_2-heavy oil system, C_3H_8-CO_2-heavy oil system and *n*-C_4H_{10}-CO_2-heavy oil system

conditions. In addition to the mole fraction of a solvent in the solvent-CO_2 mixture, therefore, pressure is another important parameter to be considered in designing an efficient solvent(s)-CO_2-based huff-*n*-puff process. A higher operating pressure generally not only leads to a higher equilibrium solubility of the solvent(s)-CO_2 mixture in heavy oil (Li *et al.*, 2011), but also enables a faster diffusion of the solvent(s)-CO_2 mixture into heavy oil. As such, more effective and efficient swelling effect and viscosity reduction can be achieved at a higher operating pressure.

7.5 Summary

Three diffusion experiments are conducted to determine the molecular diffusion coefficients for one CO_2-heavy oil system, one C_3H_8-CO_2-heavy oil system and one *n*-C_4H_{10}-CO_2-heavy oil system, respectively. GC-based composition analysis is performed to examine the composition change of gas phase during the diffusion test. During the diffusion tests, the gas-phase solvent fraction is found to decrease as diffusion proceeds, while the gas-phase CO_2 fraction decreases. As for the solvent-CO_2 mixtures tested, the molecular diffusion coefficient of solvent in heavy oil is found to be significantly larger than that of CO_2 in heavy oil.

The oil swelling is found to be significant when solvent-CO_2 mixture diffuses into heavy oil at a high pressure. At a similar starting pressure, the molecular diffusion of C_3H_8-CO_2 mixture into heavy oil tends to accelerate the swelling of heavy oil, leading to a larger degree of swelling effect after a given diffusion time, in comparison with pure CO_2. The individual molecular diffusion coefficients for C_3H_8-CO_2 in heavy oil are

determined to be 4.06×10^{-10} m^2/s and 13.34×10^{-10} m^2/s, respectively, at a starting pressure of 3799 kPa and 294.55 K. The individual molecular diffusion coefficients for *n*-C_4H_{10}-CO_2 in heavy oil are determined to be 1.92×10^{-10} m^2/s and 13.41×10^{-10} m^2/s, respectively, at a starting pressure of 1128 kPa and 294.55 K.

CHAPTER 8 CONCLUSIONS AND RECOMMENDATIONS

8.1 Conclusions

The major contributions of this dissertation can be summarized as follows.

1) A new alpha function in PR EOS is developed to more accurately predict the vapor pressure of non-hydrocarbons and hydrocarbon compounds. The acentric factor is redefined at a reduced temperature of 0.6 and incorporated into the newly developed alpha function. The new alpha function can be used to more accurately predict the vapour pressure for polar or nonpolar non-hydrocarbon substances, light hydrocarbons, and heavy hydrocarbons (up to *n*-tritetracontane) in comparison to the other existing alpha functions evaluated;
2) Well-designed experiments have been performed to measure saturation pressure, viscosity, interfacial tension, and multiphase boundaries of solvent(s)-CO_2-heavy oil systems at high pressures and elevated temperatures, while theoretical models have been developed to quantify them with a generally good accuracy; and
3) A theoretical and experimental framework is proposed to determine the individual molecular diffusion coefficient of each component of the solvent(s)-CO_2 mixture in heavy oil under reservoir conditions. The preferential diffusion of either solvent(s) or CO_2 in the solvent(s)-CO_2 mixture can be accounted for with the proposed method because the composition change at the beginning and the end of the diffusion tests are measured.

Experimental and theoretical techniques have been developed to study the phase behaviour and mass transfer of solvent(s)-CO_2-heavy oil systems under reservoir

conditions. Experimentally, the saturation pressures, swelling factors, L_1L_2V three-phase boundaries, and molecular diffusion coefficients of solvent(s)-CO_2-heavy oil systems have been measured by using a PVT setup, while the IFTs of solvent(s)-CO_2-heavy oil systems have been determined by using a ADSA technique. The following conclusions can be drawn based on the aforementioned experimental measurements,

1) It is experimentally found that significantly enhanced swelling effect and viscosity reduction of heavy oil can be obtained by adding either C_3H_8 or *n*-C_4H_{10} into CO_2 stream. Adding either C_3H_8 or *n*-C_4H_{10} into CO_2 can also cause the emergence of L_1L_2V three phases under reservoir conditions. Under the same conditions, C_3H_8 and/or *n*-C_4H_{10} is found to be much soluble in heavy oil compared to CO_2. A significantly increased swelling effect of heavy oil can be obtained by adding either C_3H_8 or *n*-C_4H_{10} into CO_2 stream. An enhanced viscosity reduction of the CO_2-heavy oil system can also be achieved in the presence of either C_3H_8 or *n*-C_4H_{10};
2) It is experimentally revealed that the addition of C_3H_8 and/or *n*-C_4H_{10} into CO_2 stream can also lead to an obvious reduction of interfacial tension (IFT) between CO_2 and heavy oil. The measured equilibrium IFTs for CO_2-, C_3H_8- and *n*-C_4H_{10}-heavy oil systems indicate that, at the same temperature and pressure, *n*-C_4H_{10} leads to the lowest IFT while CO_2 results in the highest IFT. Addition of rich solvent(s) C_3H_8 and/or *n*-C_4H_{10} into CO_2 stream leads to an obvious reduction of IFT between CO_2 and heavy oil, though the degree of IFT reduction is dependent on the amount of the rich solvent(s) added. The IFT reduction of CO_2-heavy oil

system due to addition of rich solvent(s) results in an increased capillary number, which is beneficial for achieving a higher heavy oil recovery;

3) The L_1L_2V three-phase equilibria occur in the CO_2-heavy oil system mainly because of the presence of excessive CO_2. Adding an alkane solvent, either C_3H_8 or *n*-C_4H_{10}, to the CO_2-heavy oil system tends to expand the pressure span of the L_1L_2V phase boundary. The measured L_1L_2V phase boundaries of the solvent(s)-CO_2-heavy oil system is found to be located at the higher-temperature and lower-pressure side of the *P-T* diagram compared to the measured L_1L_2V phase boundary of CO_2-heavy oil system. The extended span of L_1L_2V phase boundary observed for the solvent(s)-CO_2-heavy oil system indicates that three-phase behaviour are highly likely to occur *in-situ* when solvent(s)-CO_2 mixture is injected into heavy oil reservoirs; and
4) The pressure-decay experiments for solvent(s)-CO_2-heavy oil system indicate that the gas-phase solvent fraction decreases as diffusion proceeds, while the gas-phase CO_2 fraction increases during the test. As for the solvent(s)-CO_2 mixtures tested, the molecular diffusion coefficient of solvent in heavy oil is found to be significantly larger than that of CO_2 in heavy oil. In addition, at similar conditions, the C_3H_8-CO_2 mixture leads to an accelerated swelling-factor growth compared to pure CO_2.

Theoretically, the PR EOS together with a new alpha function is employed as the fundamental model to describe the phase behaviour of solvent(s)-CO_2-heavy oil systems. The following conclusions can be drawn based on the aforementioned theoretical modelling efforts,

1) Three BIP correlations in PR EOS are proposed for characterizing CO_2-heavy oil binaries, C_3H_8-heavy oil binaries and *n*-C_4H_{10}-heavy oil binaries, respectively, by treating heavy oil sample as a single pseudocomponent with its molecular weight and specific gravity. The PR EOS together with the BIP correlations and the new alpha function is able to predict the saturation pressures and swelling factors and three-phase boundaries of the solvent(s)-CO_2-heavy oil systems with a generally good accuracy, though the prediction accuracy is slightly reduced at temperatures close to the critical temperature of a pure solvent;
2) The mechanistic parachor model with optimized parachor of Lloydminster heavy oil and mass transfer exponent can qualitatively represent the measured IFTs between solvent(s) and heavy oil in the liquid-vapour phase region; and
3) A one-dimensional and one-way diffusion model is developed to describe the molecular diffusion of solvent(s)-CO_2 mixture in heavy oil. The individual molecular diffusion coefficients for each component in the mixture can be determined by minimizing the discrepancy between the measured composition change and the calculated composition change with the diffusion model.

In summary, the important mechanisms, including significantly enhanced swelling effect and viscosity reduction of heavy oil, IFT reduction between solvent(s)-CO_2 mixture and heavy oil, and an accelerated growth in swelling factor, are shown to take place when solvent(s)-CO_2 mixture comes into contact with heavy oil. These beneficial mechanisms imply that many established CO_2-based heavy oil recovery methods, for example, CO_2 cyclic injection, CO_2 huff-*n*-puff, continuous CO_2 injection, and water-

alternating-CO_2 injection can be further improved or modified by adding an appropriate amount of gas alkanes into CO_2 stream.

8.2 Recommendations

The enhanced swelling effect and viscosity reduction caused by adding either C_3H_8 or *n*-C_4H_{10} into CO_2 stream imply that solvent(s)-enriched CO_2 processes is a highly promising technique to recover heavy oil resources where other recovery techniques are not economically or efficiently available. Therefore, it is necessary to conduct the following experiments and possible pilot tests to determine the potential of applying variants of solvent(s)-enriched CO_2 processes for effective heavy-oil recovery purposes. Relevant research topics are recommended as follows.

1) The emergence of solid phase, i.e., asphaltene precipitation, is not elaborated in the present study, though it is also an important aspect of the phase behaviour of solvent(s)-CO_2-heavy oil systems. Asphaltene precipitation plays an important role in affecting the physical properties of solvent-diluted heavy oil and consequently the fluid flow in porous media. It is, therefore, necessary to conduct experiments to measure the onset and quantity of asphaltene precipitation in heavy oil when the heavy oil is diluted with solvent(s)-CO_2 mixtures. More accurate EOS-based thermodynamic model needs to be developed to well represent the experimental asphaltene-precipitation data considering the complexity of asphaltene precipitation phenomenon;

2) The importance of second-liquid phase in L_1L_2V behaviour of the solvent(s)-CO_2-heavy oil systems needs further investigation and clarification since it may be inevitable to encounter formation of the second-liquid phase when injecting C_3H_8- or *n*-C_4H_{10}-enriched CO_2 stream, in particular, with a high enrichment level, into heavy-oil reservoirs. Non-equilibrium mass transfer tests considering three phases, instead of only considering gas-heavy-oil two phases, might be able to reveal whether the occurrence of the second liquid-phase is beneficial for improving the mass transfer between solvent(s)-CO_2 mixture and heavy oil. Well-designed coreflood experiments should also be conducted to shed lights on the effect of the second liquid-phase on the heavy-oil recovery efficiency;
3) As for the heavy oil recovery in various formations, different solvent(s)-CO_2 injection methods could be evaluated both in laboratory experiments and possible pilot tests. Depending on the specific conditions of heavy oil reservoirs, the variants of these solvent(s)-enriched CO_2 processes may include huff-*n*-puff method, continuous gas flooding, vapour extraction utilizing horizontal-well technology, and water-alternating-gas injection. In addition, in these processes, it is necessary to compare the performance of two generic injection methods: the injection of bulk solvent(s)-CO_2 mixture and the cyclic injection of solvent(s) slugs and CO_2 slugs; and
4) When implementing a solvent(s)-CO_2-based process in a field, field-scale economic analysis must be carefully addressed in a comprehensive manner with the primary consideration of the large expenses associated with

purchasing solvent(s), recycling solvent(s), retrieving solvent(s) during production, and possible loss of unrecoverable rich solvent(s) that flee into thief zones or atmosphere.

REFERENCES

Ahmed, T.: *Hydrocarbon Phase Behaviour*. Gulf Publishing, Houston, TX (1989)

Al-Abri, A. and Amin, R.: Phase Behaviour, Fluid Properties and Recovery Efficiency of Immiscible and Miscible Condensate Displacements by $SCCO_2$ Injection: Experimental Investigation. *Transport Porous Med.*, 85(3), 743-756 (2010)

Al-Bahlani, A. and Babadagli, T.: Steam-Over-Solvent Injection in Fractured Reservoirs (SOS-FR) Technique as a New Approach for Heavy-Oil and Bitumen Recovery: an Overview of the Method. *Energy Fuels*, 25(10), 4528-4539 (2011)

Alston, R.B., Kokolis, G.P., and James, C.F.: CO_2 Minimum Miscibility Pressure: a Correlation for Impure CO_2 Streams and Live Oil Systems. *SPE J.*, 25(2), 268-274 (1985).

Ambrose, D., Counsell, J.F., and Davenport, A.J.: The Use of Chebyshev Polynomials for the Representation of Vapour Pressures Between the Triple Point and the Critical Point. *J. Chem. Thermodyn.*, 2(2), 283-294 (1970)

Ambrose, D. and Sprake, C.H.S.: Thermodynamic Properties of Organic Oxygen Compounds XXV. Vapour Pressures and Normal Boiling Temperatures of Aliphatic Alcohols. *J. Chem. Thermodyn.*, 2(5), 631-645 (1970)

Ambrose, D. and Lawenson, I.J.: The Vapor Pressure of Water. *J. Chem. Thermodyn.*, 4(5), 755-761 (1972)

Ambrose, D., Sprake, C.H.S., and Townsend, R.: Thermodynamic Properties of Organic Oxygen Compounds XXXIII. The Vapour Pressure of Acetone. *J. Chem. Thermodyn.*, 6(7), 693-700 (1974)

Ambrose, D., Sprake, C.H.S., and Townsend, R.: Thermodynamic Properties of Organic Oxygen Compounds XXXVII. Vapour Pressures of Methanol, Ethanol, Pentan-1-ol, and Octan-1-ol from the Normal Boiling Temperature to the Critical Temperature. *J. Chem. Thermodyn.*, 7(2), 185-190 (1975)

Ambrose, D., Ellender, J.H., Sprake, C.H.S., and Townsend, R.: Thermodynamic Properties of Organic Oxygen Compounds XLV. The Vapour Pressure of Acetic Acid. *J. Chem. Thermodyn.*, 9(8), 735-741 (1977)

Ambrose, D., Ewing, N.B., Ghiassee, J.C., and Sanchez, O.: The Ebulliometric Method of Vapour-Pressure Measurement: Vapour Pressures of Benzene, Hexafluorobenzene, and Naphthalene. *J. Chem. Thermodyn.*, 22(6), 589-605 (1990)

Aparicio-Martínez, S. and Hall, K.R.: Use of PC-SAFT for Global Phase Diagrams in Binary Mixtures Relevant to Natural Gases. 1. *n*-Alkane + *n*-Alkane. *Ind. Eng. Chem. Res.*, 46(1), 273-284 (2007)

Ayirala, S.C. and Rao, D.N.: A New Mechanistic Parachor Model to Predict Dynamic IFT and Miscibility in Multicomponent Hydrocarbon Systems. *J. Colloid Interface Sci.*, 299(1), 321-331 (2006)

Bachu, S. and Stewart, S.: Geological Sequestration of Anthropogenic Carbon Dioxide in the Western Canada Sedimentary Basin: Suitability Analysis. *J. Can. Pet. Technol.*, 41(2), 32-40 (2002)

Badamchi-Zadeh, A., Yarranton, H.W., Svrcek, W.Y., and Maini, B.B.: Phase Behaviour and Physical Property Measurements for VAPEX Solvents: Part I. Propane and Athabasca Bitumen. *J. Can. Pet. Technol.*, 48(1), 54-61 (2009a)

Badamchi-Zadeh, A., Yarranton, H.W., Maini, B.B., and Satyro, M.A.: Phase Behaviour and Physical Property Measurements for VAPEX Solvents: Part II. Propane, Carbon Dioxide and Athabasca Bitumen. *J. Can. Pet. Technol.*, 48(3), 57-65 (2009b)

Baehr, H.D.: The Vapour Pressure of Lliquid Ammonia New Measurements above 328 K and a Rational Vapour-Pressure Equation. *J. Chem. Thermodyn.*, 8(2), 113-119 (1976)

Baker, L.E., Pierce, A.C., and Luks, K.D.: Gibbs Energy Analysis of Phase Equilibria. *SPE J.*, 22(5), 731-742 (1982)

Bich, E., Lober, T., and Millat, J.: Quasi-Isochoric pρT Measurements, 2nd Virial Coefficient and Vapor Pressure of n-Hexane. *Fluid Phase Equilib.*, 75(14), 149-161 (1992)

Blunt, M., Fayers, F.J., and Orr, F.M.: Carbon Dioxide in Enhanced Oil Recovery. *Energ. Convers. Manage.*, 34(9-11), 1197-1204 (1993)

Boustani, A. and Maini, B.B.: The Role of Diffusion and Convective Dispersion in Vapour Extraction Process. *J. Can. Pet. Technol.*, 40(4), 68-77 (2001)

Bowers, B. and Drummond, K.: Conventional Crude Resources of the Western Canadian Sedimentary Basin. *J. Can. Pet. Technol.*, 36(2), 56-63 (1997)

Carmichael, L.T., Sage, B.H., and Lacey, W.N.: Phase Equilibria in Hydrocarbon Systems. Volumetric Behavior of *n*-Nonane. *Ind. Eng. Chem.*, 45(12), 2697-2699 (1953)

Chatzis I. and Morrow, N.R.: Correlation of Capillary Number Relationships for Sandstone. *SPE J.*, 24(5), 555-562 (1984)

Chen, Q., Hong, R.H., and Chen, G.M.: Vapor Pressure Measurements of Ethyl Fluoride. *J. Chem. Eng. Data*, 50(5), 1586-1588 (2005)

Chickos, J.S. and Wilson, J.A. J.: Vaporization Enthalpies at 298.15 K of the *n*-Alkanes from C_{21} to C_{28} and C_{30}. *J. Chem. Eng. Data*, 42(1), 190-197 (1997)

Chirico, R.D., Nguyen, A., Steele, W.V., and Strube, M.M. J.: The Vapor Pressure of n-Alkanes Revisited. New High-Precision Vapor Pressure Data on n-Decane, n-Eicosane, and *n*-Octacosane. *Chem. Eng. Data*, 34(2), 149-156 (1989)

Chung, J.G.: Estimation of Vapor Pressure of Liquid Oxygen Between the Triple and Critical Points. *Korean J. Chem. Eng.*, 14(3), 209-212 (1997)

Chung, F.T.H., Jones, R.A., and Nguyen, H.T.: Measurements and Correlations of the Physical Properties of CO_2/Heavy-Crude-Oil Mixtures. *SPE Reservoir Eng.*, 3(3), 822-828 (1988)

Computer Modelling Group Ltd.: WINPROP Phase Property Program. Calgary, AB, Canada (2009)

Cragoe, C.S.: Changes in the Viscosity of Liquids with Temperature, Pressure, and Composition. Paper 201, proceedings of the 14th World Petroleum Congress, London, 2, 529-541 (1933)

Das, S.K. and Butler, R.M.: Diffusion Coefficients of Propane and Butane in Peace River Bitumen. *Can. J. Chem. Eng.*, 74(6), 985-992 (1996)

Deo, M.D., Wang, C.J., and Hanson, F.V.: Solubility of Carbon Dioxide in Tar Sand Bitumen: Experimental Determination and Modeling. *Ind. Eng. Chem. Res.*, 30(3), 532-536 (1991)

DeRuiter, R.A., Nash, L.J., and Singletary, M.S.: Solubility and Displacement Behavior of a Viscous Crude with CO_2 and Hydrocarbon Gases. *SPE Reservoir Eng.*, 9(2), 101-106 (1994)

Díaz, O.C., Modaresghazani, J., Satyro, M.A., and Yarranton, H.W.: Modeling the Phase Behaviour of Heavy Oil and Solvent Mixtures. *Fluid Phase Equilib.*, 304(1-2), 74-85 (2011)

Douslin, D.R. and Harrison, R.H.: Pressure, Volume, Temperature Relations of Ethane. *J. Chem. Thermodynamics*, 5(4), 491-512 (1973)

Dyer, S.B. and Farouq Ali, S.M.: Linear Model Studies of the Immiscible CO_2 WAG Process for Heavy-Oil Recovery. *SPE Reservoir Eng.*, 9(2), 107-111 (1994)

Emera, M.K. and Sarma, H.K.: A Genetic Algorithm-based Model to Predict CO_2-Oil Physical Properties for Dead and Live Oil. *J. Can. Pet. Technol.* 47(2): 52-61 (2008).

Etminan, S.R., Maini, B.B., Chen, Z., and Hassanzadeh, H.: Constant-pressure Technique for Gas Diffusivity and Solubility Measurements in Heavy Oil and Bitumen. *Energy Fuels*, 24 (1): 533-549 (2010)

Fadaei, H., Scarff, B., and Sinton, D.: Rapid Microfluidics-based Measurement of CO_2 Diffusivity in Bitumen. *Energy Fuels*, 25(10): 4829-4835 (2011)

Fall, J.L. and Luks, K.D.: Effect of Additive Gases on the Liquid-Liquid-Vapor Immiscibility of the Carbon Dioxide + *n*-Nonadecane Mixture. *J. Chem. Eng. Data*, 31(3), 332-336 (1986)

Farouq Ali, S.M.: Heavy Oil-Evermore Mobile. *J. Pet. Sci. Eng.*, 37(1-2), 5-9 (2003)

Feizabadi, S.A., Abedi, J., and Chen, Z.: Importance of a Second Liquid Phase Formation in CO_2 Injection into Bitumen Reservoirs and its Effect on Production. Paper SPE

153712, presented at the SPE Improved Oil Recovery Symposium, Tulsa, OK, April 14-18 (2012)

Firoozabadi, A., Katz, D.L., Saroosh, H., and Sajjadian, V.A.: Surface Tension of Reservoir Crude Oil/Gas Systems Recognizing the Asphalt in the Heavy Fraction. *SPE Reservoir Eng.*, 3(1), 265-272 (1988)

Frauenfeld, T., Jossy, C., Rispler, K., and Kissel, G.: Evaluation of the Bottom Water Reservoir VAPEX Process. *J. Can. Pet. Tech.*, 45(9), 29-35 (2006)

Freitag, N.P., Sayegh, S.G., and Exelby, R.: A New Semiautomatic PVT Apparatus for Characterizing VAPEX Systems. Paper SPE 97783, presented at the SPE/PS-CIM/CHOA International Thermal Operations and Heavy Oil Symposium, Calgary, AB, November 1-3 (2005)

Fu, C.T., Puttagunta, V.R., and Vilcsak, G.: Vapour-Liquid Equilibrium Properties for Pseudo-Binary Mixtures of CO_2-Athabasca Bitumen and N_2-Athabasca Bitumen. *AOSTRA J. Research*, 2(2), 73-81 (1985)

Ganapathi, K.: *Solubility and Diffusivity Study for Light Gases in Heavy Oil and Its Fractions*. MASc Thesis, Industrial Systems Engineering, Faculty of Engineering and Applied Science, University of Regina (2009).

Gao, W., Robinson, Jr., R.L., and Gasem, K.A.M.: Improved Correlations for Heavy n-Paraffin Physical Properties. *Fluid Phase Equilib.*, 179(1-2), 207-216 (2001)

Gasem, K.A.M., Gao, W., Pan, Z., and Robinson, Jr., R.L.: A Modified Temperature Dependence for the Peng-Robinson Equation of State. *Fluid Phase Equilib.*, 181(1-2), 113-125 (2001)

Goncalves, F.A.M.M., Trindade, A.R., Costa, C.S.M.F., Bernardo, J.C.S., Johnson, I., Fonseca, I.M.A., and Ferreira, A.G.M.: PVT, Viscosity, and Surface Tension of Ethanol: New Measurements and Literature Data Evaluation. *J. Chem. Thermodynamics*, 42(8), 1039-1049 (2010)

Green, D.W. and Perry, R.H.: *Perry's Chemical Engineers' Handbook*, McGraw-Hill, New York (2008)

Gregorowicz, J., Kiciak, K., and Malanowski, S.: Vapour Pressure Data for 1-Butanol, Cumene, *n*-Octane and *n*-Decane and Their Statistically Consistent Reduction with the Antoine Equation. *Fluid Phase Equilib.*, 38(1-2), 97-107 (1987)

Han, B.X., Yang, G.Y., Ke, J., Mao, C., and Yan, H.K.: Phase Equilibria of Supercritical Propane-Fengcheng Bitumen System and the Density and Viscosity of the Liquid Phase. *Fluid Phase Equilib*., 143(1-2), 205-211 (1998)

Hatzignatiou, D.G. and Lu, Y.: Feasibility Study of CO_2 Immiscible Displacement Process in Heavy Oil Reservoirs. Paper 94-90, presented at the Annual Technical Meeting, Calgary, AB, June 12-15 (1994)

Hernández-Garduza, O., García-Sánchez, F., Ápam-Martínez, D., and Vázquez-Román, R.: Vapor Pressures of Pure Compounds Using the Peng-Robinson Equation of State with Three Different Attractive Terms. *Fluid Phase Equilib.*, 198(2), 195-228 (2002)

Heyen, G.: A Cubic Equation of State with Extended Range of Application. Proceedings of the 2nd World Congress of Chem. Eng., Montreal, QC, October 4-9, 41-46 (1981)

Hildebrand, J.H.: *Solubility of Non-Electrolytes*. American Chemical Society Monograph Series, Reinhold Publishing Corporation, New York (1936)

Holcomb, C.D. and Outcalt, S.L.: Near-Saturation (P, ρ, T) and Vapor-Pressure Measurements of NH_3, and Liquid-Phase Isothermal (P, ρ, T) and Bubble-Point-Pressure Measurements of NH_3 + H_2O Mixtures. *Fluid Phase Equilib.*, 164(1), 97-106 (1999)

Ivory, J., Chang, J., Coates, R., and Forshner, K.: Investigation of Cyclic Solvent Injection for Heavy Oil Recovery. *J. Can. Pet. Technol.*, 23(3), 29-36 (2010)

Jamaluddin, A.K.M., Kalogerakis, N.E., and Chakma, A.: Predictions of CO_2 Solubility and CO_2 Saturated Liquid Density of Heavy Oils and Bitumens Using a Cubic Equation of State. *Fluid Phase Equilib.*, 64: 33-48 (1991)

Jamialahmadi, M., Emadi, M., and Müller-Steinhagen, H.: Diffusion Coefficients of Methane in Liquid Hydrocarbons at High Pressure and Temperature. *J. Pet. Sci. Eng.*, 53(1-2): 47-60 (2006)

Joshipura, M.H., Dabke, S.P., and Subrahmanyam, N.: Development and Comparison of Cohesion Function Relationship for PR Equation of State. *Int. J. Chem. Eng. Res.*, 1(2), 123-134 (2009)

Kamal, N.J.: A Laboratory Study of Heavy Oil Recovery with Carbon Dioxide. *J. Can. Pet. Technol.*, 25(2), 54-63 (1986)

Kariznovi, M., Nourozieh, H., and Abedi, J.: Bitumen Characterization and Pseudocomponents Determination for Equation of State Modeling. *Energy Fuels*, 24(1), 624-633 (2010)

Kesler, M.G. and Lee, B.I.: Improve Predictions of Enthalpy of Fractions. *Hydro. Pro.* 55(3), 153-158 (1976)

Kleinrahm, R. and Wagner, W.: Measurement and Correlation of the Equilibrium Liquid and Vapour Densities and the Vapour Pressure along the Coexistence Curve of Methane. *J. Chem. Thermodyn.*, 18(8), 739-760 (1986)

Klins, M.A. and Farouq Ali, S.M.: Heavy Oil Production by Carbon Dioxide Injection. *J. Can. Pet. Technol.*, 21(5), 64-72 (1982)

Knorr, K.D. and Imran, M.: Extension of Das and Butler Semianalytical Flow Model. *J. Can. Pet. Tech.*, 50(6), 53-60 (2011)

Kokal, S.L. and Sayegh, S.G.: Phase Behavior Correlation of CO_2/Heavy Oil Mixtures for Enhanced Oil Recovery. *Fluid Phase Equilib*., 52, 283-290 (1989)

Kokal, S.L. and Sayegh, S.G.: Phase Behaviour and Physical Properties of CO_2 Saturated Suffield Heavy Oil and its Constituent Fractions: Experimental Data and Correlations. *AOSTRA J. Research*, 8, 79-94 (1992)

Kratzke, H., Spillner, E., and Muller, S.: Thermodynamic Properties for *n*-Butane 1. The Vapour Pressure of Liquid *n*-Butane. *J. Chem. Thermodyn.*, 14(12), 1175-1181 (1982)

Kratzke, H., Muller, S., Bohn, M., and Kohlen, R.: Thermodynamic Properties of Saturated and Compressed Liquid *n*-Pentane. *J. Chem. Thermodyn.*, 17(3), 283-294 (1985)

Kumar, R. and Mahadevan, J.: Well-Performance Relationships in Heavy-Foamy-Oil Reservoirs. *SPE Prod. Operat.*, 27(1), 94-105 (2012)

Larson, L.L., Silva, M.K., Taylor, M.A., and Orr Jr., F.M.: Temperature Dependence of $L_1/L_2/V$ Behaviour in CO_2/Hydrocarbon Systems. *SPE Reservoir Eng.*, 4(1), 105-114 (1989)

Lederer, E.L.: Viscosity of Diluted Mixtures. Paper 200, proceedings of the 14th World Petroleum Congress, London, 2, 526-528 (1933)

Lee, B.I. and Kesler, M.G.: A Generalized Thermodynamic Correlation based on Three-Parameter Corresponding States. *AIChE J.*, 21 (3), 510-527 (1975)

Lemmon, E.W. and Goodwin, A.R.H.: Critical Properties and Vapor Pressure Equation for Alkanes C_nH_{2n+2}: Normal Alkanes with $n <= 36$ and Isomers for $n = 4$ Through $n = 9$. *J. Phys. Chem. Ref. Data*, 29, 1-39 (2000)

Li. H., Qin, J., and Yang, D.: An Improved CO_2-oil Minimum Miscibility Pressure Correlation for Live and Dead Crude Oils. *Ind. Eng. Chem. Res.*, 51(8): 3516-3523 (2012)

Li, H. and Yang, D.: Modified α Function for the Peng-Robinson Equation of State to Improve the Vapor Pressure Prediction of Non-Hydrocarbon and Hydrocarbon Compounds. *Energy Fuels*, 25(1), 215-223 (2011)

Li, H., Yang, D., and Tontiwachwuthikul, P.: Experimental and Theoretical Determination of Equilibrium Interfacial Tension for the Solvent(s)-CO_2-Heavy Oil Systems. *Energy Fuels*, 26(3), 1776-1786 (2012)

Li, H. and Yang, D.: Phase Behaviour of C_3H_8-*n*-C_4H_{10}-Heavy Oil Systems at High Pressures and Elevated Temperatures. *J. Can. Pet. Technol.*, 52(1), 30-40 (2013).

Li, H., Zheng, S., and Yang, D.: Enhanced Swelling Effect and Viscosity Reduction of Solvent(s)-CO_2-Heavy Oil Systems. *SPE J.*, available on-line (http://dx.doi.org/10.2118/150168-PA).

Li, Z. and Firoozabadi, A.: General Strategy for Stability Testing and Phase-Split Calculations in Two and Three Phases. Paper SPE 129844, presented at the SPE Improved Oil Recovery Symposium, Tulsa, OK, April 24-28 (2010)

Lide, D.R.: *CRC Handbook of Chemistry and Physics*. CRC Press, Florida (2009)

Liphard, K.G., and Schneider, G.M.: Phase Equilibria and Critical Phenomena in Fluid Mixtures of Carbon Dioxide + 2,6,10,15,19,23-Hexamethyltetracosane up to 423 K and 100 MPa. *J. Chem. Thermodyn.*, 7(9), 805-814 (1975)

Liu, Z., Yang, G., Lu, Y., Han, B., and Yan, H.: Phase Equilibria of the CO_2-Jiangsu Crude Oil System and Precipitation of Heavy Components Induced by Supercritical CO_2. *J. Supercrit. Fluid.*, 16(1), 27-31 (1999)

Lobe, V.M.: *A Model for the Viscosity of Liquid-Liquid Mixtures*. M.Sc. Thesis, University of Rochester, Rochester, NY (1973)

Luo, P. and Gu, Y.: Characterization of a Heavy Oil-Propane System in the Presence or Absence of Asphaltene Precipitation. *Fluid Phase Equilib.*, 277(2), 1-8 (2007)

Luo, P., Yang, C., and Gu, Y.: Enhanced Solvent Dissolution into in-situ Upgraded Heavy Oil under Different Pressures. *Fluid Phase Equilib.*, 252(1-2), 143-151 (2007)

Luo, P., Zhang, Y., Wang, X., and Huang, S.: Propane-Enriched CO_2 Immiscible Flooding for Improved Heavy Oil Recovery. *Energy Fuels*, 26(4), 2124-2135 (2012)

Macleod, D.B.: On a Relation between Surface Tension and Density. *Trans. Faraday Soc.*, 19, 38-42 (1923)

Mangalsingh, D. and Jagai, T.: A Laboratory Investigation of the Carbon Dioxide Immiscible Process. Paper SPE 36134, presented at the SPE Latin America/Caribbean Petroleum Engineering Conference, Port-of-Spain, Trinidad, April 23-26 (1996)

Martinez-Ortlz, J.A. and Manley, D.B.: Vapor Pressures for the System Isobutane-Isobutylene-*n*-Butane. *J. Chem. Eng. Data*, 23(2), 165-167 (1978)

Mathias, P.M.: A Versatile Phase Equilibrium Equation of State. *Ind. Eng. Chem. Process Des. Dev.*, 22(3), 385-391 (1983)

Mazee, W.M.: Properties of Hydrocarbons Having more than Twenty Carbon Atoms. *Recl. Trav. Chim.*, 67(3), 197-213 (1948)

Mathias, P.M. and Copeman, T.W.: Extension of the Peng-Robinson Equation of State to Complex Mixtures: Evaluation of the Various Forms of the Local Composition Concept. *Fluid Phase Equilib.*, 13, 91-108 (1983)

McCain, W.D.: *The Properties of Petroleum Fluids*. Pennwell Publishing Co., Tulsa, (1990)

Mehra, R.K.: *The Computation of Multi-phase Equilibrium in Compositional Reservoir Studies*. Ph.D. Dissertation, University of Calgary, Calgary, AB, Canada (1981)

Mehrotra, A.K. and Svrcek, W.Y.: Correlations for Properties of Bitumen Saturated with CO_2, CH_4 and N_2, and Experiments with Combustion Gas Mixtures. *J. Can. Pet. Technol.*, 21(6), 95-104 (1982)

Mehrotra, A.K. and Svrcek, W.Y.: Measurement and Correlation of Viscosity, Density, and Gas Solubility for Marguerite Lake Bitumen Saturated with Carbon Dioxide. *AOSTRA J. Research*, 1(1), 51-62 (1984)

Mehrotra, A.K. and Svrcek, W.Y.: Viscosity, Density and Gas Solubility Data for Oil Sand Bitumen. Part II: Athabasca Bitumen Saturated with N_2, CO, CH_4, CO_2, and C_2H_6. *AOSTRA J. Research*, 1(4), 269-279 (1985a)

Mehrotra, A.K. and Svrcek, W.Y.: Viscosity, Density and Gas Solubility Data for Oil Sand Bitumen. Part III: Wabasca Bitumen Saturated with N_2, CO, CH_4, CO_2, and C_2H_6. *AOSTRA J. Research*, 2(2), 83-93 (1985b)

Mehrotra, A.K. and Svrcek, W.Y.: Properties of Cold Lake Bitumen Saturated with Pure Gases and Gas Mixtures. *Can. J. Chem. Eng.*, 66(4), 656-665 (1988)

Mehrotra, A.K., Nighswander, J.A., and Kalogerakis, N.: Data and Correlation for CO_2-Peace River Bitumen Phase Behaviour at 22-200ºC. *AOSTRA J. Research*, 5(4), 351-357 (1989)

Meldrum, A.H. and Nielsen, R.F. A Study of Three-Phase Equilibria for CO_2-Hydrocarbon Mixtures. *Prod. Monthly*, 19, 22-35 (1955)

Melhem, G.A., Saini, R., and Goodwin, B.M.: A Modified Peng-Robinson Equation of State. *Fluid Phase Equilib.*, 47(2-3), 189-237 (1989)

Memon, A.I., Gao, J., Taylor, S.D., Davies, T.L., and Jia, N.: A Systematic Workflow Process for Heavy Oil Characterization: Experimental Techniques and Challenges. Paper SPE 137006, presented at the SPE Canadian Unconventional Resources and International Petroleum Conference, Calgary, AB, October 19-21 (2010)

Michels, A.; Wassenaar, T.; Zwietering, Th.; and Smits, P.: The Vapour Pressure of Liquid Carbon Dioxide. *Physica*, 16(5), 501-504 (1950)

Michelsen, M.L.: Isothermal Flash Problem-Part I: Stability. *Fluid Phase Equilib.*, 9(1), 1-19 (1982)

Miller, M.M. and Luks, K.D.: Observation on the Multiphase Equilibria Behaviour of CO_2-Rich and Ethane-Rich Mixtures. *Fluid Phase Equilib.*, 44(1-2), 295-304 (1989)

Miller, J.S. and Jones, R.A.: A Laboratorial Study to Determine Physical Characteristics of Heavy Oil after CO_2 Saturation. Paper SPE 13598, presented at the SPE/DOE Enhanced Oil Recovery Symposium, Tulsa, OK, April 5-8 (1981)

Mohammed-Singh, L. and Singhal, A.K.: Lessons Learned from Trinidad's CO_2 Immiscible Projects. *SPE Reservoir Eval. Eng.*, 8(5), 397-403 (2005)

Mokbel, I., Rauzy, E., Loiseleur, H., Berro, C., and Jose, J.: Vapor Pressures of 12 Alkylcyclohexanes, Cyclopentane, Butylcyclopentane and Trans-Decahydronaphthalene down to 0.5 Pa. Experimental Results, Correlation and Prediction by an Aquation of State. *Fluid Phase Equilib.*, 108(1-2), 103-120 (1995)

Mokbel, I., Rauzy, E., Meille, J.P., and Jose, J.: Low Vapor Pressures of 12 Aromatic Hydrocarbons. Experimental and Calculated Data Using a Group Contribution Method. *Fluid Phase Equilib.*, 147(1-2), 271-284 (1998)

Monger, T.G. and Coma, J.M.: A Laboratory and Field Evaluation of the CO_2 Huff 'n' Puff Process for Light-Oil Recovery. *SPE Res. Eng.*, 3(4), 1168-1176 (1988)

Morgan, D.L. and Kobayashi, R. Direct Vapor Pressure Measurements of Ten *n*-Alkanes in the C_{10}-C_{28} Range. *Fluid Phase Equilib.*, 97(15), 211-242 (1994)

Mullken, C.A. and Sandler, S.I.: The Prediction of CO_2 Solubility and Swelling Factors for Enhanced Oil Recovery. *Ind. Eng. Chem. Process Des. Dev.*, 19(4), 709-711 (1980)

Nagashima, A.: Viscosity of Water Substance-New International Formulation and its Background. *J. Phys. Chem. Ref. Data*, 6(4), 1133-1166 (1977)

Neau, E., Hernández-Garduza, O., Escandell, J., Nicolas, C., and Raspo, I.: The Soave, Twu and Boston-Mathias Alpha Functions in Cubic Equations of State. Part I. Theoretical Analysis of their Variations According to Temperature. *Fluid Phase Equilib.*, 276(2), 87-93 (2009a)

Neau, E., Raspo, I., Escandell, J., Nicolas, C., and Hernández-Garduza, O.: The Soave, Twu and Boston-Mathias Alpha Functions in Cubic Equations of State. Part II. Modeling of Thermodynamic Properties of Pure Compounds. *Fluid Phase Equilib.*, 276(2), 156-164 (2009b)

Nguyen, T.A. and Farouq Ali, S.M.: Effect of Nitrogen on the Solubility and Diffusivity of Carbon Dioxide into Oil and Oil Recovery by the Immiscible WAG Process. *J. Can. Pet. Technol.*, 37(2), 24-31 (1998)

Nikitin, E.D., Pavlov, P.A., and Popov, A.P.: Vapour-Liquid Critical Temperatures and Pressures of Normal Alkanes with from 19 to 36 Carbon Atoms, Naphthalene and m-Terphenyl Determined by the Pulse-Heating Technique. *Fluid Phase Equilib.*, 141(1-2), 155-164 (1997)

Nji, G.N., Svrcek, W.Y., Yarranton, H., and Satyro, M.A.: Characterization of Heavy Oils and Bitumens 2. Improving the Prediction of Vapor Pressures for Heavy Hydrocarbons at Low Reduced Temperatures Using the Peng-Robinson Equation of State. *Energy Fuels*, 23(1), 366-373 (2009)

Nobakht, M., Moghadam, S., and Gu. Y.: Effect of Viscous and Capillary Forces on CO_2 Enhanced Oil Recovery under Reservoir Conditions. *Energy Fuels*, 21(6), 3469-3476 (2007)

Okuno, R., Johns, R.T., and Sepehrnoori, K.: Mechanisms for High Displacement Efficiency of Low Temperature CO_2 Floods. *SPE J.*, 16(4), 751-767 (2011)

Olenick, S., Schroeder, F.A., Haines, H.K. and Monger-McClure, T.G.: Cyclic CO_2 Injection for Heavy-Oil Recovery in Halfmoon Field: Laboratory Evaluation and

Pilot Performance. Paper SPE 24645, presented at the 67th SPE Annual Technical Conference and Exhibition, Washington, DC, October 4-7 (1992)

Orr, Jr., F.M.: Interpretation of Pressure-Composition Phase Diagrams for CO_2/Crude-Oil Systems. *SPE J.*, 24(5), 485-497 (1984)

Orr, Jr., F.M., Yu, A.D., and Lien, C.L.: Phase Behaviour of CO_2 and Crude Oil in Low-Temperature Reservoirs. *SPE J.*, 21(4), 480-492 (1981)

Orr, Jr., F.M. and Silva, M.K.: Equilibrium Phase Compositions of CO_2/Hydrocarbon Mixtures-Part 1: Measurement by a Continuous Multiple-Contact Measurement. *SPE J.*, 23(2), 272-280 (1983)

Orr, Jr., F.M., Silva, M.K., and Lien, C.L.: Equilibrium Phase Compositions of CO_2/Hydrocarbon Mixtures-Part 2: Comparison of Continuous Multiple-Contact and Slim-Tube Displacement Tests. *SPE J.*, 23(2), 281-291 (1983)

Orr, Jr., F.M. and Taber, J.J.: Use of Carbon Dioxide in Enhanced Oil Recovery. *Science*, 224(4649), 563-569 (1984)

Pathak, V., Babadagli, T., and Edmunds, N.R.: Heavy Oil and Bitumen Recovery by Hot Solvent Injection. *J. Pet. Sci. Eng.*, 78(3-4), 637-645 (2011)

Paulaitis, M.E., Krukonis, V.J., Kurnik, R.T., and Reid, R.C.: Supercritical Fluid Extraction. *Rev. Chem. Eng.*, 1: 181-248 (1983)

Peng, D. and Robinson, D.B.: A New Two-Constant Equation of State. *Ind. Eng. Chem. Fundam.*, 15(1), 59-64 (1976)

Peneloux, A., Rauzy, E., and Freze, R.: A Consistent Correction for Redlich-Kwong-Soave Volumes. *Fluid Phase Equilib.*, 8(1), 7-23 (1982)

Peters, C.J., Van Der Kooi, H.J., De Roo, J.L., De Swaan Arons, J., Gallagher, J.S., and Levelt Sengers, J.M.H.: The Search for Tricriticality in Binary Mixtures of Near-critical Propane and Normal Paraffins. *Fluid Phase Equilib.*, 51, 339-351 (1989)

Petersen, K.S. and Christensen, P.L.: *Phase Behaviour of Petroleum Reservoir Fluid*s. New York, Taylor & Francis Group (2006)

Pitzer, K.S.: The Volumetric and Thermodynamic Properties of Fluids. I. Theoretical Basis and Virial Coefficients. *J. Am. Chem. Soc.*, 77(13), 3427-3433 (1955)

Pitzer, K.S., Lippmann, D.Z., Curl, R.F., Huggins, C.M., and Petersen, D.E.: The Volumetric and Thermodynamic Properties of Fluids. II. Compressibility Factor, Vapor Pressure and Entropy of Vaporization. *J. Am. Chem. Soc.*, 77(13), 3433-3440 (1955)

Qazvini Firouz, A. and Torabi, F.: Feasibility Study of Solvent-based Huff-*n*-Puff Method (Cyclic Solvent Injection) to Enhance Heavy Oil Recovery. Paper SPE 157853, presented at SPE Heavy Oil Conference Canada, Calgary, AB, June 12-14 (2012)

Quail, B., Hill, G.A., and Jha, K.N.: Correlations of Viscosity, Gas Solubility, and Density for Saskatchewan Heavy Oils. *Ind. Eng. Chem. Res.*, 27(3), 519-523 (1988)

Rahmes M.H. and Nelson, W.L.: Viscosity Blending Relationship of Heavy Petroleum Oils. *Analytical Chem.*, 20, 912-915 (1948)

Redlich, O. and Kwong, J.N.S.: On the Thermodynamics of Solutions. V. An Equation of State. Fugacities of Gaseous Solutions. *Chem. Rev.*, 44(1), 233-244 (1949)

Rezaei, N., Mohammadzadeh, O., and Chatzis, I.: Warm VAPEX: a Thermally Improved Vapour Extraction Process for Recovery of Heavy Oil and Bitumen. *Energy Fuels*, 24(11), 5934-5946 (2010)

Robinson, D.B. and Peng, D.: The Characterization of the Heptanes and Heavier Fractions for the GPA Peng-Robinson Programs. Research Report 28, Gas Producers Association (GPA), Tulsa (1978)

Rojas, G. and Farouq Ali, S.M.: Scaled Model Studies of Carbon Dioxide/Brine Injection Strategies for Heavy Oil Recovery from Thin Reservoirs. *J. Can. Pet. Technol.*, 25(1), 85-94 (1986)

Rojas, G.A. and Farouq Ali, S.M.: Dynamics of Subcritical CO_2/Brine Floods for Heavy Oil Recovery. *SPE Reservoir Eng.*, 3(1), 35-44 (1988)

Rowlinson, J.E. and Swinton, F.L.: *Liquids and Liquid Mixtures*. Butterworths, London (1982)

Saber, N. and Shaw, J.M.: Rapid and Robust Phase Behavior Stability Analysis Using Global Optimization. *Fluid Phase Equilib.*, 264(1-2), 137-146 (2008)

Sahin, S., Kalfa, U., and Celebioglu, D.: Bati Raman Field Immiscible CO_2 Application-Status Quo and Future Plans. *SPE Reservoir Eval. Eng.*, 11(4), 778-791 (2008)

Sandler, S.I.: *Chemical and Engineering Thermodynamics*. John Wiley & Sons, New York (1999)

Saner, W.B. and Patton, J.T.: CO_2 Recovery of Heavy Oil: Wilmington Field Test. *J. Pet. Technol.*, 38(7), 769-776 (1986)

Saskatchewan Industry and Resources. *Oil Reserve Summary Reports*. Regina, SK, Canada (2006)

Sayegh, S.G. and Maini, B.B.: Laboratory Evaluation of the CO_2 Huff-*n*-Puff Process for Heavy Oil Reservoirs. *J. Can. Pet. Technol.*, 23(3), 29-36 (1984)

Sayegh, S.G., Rao, D.N., Kokal, S., and Najman, J.: Phase Behaviour and Physical Properties of Lindbergh Heavy Oil/CO_2 Mixtures. *J. Can. Pet. Technol.*, 29(6), 31-39 (1990)

Shaver, R.D., Robinson, Jr., R.L., and Gasem, K.A.M. A Framework for the Prediction of Saturation Properties: Vapor Pressures. *Fluid Phase Equilib.*, 64, 141-163 (1991)

Shaw, J.M. and Zou, X.: *Phase Behaviour of Heavy Oils. In Asphaltenes, Heavy Oils, and Petroleomics*, Springer, New York, 489-510 (2007)

Sheft, I., Perkins, A.J., and Hyman, H.H.: Anhydrous Hydrogen Fluoride: Vapor Pressure and Liquid Density. *J. Inorg. Nucl. Chem.*, 35(11), 3677-3680 (1973)

Shokir, E.M.E.-M.: CO_2-oil Minimum Miscibility Pressure Model for Impure and Pure CO_2 Streams. *J. Pet. Sci. Eng.*, 58(1-2), 173-185 (2007).

Shu, W.R.: A Viscosity Correlation for Mixtures of Heavy Oil, Bitumen, and Petroleum Fractions. *SPE J.*, 24(6), 277-282 (1984)

Simon, R. and Graue, D.J.: Generalized Correlations for Predicting Solubility, Swelling and Viscosity Behaviour of CO_2-Crude Oil Systems. *J. Pet. Technol.*, 17(1), 102-106 (1965)

Simon, R., Rosman, A., and Zana, E.: Phase Behaviour Properties of CO_2-Reservoir Systems. *SPE J.*, 18(1), 20-26 (1978)

Singh, R. and Babadagli, T.: Mechanics and Upscaling of Heavy Oil Bitumen Recovery by Steam-Over-Solvent Injection in Fractured Reservoirs Method. *J. Can. Pet. Technol.*, 50(1), 33-42 (2011)

Soave, G.: Equilibrium Constants from a Modified Redlich-Kwong Equation of State. *Chem. Eng. Sci.*, 27(6), 1197-1203 (1972)

Soreide, I.: *Improved Phase Behavior Predictions of Petroleum Reservoir Fluids from a Cubic Equation of State*. Ph.D. Dissertation, Norwegian Institute of Technology (NTH), Trondheim, Norway (1989)

Span, R. and Wagner, W.: A New Equation of State for Carbon Dioxide Covering the Fluid Regiona from the Triple Point Temperature to 1100 K at Pressures up to 800 MPa. *J. Phys. Chem. Ref. Data*, 25(6), 1509-1596 (1996)

Specovius, J., Leiva, M.A., Scott, R.L, and Knobler, C.M.: Tricritical Phenomena in Quasi-Binary Mixtures of Hydrocarbons. 2. Binary Ethane Systems. *J. Phys. Chem.*, 85(16), 2313 (1981)

Spencer, C.F. and Danner, R.P.: Improved Equation for Prediction of Saturated Liquid Density. *J. Chem. Eng. Data*, 17(2), 236-241 (1972)

Spivak, A. and Chima, C.M.: Mechanisms of Immiscible CO_2 Injection in Heavy Oil Reservoirs, Wilmington Field, CA. Paper SPE 12667, presented at the SPE Enhanced Oil Recovery Symposium, Tulsa, OK, April 15-18 (1984)

Srivastava, R.K., Huang, S., and Dong, M.: Comparative Effectiveness of CO_2 Produced Gas, and Flue Gas for Enhanced Heavy-Oil Recovery. *SPE Reservoir Eval. Eng.*, 2(3), 238-247 (1999)

Stewart, W.C. and Nielsen, R.F.: Phase Equilibria for Mixtures of Carbon Dioxide and Several Normal Saturated Hydrocarbons. *Prod. Monthly*, 18, 27-32 (1954)

Stryjek, R. and Vera, J.H.: PRSV: An Improved Peng-Robinson Equation of State for Pure Compounds and Mixtures. *Can. J. Chem. Eng.*, 64(2), 323-333 (1986)

Stull, D.R.: Vapor Pressure of Pure Substances. Organic and Inorganic Compounds. *Ind. Eng. Chem.*, 39(4), 517-540 (1947)

Sudgen, S.: The Variation of Surface Tension with Temperature and Some Related Functions. *J. Chem. Soc.*, 125(0), 32-41 (1924)

Suehiro, Y., Nakajima, M., Yamada, K., and Uematsu, M.: Critical Parameters of $\{xCO_2 + (1- x)CHF_3\}$ for x = (1.0000, 0.7496, 0.5013, and 0.2522). *J. Chem. Thermodyn.*, 28(10), 1153-1164 (1996)

Svrcek, W.Y. and Mehrotra, A.K. Properties of Peace River Bitumen Saturated with Field Gas Mixtures. *J. Can. Pet. Technol.*, 28(2), 50-56 (1989)

Talbi, K. and Maini, B.B.: Experimental Investigation of CO_2-based VAPEX for Recovery of Heavy Oils and Bitumen. *J. Can. Pet. Technol.*, 47(4), 1-8 (2008)

Teja, A.S. and Sandler, A.I.: A Corresponding States Equation for Saturated Liquid Densities. II. Applications to the Calculation of Swelling Factors of CO_2-Crude Oil Systems. *AICHE J.*, 26(3), 341-345 (1980)

Tharanivasan, A.K., Yang, C., and Gu Y.: Measurements of Molecular Diffusion Coefficients of Carbon Dioxide, Methane, and Propane in Heavy Oil under Reservoir Conditions. *Energy Fuels*, 20(6): 2509-2517 (2006)

Thomast, R.H.P. and Harrison, R.H.: Pressure-Volume-Temperature Relations of Propane. *J. Chem. Eng. Data*, 27(1), 1-11 (1982)

Trebble, M.A. and Bishnoi, P.R.: Development of a New Four-parameter Cubic Equation of State. *Fluid Phase Equilib.*, 35(1-3), 1-18 (1987)

Turta, A.T., Maini, B.B., and Jackson, C.: Mobility of Gas-in-Oil Dispersions in Enhanced Solution Gas Drive (Foamy Oil) Exploitation of Heavy Oil Reservoirs. *J. Can. Pet. Technol.*, 42(3): 48-55 (2003)

Tuzunoglu, E. and Bagci, S.: Scaled 3-D Model Studies of Immiscible CO_2 Flooding Using Horizontal Wells. *J. Pet. Sci. Eng.*, 26(1-4), 67-81 (2000)

Twu, C.H., Bluck, D., Cunningham, J.R., and Coon, J.E.: A Cubic Equation of State with a New Alpha Function and a New Mixing Rule. *Fluid Phase Equilib.*, 69, 33-50 (1991)

Twu, C.H. and Chan, H.S.: Rigorously Universal Methodology of Volume Translation for Cubic Equation of State. *Ind. Eng. Chem. Res.*, 48(12), 5901-5906 (2009)

Twu, C.H., Coon, J.E., and Cunningham, J.R.: A Generalized Vapor Pressure Equation for Heavy Hydrocarbons. *Fluid Phase Equilib.*, 96, 19-31 (1994)

Twu, C.H., Coon, J.E., and Cunningham, J.R.: A New Generalized Alpha Function for a Cubic Equation of State Part 1. Redlich-Kwong Equation. *Fluid Phase Equilib.*, 105(1), 49-59 (1995a)

Twu, C.H., Coon, J.E., and Cunningham, J.R.: A New Generalized Alpha Function for a Cubic Equation of State Part 2. Peng-Robinson Equation. *Fluid Phase Equilib.*, 105(1), 61-69 (1995b)

Upreti, S.R., Lohi, A., Kapadia, R.A., and El-Haj, R.: Vapor Extraction of Heavy Oil and Bitumen: A Review. *Energy Fuel*, 21(3), 1562-1574 (2007)

Upreti, S.R. and Mehrotra, A.K.: Diffusivity of CO_2, CH_4, C_2H_6, and N_2 in Athabasca Bitumen. *Can. J. Chem. Eng.*, 80(1): 116-125 (2002)

Upreti, S.R. and Mehrotra, A.K.: Experimental Measurement of Gas Diffusivity in Bitumen: Results for Carbon Dioxide. *Ind. Eng. Chem. Res.*, 39(4): 1080-1087 (2000)

Van Konynenburg, P.H. and Scott, R.L.: Critical Lines and Phase Equilibria in Binary van der Waals Mixtures. *Philos. Tr. R. Soc. S-A*, 298(1442), 495-540 (1980)

Vesovic, V., Wakeham, W.A., Olchowy, G.A., Sengers, J.V., Watson, J.T.R., and Millat, J.T.R.: The Transport Properties of Carbon Dioxide, *J. Phys. Chem. Ref. Data*, 19(3), 763-808 (1990)

Vogel, E., Kuchenmeister, C., and Bich, E.: Reference Correlation of the Viscosity of Propane. *J. Phys. Chem. Ref. Data*, 27(5), 947-970 (1998)

Wagner, W. New Vapour Pressure Measurements for Argon and Nitrogen and a New Method for Establishing Rational Vapour Pressure Equations. *Cryogenics*, 13(8), 470-482 (1973)

Wagner, W. and Pruß, A.: The IAPWS Formulation 1995 for the Thermodynamic Properties of Ordinary Water Substance for General and Scientific Use. *J. Phys. Chem. Ref. Data*, 31(2), 387-535 (2002)

Wang, J. and Sadus, R.J.: Phase Behaviour of Binary Fluid Mixtures: a Global Phase Diagram Solely in Terms of Pure Component Properties. *Fluid Phase Equilib.*, 214(1), 67-78 (2003)

Weber, L.A.: Vapor Pressure of Heptane from the Triple Point to the Critical Point. *J. Chem. Eng. Data*, 45(2), 173-176 (2000)

Weinaug, C.F. and Katz, D.L.: Surface Tensions of Methane-Propane Mixtures. *Ind. Eng. Chem.*, 35(2), 239-246 (1943)

Welker, J.R. and Dunlop, D.D.: Physical Properties of Carbonated Oils. *J. Pet. Technol.*, 15(8), 873-876 (1963)

Whitson, C.H. and Brule, M.R.: *Phase Behavior*. Richardson, TX: Monogragh Series, SPE, 20(79) (2000)

Wilke, C.R. and Chang, P.: Correlation of Diffusion Coefficients in Dilute Solutions. *AIChE J.*, 1(2), 264-270 (1995)

Yang, C. and Gu, Y.: Effects of Heavy Oil-Solvent IFT on Gravity Drainage in the Vapor Extraction (VAPEX) Process. SPE paper 97906, presented at the SPE International Thermal Operations and Heavy Oil Symposium, Calgary, AB, November 1-3 (2005)

Yang, C. and Gu, Y.: A New Method for Measuring Solvent Diffusivity in Heavy Oil by Dynamic Pendant Drop Shape Analysis (DPDSA). *SPE J.*, 11(1), 48-57 (2006a)

Yang, C. and Gu, Y.: Diffusion Coefficients and Oil Swelling Factors of Carbon Dioxide, Methane, Ethane, Propane, and their Mixtures in Heavy Oil. *Fluid Phase Equilib.*, 243, 64-73 (2006b)

Yang, D. and Gu, Y.: Interfacial Interactions between Crude Oil and CO_2 under Reservoir Conditions. *Pet. Sci. Technol.*, 23(9-10), 1099-1112 (2005)

Yang, D., Tontiwachwuthikul, P., and Gu, Y.: Interfacial Tensions of the Crude Oil + Reservoir Brine + CO_2 Systems at Pressures up to 31 MPa and Temperatures of 27°C and 58°C. *J. Chem. Eng. Data*, 50(4), 1242-1249 (2005)

Yang, D. and Gu, Y.: Determination of Diffusion Coefficients and Interface Mass-Transfer Coefficients of the Crude Oil-CO_2 System by Analysis of the Dynamic and Equilibrium Interfacial Tensions. *Ind. Eng. Chem. Res.*, 47(15), 5447-5455 (2008).

Yang, D., Tontiwachwuthikul, P., and Gu, Y.: Dynamic Interfacial Tension Method for Measuring the Gas Diffusion Coefficient and the Interface Mass Transfer Coefficient in a Liquid. *Ind. Eng. Chem. Res.*, 45(14), 4999-5008 (2006).

Yaws, C.L.: *Yaws' Handbook of Thermodynamic and Physical Properties of Chemical Compounds*. Knovel Corporation, http://www.knovel.com/knovel2/Toc.jsp (2003)

Yazdani, A. and Maini, B.B.: Measurements and Modelling of Phase Behaviour and Viscosity of a Heavy Oil/Butane System. *J. Can. Pet. Technol.*, 49(2), 9-14 (2010)

Younglove, B.A. and Ely, J.F.: Thermodynamic Properties of Fluids. II. Methane, Ethane, Propane, Isobutane, and Normal Butane. *J. Phys. Chem. Ref. Data*, 16(4), 577-798 (1987)

Yu, J., Huang, S., and Radosz, M.: Phase Behaviour of Reservoir Fluids: Supercritical Carbon Dioxide and Cold Lake Bitumen. *Fluid Phase Equilib.*, 53, 429-438 (1989)

Zhang, Y.P., Hyndman, C.L., and Maini, B.B.: Measurement of Gas Diffusivity in Heavy Oils. *J. Pet. Sci. Eng.* 25: 37-47 (2000)

Zhao, L.: Steam Alternating Solvent Process. *SPE Reservoir Eval. Eng.*, 10(2), 185-190 (2007)

Zheng, S., Li, H., and Yang, D.: Pressure Maintenance and Improving Oil Recovery with CO_2 Injection in Heavy Oil Reservoirs. Paper SPE 150169, presented at the SPE Heavy Oil Conference and Exhibition (HOCE), Kuwait City, Kuwait, December 12-14 (2011)

Zheng, S. and Yang, D.: Pressure Maintenance and Improving Oil Recovery by Means of Water-Alternating-CO_2 Processes in Thin Heavy Oil Reservoirs. *SPE Reservoir Eval. Eng.*, 16(1), 60-71 (2013)